The Handbook of Environmental Chemistry 22
Series Editors: Damià Barceló · Andrey G. Kostianoy

Evgeniy V. Yakushev *Editor*

Chemical Structure of Pelagic Redox Interfaces

Observation and Modeling

Springer

The Handbook of Environmental Chemistry

Founded by Otto Hutzinger

Volume 22

The Handbook of Environmental Chemistry

Recently Published and Forthcoming Volumes

Chemical Structure of Pelagic Redox Interfaces: Observation and Modeling
Volume Editor: E.V. Yakushev
Vol. 22, 2013

The Llobregat: The Story of a Polluted Mediterranean River
Volume Editors: S. Sabater, A. Ginebreda, and D. Barceló
Vol. 21, 2012

Emerging Organic Contaminants and Human Health
Volume Editor: D. Barceló
Vol. 20, 2012

Emerging and Priority Pollutants in Rivers: Bringing Science into River Management Plans
Volume Editors: H. Guasch, A. Ginebreda, and A. Geiszinger
Vol. 19, 2012

Global Risk-Based Management of Chemical Additives I: Production, Usage and Environmental Occurrence
Volume Editors: B. Bilitewski, R.M. Darbra, and D. Barceló
Vol. 18, 2012

Polyfluorinated Chemicals and Transformation Products
Volume Editors: T.P. Knepper and F.T. Lange
Vol. 17, 2012

Brominated Flame Retardants
Volume Editors: E. Eljarrat and D. Barceló
Vol. 16, 2011

Effect-Directed Analysis of Complex Environmental Contamination
Volume Editor: W. Brack
Vol. 15, 2011

Waste Water Treatment and Reuse in the Mediterranean Region
Volume Editors: D. Barceló and M. Petrovic
Vol. 14, 2011

The Ebro River Basin
Volume Editors: D. Barceló and M. Petrovic
Vol. 13, 2011

Polymers – Opportunities and Risks II: Sustainability, Product Design and Processing
Volume Editors: P. Eyerer, M. Weller, and C. Hübner
Vol. 12, 2010

Polymers – Opportunities and Risks I: General and Environmental Aspects
Volume Editor: P. Eyerer
Vol. 11, 2010

Chlorinated Paraffins
Volume Editor: J. de Boer
Vol. 10, 2010

Biodegradation of Azo Dyes
Volume Editor: H. Atacag Erkurt
Vol. 9, 2010

Water Scarcity in the Mediterranean: Perspectives Under Global Change
Volume Editors: S. Sabater and D. Barceló
Vol. 8, 2010

The Aral Sea Environment
Volume Editors: A.G. Kostianoy and A.N. Kosarev
Vol. 7, 2010

Alpine Waters
Volume Editor: U. Bundi
Vol. 6, 2010

Transformation Products of Synthetic Chemicals in the Environment
Volume Editor: A.B.A. Boxall
Vol. 2/P, 2009

Chemical Structure of Pelagic Redox Interfaces

Observation and Modeling

Volume Editor: Evgeniy V. Yakushev

With contributions by

Ch. Anagnostou · G. Assimakopoulou · A.L. Bryukhanov · V.K. Chasovnikov · J. Chatzianestis · M.V. Chelysheva · E.I. Debolskaya · Y. He · G. Jost · A. Kamyshny · H. Kontoyiannis · V.A. Korneeva · A.V. Kostyleva · E. Krasakopoulou · I.S. Kuznetsov · A. Newton · K. Pagou · S. Pakhomova · A. Pavlidou · N.V. Pimenov · O.I. Podymov · F. Pollehne · R. Psyllidou-Giouranovits · I.I. Rusanov · O.P. Savchuk · P.A. Sigalevich · I. Siokou–Frangou · A. Staalstrøm · E. Stanev · J. Staneva · E.L. Vinogradova · E.V. Yakushev · E.E. Zakharova · Ch. Zeri · S. Zervoudaki

Springer

Editor
Prof. Evgeniy V. Yakushev
Norwegian Institute for Water Research
Oslo, Norway

The Handbook of Environmental Chemistry
ISSN 1867-979X ISSN 1616-864X (electronic)
ISBN 978-3-642-32124-5 ISBN 978-3-642-32125-2 (eBook)
DOI 10.1007/978-3-642-32125-2
Springer Heidelberg New York Dordrecht London

Library of Congress Control Number: 2012947653

Printed on acid-free paper

Springer is part of Springer Science+Business Media (www.springer.com)

To Igor I. Volkov and Tamerlan A. Ayzatullin

Editors-in-Chief

Prof. Dr. Damià Barceló

Department of Environmental Chemistry
IDAEA-CSIC
C/Jordi Girona 18–26
08034 Barcelona, Spain
and
Catalan Institute for Water Research (ICRA)
H20 Building
Scientific and Technological Park of the
University of Girona
Emili Grahit, 101
17003 Girona, Spain
dbcqam@cid.csic.es

Prof. Dr. Andrey G. Kostianoy

P.P. Shirshov Institute of Oceanology
Russian Academy of Sciences
36, Nakhimovsky Pr.
117997 Moscow, Russia
kostianoy@gmail.com

Advisory Board

The Handbook of Environmental Chemistry Also Available Electronically

The Handbook of Environmental Chemistry is included in Springer's eBook package *Earth and Environmental Science*. If a library does not opt for the whole package, the book series may be bought on a subscription basis.

For all customers who have a standing order to the print version of *The Handbook of Environmental Chemistry,* we offer free access to the electronic volumes of the Series published in the current year via SpringerLink. If you do not have access, you can still view the table of contents of each volume and the abstract of each article on SpringerLink (www.springerlink.com/content/110354/).

You will find information about the

– Editorial Board
– Aims and Scope
– Instructions for Authors
– Sample Contribution

at springer.com (www.springer.com/series/698).

All figures submitted in color are published in full color in the electronic version on SpringerLink.

Aims and Scope

Since 1980, *The Handbook of Environmental Chemistry* has provided sound and solid knowledge about environmental topics from a chemical perspective. Presenting a wide spectrum of viewpoints and approaches, the series now covers topics such as local and global changes of natural environment and climate; anthropogenic impact on the environment; water, air and soil pollution; remediation and waste characterization; environmental contaminants; biogeochemistry; geoecology; chemical reactions and processes; chemical and biological transformations as well as physical transport of chemicals in the environment; or environmental modeling. A particular focus of the series lies on methodological advances in environmental analytical chemistry.

Series Preface

With remarkable vision, Prof. Otto Hutzinger initiated *The Handbook of Environmental Chemistry* in 1980 and became the founding Editor-in-Chief. At that time, environmental chemistry was an emerging field, aiming at a complete description of the Earth's environment, encompassing the physical, chemical, biological, and geological transformations of chemical substances occurring on a local as well as a global scale. Environmental chemistry was intended to provide an account of the impact of man's activities on the natural environment by describing observed changes.

While a considerable amount of knowledge has been accumulated over the last three decades, as reflected in the more than 70 volumes of *The Handbook of Environmental Chemistry,* there are still many scientific and policy challenges ahead due to the complexity and interdisciplinary nature of the field. The series will therefore continue to provide compilations of current knowledge. Contributions are written by leading experts with practical experience in their fields. *The Handbook of Environmental Chemistry* grows with the increases in our scientific understanding, and provides a valuable source not only for scientists but also for environmental managers and decision-makers. Today, the series covers a broad range of environmental topics from a chemical perspective, including methodological advances in environmental analytical chemistry.

In recent years, there has been a growing tendency to include subject matter of societal relevance in the broad view of environmental chemistry. Topics include life cycle analysis, environmental management, sustainable development, and socio-economic, legal and even political problems, among others. While these topics are of great importance for the development and acceptance of *The Handbook of Environmental Chemistry,* the publisher and Editors-in-Chief have decided to keep the handbook essentially a source of information on "hard sciences" with a particular emphasis on chemistry, but also covering biology, geology, hydrology and engineering as applied to environmental sciences.

The volumes of the series are written at an advanced level, addressing the needs of both researchers and graduate students, as well as of people outside the field of "pure" chemistry, including those in industry, business, government, research establishments, and public interest groups. It would be very satisfying to see these volumes used as a basis for graduate courses in environmental chemistry. With its high standards of scientific quality and clarity, *The Handbook of*

Environmental Chemistry provides a solid basis from which scientists can share their knowledge on the different aspects of environmental problems, presenting a wide spectrum of viewpoints and approaches.

The Handbook of Environmental Chemistry is available both in print and online via www.springerlink.com/content/110354/. Articles are published online as soon as they have been approved for publication. Authors, Volume Editors and Editors-in-Chief are rewarded by the broad acceptance of *The Handbook of Environmental Chemistry* by the scientific community, from whom suggestions for new topics to the Editors-in-Chief are always very welcome.

Damià Barceló
Andrey G. Kostianoy
Editors-in-Chief

Contents

Introduction: Redox Interfaces in Marine Waters

E.V. Yakushev and A. Newton

Abstract The typical features of the structure of the redox layers in a marine water column are described. The oxic, hypoxic, suboxic and anoxic layers are discussed with respect to the definitions of terms. A classification of the redox conditions is proposed based on processes typical of the redox conditions appearing during the different stages of oxygen depletion.

Oxygen depletion events are connected with anthropogenic forcing such as eutrophication. However, climatic forcing may further stimulate the formation of oxygen-depleted zones. The redox interfaces and oxygen depletion events studies will therefore require an interdisciplinary approach, which the present book reflects.

Keywords Baltic Sea, Black Sea, Oslo fjord, Redox zone

Contents

E.V. Yakushev (✉)
Norwegian Institute for Water Research, Oslo, Norway

Shirshov Institute of Oceanology RAS, Gelendzhik, Russia
e-mail: eya@niva.no

A. Newton
Norwegian Institute for Air Research, Kjeller, Norway

IMAR-FCT, Universidade do Algarve, Campus de Gambelas, 8005-139 Faro, Portugal

E.V. Yakushev (ed.), *Chemical Structure of Pelagic Redox Interfaces: Observation and Modeling*, Hdb Env Chem (2013) 22: 1–12, DOI 10.1007/698_2012_167,

Abbreviations

DO Dissolved oxygen
OM Organic matter

1 Preface

During the last decades, many studies have focused on the oxygen depletion of coastal and oceanic waters in the context of the series of projects and programmes, i.e. INCO-Copernicus, NATO, FP6 and FP7 programmes Bonus, HYPOX and SESAME. The results obtained have been published in numerous articles and monographs, many of which are listed in the reference section. This new book is well timed and urgent. It presents the "state of the art" of our knowledge and understanding of the nature of redox interfaces, structures and oxygen depletion. It synthesises the joint response of the global scientific community to the challenge of global changes in the "oxygen condition" of marine waters, new developments in observation techniques, such as the introduction of new analytical methods, and the analysis of data to identify thresholds of change using new models. Nevertheless, there are still gaps in our knowledge about the cycling of chemical elements in changing redox conditions. An understanding of the processes involved is fundamental to assess the impacts and effects of global and climatic changes and to enable an ecosystem approach of adaptive environmental management for the coastal seas and ocean basins.

2 Occurrence and Hydrophysical Structure

The occurrence of oxygen-depleted and anoxic water depends on the combined influence of eutrophication (organic matter and nutrient loads) and hydrodynamics (intensity of mixing and water renewal). Oxygen depletion zones form when there is an imbalance between the supply of organic matter (OM) and the supply of dissolved oxygen (DO) for its decomposition. This may occur when a hydrophysical structure, such as temperature stratification, restricts the aeration of the water column. The existence of low-oxygen structures can be temporary or permanent, correspondingly creating zones of temporary or permanent hypoxia and anoxia.

Oxygen depletion and anoxia in the water column are increasingly common features observed in the World Ocean, inland seas and coastal areas. Observations show a decline in the dissolved oxygen concentrations at continental margins in many regions, and these are related to both an increase in anthropogenic nutrient loadings and a decrease in vertical mixing (e.g. [1–3]). Observations of decreases in oxygen are also reported in the tropical oceans [4–9]. Low-oxygen "dead zones" have spread exponentially since the 1960s [1]. The decrease in DO throughout the

open ocean basins may be a long-term, nonperiodic trend related to climate change, or the result of natural cyclical processes, or a combination of both [6]. Within the marine science community, there is increasing interest to these events in recent years because of their global character.

The scales of processes that affect the formation of each system's hydrophysical structure vary from molecular diffusion to climatic variability. However, in lakes and fjords, some processes, such as transport of water with geostrophic currents or mesoscale eddies, are unimportant, leading to less intense mixing than under marine conditions. Therefore, the chemical structure of redox interfaces in fjords and lakes is characterised by sudden changes in redox conditions and steep chemical gradients. In comparison to lakes and fjords, oxidation–reduction features at marine redox interfaces are characterised by gradual gradients, and gradually varying temporal changes as well. For example, the boundary of anoxic zone of the Cariaco Basin is influenced by mesoscale eddies that periodically supply dense water with high oxygen content to the anoxic zone [10]. In the Baltic Sea, under certain winter weather conditions in particular years, there is an influx of oxygen-rich saline northern Sea waters to the deep anoxic layers [11, 12]. The Black sea oxic/anoxic interface appears to be more stable, because the Bosphorus plume waters influence only the south-western part of the Black Sea. The central and peripheral Black Sea are characterised by the stability of the chemical features (i.e. maximum positions, onset levels) in the density field [13, 14]. Such a *chemotropicity* implies that there are no horizontal gradients of chemical variables along the same density surface, supporting the use of a 1D model for describing the processes responsible for the maintenance of the redox-layer chemical structure.

3 Global Distribution

Permanent anoxic conditions are observed in numerous lakes, lagoons, fjords, seas and also in some regions of the World Ocean. They include examples of very different systems under the simultaneous influence of saline and brackish waters and suffering from restricted ventilation [15]. The most notable and stable example is in the Black Sea [16, 17]. Other examples include the Cariaco Trench of Venezuela [10, 18], the Gotland Deep of the Baltic Sea [19, 20], Drammensfjord [21], Framvaren [22], Hemmelsdorfer See [23], Gulf of Mexico [2], coastal salt ponds along the US coast [24], Saanich Inlet (Vancouver Island) [25], Elefsis Bay [26] and meromictic lakes in the Vestfold Hills in Antarctica (e.g. [27]).

4 Effects on Chemistry, Biochemistry and Ecosystem Function

The redox interface is a layer where oxic and anoxic conditions are adjacent. It is very complex because of the many chemical reactions and biogeochemical mineralisation processes that can be oxic, suboxic and anoxic. The decline in DO

concentration therefore affects the biogeochemical cycles of N, P, S, as well as the carbonate system and trace metals equilibria. Water layers that are already depleted with respect to DO may be close to the threshold between suboxic and anoxic conditions and are the water bodies most vulnerable to the effects of the globally observed deoxygenation trend [28]. It is necessary to better understand the physical processes leading to anoxia, the biogeochemical structure of the oxic/anoxic interfaces and the ecological consequences of oxygen depletion in order to predict the possible effect of global changes in oxygen conditions.

Oxygen depletion significantly affects the water quality and ecosystem function. Absence of oxygen impairs the oxic ecosystem both directly and indirectly. Increased occurrence and volumes of anoxic water threaten the functioning of healthy aerobic ecosystems and thereby have a direct impact to human welfare and ecosystem services. There can be an additional, indirect impact at the water–sediment interface, where redox equilibria control the rate of supply of phosphorus from the sediments and the release of hazardous substances, e.g. methyl mercury.

There is a normal sequence or succession of processes during the transition from oxic to anoxic. The bacterial decomposition of organic matter is an oxidative process. If there is an excess of organic material to be decomposed once the DO has been used, bacterial activity will substitute the DO with a series of other electron acceptors that usually ends with reduction of sulphate, a major constituent in seawater. This last process produces hydrogen sulphide, which is toxic to aerobic life forms. Conversely, the oxidation of reduced inorganic compounds in the anoxic zone also fuels the microbial production of OM via chemosynthesis [17, 29, 30]. It is necessary to emphasise that the synthesis of organic matter happens in all the oxygen conditions via photosynthesis (oxic and anoxygenic) or chemosynthesis.

5 Terminology, Definitions, Boundaries and Thresholds

The oxygen condition of natural waters is an important element of water quality legislation, e.g. in the Water Framework Directive (EC 2000). However, there are several terms that are in use to describe the changes in oxygen condition, i.e. *oxic*, *oxygen-deficient*, *hypoxic*, *suboxic*, *anoxic*, but these are not be precisely defined. The terms reflect different DO conditions and the associated processes. For example, the term "oxygen-deficient" is widely used for a wide range of low oxygen concentrations, from below 80% saturation to suboxic levels. Nevertheless, the boundaries in terms of oxygen concentrations are rather arbitrary, and therefore, there are several problems to the currently used definitions. Biochemical thresholds provide less arbitrary boundaries.

A frequently used boundary between *oxic* and *hypoxic* conditions is set at 2 mg O_2 L^{-1} (~63 μM O_2 i.e. [31]) or 2 ml O_2 L^{-1} (~89 μM O_2 i.e. [1, 32]). The threshold of tolerance, stress responses and morbidity of pelagic and benthic

animals is usually in the range of 1–4 mg O_2 L^{-1} (e.g. [32–34]), which corresponds to a threshold molar concentrations of ~75 μM O_2.

The boundary between *hypoxic* and *suboxic* conditions is also arbitrary, and there has been opposition to the use of the term "suboxic" once oxygen is no longer present [35]. In the Black Sea, for example, the reported suboxic values range from 4.5 μM O_2 [36] to 15 μM O_2 [37]. A value of 10 μM [13] is often used, which corresponds to the water layers with enhanced nitrification due to an upward flux of ammonia [28]. However, this boundary should correspond to the biochemical threshold after which the dominant electron acceptors are oxidised ions of N (nitrate, nitrite) or oxidised species of metals [Mn(IV), Fe(III)], whereas DO becomes an auxiliary oxidant.

The *suboxic* layer may be further divided into "suboxidised" layer, where DO is present, and "subreduced" layer, where DO is absent [38]. The *suboxidised* layer is therefore a layer where DO is present with a threshold molar concentration of ~15 μM O_2 as an "upper" boundary. The *subreduced* layer, where there is no longer any DO but H_2S is not yet present, should correspond to the conditions necessary for the onset of processes such as anammox [39] or formation of Mn(III) [40], that are inhibited by both oxygen and hydrogen sulphide.

Once the oxidised species of nitrogen, manganese or iron and DO is completely depleted, OM microbial decomposition uses sulphate as the next electron acceptor for oxidation. This is the appropriate threshold for the term *anoxic*.

The main biogeochemical processes change in intensity dependent on the oxygen conditions as summarised in Table 1. A schematic of the corresponding layers and different redox conditions with respect to the distributions of DO, H_2S, speciation of Mn and N is shown in Fig. 1.

6 The Redox Layers in a Marine Water Column

The transition layer between the oxic and anoxic conditions in the water column is often called "redoxcline" or "redox layer". The redox boundaries in the water column are established and controlled by two opposite fluxes: the upward flux of reduced chemical species and the downward flux of oxidised chemical species. The redox layer covers the layer of transformation from the oxic conditions to anoxic. A nitrate maximum can be taken as the upper boundary of the redox layer. This corresponds to σ_θ ~ 15.3 kg m^{-3} for the Black Sea [41]. The lower boundary of this layer corresponds to the disappearance of oxidised manganese species, σ_θ ~ 16.15 kg m^{-3} for the Black Sea.

In the stratified water bodies, these counter fluxes generate a wide range of redox potentials within narrow zones in the water [42]. The biogeochemical processes occur in a predictable sequence according to their redox potential (i.e. [13]) and the products of these reactions appear in the water according to the laws of thermodynamics. The vertical distributions of the chemical compounds result from the

Table 1 Basic biogeochemical processes and corresponding oxygen condition

Oxygen conditions	Oxic	Hypoxic	Suboxic		Anoxic
			Suboxidised	Subreduced	
DO concentration	>75 μM	15–75 μM	0–15 μM	0 μM	
H_2S concentration					>0 μM
Oxic mineralisation of OM and nitrification	+	+			
Oxidation with DO of reduced species of S, Mn, Fe, C, N		+	+		
Denitrification and mineralisation of OM with metals			+	+	
Anammox, accumulation of Mn(III)				+	
Reduction of oxidised species of S, Mn, Fe, C				+	+
Sulphate reduction, methanogenesis					+
Increased mortality		+	+	+	+
Synthesis of OM	+	+	+	+	+

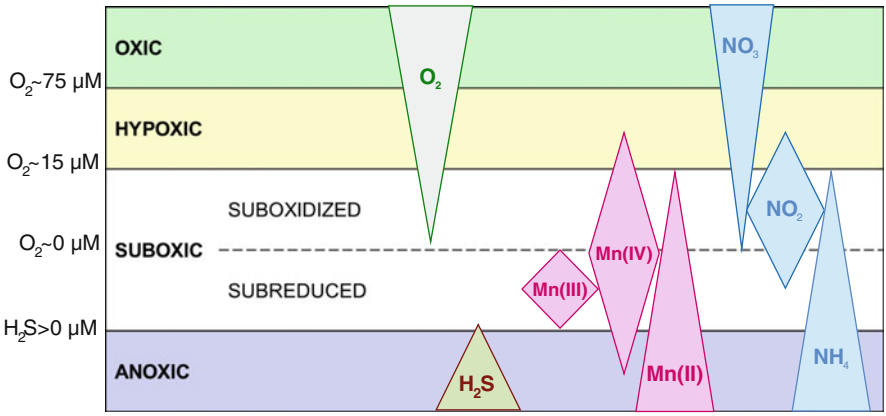

Fig. 1 A redox framework for the structure of the oxygen condition of a water column with respect to the distributions of DO, H_2S and indicative speciation of Mn and N

reactions that can occur in narrow layers, i.e. 2–5 m in the Black Sea [43] and several dm in the fjords.

There are common features of the water column redox interfaces for the different marine basins [44]. These characteristics are:

- A nitrate maximum is observed at the depth where the vertical gradient of oxygen decreases (lower part of oxycline).
- Onset depths of concentrations of ammonia and dissolved manganese correspond to oxygen depletion and the position of the "shallow" phosphate minimums.
- Hydrogen sulphide appears in deeper waters, about 10 m in the Black Sea.

Organic matter is the main reducing agent in the redox zone [45]. It is a product of photosynthesis and is transported downwards from the euphotic zone. Organic matter is also generated in the redox zone by chemosynthesis. Organic matter serves as a carbon source for the reduction of DO and thereafter, nitrate, nitrite, Mn oxide, Fe oxide and sulphate.

The biogeochemical structure of the water column redox layer is characterised by an absence of overlap between dissolved oxygen and hydrogen sulphide [13, 46–48]. Reduced and oxidised forms of several elements (N, S, C, Mn, Fe) can be observed in the redox layer, which reflects the complexity of the chemical processes. The role of the biogeochemical cycles of the different elements in the formation and support of the redox-layer structure is still not clear.

Oxygen disappears at a depth where the onset of ammonia and dissolved manganese is observed, while hydrogen sulphide appears deeper (approximately 5–10 m in the Black Sea).

The depth at which H_2S is first observed also depends on the equilibrium between the transport of electron acceptors and organic matter (e.g. [28, 49, 50]).

The suboxic (subreduced) zone phenomenon where both oxygen and hydrogen sulphide are absent [13] is not clearly understood. It may be due to the peculiarities of the manganese cycle: the formation of a significant amounts of the particulate Mn(IV) that can precipitate from the depth at which it is formed due to the reaction between oxygen and dissolved Mn(II) [51, 52]. Mn(III) has been observed in the marine environment [40]. It is an important intermediate product of the Mn cycle that could be formed both by Mn(II) oxidation [53] and by Mn(IV) reduction [54, 55]. This dissolved, oxidised Mn(III) could explain the distribution of other elements at redox interfaces, such as phosphate. Mn(III) permits the formation of P-containing complexes [53]. Studies of this oxidised and dissolved species of Mn are recent (Luther, p.c. [56]). This species was not represented in previous suboxic zone models that seek to describe the flow of primary nutrients such as nitrogen, phosphate and carbon as well as heavy metals through the oxic/anoxic boundary.

7 Modelling

The study of the processes responsible for the maintenance of redox interfaces should combine field observations and experimental measurements. These should be supplemented by modelling to allow a joint analysis of the complex processes studied by the different scientific disciplines. Models are oversimplifications of real system, sometimes overemphasising particular characteristics, as in a caricature. Nevertheless, modelling seems to be appropriate for use as a diagnostic tool. Models can be used to test the hypothesis of which processes are responsible for the observed distributions. Thus, modelling and observations mutually complement each other.

Nutrient cycling in the oxic conditions can be described for individual elements, and it is possible to use the Redfield ratios to estimate the other

elements changes. However, the modelling of oxic/anoxic transformation requires the parameterisation of cycles of several elements simultaneously [52, 57].

In contrast to modelling in the typical oceanic and marine waters oxic conditions, the modelling of the oxic/anoxic transformation cannot only give numerical estimates but can reveal the mechanisms of the main processes occurring. This is particularly useful because there are still many knowledge gaps. The main goal of oxic/anoxic modelling is therefore to use the knowledge of events, processes and systems to analyse and understand the observed situation and distribution of observed chemical species.

The choice of list of variables and complexity of a model should depend on the time and space scale of the studying event. Nevertheless, the model should at least parameterise all those listed in Table 1 processes. The model should also establish the thresholds that provide the boundaries or "switches" between the different redox processes.

8 Structure of the Monograph

This monograph is characterised by the following features. First of all, it is multidisciplinary since it deals with the principal processes that form the physical, biogeochemical and biological structures of the redox interfaces. Secondly, it assesses the issues connected with predicting the development interannual oxygen depletion and mathematical modelling.

The book consists of 11 chapters, which may be conventionally joined into the sections devoted to the general features of the redox-layer biogeochemical and microbiological structure (3 chapters), cycling of selected elements (2 chapters), interannual estimates (3 chapters) and modelling (3 chapters).

Thus, this book presents a description of the knowledge accumulated to date (2012) on pelagic redox interfaces. Nevertheless, it is not a collection of individual papers but rather a monograph written by a team of scientists joined by a common understanding of the complicated phenomena and processes that are connected with the redox-interfaces structure formation and oxygen depletion development. The publication is based on numerous observational data, collected by the authors of the chapters during sea and shore expeditions, on the archive data of P.P. Shirshov Institute of Oceanology RAS, Winogradsky Institute of Microbiology, Water Problems Institute RAS, Faculty of Biology, Lomonosov Moscow State University (Russia), Norwegian Institute for Water Research (Norway), Leibniz Institute for Baltic Sea Research, Warnemuende, Helmholtz-Zentrum Geesthacht, Max Planck Institute for Marine Microbiology (Germany), Hellenic Centre for Marine Research, Institute of Oceanography (Greece), Baltic Nest Institute, Stockholm University (Sweden) and others, as well as on a wide scientific literature. These data are complemented by the results of a series of national and international projects listed below, where an extensive research was carried out over the past decades.

This book is addressed to the specialists working in various fields of physical oceanography, marine chemistry, pollution studies and biology and studying a cascade of problems from regional climate to mesoscale processes and from remote sensing of the sea to numerical and laboratory modelling. It may also be useful to the students and postgraduates specialising in the oceanographic research of the seas. The editors and authors expect that this monograph would help the readers to complement the information on the nature of the oxygen depletion and the redox interfaces phenomena. More information on special issues may be derived using the reference lists contained in each chapter.

The studies of the authors of this book were supported by FP7 project HYPOX (No. EC Grant 226213), SESAME, Norwegian Research Council grant 211227/F11, Russian Foundation for Basic Research grants 10-05-00653, 10-04-00220, Russian World Ocean Federal Research Programme (project 7), the "World Ocean", CRDF Grant (RUG1-2828-KS-06), Max Planck Society, Norwegian Institute for Water Research project 29083 and institutional funding of the IOW.

On behalf of the authors, we would like to thank Springer-Verlag Publishers for the timely interest in the topic and the support of the publication presented.

In the final stage of the chapter's preparation, the discussions with colleagues Jens Skei and Violeta Velikova were all of enormous importance.

Finally, we would like to express our deep appreciation to colleagues and the administrations at the Shirshov Institute of Oceanology RAS (in Gelendzhik and Moscow), at the Norwegian Institute for Water Research (NIVA) for their patience and understanding for the time spent working on this book.

References

1. Diaz R, Rosenberg R (2008) Spreading dead zones and consequences for marine ecosystems. Science 321:926–929
2. Rabalais NN, Turner RE, Weisman WJ Jr (2002) Gulf of Mexico hypoxia a.k.a. "The dead zone". Annu Rev Ecol Syst 33:235–263
3. Richardson K, Jørgensen BB (1996) Eutrophication: definition, history and effects. In: Jorgenson BB, Richardson K (eds) Eutrophication in coastal marine ecosystems. Coastal and Estuarine studies, vol 52. AGU, Washington, pp 1–19
4. Deutsch C, Brix H, Ito T, Frenzel H, Thompson L (2011) Climate-forced variability of ocean hypoxia. Science 333(6040):336–339
5. Emerson S, Watanabe YW, Ono T, Mecking S (2004) Temporal trends in apparent oxygen utilization in the upper pycnocline of the North Pacific: 1980–2000. J Oceanogr 60:139–147
6. Falkowski PG, Algeo T, Codispoti L, Deutsch C, Emerson S, Hales B, Huey RB, Jenkins WJ, Kump LR, Levin LA, Lyons TW, Nelson NB, Schofield OS, Summons R, Talley LD, Thomas E, Whitney F, Pilcheret CB (2011) Ocean deoxygenation: past, present, and future. Eos Trans AGU 92(46):409–420
7. Keeling RE, Kortzinger A, Gruber N (2010) Ocean deoxygenation in a warming world. Annu Rev Mar Sci 2:199–229
8. Paulmier A, Ruiz-Pino D (2009) Oxygen minimum zones (OMZs) in the modern ocean. Prog Oceanogr 80:113–128

9. Whitney FA, Freeland HJ, Robert M (2007) Persistently declining oxygen levels in the interior waters of the eastern subarctic Pacific. Prog Oceanogr 75:179–199
10. Scranton MI, McIntyre M, Taylor GT, Muller-Karger F, Fanning K, Astor Y (2006) Temporal variability in the nutrient chemistry of the Cariaco Basin. In: Neretin LN (ed) Past and present water column anoxia, NATO Sci Ser. Springer, Amsterdam, pp 139–160
11. Feistel R, Nausch G, Wasmund N (eds) (2008) State and evolution of the Baltic Sea, 1952–2005. Wiley, New Jersey
12. Schneider B, Nausch G, Kubsch H, Peterson I (2002) Accumulation of total CO_2 during stagnation in the Baltic deep water and its relationship to nutrient and oxygen concentrations. Mar Chem 77:277–291
13. Murray JW, Codispoti LA, Friederich GE (1995) Oxidation–reduction environments. The suboxic zone in the Black Sea. In: Huang CP et al (eds) Aquatic chemistry: interfacial and interspecies processes. ACS Adv Chem Ser 244:157–176
14. Vinogradov ME, Nalbandov YR (1990) Oceanology 30:769
15. Ström TE, Klaveness D (2003) Hennebont: a seawater basin transformed by natural and anthropogenic processes. Estu Coast Shelf Sci 56(5–6):1177–1185
16. Andrusov NI (1890) Predvaritelnii otchyot ob uchastii v Chernomorskoi glubomernoi ekspiditsii 1890 g (preliminary report on participation in the 1890 Black Sea fathometer expedition). Izvestiya Russkogo Geograficheskogo Obschestva (Proc Russ Geogr Soc) 26 (5):398–409 (in Russian)
17. Sorokin Yu I (2002) The Black Sea. Ecology and oceanography. Backhuys Publishers, Leiden, p 875
18. Deuser WG (1973) Cariaco trench: oxidation of organic matter and residence time of anoxic water. Nature 242:601–603
19. Fonselius S (1981) Oxygen and hydrogen sulphide conditions in the Baltic Sea. Mar Pollut Bull 12:187–194
20. Kautsky L, Kautsky N (2000) The Baltic Sea, including Bothnian Sea and Bothnian Bay. In: Sheppard CRC (ed) Seas at the millennium: an environmental evaluation, vol 1, Regional seas: Europe, The Americas and West Africa. Elsevier Science Ltd./Pergamon Press, Oxford, pp 121–133
21. Richards FA (1965) Anoxic basins and fjords. In: Riley JP, Skirrow G (eds) Chemical oceanography. Academic, London, pp 611–645
22. Skei JM (1988) Framvaren – environmental setting. Mar Chem 23:209–218
23. Halbfass W (1923) Grundzüge einer vergleichenden Seenkunde. Borntraeger, Berlin, p 354
24. Conover RJ (1961) A study of Charlestown and Green Hill ponds, Rhode Island. Ecology 42:119–140
25. Grant Gross M, Gucluer SM, Creager JS, Dawson WA (1963) Varved marine sediments in a stagnant fjord. Science 141:918–919
26. Pavlidou A, Kontoyiannis H, Anagnostou Ch, Siokou-Frangou I, Pagou K, Krasakopoulou E, Assimakopoulou G, Zervoudaki S, Zeri Ch, Chatzianestis J, Psyllidou-Giouranovits R (2010) Biogeochemical Characteristics in the Elefsis Bay (Aegean Sea, Eastern Mediterranean) in Relation to Anoxia and Climate Changes. In: Yakushev EV (ed) Chemical structure of pelagic redox interfaces: observation and modelling. Springer, Heidelberg. Hdb Environ Chem. doi:10.1007/698_2010_55
27. Gallagher JB, Burton HR, Calf GE (1989) Meromixis in an Antarctic Fjord: a precursor to meromictic lakes on an isostatically rising coastline. Hydrobiologia 172:235–254
28. Jost G, Pollehne F (2011) The energetic balance of microbial exploitation of pelagic redox gradients. In: Yakushev EV (ed) Chemical structure of pelagic redox interfaces: observation and modelling. Springer, Heidelberg. Hdb Environ Chem. doi:10.1007/698_2011_104
29. Canfield DE, Thamdrup B, Kristensen E (2005) Aquatic geomicrobiology. In: Southward AJ, Tyler PA, Young CM, Fuiman LA (eds) Advances in marine biology, vol 48. Elsevier Academic Press, Amsterdam, p 640

30. Nealson KN, Stahl DA (1997) Microorganisms and biogeochemical cycles: what can we learn from layered microbial communities? In: Banfield JF, Nealson KN (eds) Reviews in mineralogy, vol 35, Geomicrobiology: interactions between microbes and minerals. Mineralogical Society of America, Washington, p 5
31. CENR (2000) Integrated assessment of hypoxia in the Northern Gulf of Mexico. National Science and Technology Council Committee on Environment and Natural Resources, Washington, 58 pp
32. Savchuk O (2010) Large-scale dynamics of hypoxia in the Baltic Sea. In: Yakushev EV (ed) Chemical structure of pelagic redox interfaces: observation and modelling. Springer, Heidelberg. Hdb Environ Chem. doi:10.1007/698_2010_53
33. Diaz RJ (2001) Overview of hypoxia around the world. J Environ Quality 30:275–281
34. Vaquer-Sunyer R, Duarte CM (2008) Thresholds of hypoxia for marine biodiversity. Proc Natl Acad Sci USA 105:15452–15457
35. Canfield DE, Thamdrup B (2009) Towards a consistent classification scheme for geochemical environments, or, why we wish the term "suboxic" would go away. Geobiology 7:385–392
36. Lam P, Jensen MM, Lavik G et al (2007) Linking crenarchaeal and bacterial nitrification to anammox in the Black Sea. Proc Natl Acad Sci USA 104:7104–7109
37. Zubkov MV, Sazhin AF, Flint MV (1992) The microplankton organisms at the oxic-anoxic interface in the pelagial of the Black Sea. FEMS Microbiol Ecol 101:245–250
38. Stunzhas PA (2005) Application of continuous oxygen profiles to redox zone studies in a coastal anticyclonic eddy. Oceanology 45:S93–S101
39. Kuypers MMM, Sliekers AO, Lavik G, Schmid M, Jorgensen BB, Kuenen JG, Sinnenghe Damste JS, Strous M, Jetten MSM (2003) Anaerobic ammonium oxidation by anammox bacteria in the Black Sea. Nature 422:608–611
40. Trouwborst RE, Brian GC, Tebo BM, Glazer BT, Luther GW III (2006) Soluble Mn(III) in suboxic zones. Science 313:1955–1957
41. Yakushev EV, Lukashev YuF, Chasovnikov VK, Chzhu VP (2002) Modern notion of the vertical hydrochemical structure of the Black Sea redox zone. In: Zatsepin AG, Flint MV (eds) Complex investigation of the Northeastern Black Sea. Nauka, Moscow, pp 119–132 (in Russian)
42. Lewis BL, Landing WM (1991) The biochemistry of manganese and iron in the Black Sea. Deep-Sea Res II 38:S773–S803
43. Volkov II, Kontar EA, Lukashev Yu F, Neretin LN, Niffeler F, Rozanov AG (1997) The upper boundary of hydrogen sulfide and redox nefeloid layer in water of the Caucasian slope in the Black sea. Geochemistry 7:540–550
44. Yakushev EV, Chasovnikov VK, Murray JW, Pakhomova SV, Podymov OI, Stunzhas PA (2008) Vertical hydrochemical structure of the Black Sea. In: Kostyanoy AG, Kosarev AN (eds) The handbook of environmental chemistry, vol 5, The Black Sea environment. Springer, Heidelberg, pp 277–307
45. Rosanov AG (1995) Redox stratification of the Black Sea water. Oceanology 35:544
46. Konovalov SK, Tugrul S, Basturk O, Salihoglu I (1997) Spatial isopycnal analysis of the main pycnocline chemistry of the Black Sea: seasonal and interannual variations. In: Ozsoy E, Mikaelyan A (eds) Sensitivity to change: Black Sea, Baltic Sea and North Sea, NATO ASI, 2/27. Kluwer Academic Publishes, Dordrecht, pp 197–210
47. Lukashev YuF, Yakushev EV (1999) Dissolved oxygen content measurements on the border of the sulfide zone of the Black Sea . In: PACON-99 symposium, abstracts, Russian Academy of Sciences, Moscow, 23–25 June 1999,167 pp
48. Stunzhas PA (2000) On the structure of the interaction zone of aerobic and anaerobic water in the Black Sea on the base of measurements by membrane-free oxygen sensor. Oceanology 40:503–509
49. Grote J, Labrenz M, Pfeiffer B et al (2007) Quantitative distributions of *Epsilonproteobacteria* and a *Sulfurimonas* subgroup in pelagic redoxclines of the central Baltic Sea. Appl Environ Microbiol 73:7155–7161

50. Vetriani C, Tran HV, Kerkhof LJ (2003) Fingerprinting microbial assemblages from the oxic/anoxic chemocline of the black sea. Appl Environ Microbiol 69:6481–6488
51. Yakushev EV, Debolskaya EI (2000) Particulate manganese as a main factor of oxidation of hydrogen sulfide in redox zone of the Black Sea. In: Oceanic fronts and related phenomena. Konstantin Fedorov Memorial Symposium. Pushkin, Saint-Petersburg. 18–22 May 1998. Proceedings. IOC Workshop Report No. 159. Kluwer Academic Publisher, pp 592–597
52. Yakushev EV, Pollehne F, Jost G, Umlauf L, Kuznetsov I, Schneider B (2007) Analysis of the water column oxic/anoxic interface in the Black and Baltic seas with a redox-layer model. Mar Chem 107:388–410
53. Webb SM, Dick GJ, Bargar JR, Tebo BM (2005) Evidence for the presence of Mn(III) intermediates in the bacterial oxidation of Mn(II). Proc Natl Acad Sci USA 102:5558–5563
54. Ali K, Ashiq U (2004) Study of the kinetics and activation parameters of reduction of Mn(III) to Mn(II) by SO_3^{2-} ion in $(MnSiW_{11}O_{40}H_2)_{5-}$ heteropoly ion. J Iran Chem Soc 1:122–127
55. Kostka JE, Luther GW III, Nealson KH (1995) Chemical and biological reduction of Mn(III)-pyrophosphate complexes: potential importance of dissolved Mn(III) as an environmental oxidant. Geochim Cosmochim Acta 59:885–894
56. Pakhomova SV, YakushevEV (2011) On the role of iron and manganese species in the formation of the redox-interface structure in the Black Sea, Baltic Sea and Oslo Fjord. In: Yakushev EV (ed) Chemical structure of pelagic redox interfaces: observation and modelling. Springer, Heidelberg. Hdb Environ Chem. doi:10.1007/698_2011_98
57. Yakushev EV (2012) Redox layer model: a tool for analysis of the water column oxic/anoxic interface processes. In: Yakushev EV (ed) Chemical structure of pelagic redox interfaces: observation and modelling. Hdb Environ Chem. doi:10.1007/698_2012_145

Biogeochemical Peculiarities of the Vertical Distributions of Nutrients in the Black Sea

M.V. Chelysheva, E.V. Yakushev, E.L. Vinogradova, and V.K. Chasovnikov

Abstract Analysis of the vertical distributions of the ratios between C, S, Si, N, and P revealed the layers with significant systematic differences from the theoretical Redfield and Richards values. These anomalies can testify to the presence of such processes as denitrification/anammox and the processes of the "phosphate dipole" formation. Based on the ratios to Si, which concentrations do not change under the redox conditions variability, we estimated numerically the other elements deficiencies and the rates of the processes that form these deficiencies. The calculated rates of denitrification/anammox (0.012–0.046 μM per day) correspond well to the present observations data. The calculated possible rates of the processes controlling the shallower phosphate minimum formation equal to 0.008–0.032 μM per day, and the rates of the deeper phosphate minimum formation are in the range of 0.006–0.024 μM per day. The C_t/S_t ratio showed that bacterial sulfate reduction was the only significant process in the anaerobic mineralization of organic matter in the anoxic zone of the Black Sea that lead to a constant stoichiometric C/S ratio close to the theoretical one of 2.

Keywords Black Sea, Hydrogen sulfide, Nutrients, Redfield ratio, Redox layer, Richards ratio

M.V. Chelysheva and E.L. Vinogradova
P.P. Shirshov Institute of Oceanology, RAS, Moscow, Russia

E.V. Yakushev (✉)
Norwegian Institute for Water Research, Gaustadalleen 21, 0349 Oslo, Norway

Southern Branch of P.P. Shirshov Institute of Oceanology, Russian Academy of Sciences, Okeanologiya, Gelendzhik-7, 353470 Krasnodarsky Kray, Russia
e-mail: e_yakushev@yahoo.com

V.K. Chasovnikov
Southern Branch of P.P. Shirshov Institute of Oceanology, Russian Academy of Sciences, Okeanologiya, Gelendzhik-7, 353470 Krasnodarsky Kray, Russia

E.V. Yakushev (ed.), *Chemical Structure of Pelagic Redox Interfaces: Observation and Modeling*, Hdb Env Chem (2013) 22: 13–26, DOI 10.1007/698_2011_119,

Contents

1 Introduction

The Black Sea is the largest meromictic basin in the world. The presence of oxic layer in the upper 100–200 m, anoxic layer from 100 to 200 m to the bottom (2,000–2,200 m), and redox boundary layer between them affects the vertical hydrochemical structure and, in particular, the distributions of nutrients and of the carbonate system parameters. A characteristic feature of the Black Sea redox layer is that certain redox reactions occur in very narrow layers (2–5 m) of a constant water density. That leads to the correspondence of vertical chemical distributions to specific density levels [1–4]. For instance, the nitrate maximum is located at the density level of $\sigma_\theta \approx 15.50$ kg m^{-3}; ammonia increases initially at $\sigma_\theta \approx 16.05$ kg m^{-3}; phosphate minimum and maximum are located at $\sigma_\theta \approx 15.90$ kg m^{-3} and $\sigma_\theta \approx 16.15$ kg m^{-3}, respectively. Calculated on the basis of averaged observations data, typical nutrients distribution versus density in the Black Sea is presented in Fig. 1. The existing relationship between the vertical distributions of hydrochemical

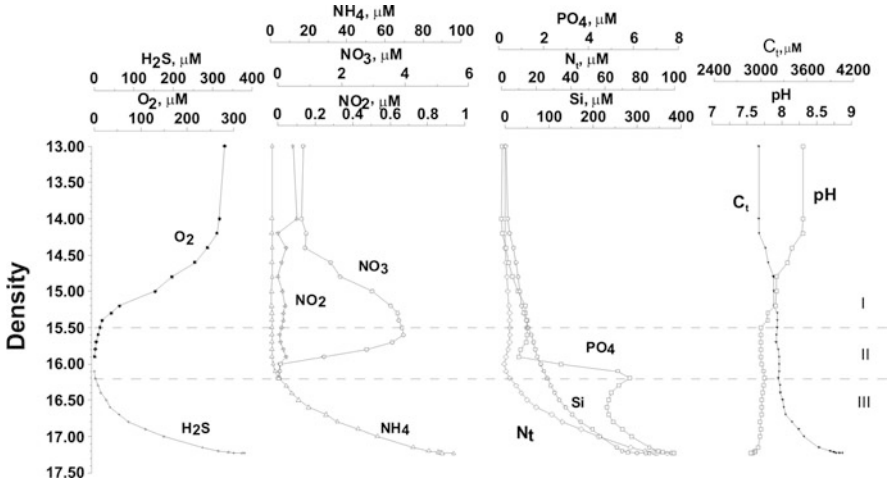

Fig. 1 Vertical distribution of nutrients, dissolved oxygen, hydrogen sulfide, pH, and salinity in the Black Sea versus density, based on data of observations during cruises R/V Akvanavt in 1997–2006 (averaged of isopycns using VERTA programme [32]: *I*, oxygen layer; *II*, redox layer; *III*, hydrogen sulfide layer

parameters and the water density simplifies the hydrochemical structure general features all over the Black Sea with the exception of the Bosporus Strait area.

As mentioned above, the vertical Black Sea structure can be divided into three layers: oxic layer, redox layer, and hydrogen sulfide layer. The mineralization of organic matter (OM) under aerobic conditions follows the classical Redfield [5] reaction (1):

$$(CH_2O)_{106}(NH_3)_{16}H_3PO_4 + 138O_2 \rightarrow 106CO_2 + 122H_2O + 16HNO_3 + H_3PO_4 \quad (1)$$

Hence, the mineralization of 1 mol of OM utilizes 276 oxygen atoms and releases 106 carbon atoms, 16 nitrogen atoms, and 1 phosphorus atom. In this model, 31 atoms of silicon should be added to reflect the diatoms presence which constitutes 77% of the World Ocean plankton [6–8]. Taking into account that the largest share of the Black Sea phytoplankton belongs to the diatoms [9] herewith the stoichiometric relationships between the nutrients can be assumed as O:C:Si:N:P = (−276):106:31:16:1.

The upper boundary of the redox layer can be detected by the depth of the nitrate maximum and the position of the oxycline. In the redox layer, extremes of oxidized, reduced, and intermediate forms of chemical elements (nitrate, nitrite, suspended manganese, thiosulfate, and elemental sulfur) can be found. At the lower boundary of the redox layer, where Eh values become negative, reduced compounds such as sulfide hydrogen, ammonia, and methane appear in the water. The mineralization of OM in the redox layer follows the Richards reaction [10], where nitrate is used for the OM mineralization:

$$(CH_2O)_{106}(NH_3)_{16}H_3PO_4 + 84.8NO_3^- + 100.8H^+ \rightarrow 106CO_2 + 16NH_3 + 42.4N_2 + H_3PO_4 + 148.4H_2O \quad (2)$$

In this case, the mineralization of OM leads to a release of inorganic carbon, silicate, nitrogen, and phosphorus in the ratio of C:Si:N:P = 106:31:(−84.8 + 16):1.

If anammox, a reaction between nitrite and ammonia [11, 12] is involved, then the mineralization of OM will follow (3):

$$(CH_2O)_{106}(NH_3)_{16}H_3PO_4 + 94.4HNO_3 \rightarrow 106CO_2 + 55.2N_2 + 177.2H_2O + H_3PO_4 \quad (3)$$

This kind of mineralization corresponds to a different stoichiometric relationship: C:Si:N:P = 106:31:(−94.4):1. But due to scarce data and poor understanding of the anammox mechanism and scale, we followed the first mechanism of OM mineralization for the calculations presented.

The mineralization of OM in the anaerobic zone follows the reaction [10]:

$$(CH_2O)_{106}(NH_3)_{16}H_3PO_4 + 53SO_4^{2-} \rightarrow 106HCO_3^- + 16NH_4^+ + 16HS^- + 37H_2S + H_3PO_4 \quad (4)$$

The relationship between nutrients is C:S:Si:N:P = 106:(−53):31:16:1.

The neutrality of silicon in regard to the redox condition changes is explained as follows. Dissolved silicon is consumed by diatoms in the surface euphotic layer only and it returns back to a dissolved form in the aphotic water column independently on the redox potential changes.

The other nutrients (C, N, and P) distributions are also affected by photosynthesis and mineralization of OM, and additionally by a number of redox dependent processes and chemosynthesis that occur in the vicinity of the redox layer. The main redox reactions, which may occur in the sea water, are given in Table 1. They take place in accordance with the thermodynamical preference determined by the Gibbs energy and by changes in the equilibrium redox potential (Eh). These processes can influence the formation of the vertical biogeochemical structure of the Black Sea. However, their quantitative role in the formation of this structure features is unknown, as well as it is not clear which peculiarities of the vertical distributions of nutrients can be explained by the presence of certain process (or several processes) there. The present study focuses on the revealing of anomalies in the vertical distributions of nutrients in the Black Sea and on estimating the rates of biogeochemical processes that are responsible for these anomalies formation and existence.

2 Materials and Methods

We analyzed the vertical variability of main nutrients ratios in the changeable redox conditions of the Black Sea water column. Approaches in estimating the biogeochemical processes rates connected with the redox condition changes on the base of the main nutrients ratios are widely applied [13–16].

We used the observations data collected in the expeditions of the Shirshov Institute of Oceanology in the Black Sea in the period of 1997–2006. Most of the data used were collected in the north-eastern part of the Black Sea on the base of the systematic observations carried out in this region during R/V “Akvanavt” and R/V “Ashamba” cruises. These data used cover all the seasons, a list of cruises used is given in Yakushev et al. [4]. The sampling and processing of samples of dissolved oxygen, hydrogen sulfide, nitrate, nitrite, ammonia, silicate, phosphate, pH, and total alkalinity were performed by standard methodologies [17, 18].

The data were quality controlled and doubtful values (outliers) were excluded. We considered the distribution of hydrochemical parameters vertically versus depth

Table 1 The main redox reactions in the Black Sea water

Main processes	Reaction	Characteristics of depth	Density	Eh, V	Microorganisms
Photosynthesis	$CO_2 + H_2O = CH_2O + O_2$ [2]	Maximum of O_2			Phytoplankton
Aerobic oxidation of organic matter	$O_2 + C = CO_2$ [2]	Decrease of concentration O_2		0.74	Heterotrophic organisms (saprophytes)
Nitrification	$2NH^{4+} + 3O_2 = 2NO_2^- + 4H^+ + 2H_2O$, $2NO_2^- + O_2 = 2NO_3^-$[2]	Maximum of NO_3^- and NO_2^-, minimum of O_2	15.4		Chemotrophs (nitrificators)
Denitrification	$3NO_3^- + C = 2NO_2^- + CO_2$, $2NO_2 + C = N_2 + 2CO_2$ [2]	Decrease of NO_3^- maximum of NO_2^-	16.0	0.59	Heterotrophic organisms (nitrificators), chemoautotrophs (thiodenitrificators)
Oxidation of Mn	$2 Mn^{2+} + O_2 + 2H_2O = 2MnO_2 + 4H^+$ [2]	Maximum of MnO_2	16.1		Chemoautotrophs
Oxidation of Fe	$2Fe^{2+} + MnO_2 + 2H_2O = 2FeOOH + Mn^{2+} + 2H^+$ [2]	Maximum of FeOOH	16.2		Chemoautotrophs (ferrobacterias)
Thiodenitrification	$HS^- + NO_3 + H_2O + H^+ = SO_4^{2-} + NH_4^+$ [19]	Increase of ammonia content	16.0		
Anammox	$NH_4^+ + NO_2 = N_2 + 2H_2O$ [11]	Decrease of total nitrogen content	16.0		Planctomycetes
Reduction of Mn	$2MnO_2 + C + 4H^+ = 2Mn^{2+} + CO_2 + 2H_2O$ [2], $H_2S + MnO_2 = S^0 + Mn^{2+} + 2OH^-$ [19]	Maximum of Mn^{2+}	16.5	0.47	Heterotrophic organisms (manganese reduced)
Oxidation of hydrogen sulfide	$H_2S + 2O_2 = H_2SO_4$ [19], $2H_2S + O_2 = 2S^0 + 2H_2O$ [19], $5H_2S + 8NO_3^- = 4N_2 + 5SO_4 + 2H^+ + 4H_2O$ [19], $H_2S + NO_3^- + H_2O = SO_4^{2-} + NH_4^+$ [19], $S^{2-} + 2FeOOH = SO_4^{2-} + 2Fe^{2+} + 2H^+$ [2], $H_2S + 4MnO_2 + 2H_2O = SO_4^{2-} + 4Mn^{2+} + 6OH^-$ [19]	Maximum of SO_4^{2-}	16.2		Chemoautotrophs (thionic)
Reduction of Fe	$4FeOOH + C + 8H^+ = 4Fe^{2+} + CO_2 + 6H_2O$ [2], $2Fe^{2+} + MnO_2 + 2OH^- = 2FeOOH + Mn^{2+}$ [19]	Maximum of Fe^{2+}	16.5	0.24	Heterotrophic organisms (ferrobacterias)

(continued)

Table 1 (continued)

Main processes	Reaction	Characteristics of depth	Density	Eh, V	Microorganisms
Sulfate reduction	$SO_4^{2-} + 2C + 2H^+ = H_2S + 2CO_2$ [16]	Increase of hydrogen sulfide	16.15	−0.24	Heterotrophic organisms
Oxidation of methane	$CH_4 + CO_2 = 2CH_2O$ [2], $CH_4 + CO_2 = CH_3COOH$ [2], $CH_4 + SO_4^{2-} = HS^- + HCO_3 + H_2O$ [19]	Decrease of CO_2 concentration			Chemoautotrophs
Methane formation	$CO_2 + 4H_2 = CH_4 + 2H_2O$ [19], $CH_3COOH \rightarrow CH_4 + CO_2$ [19]	Increase of methane concentration	16.5	−0.35	Chemoautotrophs or heterotrophic organisms
Formation of H_2	$C_6H_{12}O_6 + 6H_2O = 12H_2 + 6CO_2$ [2]				Fermentation
Oxidation of H_2	$12H_2 + 6CO_2 = C_6H_{12}O_6 + 6H_2O$ [2]				Chemoautotrophs

and density. Statistical processing of data and averaging to isopycns was performed by DB VERTA (Podymov 2008).

Total alkalinity was calculated using the equation:

$$A_t = \left[HCO_3^-\right] + 2\left[CO_3^{2-}\right] + \left[B\left(OH_4^-\right)\right] + \left[SiO(OH)_3^-\right] + [HS^-] + 2\left[S^{2-}\right] + \left[HPO_4^{3-}\right] + 2\left[PO_4^{2-}\right] + [NH_3] + [OH^-] + [H^+] \quad (5)$$

with the inclusion of sulfide, phosphate, and ammonia components. The calculations of the carbonate system parameters were performed applying a standard approach [15, 16, 19, 20].

The details of the main nutrients ratios calculations are described below.

3 Results and Discussions

The calculated ratios between the total inorganic carbon, phosphorus, silicon, hydrogen sulfide, and dissolved inorganic nitrogen (a sum of nitrate, nitrite, and ammonia) versus density are shown in Fig. 2. The calculations were aimed to reveal those changes in the aphotic zone which were connected with the processes in the redox and anaerobic layer (e.g., the water column beneath the oxycline in the density range of $\sigma_\theta \approx 15.5$–$17.5$ kg m^{-3}). The C_t/P_t ratio was calculated as $(C_i - C_o)/(P_i - P_o)$, where C_i and P_i are the concentrations of total inorganic carbon and phosphorus at the depth under studies, $C_o = 3{,}157$ μM and $P_o = 1$ μM are the year-averaged concentrations of inorganic carbon and phosphorus at the upper boundary of the redox layer (depth 100–120 m). The ratios of the other nutrients were calculated in a similar way.

The calculated C_t/P_t ratio increased with depth from 0 near the upper boundary of the redox layer to 105 at the bottom (Fig. 2). In the density layer, $\sigma_\theta \approx 15.5$–$16.0$ kg m^{-3}, the C_t/P_t ratio increased at practically constant C_t values that testified to a consumption of phosphate there. Meanwhile, deeper in the layer of $\sigma_\theta \approx 16.0$–$16.2$ kg m^{-3}, the C_t/P_t ratio slightly decreased, that can be an evidence for the production of phosphate. At the near-bottom layers, C_t/P_t values approach the stoichiometric one of about 106.

C_t/Si_t ratio was calculated as $(C_i - C_0)/(Si_i - Si_0)$, where $Si_0 = 53$ μM is the year averaged concentration of silicon at the depth of 100–120 m. The calculated C_t/Si_t ratio changed from 0 to 3.2. At the near-bottom, the C_t/Si_t ratio approached the stoichiometric one of 3.4. The decreased values of C_t/Si_t ratio (less than 1) in the redox layer and in the upper part of the sulfidic zone can be well connected with the chemosynthesis occurring there.

The ratio Si_t/P_t varied in the investigated water column from 0 to 32, as the theoretical value of about 31 was reached in the near-bottom layer. The typical for all observed stations sudden increase of Si_t/P_t values to 23 in the upper part of

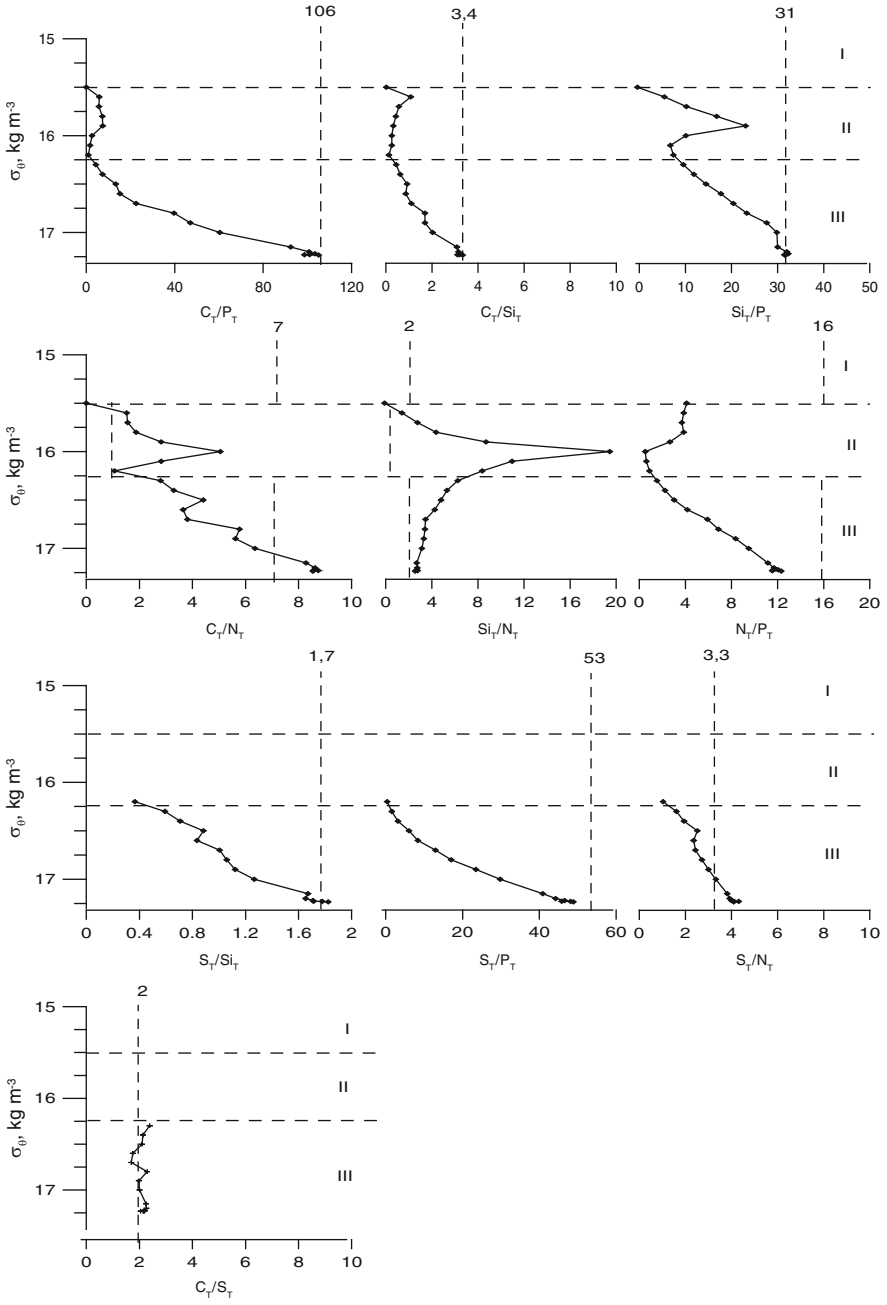

Fig. 2 Vertical distributions of ratios between total inorganic carbon, silicate, phosphate, hydrogen sulfide, ammonia versus density. *Dotted vertical lines* show stoichiometric relationships without anammox effect [5, 10]: *I*, oxygen layer; *II*, redox layer; *III*, sulfidic layer

the redox layer ($\sigma_\theta \approx 15.7$–$16.0$ kg m^{-3}), and the following decrease to 7 in the deeper part of the redox layer ($\sigma_\theta \approx 16.10$–$16.30$ kg m^{-3}) evidence the presence of two corresponding processes – phosphate consumption at the phosphate shallow minimum depth and phosphate production at the phosphate deep maximum depth.

The C_t/N_t ratio (with an annual concentration of the total nitrogen at the depth of 100–120 m assumed as $N_0 = 5$ μM) changed from 0 to 9 (Fig. 2). The C_t/N_t value approached to the stoichiometric one of 7 in the near-bottom water. The decrease of the C_t/N_t to 5 at $\sigma_\theta \approx 16.0$ kg m^{-3} could be connected to the processes of the bound nitrogen removal, i.e., denitrification and anammox.

The Si_t/N_t ratio changed in the range of 2–19 with the theoretical value of about 2 in the near-bottom layer observed and with a maximum of 19 in the vicinity of $\sigma_\theta \approx 16.0$ kg m^{-3} recorded. The latter testified again to the presence of nitrogen consumption processes there.

The N_t/P_t ratio varied from 1 to 12 with a minimum of 1–2 at $\sigma_\theta \approx 16.0$–$16.4$ kg m^{-3}. This minimum evidences that the decrease of nitrogen related to denitrification/anammox is more intensive than the decrease of phosphorus which occurs due to phosphorus consumption processes at the phosphate minimum depth.

The S_t/Si_t and S_t/P_t ratios practically evenly increase from 0 to 1.7 and from 5 to 53. In the near-bottom water, their values approach to the stoichiometric ones of 1.7 and 53, respectively.

The S_t/N_t ratio increases from 1 to 4 and approaches to the Redfield one (3.3) in the near-bottom water.

The calculated ratio between the total inorganic carbon and total hydrogen sulfide is 2.13, by less than 4% exceeding the theoretical one of 2.0. The latter supports the theory that the process of bacterial sulfate reduction is the main process of mineralization of OM under anaerobic conditions, and this process occurs throughout the entire water column, from the low boundary of the redox layer to the bottom, with practically stoichiometric C_t/S_t ratio near 2 [16, 21].

Using a simple one-dimensional vertical transport model, it was possible to estimate the rates of biogeochemical processes in the redox layer leading to decrease in nitrogen content (denitrification/anammox) and of processes responsible for the formation of the shallow minimum and deep maximum of phosphate based on the following. We assumed that changes of the nutrient concentrations are compensated by their transport with the vertical turbulent flux. As it was already mentioned, silicon is not involved in the redox biogeochemical processes. This fact allows estimating the vertical variability of other nutrients on the basis of comparison of their distributions with the silicon's one.

The rates of reaction were calculated with the following formula (6):

$$R_c = k_c \frac{\partial^2 c}{\partial z^2}, \tag{6}$$

where R_c is the rate of the reaction;

c is the concentration of nutrient;

k_c is a coefficient of the vertical turbulent exchange;

z is the depth.

The calculations of k_c for the redox layer were performed with the Gargett formula [22], which is based on data of density vertical distribution: $k_c = a_0 N^{-q}$, where $N = \sqrt{-\frac{g}{\rho}\frac{\partial \rho}{\partial z}}$, a_0 and q are empirical coefficients, g is the acceleration of gravity and ρ is the density.

For the Black Sea redox layer, we used the parametrization of a_0 and q proposed by Konovalov et al. [23]: $k_c = 1.62 \times 10^{-3}\left(-\frac{g}{\rho}\frac{\mathrm{d}\rho}{\mathrm{d}z}\right)^{-0.5}$. This gives us the k_c value of 10^{-5} m^2 s^{-1}. A slightly lower value (5.2×10^{-6} m^2 s^{-1}) was used by Neretin for the redox layer of the Gotland deep, Baltic Sea [24]. Analyzing the distribution of ^{137}Cs after the Tchernobyl accident, Stokozov [25] received for the Central Black Sea Basin $k_c = (1 - 3) \times 10^{-5}$ m^2 s^{-1}, and for the RIM-corrent $k_c = (3 - 11) \times 10^{-5}$ m^2 s^{-1}.

We used the values of k_c in the range of (0.5–2) $\times$ 10^{-5} m^2 s^{-1} for the layer $\sigma_\theta \approx$ 15.7–16.21 kg m^{-3}.

The distributions of all the nutrients depend on the mineralization of the euphotic layer origin OM and on the vertical mixing. The nitrogen and phosphorus distributions are complicated by the reactions in the redox layer (i.e., chemosynthesis and redox reactions), while the distribution of silicate is not affected by these processes. On the basis of the stoichiometric ratios, it is possible to estimate the shares of nitrogen and phosphorus ($N_f = Si_i/2$ and $P_f = Si_i/32$), which distributions are determined by the same processes as for silicon. The difference between these shares (N_f and P_f) and the observed concentrations (P_i and N_i) will give us a share that can be explained by the reactions in the redox layer ($N_p = N_f - N_i$ and $P_p = P_f - P_i$).

The maximal rate of decrease of nitrogen, hypothetically connected with denitrification/anammox, calculated for the depth of nitrogen minimum (120 m, Table 2, Fig. 3) is:

$$R_N = k_c \frac{\partial^2 N_p}{\partial z^2} = 0.012 - 0.046 \ \ \mu\text{M per day}.$$

According to the observations, the rate of denitrification is 0.002 μM per day for the Black Sea [26] and 0.044–0.110 μM per day for the Baltic Sea [27]. A rate of thiodenitrification was calculated earlier for the Baltic Sea as 0–2.7 μM per day [28]. The rate of anammox was estimated to be 0.007 μM per day for the Black Sea [24] and 0–0.05 μM per day for the Baltic Sea [28]. The calculated value in the present study is close to the mentioned results of observations for denitrification or anammox [24, 26, 28]. Therefore, the same approach could be applied to calculate the rates of processes which form the shallow minimum and deep maximum of phosphates.

According to our calculations, the rate of the shallow phosphate minimum (110 m) formation is:

Table 2 Stoichiometric relationships Si/N, Si/P, changed concentrations of total nitrogen N_p and phosphorus P_p due to reactions in the redox layer, first and second derivatives $\frac{\partial N_p}{\partial z}$, $\frac{\partial^2 N_p}{\partial z^2}$, $\frac{\partial P_p}{\partial z}$, $\frac{\partial^2 P_p}{\partial z^2}$

Depth m	Si/N	N_p, μM	$\frac{\partial N_p}{\partial z}$	$\frac{\partial^2 N_p}{\partial z^2}$	Si/P	P_p μM	$\frac{\partial P_p}{\partial z}$	$\frac{\partial^2 P_p}{\partial z^2}$
80	1.41	25.08	0.3115	−0.0045	5.44	0.68	0.022142	0.001492
90	2.76	28.20	0.2665	0.0091	10.20	0.90	0.037058	−0.001604
100	4.36	30.86	0.3575	0.0105	16.81	1.27	0.021016	−0.018485
110	8.71	34.44	0.4625	−0.02675	23.07	1.48	−0.16383	−0.006328
120	19.44	39.06	0.195	−0.001	10.11	−0.16	−0.22711	0.01986
130	10.96	41.01	0.185	−0.0087	6.72	−2.43	−0.02851	0.010191
140	8.37	42.86	0.098	0.0021	7.40	−2.71	0.073406	−0.001422
150	6.25	43.84	0.119	−0.0022	9.56	−1.98	0.05919	−0.003905
160	5.31	45.03	0.097	0.0003	11.86	−1.39	0.020145	0.00096
170	5.12	46.00	0.1	−0.006	12.90	−1.19	0.029745	−0.000455
180	4.79	47.00	0.04	−0.0015	14.46	−0.89	0.02519	0.000362
190	4.38	47.40	0.025	−0.0028	15.94	−0.64	0.028806	−0.002113
200	3.98	47.65	−0.003	0.00146	17.71	−0.35	0.007677	1.16E-05

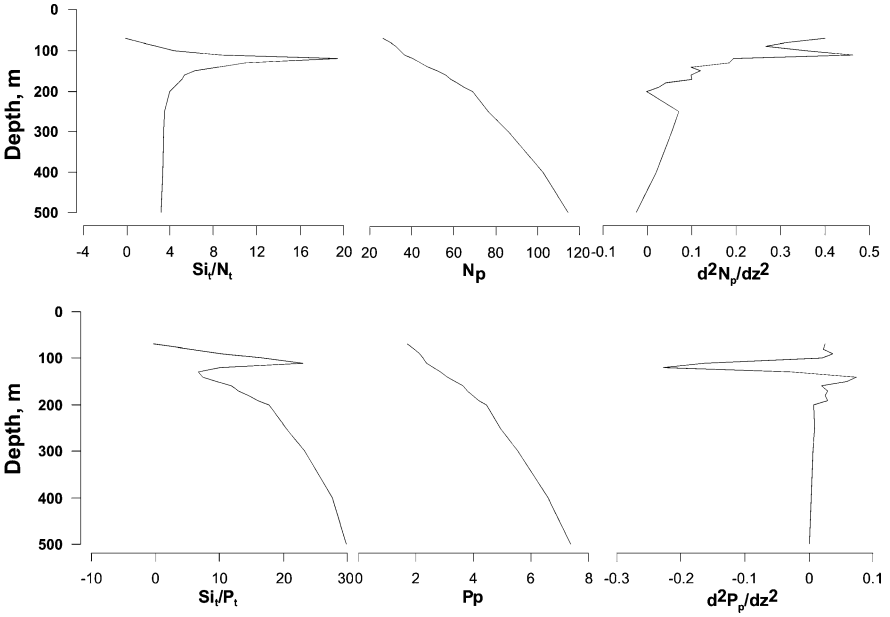

Fig. 3 Vertical distributions of Si_t/N_t, N_p, $\frac{\partial^2 N_p}{\partial z^2}$ (*top line*), Si_t/P_t, P_p, $\frac{\partial^2 P_p}{\partial z^2}$ (*bottom line*) versus depth. Explanations are in the text

$$R_{P_{min}} = k_c \frac{\partial^2 P_p}{\partial z^2} = 0.008 - 0.032\,\mu\text{M per day},$$

and the rate of forming of the deep phosphate maximum (140 m) formation is:

$$R_{\mathrm{P}_{\max}} = k_c \frac{\partial^2 \mathrm{P}_\mathrm{p}}{\partial z^2} = 0.006 - 0.024\,\mu\mathrm{M\ per\ day}.$$

The processes leading to the formation of the phosphate minimum and maximum can be connected with chemosyntheses [29], coprecipitation of phosphates with metal hydroxides [30], or formation of complexes between Mn(III) and pyrophosphate [4]. The latter was confirmed by observations on the distributions of Mn(III) and polyphosphate and was discussed in details in [31].

4 Conclusions

Based on the analyses of stoichiometric ratios between the main nutrients we have revealed, the ranges of depth and density for reactions which control the decrease of nitrogen (denitrification/anammox) ($\sigma_\theta \sim 16.0$ kg m^{-3}; 100–120 m), and the formation of the shallow minimum and deep maximum of phosphate in the redox layer ($\sigma_\theta \approx 15.85$–$16.05$ kg m^{-3}; $\sigma_\theta \approx 16.15$–$16.25$ kg m^{-3}).

Based on the assumption that silicate concentration does not change under the conditions of the redox layer, the rates of the processes of nitrogen decrease (denitrification/anammox) were calculated. According to these calculations, the range of the probable denitrification/anammox rates is (0.012–0.046) μM per day, which is in agreement with existing results of these processes measurements. Based on the same approach, the rates of formation of the shallow phosphate minima (0.008–0.032) μM per day, and the deep phosphate maxima (0.006–0.024) μM per day were calculated.

The obtained estimates of the rates of transformations of the main nutrients at the redox interface have a large significance for studying of the phosphorus and nitrogen dynamics at the seasonal and interannual scales in connection with different scenarios of climate variability and anthropogenic forcing.

Acknowledgments Authors express their gratitude to professor I. Volkov for valuable remarks and discussions while writing on the subject. This research was supported by the FTP "World Ocean"; RFBR: CRDF (RUG1-2828-KS-06).

References

1. Murray JW, Codispoti LA, Friederich GE (1995) The suboxic zone in the Black Sea. In: Huang CP, O'Melia R, Morgan JJ (eds) Aquatic chemistry: interfacial and interspecies processes, vol 244. American Chemical Society, Washington, DC, pp 157–176
2. Rozanov AG (1995) Redox stratification of the Black Sea. Oceanology 35(4):544–549

3. Vinogradov MV, Nalbandov YuR (1990) Affect of water density on disributions of phisycal, chemical, and biological characteristics of pelagic ecosysem of the Black Sea. Oceanology 30(5):769–777
4. Yakushev EV, Chasovnikov VK, Debolskaya EI, Egorov AV, Makkaveev PN, Pakhomova SV, Podymov OI, Yakubenko VG (2006) The northeastern Black Sea redox zone: hydrochemical structure and its temporal variability. Deep Sea Research II 53:1764–1786
5. Redfield AC (1934) On the proportion of organic derivatives in sea water and their relation to the composition of plankton. James Johnstone Memorial Volume University Press, Liverpool, pp 176–192
6. Canfield DE, Thamdrup B, Kristensen E (2005) Aquatic geomicrobiology. In: Southward AJ, Tyler PA, Young CM, Fuiman LA (eds) Advances in marine biology, vol 48. Elsevier Academic Press, Amsterdam, p 640
7. Ivanenkov VN (1979) General features of nutrient distribution in the World Ocean. In: Bordovskiy OK, Ivanenkov VN (eds) Chemistry of the ocean. V.1 Chemistry of the ocean waters. M. Nauka, Moscow, pp 188–229 (In Russian)
8. Sverdrup H, Johnson M, Fleming R (1942) The oceans. Prentice-Hall Inc, New York
9. BSC (2008) State of the environment of the Black Sea (2001 - 2006/7). In: Oguz T (ed) Publications of the Commission on the Protection of the Black Sea against Pollution (BSC) 2008–3, Istanbul, Turkey, 448 pp
10. Richards FA (1965) Anoxic basin and fjords. Chemical oceanography, vol 1. Academic Press, London and New York
11. Dalsgaard T, Canfield DE, Paterson J, Thamdrup B, Aguna-Gonzalea J (2003) N_2 production by the anammox reaction in the anoxic water column of Golfo Dulche, Costa Rica. Nature 422:606–608
12. Kuypers MM, Sliekers AO, Lavik G, Schmid M, Jorgensen BB, Kuenen JG, Sinnenghe Damste JS, Strous M, Jetten MSM (2003) Anaerobic ammonium oxidation by anammox bacteria in the Black Sea. Nature 422:608–611
13. Paulmier A, Ruiz-Pino D, Garcon V, Farias L, Ulloa O (2006) Biogeochemical anomalies in the OMZ off Chile. Gayana 70:135
14. Scranton M, McIntyre M, Astor Y, Taylor GT, Muller-Karger F, Fanning K (2006) Temporal variability in the nutrient chemistry of the Cariaco basin. In: Neretin LN (ed) Past and present water column anoxia, vol 64, NATO science series IV. Springer, Dordrecht, pp 105–138
15. Volkov II, Rozanov AG (2006) Introduction in biohydrochemistry of anaerobic basins. Oceanology 6(5):854–867
16. Volkov II, Rozanov AG, Dyrsen D (1998) Problem of water alkalinity and anaerobic mineralization of organic matter in the Black Sea. Geochemistry 1:78–87
17. Bordovskiy OK, Chernyakova AM (eds) (1992) Modern methods of the ocean hydrochemical investigations. P.P. Shirshov Institute of Oceanology, Moscow, p 200 (In Russian)
18. Grashoff K, Kremling K, Ehrhard M (1999) Methods of seawater analysis, 3rd edn. Wiley-VCH, Weinheim, completely revised and extended edition
19. Dyrsen D, Haraldson C, Weterlung S, Aren K (1986) Report on the chemistry seawater. XXXII, Department of Analytical and Marine Chemistry, Chalmers University, Goteborg, Sweden. 57p
20. Makkaveev PN (2002) Calculations of the component of the total titrated alkalinity in the Black Sea waters. In: Zatsepin AG, Flint MV (eds) Complex investigation of the northeastern Black Sea. Nauka, Moscow, p 447
21. Neretin LN, Volkov II, Rozanov AG, Demidova TP, Falina AS (2005) Biogeochemistry of the Black Sea anoxic zone with a reference to sulfur cycle. In: Neretin LN (ed) Past and present water column anoxia, vol 64, NATO science series IV. Springer, Dordrecht, p 69
22. Gargett AE (1984) Vertical eddy diffusivity in the ocean interior. J Marine Res 42:359–393
23. Konovalov SK, Luther GW, Friederic GE, Nuzzio DB, Tebo BM, Oguz T, Glazer B, Trouwborst RE, Clement B, Murray KJ, Romanov AS (2003) Lateral injection of oxygen

with Bosporus plume – fingers of oxidizing potential in the Black Sea. Limnol Oceanogr 48:2367–2376
24. Neretin L, Pohl C, Jost G, Leipe T, Pollehne F (2003) Manganese cycling at the oxic/anoxic interface in the Gotland deep, Baltic Sea. Mar Chem 82:125–143
25. Stokozov NA (2004) Long-term radionuclides ^{137}Cs and ^{90}Sr in the Black Sea after Tchernobyl accident and their using as tracers into the water with changing processes. PhD Thesis, Institute of Biology of the Southern Seas (In Russian)
26. Ward BB, Kilpatrick KA (1991) Nitrogen transformations in the oxic layer of permanent anoxic basins: the Black Sea and the Cariaco Trench. In: Izdar E, Murray JW (eds) Black Sea oceanography. Kluwer, Norwell, pp 111–124
27. Brettar I, Rheinheimer G (1991) Denitrification in the Central Baltic: evidence for H_2S-oxidation as motor of denitrification at the oxic-anoxic interface. Mar Ecol Progr 77:157–169
28. Hannig M, Lavik G, Kuypers M, Wobken D, Martens-Habben W, Jurgens K (2007) Shift from denitrification to anammox after inflow events in the central Baltic Sea. Limnol Oceanogr 52(4):1336–1345
29. Sorokin I (2002) The Black Sea. Ecology and oceanography. Backhuys, Leiden, p 875
30. Shaffer G (1986) Phosphorus pumps and shuttles in the Black Sea. Lett Nat 321:515–517
31. Pakhomova SV, Yakushev EV (2011). On the role of iron and manganese species in the formation of the redox-interface structure in the Black Sea, Baltic Sea and Oslo Fjord. In: Yakushev EV (ed) Chemical structure of Pelagic Redox Interfaces: observation and modeling. Handbook of Environmental Chemistry. Springer, Berlin. doi:10.1007/698_2011_98
32. Podymov OI (2008) Use of a problem-oriented database for statistical analysis of the hydrochemical characteristics of the redox layer of the Black Sea. Oceanology 48(5):656–663

Anaerobic Microbial Community in the Aerobic Water and at the Oxic/Anoxic Interface in the Black Sea

N. V. Pimenov, A. L. Bryukhanov, V. A. Korneeva, E. E. Zakharova, P. A. Sigalevich, I. I. Rusanov, E. V. Yakushev, and V. K. Chasovnikov

Abstract Fluorescent in situ hybridization (FISH) was used to analyze the abundance and phylogenetic composition of physiologically active anaerobic microbial communities [sulfate-reducing bacteria (SRB) and methanogenic archaea] in the aerobic waters and in the oxic/anoxic transitional zone (chemocline) of the Black Sea. Biogenic sulfate reduction and methane formation were detected at these horizons by radioisotope techniques. Numerous SRB phylogenetically related to *Desulfotomaculum* (30.5% of detected bacterial cells), *Desulfovibrio* (29.6%), and *Desulfobacter* (6.7%) were detected in the aerobic zone at a depth of 30 m, whereas *Desulfomicrobium*-related bacteria (33.5%) were prevalent in chemocline at a depth of 150 m. In the oxic subsurface water layer, Methanomicrobiales-related archaea and subgroup 1 methanogens constituted up to 62 and 35.3% of archaeal cell, respectively. The active cells of sulfate-reducing and methanogenic microorganisms were much more abundant in the samples collected in summer than in winter from the deep-sea zone. The presence of physiologically active anaerobic microorganisms in oxic and chemocline waters of the Black Sea correlates with the hydrochemical data on the presence of sulfide and methane at corresponding depths.

Keywords Black Sea, Chemocline, Fluorescent in situ hybridization, Meromictic basins, Methanogenic archaea, Oxic surface waters, Sulfate-reducing bacteria

N.V. Pimenov (✉), E.E. Zakharova, P.A. Sigalevich, and I.I. Rusanov
Winogradsky Institute of Microbiology, Russian Academy of Sciences, Moscow, Russia
e-mail: npimenov@mail.ru

A.L. Bryukhanov and V.A. Korneeva
Faculty of Biology, Lomonosov Moscow State University, Moscow, Russia

E.V. Yakushev
Norwegian Institute for Water Research, Oslo, NO-0349, Norway
Shirshov Insititute of Oceanology, Russian Academy of Sciences, Moscow, Russia

V.K. Chasovnikov
Shirshov Insititute of Oceanology, Russian Academy of Sciences, Moscow, Russia

E.V. Yakushev (ed.), *Chemical Structure of Pelagic Redox Interfaces: Observation and Modeling*, Hdb Env Chem (2013) 22: 27–46, DOI 10.1007/698_2010_84,

Contents

Abbreviations

ANAMMOX	Anaerobic ammonium oxidation
EDTA	Ethylenediaminetetraacetate
FISH	Fluorescent in situ hybridization
PBS	Phosphate-buffered saline
RV	Research vessel
SRB	Sulfate-reducing bacteria

1 Introduction

The Black Sea is the world's largest meromictic basin and a great reservoir of dissolved methane, sulfide, and CO_2. In the central part of the sea, the aerobic zone is 90–100 m deep, while its lower border above the continental shelf is somewhat deeper, at 140–175 m [1, 2]. Below the oxic zone, the water is more saline and contains sulfide (up to 335–370 μM at 1,500–2,000 m).

A series of publications confirmed the major role of sulfate-reducing bacteria (SRB) of the anaerobic water column in sulfide production in the Black Sea [3]. However, hydrochemical investigation revealed the presence of reduced sulfur compounds in aerobic water [4], probably resulting from bacterial sulfate reduction. Below the halocline, apart from sulfide, dissolved biogenic methane (11–15 μM) is also present, the terminal product of decomposition of organic matter by methanogenic archaea. Due to activity of aerobic and anaerobic methanotrophic bacteria in the water column, methane concentration decreases to 56–250 nM in the chemocline and to 1–8 nM at the surface [5].

Community structure and the rates of microbial processes in the oxic–anoxic interface of the water column (suboxic zone or chemocline zone) are of special interest. In this zone, activity of various physiological groups of microorganisms is

determined by flows of oxidized and reduced compounds of biogenic elements, gases, and variable-valency metals. High abundance of many microbial groups has been demonstrated in the chemocline [6], as well as high activities of microbial processes (dark CO_2 fixation, chemoautotrophic production, transformation of sulfur compounds, and production and oxidation of methane) [7, 8].

SRB and especially methanogenic archaea are traditionally considered strict anaerobes. Some species of sulfate reducers, however (e.g., many *Desulfovibrio* and *Desulfotomaculum* species), possess efficient protective mechanisms and are able to survive and even to retain their metabolic activity in the environments regularly affected by oxygen [9, 10]. Some methanogenic archaea are also able to survive temporary aerobiosis and to form communities with facultative anaerobes [10].

Application of molecular biological techniques, in particular fluorescent in situ hybridization (FISH) with 16S rRNA-specific oligonucleotide probes and its combinations with microradioautography, is presently widespread in research on marine bacterioplankton. This rapid and sensitive technique provides information on the qualitative and quantitative composition of marine microbial communities, which is especially important for determination of the phylogenetic position of uncultured microorganisms [11], and makes it possible to assess the ecological role of specific community components directly in the environment [12].

Few publications exist on the application of FISH for investigation of bacterioplankton in the Black Sea water column [8]. The results of the first detailed FISH investigation of vertical distribution of the major prokaryotic groups in the Black Sea were published in 2005–2006 [5, 6]; the authors concentrated mainly on the structure of the microbial community involved in methane turnover in the chemocline. The distribution of SRB in the Black Sea water column was analyzed with the SRB385 probe, which is most commonly used for detection of sulfate reducers [6].

The goal of the present work was application of FISH to investigation of abundance and taxonomic diversity of biogeochemically important anaerobic microorganisms (SRB and methanogenic archaea) in the aerobic surface water and in the chemocline of the Black Sea and comparison of these results with the measured rates of sulfate reduction and methanogenesis.

2 Materials and Methods

Water from the depths of 30 to 600 m was collected in sterile 50-ml Falcon tubes in May 2007 and June 2008 onboard RV *Aquanavt* at station 2900 located in the Russian sector of the Black Sea, 10–12 miles from the Golubaya Bay at the continental slope near Gelendzhik (44°.458 N, 37°.882 E; 1,300 m deep). In March 2009, water samples were collected from RV *Professor Shtokman* in the Russian sector of the deep-water zone of the Black Sea (station 20, 44°.052 N, 36°.632 E; depth 1,940 m).

Water samples from different depths were collected in 5-l Niskin bottles attached to a rosette. The physical structure of the water column was recorded by

a conductivity-temperature-depth (CTD) unit (Seabird 19) equipped with a device for measuring turbidity backscatter signals (Dr. Haardt, Kiel).

Oxygen concentrations were determined by Winkler titration in 100 ml glass bottles [13] using a Metrohm potentiometric titrator. Nutrients were measured photometrically according to [14], and sulfide was determined colorimetrically with *N*,*N*-dimethyl-*p*-phenylenediamine [15] on a HACH DR-2800 spectrophotometer.

Enrichment cultures of SRB were isolated from the samples collected in the deep-water zone of the Black Sea from the depths of 30, 70, 120, and 165 m (station 20). Liquid Widdel medium for marine forms was used [16], supplemented with vitamins and trace elements [17]. The media were prepared using the Hungate anaerobic technique [18]. The tubes with enrichment cultures were incubated for 7–21 days at 22–23°.

Growth of SRB was assessed by increase in sulfide content compared to the control. For enumeration and identification of microorganisms, water samples and enrichment cultures were fixed with fresh solution of 40% formaldehyde in phosphate-buffered saline (PBS), pH 7.0 at the final formaldehyde concentration of 4% and stored at 4°C in the dark.

Microbial cells (7–15 ml for water samples and 40–400 μl for enrichment cultures) were concentrated on black polycarbonate membrane filters GTBP 2500 (25 mm diameter, 0.2 μm pore size, Millipore, USA). The filters were washed with PBS/ethanol mixture (1:1), air-dried, and stored at −20°C.

For hybridization, sectors of the filters were placed on microscopic slides and treated with 9 μl of the freshly prepared hybridization buffer with 1 μl of Cy3-labeled 16S rRNA-specific oligonucleotide probe (50 ng μl^{-1}). The hybridization buffer contained the following: 0.9 M NaCl, 0.01% sodium dodecyl sulfate, 20 mM Tris–HCl (pH 7.5), and 0.2% blocking reagent (Roche Diagnostics, Switzerland), supplemented with formamide (MP Biomedicals, USA) in the concentration adjusted for each probe in order to obtain precise and specific hybridization [19–21]. Hybridization was carried out for 2 h in a moist chamber in a BD 53 thermostat (Binder, Germany) at the recommended temperature.

The fluorochrome-labeled oligonucleotide probes (Syntol, Russia) used in the work are listed in Table 1. The probes for identification of bacteria [22], archaea [23], and methanogenic archaea [24, 25] were used, as well as the more specific ones for differentiation between SRB groups [26–29]. The probeBase database (http://www.microbial-ecology.net/probebase) was used to select the relevant probes. Hybridization efficiency was tested on pure cultures of *Escherichia coli* TG-1 (Stratagene, USA), *Desulfotomaculum nigrificans* ssp. *salinus* strain 435 (Laboratory of Microbiology of Anthropogenic Habitats, Winogradsky Institute of Microbiology), *Desulfovibrio vulgaris* Hildenborough ATCC 29579, and *Methanosarcina barkeri* Fusaro DSMZ 804 as positive and negative controls. Filter sectors without a probe were used as controls for the possible autofluorescence (especially in the case of methanogenic archaea).

In order to remove the unbound probe, the filters were washed in the dark with sterile deionized water and incubated for 10 min at hybridization

Table 1 Cyanine 3-labeled 16S rRNA-specific oligonucleotide probes used in the work

Probe	Phylogenetic specificity	Nucleotide sequence (5′ → 3′)	16S rRNA target fragment	T_m, °C	Formamide, %
EUB338 + EUB338 II	Most *Bacteria*	GCTGCCTCCCGTAGGAGT	338–355	55	30
		GCAGCCACCCGTAGGTGT	338–355	55	30
ARCH344 + ARCH915	*Archaea*	TTCGCGCCTGSTGCRCCCCG	344–363	58	20
		GTGCTCCCCCGCCAATTCCT	915–934	58	20
DSB129	Most *Desulfobacter*	CAGGCTTGAAGGCAGATT	129–146	48	15
DSB985	*Desulfobacter*, *Desulfobacula*, *Desulfospira*, *Desulfotignum*	CACAGGATGTCAAACCCAG	985–1,003	51	20
DSV214	Most *Desulfomicrobium*	CATCCTCGGACGAATGC	214–230	49	10
DSV698	Some *Desulfovibrio*, *Bilophila wadsworthia*, *Lawsonia intracellularis*	GTTCCTCCAGATATCTACGG	698–717	52	35
DSV1292	Some *Desulfovibrio*, *Bilophila wadsworthia*	CAATCCGGACTGGGACGC	1,292–1,309	55	35
Dtm229	*Desulfotomaculum* (cluster I), other *Firmicutes*	AATGGGACGCGGATCCAT	229–246	50	15
SRB385	Most *Desulfovibrionales*, most δ-*Proteobacteria* sulfate reducers	CGGCGTCGCTGCGTCAGG	385–402	59	35
MB1174	Subgroup 1 methanogens (*Methanobacterium*, *Methanobrevibacter*, *Methanosphaera*)	TACCGTCGTCCACTCCTTCCTC	1,175–1,196	59	45
MG3	Some methanogenic archaea, *Halobacterium*, *Pyrococcus*, *Sulfolobus*, *Thermofilum* sp., *Pyrobaculum* sp.	GGGCGGTGTGTGCAAGGAG	–	58	20
MG1200b	Most *Methanomicrobiales*	CTGATAATTCGGGGCATGCTG	1,200–1,220	54	20

temperature in preheated washing buffer. The washing buffer contained the following: 5 mM EDTA (pH 8.0), 20 mM Tris–HCl (pH 7.5), 0.01% sodium dodecyl sulfate, and 70–440 mM NaCl, depending on the formamide concentration used. The filters were washed with water and air-dried on clean microscopic slides.

Total microbial numbers were determined by staining with 0.5 ng μl^{-1} 4′,6-diamidino-2-phenylindole (DAPI), 10 μl per filter sector. After 15-min incubation in the dark at room temperature, the filters were washed with water and air-dried. The preparations were mounted in a 4:1 mixture of Citifluor AF1 (Citifluor Ltd., UK) and Vectashield (Vector Laboratories, Canada) under a long coverslip and stored in the dark at −20°C. Microscopy was carried out at ×1,000 magnification under an Axio Imager.D1 epifluorescence microscope (Carl Zeiss, Germany) equipped with an Axio Cam HRc digital camera, filters (Zeiss 20 for Cy3-labeled probes and Zeiss 49 for DAPI staining), and the Axio Vision software package.

The cells were counted in 25–30 fields of view of the camera (in average, 100–120 DAPI-stained cells per field) for each filter sector. Cell number (N) per 1 ml was calculated as $N = n \times (S_{filter}:S_{field}):V$, where n is the average cell number per field, V is the filtered volume, and S_{filter} and S_{field} are the areas of the filter and the field of view, respectively.

Sulfate reduction rate was determined by the radioisotope method with $^{35}S–SO_4^{2-}$ as described previously [8]. The samples in 30-ml glass vials were incubated with the substrate for 2–3 days at 7–8°C and fixed with 1 ml of 2 N NaOH. The final concentration of $^{35}S–SO_4^{2-}$ in the sample was 10 μCi. Before fixation, 0.2 ml of 0.05 M Na_2S was added to the samples in order to prevent the oxidation of reduced sulfur compounds.

For determination of methanogenesis rates, 30-ml glass vials were filled to capacity with seawater and sealed with gas-tight butyl rubber stoppers. The water samples were supplemented with 0.2 ml of sterile $NaH^{14}CO_3$ solution to the final concentration of 20 μCi and incubated for 2–3 days at 7–8°C. After incubation, the samples were fixed with 1 ml of 2 N NaOH, transported to the laboratory, and treated as described previously [30].

3 Results

3.1 *Rates of Sulfate Reduction and Methanogenesis in the Water Column of the Black Sea*

Depth profiles of O_2, H_2S, and the rates of sulfate reduction in the water column over the continental shelf are presented in Fig. 1. Similar to our earlier determination of sulfate reduction rates [8], anaerobic waters at 190–400-m depth exhibited elevated sulfate reduction rates (Fig. 1b). Some peaks were, however, revealed in the aerobic zone, not only at 150-m depth, where oxygen concentration was close to

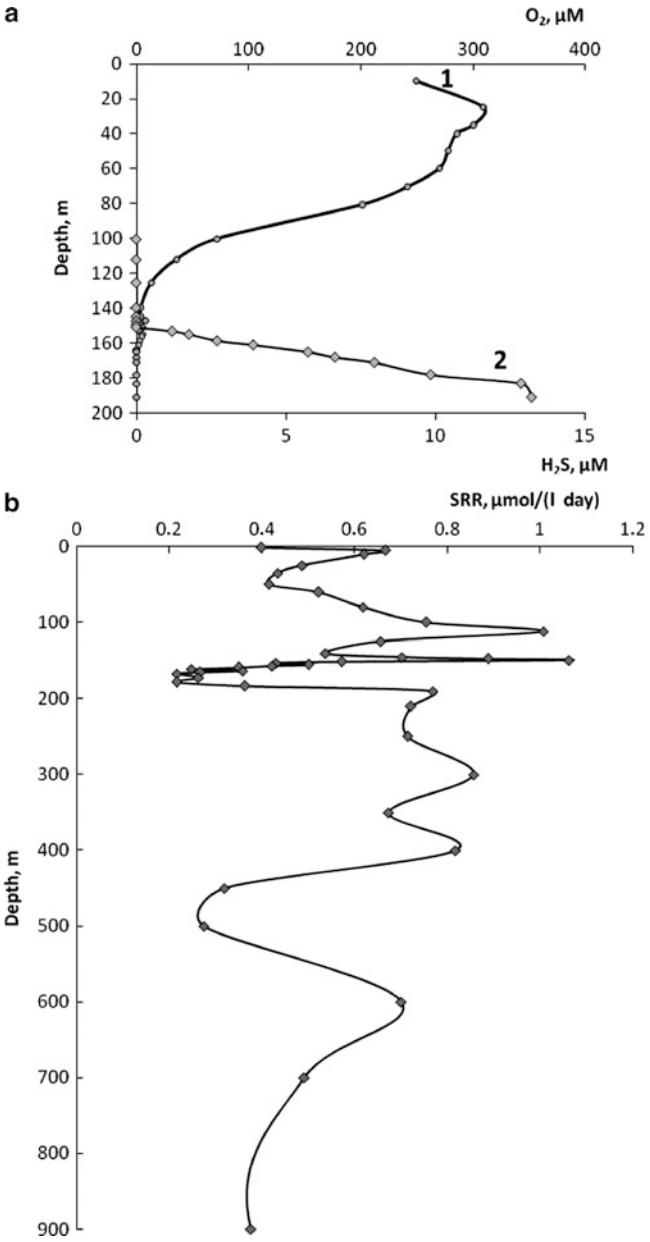

Fig. 1 Oxygen and sulfide concentrations (**a**) and sulfate reduction rates (**b**) in the water column of the Black Sea deep-water zone near Gelendzhik (St. 2900, depth 1,300 m)

the limit of the Winkler method (~3 μM), but also at the 100–110-m depth and in subsurface water (Fig. 1).

Methane content in the water column is typical of the Black Sea deep-water zone, with a sharp increase in methane content below 150 m. However, a certain

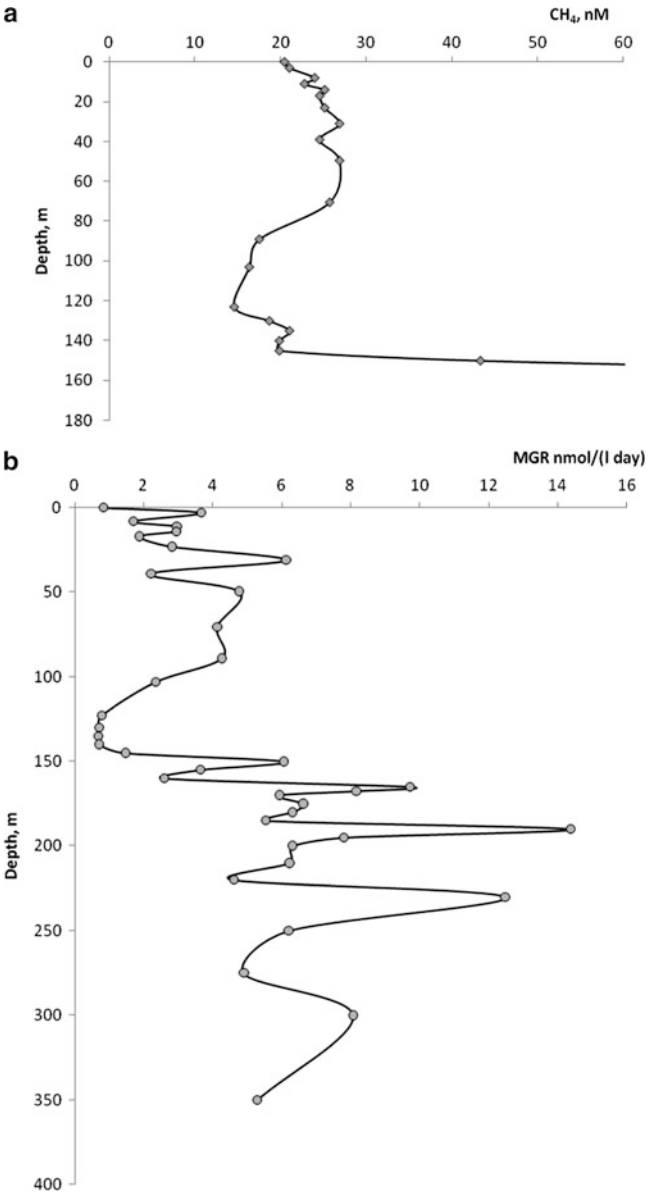

Fig. 2 Methane concentration (**a**) and methanogenesis rates (**b**) in the water column of the Black Sea deep-water zone near Gelendzhik (St. 2900, depth 1,300 m)

increase in CH_4 concentration was detected in the aerobic zone (10–70 m) (Fig. 2a). Radioisotope measurements confirmed hydrogenotrophic methanogenesis in aerobic waters with its highest rates at 30–90-m depth (Fig. 2b).

3.2 Detection of SRB and Methanogenic Archaea in Aerobic Surface Waters

At the depth of 30 m, most prokaryotic cells (~75% of the total number of DAPI-stained cells) belonged to bacteria (probes EUB338 + EUB338 II). The number of archaea (probes ARCH915 + ARCH344) in surface water did not exceed 11% of the total microbial number. Cocci and short rods were predominant at small depths (~90%), while filamentous forms were not revealed.

In the aerobic zone of the continental slope (300 μM O_2, 8.82×10^5 DAPI-stained cells ml^{-1}), SRB of the genera *Desulfotomaculum*, *Desulfovibrio*, and *Desulfobacter* were numerous, constituting 22.9, 21.15, and ~5% of the total microbial number, respectively (Table 2; Fig. 3). Members of these genera were found at this depth in the central part of the Black Sea. Active *Desulfotomaculum* cells (probe Dtm229) were almost never retrieved from greater depths.

While the number of subgroup 1 methanogenic archaea (probe MB1174 for *Methanobacterium*, *Methanobrevibacter*, and *Methanosphaera*) in oxygen-rich surface water was low (~4%), they still constituted ~35% of archaeal cells in the aerobic zone (Table 2; Fig. 3f). Unexpectedly, the remaining 62% of archaea in the surface water were hybridized with the probe MG1200b for *Methanomicrobiales* (subgroup 2 methanogenic archaea; Table 2). Since dividing cells emitted the brightest signals, these results demonstrate the presence of active methanogens in the uppermost horizons of the Black Sea water column.

3.3 Structure of Anaerobic Microbial Communities in the Chemocline of the Black Sea

The average total microbial number in the upper zone of the chemocline at the continental slope (149–152 m, 3–6 μM O_2) was 20% higher than in the upper oxic layers. While coccoid forms still prevailed among bacteria, their ratio decreased from 75 to 40% of the total number of microorganisms, whereas the number of archaea increased to 36–47% of DAPI-stained cells. Unlike surface waters, rod-shaped cells were found, often in filament-like chains. In the chemocline and below, the ratio of rod-shaped forms, both bacterial and archaeal, increased with depth, reaching 10.5 and 33%, respectively.

Desulfomicrobium species were the dominant phylogenetic group of sulfate reducers in the chemocline [13.4% of the total microbial number, 1.06×10^6 cells ml^{-1} (Table 2; Fig. 4)]. In the central deep-water zone of the Black Sea, at the depth of 115 m (3 μM O_2), *Desulfomicrobium* sp. predominated among sulfate reducers. Almost no *Desulfomicrobium* cells were found in the oxidized surface water and in anaerobic deep horizons.

In the water column of the continental slope at 157.5 m, where traces of sulfide appeared, the number of microbial cells was about 30% lower than in the upper

Table 2 Distribution of sulfate-reducing bacteria and methanogenic archaea in the water column of the Black Sea continental slope

Probe/stain	Cells, ml^{-1}					
	30 m	150 m	157.5 m	167.5 m	210 m	600 m
DAPI	8.82×10^5	1.06×10^6	7.11×10^5	1.23×10^6	1.60×10^6	2.58×10^5
EUB338 + EUB338 II	6.60×10^5 (74.8%)	4.24×10^5 (40.0%)	2.72×10^5 (38.2%)	5.62×10^5 (45.7%)	5.49×10^5 (34.3%)	8.80×10^4 (34.1%)
ARCH344 + ARCH915	1.02×10^5 (11.6%)	4.77×10^5 (45.0%)	3.35×10^5 (47.1%)	4.47×10^5 (36.3%)	4.43×10^4 (2.8%)	3.87×10^3 (1.5%)
DSB129	4.40×10^4 (6.7%)	ND	ND	ND	ND	ND
DSV214	ND	1.42×10^5 (33.5%)	6.60×10^4 (24.3%)	ND	4.04×10^3 (0.7%)	2.40×10^3 (2.7%)
DSV698	1.95×10^5 (29.6%)	ND	ND	ND	ND	ND
DSV1292	1.23×10^5 (18.6%)	4.10×10^4 (9.7%)	1.91×10^4 (7.0%)	2.58×10^4 (4.6%)	4.01×10^3 (0.4%)	3.3×10^3 (3.75%)
Dtm229	2.01×10^5 (30.5%)	ND	ND	ND	ND	ND
MB1174	3.60×10^4 (35.3%)	ND	ND	4.93×10^4 (11.0%)	3.01×10^4 (67.9%)	2.39×10^3 (61.8%)
MG3	4.75×10^4 (46.6%)	6.25×10^4 (13.1%)	5.23×10^4 (15.6%)	ND	ND	ND
MG1200b	6.32×10^4 (62.0%)	ND	ND	2.46×10^4 (7.3%)	ND	ND

ND, not detected or individual cells

The percentage of bacteria (probes EUB338 + EUB338 II) and archaea (probes ARCH344 + ARCH915) from the total number of DAPI-stained microbial cells is presented

For sulfate reducers and methanogens, the percentage of the number of bacterial and archaeal cells, respectively, is presented

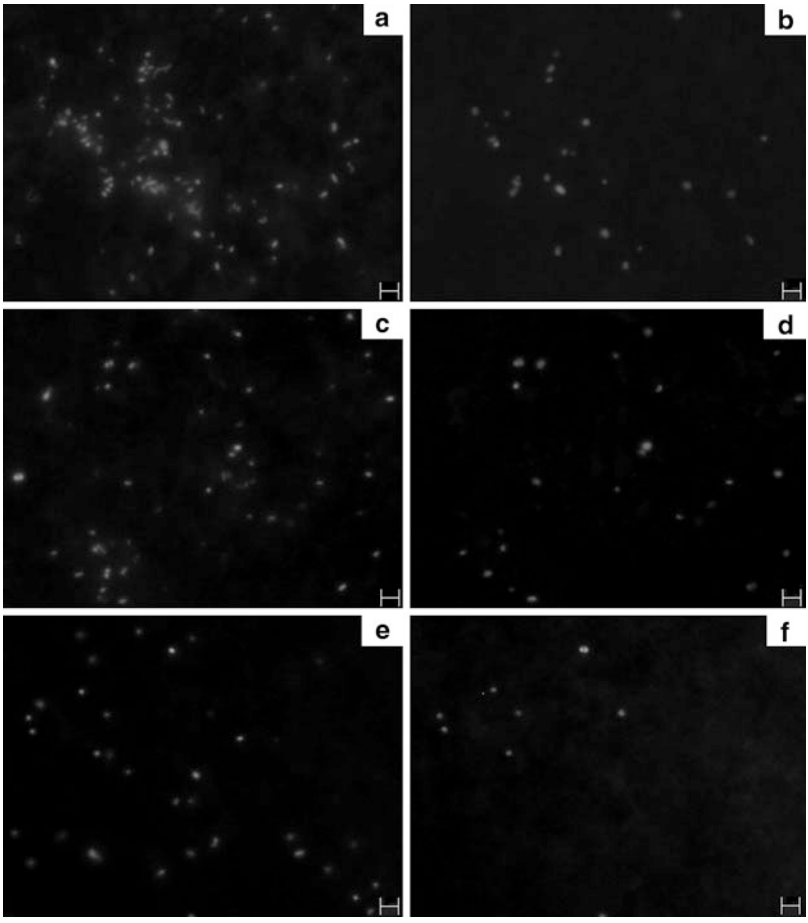

Fig. 3 Digital micrographs of the total microbial population (DAPI staining) (a, c, e), SRB *Desulfotomaculum* (probe Dtm229) (b) and *Desulfovibrio* (probe DSV698) (d), and subgroup 1 methanogenic archaea (probe MB1174) (f) from the water sample collected at the continental shelf at 30 m (aerobic waters). Scale bar on Figs. 3 and 4 is 2 μm

chemocline zone. Sulfate reducers of the genus *Desulfomicrobium* were still present. The results obtained with the probe DSV1292 demonstrated the presence of *Desulfovibrio* species at this depth (5–10% of the total bacterial number), while the probe DSV698 (specific to 16S rRNA of 14 *Desulfovibrio* species) did not detect sulfate reducers (Table 2). The probe DSB985, specific to *Desulfobacter*, *Desulfobacula*, *Desulfospira*, and *Desulfotignum*, also gave almost no hybridization signal in the chemocline.

In the chemocline zone, methanogens ($5–6 \times 10^4$ cells ml^{-1}) were revealed only with the MG3 universal probe. The probe MB1174, specific to *Methanobacterium*, *Methanobrevibacter*, and *Methanosphaera* (subgroup 1 methanogens), gave practically no hybridization signals at the depths of 150 and 157.5 m (Table 2).

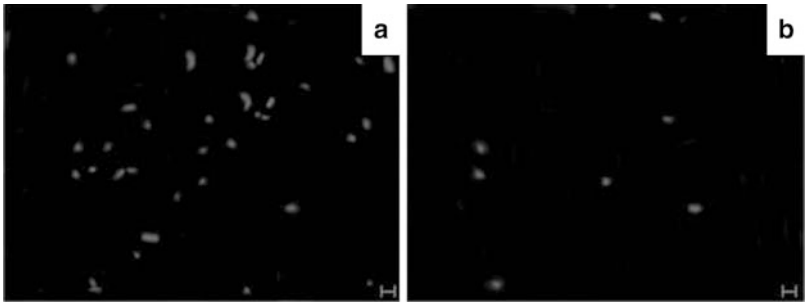

Fig. 4 Digital micrographs of the total microbial population (DAPI staining) (**a**) and *Desulfomicrobium* sulfate-reducing bacteria (probe DSV214) (**b**) from the water sample collected at the continental shelf at 150 m (chemocline zone)

The border between oxidized and reduced water layers at the continental slope station was at 165–167-m depth. Below 167 m, sulfide was present in the water and the concentration of dissolved methane increased drastically. The number of prokaryotic cells increased. Cells of methanogens of subgroups 1 and 2 were detected at the depth of 167.5 m; 11 and 7.3% of all archaeal cells were revealed by the probes MB1174 and MG1200b, respectively (Table 2).

Detection of SRB and methanogenic archaea in the aerobic zone correlates with the profiles of sulfate reduction and methanogenesis. Four peaks of sulfate reduction (5, 25, 120, and 180 m) and five peaks of methanogenesis (5, 15, 30, 150, and 165 m) can be seen at the depths from 0 to 200 m (Figs. 1, 2).

3.4 Identification of SRB from Enrichment Cultures Isolated from Aerobic Water and the Chemocline Zone

In enrichment cultures from the depths of 30 and 70 m, the number of active bacterial cells revealed with EUB338 + EUB338 II did not exceed 39% of the total cell number (Table 3). From 120 m (lower chemocline) and 165 m (anaerobic sulfide-containing water), SRB enrichments were obtained containing 63 and 67% of active bacterial cells, respectively.

In anaerobic SRB enrichments isolated from the aerobic zone of the Black Sea (30 and 70 m), *Desulfomicrobium*-related organisms were predominant (6.2 and 20% of total bacterial cell numbers, respectively), while the probe SRB385 for sulfate-reducers of the δ-*Proteobacteria* group revealed 11% of the cells (Table 3). SRB enrichments obtained from the water samples of the lower chemocline in the deep part of the Black Sea contained species of the genera *Desulfovibrio* (DSV1292, 23%), *Desulfotomaculum* (7.6%), and *Desulfomicrobium* (up to 4%). The probe SRB385 revealed 9% of the cells. No *Desulfobacter* sp. cells were detected (Table 3).

Table 3 Numbers of sulfate-reducing bacterial cells in enrichment cultures obtained from the samples of the central zone of the Black Sea (RV *Professor Shtokman*, station 20, March 2009)

Probe/stain	Cells, ml^{-1}			
	30 m, aerobic zone	70 m, aerobic zone	120 m, lower chemocline	165 m, anaerobic zone
DAPI	1.03×10^7	2.20×10^7	2.33×10^8	4.41×10^8
EUB338 + EUB338 II	3.80×10^6 (36.9%)	8.60×10^6 (39.1%)	1.49×10^8 (63.9%)	2.96×10^8 (67.1%)
DSB129	2.20×10^5 (5.6%)	7.90×10^4 (0.9%)	ND	ND
DSV214	2.40×10^5 (6.2%)	1.70×10^6 (20.0%)	5.65×10^6 (3.8%)	5.65×10^6 (1.9%)
DSV698	ND	ND	ND	ND
DSV1292	1.40×10^5 (3.5%)	6.80×10^4 (0.8%)	3.44×10^7 (23.1%)	3.07×10^7 (10.4%)
Dtm229	1.60×10^5 (4.3%)	2.80×10^5 (3.3%)	1.13×10^7 (7.6%)	1.32×10^7 (4.5%)
SRB385	4.30×10^5 (11.1%)	9.50×10^5 (11.0%)	1.34×10^7 (9.0%)	ND

ND, not detected or individual cells

The percentage of bacteria (probes EUB338 + EUB338 II) from the total number of DAPI-stained microbial cells is presented

For sulfate reducers, the percentage of the number of bacterial cells is presented

3.5 *Detection of Active Prokaryotic Cells in the Anaerobic Water of the Black Sea*

For the water horizons below 200 m, hybridization with the most probes for the major groups of sulfate-reducers and methanogens was either absent or close to the lower limit of sensitivity for the FISH method (below 4%) both in winter and in summer (Table 2). Only the probe MB1174 (for subgroup 1 methanogens) produced a positive signal for about 11 and 5.3–5.5% of the total cell number (for 186 and 250–600 m, respectively).

At the upper border of sulfide-containing water (210 m, continental slope), the number of microorganisms (over 1.60×10^6 cells ml^{-1}) was the highest for the water column. It was 187% of their number at 30-m depth and 130–150% of microbial numbers in the central part of the chemocline. In the central part of the Black Sea, microbial numbers peaked at the depths of 80 and 115 m, i.e., in the lower chemocline and the upper border of sulfide-containing waters (7.66×10^5 and 7.16×10^5 cells ml^{-1}, respectively). Microbial numbers then gradually decreased to 1.80×10^5 cells ml^{-1} at 600 m. By 600 m, the ratio of archaea decreased to several percent; numerous filamentous prokaryotic forms (up to 15% of the total microbial number) were found at big depths. At the greatest depths of 1,500–1,940 m, the number of microorganisms was $2.1–2.7 \times 10^5$ cells ml^{-1}, with significant predominance of bacteria.

However, the universal bacterial and archaeal probes demonstrated the presence of active microorganisms (up to 10^5 cells ml^{-1}) in the deep-water zone, although the ratio of the cells detected with EUB338 + EUB338 II and ARCH344 + ARCH915 to the total number of DAPI-stained cells decreased significantly (34–45%).

4 Discussion

Our data on prokaryote numbers in the surface Black Sea waters correlate well with the results of previous works [5, 8], reporting elevated microbial numbers in the oxic surface waters of the Black Sea ($3.04–8.48 \times 10^5$ cells ml^{-1}), with bacteria as the dominant group (up to 65–77% of the cells).

The number of prokaryotic cells determined by FISH with universal bacterial and archaeal primers was somewhat lower than the number of microorganisms determined by staining with DAPI, a universal DNA stain. However, in some experiments in the aerobic and chemocline zones, application of these domain-specific probes resulted in total microbial numbers as high as 82–86% of DAPI-stained cells (Table 2). Moreover, although DAPI is considered a DNA-specific stain and a de facto standard for enumeration of microorganisms, nonspecific staining of nonmicrobial particles has been reported [31]. Thus, FISH provides sufficiently reliable data for quantitative assessment of microbial communities in the upper part of the water column. High numbers of metabolically active microorganisms in the aerobic horizons result probably from high levels of available organic matter, both produced by photosynthesis and arriving with river flow.

A mixture of two known probes for the *Archaea* domain (ARCH915 and ARCH344) was used in order to achieve the highest possible retrieval. Application of the universal probe EUB338 for the *Bacteria* domain is reasonable for detection of bacterial cells in the aerobic and chemocline zones, while its combination with EUB338 II (for *Planctomycetes*, including the ANAMMOX bacteria) should be recommended for anaerobic Black Sea waters.

Investigation of the structure of methanogenic archaeal communities of the Black Sea waters suggested that a combination of the probes MB1174 (for subgroup 1 methanogens *Methanobacterium*, *Methanobrevibacter*, and *Methanosphaera*) and MG1200b (for subgroup 2 *Methanomicrobiales*) is preferable to the universal probe MG3, which is insufficiently specific for identification of methanogens.

Detection of viable SRB in Black Sea aerobic waters correlates with the hydrochemical data [4], confirming the traces of reduced sulfur compounds in aerobic seawater, and with our measurements of sulfate reduction rates (Fig. 1). Our measurement of methane distribution in the aerobic waters of the Black Sea (Fig. 2) and the data of [32] revealed CH_4 in the depth range from 30 to 40 m; methanogenesis was detected there by the radioisotope method ([33]; our data, Fig. 2). Thus, although sulfate reducers and methanogens, as strictly anaerobic organisms, should have been expected to occur only in deep, anaerobic horizons,

their active cells were present in significant numbers in upper, aerobic waters. It has been earlier demonstrated that pronounced isotopic fractionation of methane in the chemocline correlated with increased numbers of bacteria and archaea involved in methane oxidation [5].

The previous investigation of Black Sea SRB with only one probe (SRB385) revealed a peak of (not identified more precisely) sulfate reducers immediately above the upper boundary of anaerobic, sulfide-containing waters, i.e., in the chemocline zone; these results were described as paradoxical [6]. Moreover, real-time PCR was used to assess the copy number of the *dsrA* functional gene, encoding the (bi)sulfite reductase α subunit, in the Black Sea water column. These data confirmed the peaks of SRB numbers at 95 m (in the chemocline) and 150 m (upper anoxygenic zone) [34]. This research established the SRB ratio among bacterial cells of only 0.1% in the surface water, up to 1.9% in the chemocline, and up to 4.7% in anoxic water, with deep-water SRB belonging to the *Desulfonema–Desulfosarcina* cluster [34]. We attempted more detailed investigation of SRB distribution in the Black Sea upper horizons with specific probes to the known genera of sulfate reducers.

Diversity of the antioxidant protective mechanisms in some sulfate reducers, especially in *Desulfovibrio* and *Desulfotomaculum* species, makes it possible for them to occupy the econiches and even to reduce sulfate in microaerobic zones of heterogeneous habitats (temporarily flooded soils, the photic zone of cyano–bacterial mats, biofilms, groundwater, etc.) [9, 10]. They thus gain advantage in competition for the substrates and may survive under varying environmental conditions. Such hydrological processes as advective penetration of deep water, resulting in mixing of the water layers and of microbial populations, are another, albeit less probable explanation for the presence of SRB in significant numbers in the upper horizons of the Black Sea water.

Although methanogens are strict anaerobes, some of them may also survive oxygen due to the antioxidant protective enzymes, by formation of cell aggregates, or in consortia with facultative anaerobes. It is presently maintained, however, that methanogenesis may be carried out only in anaerobic microniches [10]. The fact that many of methanogens' cells retrieved from 30-m depth were inside cell aggregates or were surrounded by particles (probably organic) seems to support this notion.

In the chemocline of the continental slope, *Desulfomicrobium* was the dominant SRB, while the number of *Desulfovibrio* was significantly lower than in aerobic waters. *Desulfobacter* and *Desulfotomaculum* cells, which were present in the aerobic layers, were not detected in the chemocline samples (Table 2).

The structure of the SRB community in enrichment cultures differed significantly from that observed in native water samples, since conventional enrichment cultures did not reproduce in situ conditions, especially those of the aerobic marine environment. For example, while *Desulfotomaculum* and *Desulfovibrio* species prevailed in the samples from the surface oxic layers (Dtm229 and DSV698 or DSV1292, 30.5 and 18.6–29.6% of the total number of bacterial cells, respectively), in enrichment cultures from the aerobic zone, only 4.3 and 3.5% of the cells were

revealed by the probes Dtm229 and DSV1292, respectively. While Dtm229 was designed as a specific probe for *Desulfotomaculum* [28], it also targets other *Firmicutes*. The high *Desulfotomaculum* numbers revealed with this probe may therefore be an overestimate; however, high numbers of targeted microorganisms, which are mostly anaerobes, still deserve consideration. In any case, the enrichment conditions favoring SRB growth were probably less favorable to other bacteria hybridizing with Dtm229. For the chemocline zone, significant differences between the native samples and SRB enrichments were also observed. For example, in the samples collected from the lower chemocline, DSV214 and DSV1292 revealed ~24 and 7% of bacterial cells, respectively, while Dtm229 detected no microorganisms. For the relevant enrichments, the values obtained with these probes are 3.8, 23.1, and 7.6%, respectively (Tables 2 and 3). Thus, enrichment cultures should not be relied upon in assessment of the SRB community structure in marine environments.

Importantly, in the samples collected in March in the central part of the Black Sea, the number of detected prokaryotic cells both in the surface waters and in the chemocline zone was about 1.5 times lower than in the samples collected in summer from the continental slope near Gelendzhik. In the chemocline, the ratio of archaeal cells decreased significantly, to several percent of the total microbial number. The number of active SRB revealed by FISH also decreased drastically (3–5 times lower than in the summer samples), although the distribution of the phylogenetic groups of sulfate reducers resembled that obtained for the water column of the continental slope. In this case, the ratio of methanogens (probe MB1174) in the chemocline zone was only 0.5–0.7% of the total cell number. This decrease in microbial numbers is probably associated with the sharp decrease in bacterioplankton concentration (and consequently in the content of available organic matter) in winter.

The universal and specific probes for methanogens used in this work exhibited significantly lower hybridization in the deep water of the Black Sea. This may result from low RNA content in the cells of deep-water microorganisms, exhibiting low metabolic activity, as well as from the possible presence of prokaryotes of the phylogenetic groups not detected by the probes applied in statistically significant amounts. These results correlate with the data of earlier investigations, also reporting low detection of prokaryotes, especially archaea, in Black Sea anaerobic waters, compared to other marine environments [6]. Moreover, application of FISH for detection of marine prokaryotes has certain limitations depending on their metabolic activity [35]. According to [6], in the Black Sea water column the average number of cells detected with EUB338 + ARCH915 was 55% of the number determined by DAPI staining, while this ratio reached 82% in the meromictic marine Cariaco Basin. It has been previously demonstrated that the ratio of sulfate reducers in anaerobic Black Sea waters was 3–7%, and the total number of DAPI-stained microorganisms in this environment was about $2.11–4.47 \times 10^5$ cells ml^{-1}, with *Bacteria* being the main and predominant group [5, 8]. While the number of prokaryotic cells (bacteria and archaea) detected by FISH was about 85% of the number of DAPI-stained cells in the aerobic water and the chemocline zone, at depths exceeding 167.5 m it decreased significantly to less than 40% of the total cell number.

Members of archaeal groups ANME-1 and ANME-2 found in the chemocline and anaerobic waters (anaerobic methanotrophs) probably formed consortia with SRB present in the same horizons [5, 35, 36]. The members of *Bacteria* (probe EUB338), depending on depth, constituted 21–65% of the total number of free-living microorganisms. It was impossible to determine the phylogenetic position of a significant part of the Black Sea bacteria (~57%) with the probes specific for the major bacterial subdomains (α-, β-, and γ-*Proteobacteria*, sulfate-reducing δ-*Proteobacteria*, and the CFB group) [6].

It was also found [6] that the average number of archaea (hybridization with ARCH915) in the central part of the Black Sea was 14% for the chemocline zone, while it was 2% in the surface water (0–30 m) and 7% in the anaerobic layers (115–2,000 m). Throughout the Black Sea water column, most of the identified archaea belonged to *Crenarchaeota*, with the highest content of this group in the central part of the sea at 77-m depth.

Our detection of physiologically active SRB and methanogenic archaea in aerobic water layers and in the oxic–anoxic interface correlates with our data on radioisotope measurement of the rates of microbial processes, which demonstrated the highest activity of microbial communities of the Black Sea deep waters in the 100–300-m depth range, i.e., close to the boundary between reduced and oxidized waters [8].

The probes for detection of sulfate-reducing archaea were not used in the present work. While oligonucleotide probes suitable for reliable detection of *Archaeoglobus* cells by FISH exist presently [37], these hyperthermophilic archaea, according to the published data, have never been recovered from the water column of meromictic basins.

Thus, the results of both FISH and radioisotope measurement of the rates of sulfate reduction and methanogenesis indicate active sulfate reduction in the aerobic waters of the Black Sea. The aerobic surface waters and the boundary between aerobic and anaerobic waters (chemocline zone) differed in both the total microbial numbers and the phylogenetic composition of the physiologically active anaerobic microbial community. High abundance of SRB of the genera *Desulfotomaculum* and *Desulfovibrio*, which exhibit relatively high aerotolerance, was discovered in the oxidized surface horizons. In the chemocline zone, the cells of *Desulfomicrobium* and, to a lesser degree, *Desulfovibrio* were found. However, *Desulfomicrobium* and *Desulfovibrio* prevailed in anaerobic enrichment cultures obtained from the water samples of the aerobic and chemocline zone, respectively.

Our results demonstrate a significant biogeochemical and ecological role of SRB and methanogenic archaea in the aerobic zone, chemocline, and upper anaerobic horizons of the Black Sea. Our subsequent research will be focused on better understanding of the complex structure of the Black Sea microbial communities (including isolation of pure cultures) and the ecophysiology of microbial activity in the water column, depending on the season, distribution of electron donors and acceptors, rates of substrate utilization, and other variable environmental parameters.

Acknowledgments The authors are grateful to the crew of RV *Aquanavt* for their help in organization of the expedition and water sampling, and Laboratory of Marine Chemistry, Southern Branch of Shirshov Institute of Oceanology for providing of chemical analyses. This work was supported by the Russian Foundation for Basic Research, project no. 10-04-00220-a.

References

1. Skopintsev BA (1975) Formirovanie sovremennogo gidrokhimicheskogo sostava Chyornogo morya (Formation of the modern chemical composition of the Black Sea). Hydrometeoizdat, Leningrad, p 336
2. Murray JW, Jannash HW, Honjo S, Anderson RF, Reeburgh WS, Top Z, Friederich GE, Codispoti LA, Izdar E (1989) Unexpected changes in the oxic/anoxic interface in the Black Sea. Nature 338:411–413
3. Ivanov MV, Lein AYu, Karnachuk OV (1992) New evidence of the biogenic nature of Black Sea H_2S. Geokhimiya 8:1186–1194 (in Russian)
4. Volkov II, Rozanov AG, Demidova TP (1992) Winter state of the ecosystem of the open Black Sea. In: Vinogradov ME (ed) Inorganic reduced sulfur compounds and reduced manganese in Black Sea water. IO RAN, Moscow, pp 38–50 (in Russian)
5. Durisch-Kaiser E, Klauser L, Wehrli B, Schubert C (2005) Evidence of intense archaeal and bacterial methanotrophic activity in the Black Sea water column. Appl Environ Microbiol 71:8099–8106
6. Lin X, Wakeham SG, Putnam IF, Astor YM, Scranton MI, Chistoserdov AY, Taylor GT (2006) Comparison of vertical distributions of prokaryotic assemblages in the anoxic Cariaco Basin and Black Sea by use of fluorescence in situ hybridization. Appl Environ Microbiol 72:2679–2690
7. Pimenov N, Neretin L (2006) Composition and activities of microbial communities involved in carbon, sulfur, nitrogen and manganese cycling in the oxic/anoxic interface of the Black Sea. In: Neretin L (ed) Past and present water column anoxia, NATO Science Series. Springer, New York, pp 501–522
8. Pimenov NV, Rusanov II, Yusupov SK, Fridrich J, Lein AYu, Wehrli B, Ivanov MV (2000) Microbial processes at the aerobic–anaerobic interface in the deep-water zone of the Black Sea. Microbiology 69:527–540
9. Dolla A, Fournier M, Dermoun Z (2006) Oxygen defence in sulfate-reducing bacteria. J Biotechnol 126:87–100
10. Brioukhanov AL, Netrusov AI (2007) Aerotolerance of strictly anaerobic microorganisms and factors of defense against oxidative stress: a review. Appl Biochem Microbiol 43:567–582
11. DeLong EF, Taylor LT, Marsh TL, Preston CM (1999) Visualization and enumeration of marine planctonic archaea and bacteria by using polyribonucleotide probes and fluorescent in situ hybridization. Appl Environ Microbiol 65:5554–5563
12. Cottrell MT, Kirchman DL (2000) Community composition of marine bacterioplankton determined by 16S rRNA gene clone libraries and fluorescence in situ hybridization. Appl Environ Microbiol 66:5116–5122
13. Hansen HP (1999) Determination of oxygen. In: Grashoff K, Kremling K, Ehrhard M (eds) Methods of seawater analysis. 3d, completely revised and extended edition. Wiley-VCH, Weinheim-New York-Chichester-Brisbane-Singapore-Toronto, pp 75–90
14. Hansen HP, Koroleff F (1999). Determination of nutrients. In: Grashoff K, Kremling K, Ehrhard M (eds) Methods of seawater analysis. 3d, completely revised and extended edition. Wiley-VCH, Weinheim-New York-Chichester-Brisbane-Singapore-Toronto, pp 149–228
15. Trüper HG, Schlegel HG (1964) Sulfur metabolism in Thiorhodaceae. I. Quantitative measurements in growing cells of *Chromatium okenii*. Antonie van Leeuwenhoek J Microbiol Serol 30:225–238

16. Widdel F, Back F (1992) The genus *Desulfotomaculum*. In: Dworkin M, Falkow S, Rosenberg E, Schleifer K-H, Stackebrandt E (eds) The prokaryotes (Ecophysiology and Biogeochemistry), vol 4. Springer, New York, pp 787–794
17. Widdel F, Pfennig N (1981) Studies on dissimilatory sulfate-reducing bacteria that decompose fatty acids. I. Isolation of new sulfate-reducing bacteria enriched with acetate from saline environments. description of *Desulfobacter postgatei* gen. nov., sp. nov. Arch Microbiol 129: 395–400
18. Hungate RE (1969) A roll tube method for the cultivation of strict anaerobes. In: Norris JR, Ribbons DW (eds) Methods in microbiology, vol 3B. Academic, New York, pp 117–132
19. Amann RI, Zarda B, Stahl DA, Schleifer K-H (1992) Identification of individual prokaryotic cells by using enzyme-labeled, rRNA-targeted oligonucleotide probes. Appl Environ Microbiol 58:3007–3011
20. Glockner FO, Amann R, Alfreider A, Pernthaler J, Psenner R, Trebesius K, Schleifer K-H (1996) An in situ hybridization protocol for detection and identification of planctonic bacteria. Syst Appl Microbiol 19:403–406
21. Pernthaler A, Pernthaler J, Amann R (2002) Fluorescence in situ hybridization and catalyzed reporter deposition for the identification of marine bacteria. Appl Environ Microbiol 68: 3094–3101
22. Amann RI, Binder BJ, Olson RJ, Chisholm SW, Devereux R, Stahl DA (1990) Combination of 16S rRNA-targeted oligonucleotide probes with flow cytometry for analyzing mixed microbial populations. Appl Environ Microbiol 56:1919–1925
23. Stahl DA, Amann RI, Poulsen LK, Raskin L, Capman WC (1995) Use of fluorescent probes for determinative microscopy of methanogenic archaea. In: Sowers KR, Schreier HJ (eds) Archaea: Methanogens: a laboratory manual. Cold Spring Harbor Laboratory Press, New York, pp 111–121
24. Raskin L, Stromley JM, Rittmann BR, Stahl DA (1994) Group-specific 16S rRNA hybridization probes to describe natural communities of methanogens. Appl Env Microbiol 60: 1232–1240
25. Crocetti G, Murto M, Björnsson L (2006) An update and optimisation of oligonucleotide probes targeting methanogenic archaea for use in fluorescence in situ hybridisation (FISH). J Microbiol Methods 65:194–201
26. Devereux R, Kane MD, Winfrey J, Stahl DA (1992) Genus- and group-specific hybridization probes for determinative and environmental studies of sulfate-reducing bacteria. Syst Appl Microbiol 15:601–609
27. Manz W, Eisenbrecher M, Neu TR, Szewzyk U (1998) Abundance and spatial organization of gram-negative sulfate-reducing bacteria in activated sludge investigated by in situ probing with specific 16S rRNA targeted oligonucleotides. FEMS Microbiol Ecol 25:43–61
28. Hristova KR, Mau M, Zheng D, Aminov RI, Mackie RI, Gaskins HR, Raskin L (2000) *Desulfotomaculum* genus- and subgenus-specific 16S rRNA hybridization probes for environmental studies. Environ Microbiol 2:143–159
29. Lücker S, Steger D, Kjeldsen KU, MacGregor BJ, Wagner M, Loy A (2007) Improved 16S rRNA-targeted probe set for analysis of sulfate-reducing bacteria by fluorescence in situ hybridization. J Microbiol Methods 69:523–528
30. Ivanov MV, Pimenov NV, Rusanov II, Lein AYu (2002) Microbial Processes of the Methane Cycle at the North-western Shelf of the Black Sea. Estuarine, Goastal and Shelf Sci 54:589–599
31. Weinbauer MG, Beckmann C, Höfle MG (1998) Utility of Green fluorescent nucleic acid dyes and aluminum oxide membrane filters for rapid epifluorescence enumeration of soil and sediment bacteria. Appl Environ Microbiol 64:5000–5003
32. Egorov AV (2002) Patterns of methane distribution in the water column of northeastern Black Sea in complex investigation of northeastern Black Sea. Nauka, Moscow, pp 183–190 (in Russian)

33. Rusanov II, Yusupov SK, Savvichev AS, Lein AYu, Pimenov NV, Ivanov MV (2004) Microbial production of methane in the aerobic water layer of the Black Sea. Doklady Acad Sci 399:493–495
34. Neretin LN, Abed RM, Schippers A, Schubert CJ, Kohls K, Kuypers MM (2007) Inorganic carbon fixation by sulfate-reducing bacteria in the Black Sea water column. Environ Microbiol 9:3019–3024
35. Karner M, Furner J (1997) Determination of active marine bacterioplankton: a comparison of universal 16S rRNA probes, autoradiography, and nucleoid staining. Appl Environ Microbiol 63:1208–1213
36. Vetriani C, Tran HV, Kerkhof LJ (2003) Fingerprinting microbial assemblages from the oxic/anoxic chemocline of the Black Sea. Appl Environ Microbiol 69:6481–6488
37. Loy A, Lehner A, Lee N, Adamczyk J, Meier H, Ernst J, Schleifer KH, Wagner M (2002) Oligonucleotide microarray for 16S rRNA gene-based detection of all recognized lineages of sulfate-reducing prokaryotes in the environment. Appl Environ Microbiol 68:5064–5081

The Energetic Balance of Microbial Exploitation of Pelagic Redox Gradients

G. Jost and F. Pollehne

Abstract In marine environments and especially in marginal seas, pelagic redox gradients with underlying sulfidic water layers are a known phenomenon. General explanations for the observed spatial distribution and amount of chemolithoautotrophic carbon dioxide fixation within these redox zones persisted for decades. Here, we try to combine the assessment of fluxes of electron acceptors and donors which fuel chemolithoautotrophy, including energetic aspects of different reactions with observations on the microbial taxonomic structure within marine redox gradients. Although modern molecular techniques help to identify the acting organisms and verify chemolithoautotrophy on the process level, there are still gaps that need to be solved. Within the energetic frame of contributing reactions, there is still the option of the presence of hitherto undescribed physiological pathways. In this environment, characterized by strong gradients, new approaches need verification by incubation-independent methods to eliminate artifacts.

Keywords Carbon dioxide fixation, Chemolithoautotrophy, Electron acceptors, Electron donors, Microbial communities, Pelagic redox zones

Contents

G. Jost (✉) and F. Pollehne
Leibniz Institute for Baltic Sea Research Warnemünde, Seestrasse 15, 18119 Rostock, Germany
e-mail: guenter.jost@io-warnemuende.de

E.V. Yakushev (ed.), *Chemical Structure of Pelagic Redox Interfaces: Observation and Modeling*, Hdb Env Chem (2013) 22: 47–66, DOI 10.1007/698_2011_104,

Abbreviations

DAPI	4′,6-Diamidino-2-phenylindole, a fluorescence stain that binds strongly to nucleic acids
MICRO-CARD-FISH	Fluorescence in situ hybridization combined with micro-autoradiography
OMZ	Oxygen minimum zone

1 Introduction

Organisms living below the euphotic zone in marine environments are dependent on the organic matter supplied to this environment. Here, the quantity and quality of organic carbon is in most cases the limiting factor for heterotrophic growth. In some cases, also oxygen becomes limiting for metabolic processes in deeper layers, mostly as an effect of reduced water circulation. These oxygen minimum zones (OMZ) are well-known phenomena in oceanography. It is assumed that the extension of hypoxic zones will increase especially in coastal marine waters due to both eutrophication and global warming [1] with severe effects on these ecosystems. The supply of both oxygen and organic carbon to layers below the euphotic zone of most marine systems is essential to maintain lives of higher organisms, as nearly all living organisms beyond the prokaryotic level depend on oxygen as terminal electron acceptor generating energy by respiration of organic material.

OMZs in the open ocean like in the Arabian Sea or in the central Pacific are under recent conditions not exhausting the total oxygen and nitrate inventory, as the organic input from the oligotrophic surface layer is comparatively low. Hypoxia in coastal waters (oxygen concentration below 2 mL L^{-1} or <90 μM) has a higher capacity of exhausting these resources of oxidants, and the system might turn to sulfate as electron acceptor because of higher biomasses, metabolic rates, concentrations of organics, and turnover of nutrients.

This shift is common within sediments, particularly in coastal areas [2]. Due to the reduced mobility of sedimentary pore-waters and the constant oxidation in surface sediments, this process remains largely unnoticed, since in most cases only the depth of the oxic–anoxic interface moves upward under reduced supply of electron acceptors. Most of the produced H_2S in sediments will be buried as pyrite in anoxic sediments [3] as long as iron is in good supply, but certain amounts of it will diffuse upward. Depending on the organic load of the sediment and the reduced flux of electron acceptors from supernatant water, which is already free of oxygen, the export of reduced compounds from sediments can push the redoxcline into the open water. This leads to higher H_2S concentrations in the overlying water than sulfate reduction processes within this water body could provide.

Pelagic redox gradients differ from benthic gradients, as they allow particulate phases to be sinking into deeper layers and therefore are selectively separating

elements. In a lot of coastal and marginal seas, pelagic redox zones are unstable on a regular seasonal basis or triggered by hydrographic events. This sometimes leads to the transport of oxygen-free or even sulfidic water into the surface layer and provokes undesired effects on higher organisms including humans. The occurrence of hydrogen sulfide in the water column documents an advanced stage in the development of hypoxia due to a larger imbalance in the fluxes of electron acceptors and electron donors. The depths, where such pelagic chemoclines [defined as the first appearance of H_2S (e.g., [4, 5])] are observed, depend on the equilibrium between the transport of electron acceptors and organic matter.

Although the term "suboxic" is widely used in oceanographic literature, the exact boundaries in terms of oxygen concentrations are rather diffuse. Values for the Black Sea range from 4.5 μM O_2 (e.g., [6]) to 15 μM O_2 [7]. More often a value of 10 μM is used [8]. Canfield and Thamdrup [9] argue for a stricter definition of this term, which is the base for a differentiation of biogeochemical processes. We advocate the value of about 10 μM O_2 thereby integrating water layers with enhanced nitrification from upward flux of ammonia, so that the major coupled nitrogen conversion processes are included. Here, we define the upper border of a pelagic redox zone as the layer, where denitrification is not detectable (which otherwise is often marked by a secondary nitrite peak) and nitrification is the dominant chemolithotrophic process. This usually is the case at oxygen concentrations of around 10 μM. The lower boundary is within the sulfidic layer at a concentration of about 10–15 μM hydrogen sulfide. This sulfide concentration seems to be the upper limit for a peak of enhanced carbon dioxide fixation [10–12], which is supposed to have a functional relation to the redox gradient. The absolute vertical extension of the pelagic redox gradient varies between the different ecosystems and shows a seasonal variability. This is due to the different strength of vertical mixing that merges sulfide from the deeper and oxygen from the surface layers.

Seasonal hypoxia often occurs at ocean margins dominated by large rivers, in estuaries and in brackish marginal seas [13]. Since decades, pelagic chemoclines have been quite well investigated in marine areas such as the Black Sea [14–16], the Cariaco Basin [17–19], the deep basins of the Baltic Sea [20–22], and several fjords like Framvaren [23, 24]. One of the largest hypoxic areas, besides the central Black Sea, is found in the Baltic [25, 26]. Here, changing areas of hypoxic bottom water are accompanied by often perennial anoxic bottom waters in the central basins.

Pelagic redox gradients are much more affected by lateral transport processes than their sedimentary images. Dependent on the basin morphology of different marine areas with pelagic redox zones, there are distinct depths at which lateral intrusions of water can occur, which then cause fluctuations in the depth of the oxycline or instabilities above the redox zone. Examples of these lateral intrusions are reported as inflow events into the western Black Sea [27, 28], in the Gotland Basin of the Baltic Sea [29], and in the Cariaco Basin [30].

A unique property of oxic/sulfidic pelagic redox zones is a pronounced peak in dark carbon dioxide fixation which was found in any of the investigated gradients. First, Sorokin [14] measured carbon dioxide fixation in the redox zone of the Black Sea and attributed it to bacterial chemosynthesis fueled by oxidation of reduced

sulfur compounds. It took about 15 years until this feature was observed in Cariaco Basin [31]. Earlier investigations by the same authors showed the occurrence of sulfide- and thiosulfate-oxidizing bacteria at the redox zones of the Black Sea and the Cariaco Basin, and also their potential to use thiosulfate for dark fixation of carbon dioxide [32]. But up to now any attempt to explain the high rates of carbon dioxide fixation quantitatively failed. We therefore want to review and discuss the existing data and hypotheses concerning this process focusing on three topics:

(a) Microbial communities across pelagic redox gradients
(b) Flux of electron acceptors and donors as source of energy
(c) Observed carbon dioxide fixation and quantitative explanation

2 Microbial Communities Across Pelagic Redox Gradients

Although in most pelagic redox zones gradients of temperature and salinity provide the density gradient, which inhibits vertical mixing, these gradients itself are rarely so strong that they exert direct effects on biological diversity and activity. The resulting gradients of the different electron acceptors and donors are much more directly influencing the abundance of bacteria across these water layers. There is, however, not a general pattern in bacterial biomass and diversity. Ho et al. [33] reported a significant increase in bacterial numbers at the suboxic/anoxic interface which at least in some cases showed more than twice the number of cells compared to the layers above or below. Similar conditions were later reported by [34, 35]. Bacterial abundances in the pelagic redox zone of the Black Sea are much more variable compared to the layers above and below. Bird and Karl [36] could only find an "absence of a general enrichment in total microbial or bacterial biomass across the oxic-to-anoxic boundary". Sorokin et al. [37] reported a stock of bacterial numbers and biomass within the redox zone, which was nearly twice as high as that in the water layer between redox and thermocline (40–100 m). Sometimes, the differences in bacterial numbers between these layers do not seem to be so high [38–40]. In pelagic redox zones of the Cariaco Basin and the Black Sea, bacterial cell numbers between 0.3 and 0.5 $\times$ 10^6 mL^{-1} were most often found, although these numbers range from less than 0.2 to more than 1 $\times$ 10^6 mL^{-1} for the Black Sea and the Cariaco Basin, respectively. Bacterial numbers are about twice as high for Baltic Sea redox gradients (mean between 0.8 and 1.2 $\times$ 10^6 mL^{-1}, ranging from 0.5 to more than 2 $\times$ 10^6 mL^{-1}) (e.g., [41–44]).

During transition from oxic-to-anoxic conditions in the Gotland Basin, also higher cell volumes of bacteria with increasing depths were reported [37, 41]. Especially in the Black Sea, the occurrence of filaments at the redox zone was reported [39], but this was already observed in samples from sulfidic water layers by Kriss [45].

Table 1 Bacterial growth estimations around redox zones of the Black Sea, Cariaco Basin, and Baltic Sea

Location	Bacterial production (μgC L^{-1} day^{-1})	Growth rate (day^{-1})	References
Baltic Sea	0.3–3.4[a]	0.04–0.4[b]	[46]
Black Sea	3.2–18.6	0.2–0.6	[37]
Black Sea	1.6–6		[47]
Black Sea	0,15	0.02–0.15	[39]
Cariaco Basin	0.02–1.2	0.02–0.2	[34]

[a]Assuming 20 fg C per cell
[b]Calculated from given ranges of biomass and production

Estimates of bacterial production in the different redox zones were published infrequent and also performed with quite different methods. From the values provided in Table 1, we conclude that the earlier estimations [37, 47] were probably too high. Growth rates of about 0.1 day^{-1} seem to be in the mean range. In the Baltic Sea, the bacterial production and the growth rates were higher as the values reported more recently from the Black Sea and Cariaco Basin (Table 1; [46]).

The DOC concentration is slightly decreasing with depth in the Black Sea [48], the Cariaco Basin [33], and the Baltic Sea [49]. Since most of the prokaryotic organisms are heterotrophs, they gain decreasing amounts of energy over the redox gradient by respiration of the same amount of dissolved organic matter, because of the decreasing energy gain by using different electron acceptors. This combination should result in at least slightly decreasing bacterial productivity with depth.

Within all three pelagic oxic–anoxic transition zones, mentioned above, pronounced shifts in the composition of bacterial communities are observed [4, 19, 50, 51]. Within the prokaryotic organisms, *Eubacteria* are dominant. Also common for all of these areas are higher proportions of *Epsilonproteobacteria* at the redox zone, accounting for up to 27% and 20% of the DAPI counts for the Cariaco Basin and the Black Sea, respectively [50]. For the Baltic Sea redox zone, up to 16% of the DAPI counts were related to the *Epsilonproteobacteria* [5]. For the Cariaco Basin and the Black Sea, comparable, but low abundances of *Gammaproteobacteria* of around 2–4% of the DAPI counts were reported [50], whereas in both regions peaks of around 8% were detected just above the chemocline. Using fingerprinting techniques, Labrenz et al. [51] could detect bands from *Alpha-*, *Gamma-*, *Delta-*, and *Epsilonproteobacteria* from the suboxic to the sulfidic layer at the central Baltic redox zone.

In many marine systems, also *Crenarchaeota* are at least partly involved in ammonia oxidation. *Crenarchaeota* dominate the variable proportions of archaea in all basins [50, 51]. Especially in the suboxic part of the redox zone, these *Crenarchaeota* seem to be mainly composed of nitrifying organisms related to the *Candidatus* "Nitrosopumilus maritimus" [52, 53]. These nitrifying *Crenarchaeota* seem to be well adapted to low oxygen conditions in marine environments [54–56].

Their contribution to ammonia oxidation was proven for the Black Sea [6, 52] and indicated for the Cariaco Basin [50]. In the suboxic part of the Baltic Sea redox zone, a peak of transcripts of amoA from *Crenarchaeota* just above the chemocline supports the importance of these organisms versus ammonia-oxidizing bacteria

[53]. These *Crenarchaeota* were recently detected in nearly all, especially suboxic, marine waters [54, 57, 58].

The existence of chemolithoautotrophic bacteria in pelagic redox zones is acknowledged since decades. Already Kriss [45] described the filamentous bacteria found in sulfidic waters as autotrophs oxidizing hydrogen sulfide. He, however, assumed that they used the energy from radioactive disintegrations. First measurements of chemosynthetic production by autotrophs at the pelagic redox zone of the Black Sea were reported by Sorokin [14], who addressed it to thio-oxidizing bacteria. Tuttle and Jannasch [59] reported the isolation of bacteria from the Black Sea oxidizing different reduced sulfur compounds, capable for autotrophic growth as well as for surviving under anoxic conditions. They later repeated that with material from the pelagic redox zone of the Cariaco Basin [32].

Although at least since the late 1980s a peak of elevated dark carbon dioxide fixation at the redox zone of the Baltic Sea is known [60, 61]. Until the work of Labrenz et al. [62] resulted in enrichment cultures, there are no attempts known to isolate these chemolithoautotrophic bacteria.

Since only a few metazoans are adapted to very low oxygen concentrations or even anoxic waters, protozoa seem to be the only organisms left to fulfill the function of grazers, preying on either other protozoa, flagellates, or prokaryotes [7]. Their abundance decreases with increasing concentrations of H_2S. In the central Baltic redox zone, ciliates instead of heterotrophic nanoflagellates seem to be the major grazers of bacteria within the suboxic part of the redox zone showing a peak at the oxic–anoxic interface [63]. Already Detmer et al. [61] reported a peak of ciliates at the chemocline followed by a drastic decrease further downward in the sulfidic water. This results in a decrease in grazing pressure on the prokaryotic populations over the pelagic redox zone, which might at least compensate the effect of reduced bacterial productivity on the standing stock of prokaryotes. A more pronounced increase in prokaryote abundance below the redox zone might be limited by increased mortality due to bacteriophages [46]. This might be also supported by a higher ratio of virus-like particles to bacteria as found in the anoxic part of the Cariaco Basin [34].

3 Flux of Electron Acceptors and Donors as Source of Energy

A shift in the composition of bacterial communities across oxic–anoxic transition zones is not surprising since the main electron acceptor oxygen and is gradually replaced by other oxidants. The next energetically favorable electron acceptor is nitrate, followed by oxidized iron, manganese, and, finally, sulfate. This microbial redox sequence based on the energy gained by the different electron acceptors describes principally the temporal succession of the exhausted electron acceptors and their spatial disappearance [2]. While such cascades in sediments happen often

within several millimeters or centimeters, we have to assume spacial scales of decimeters for strong gradients like in several fjords [24] to several meters like in the Cariaco Basin [11]. The availability of the electron acceptors will cause a transition from aerobic via facultative anaerobic to anaerobic microbial metabolisms. Following this succession, not only the energy gain for bacterial growth by alternative electron acceptors will be reduced drastically, but also alternative bacterial metabolism becomes dominant as reflected by the shift in the community structure.

Below we will focus our attention on compounds that are known to fuel chemolithoautotrophic growth of microorganisms. A number of different bacteria are specialized to gain their energy by oxidation of inorganic or one-carbon compounds and assimilating carbon dioxide [64]. The number of compounds that could react as electron acceptors and/or as electron donors for microbial carbon dioxide fixation is relatively limited. A list of the most probable compounds used by chemolithotrophic microorganisms is shown in Table 2. We will focus our attention on oxygen and nitrate as the most important electron acceptors. Less-oxidized nitrogen compounds can be detected in significantly lower concentrations during different redox transitions as intermediates and can therefore be included in the nitrate inventory. Particulate manganese oxides are important due to their different transport behavior. In contrast to dissolved substances that are dependent on enhanced eddy diffusion for their vertical distribution, these manganese particles are transported much faster by sinking [22, 65]. The highest energy gain can be achieved by chemolithoautotrophic oxidation of hydrogen or methane by oxygen or even nitrate [64], but both compounds can only be found close to the detection limit (hydrogen) or in the nMol range at pelagic chemoclines ([66], Heyer, personal communication). Therefore, the contribution of these oxidation pathways can be considered a minor contribution to the observed carbon dioxide fixation. According to the measured concentration gradients and calculated fluxes, this leaves only

Table 2 Inorganic electron acceptors and/or donors which could enable chemolithoautotrophic bacterial growth

Electron acceptors	Electron donors
Oxygen	Hydrogen
Nitrate	Methane
Nitrite[a]	Ammonia
Other partly oxidized nitrogen compounds[a]	Nitrite[a]
Oxidized iron	Other partly oxidized nitrogen compounds[a]
Oxidized manganese	Reduced iron
Carbon monoxide	Reduced manganese
Thiosulfate[a]	Hydrogen sulfide
Elemental sulfur[a]	Thiosulfate[a]
Other partly oxidized sulfur compounds[a]	Elemental sulfur[a]
Sulfate	Other partly oxidized sulfur compounds[a]

Underlined are the compounds (most oxidized/reduced) assumed to be most important

[a]Intermediate compounds, which could be further oxidized or reduced depending on environmental conditions

ammonia, sulfide, and manganese to contribute substantially to chemolithotrophy. Other more oxidized sulfur compounds such as elemental sulfur and thiosulfate can be included in the sulfide budget since they remain most probably intermediates within the redox zone. According to the vertical profiles, a vertical transport of these compounds from sediments to the pelagic redox zone in the Baltic Sea [67] or in the Cariaco Basin [68] is rather unlikely.

Biological turnover in the redox gradient is largely dependent on the downward flux of the most oxidized and upward flux of the most reduced chemical species into the pelagic redox zone. Intermediates that can be used as either electron donor or acceptor are mainly involved in cyclic processes within the system and not relevant for import or export.

The successive disappearance of the different electron acceptors with depth following the decreasing amount of energy gained by their use is well known from sediments. Like in sediments, the decline of oxygen with depth in pelagic redox zones is as well followed by a decline of nitrate. Denitrification already starts under suboxic conditions. For oceanic denitrification, oxygen concentrations above around 2 μM seem to be inhibiting [69, 70]. In the suboxic water of the Gotland Basin, denitrification was detectable at oxygen concentrations below 9 μM [71]. But already Brettar and Rheinheimer [21] reported that heterotrophic denitrification in the suboxic water column was hard to measure and assumed that the main nitrogen loss process is coupled to oxidation of reduced sulfur compounds. They concluded that heterotrophic denitrification is limited especially by the quality of available organic matter [21, 72]. The importance of chemolithotrophic denitrification as the main loss factor for nitrogen at pelagic redox zones of the Baltic Sea was also stressed by Hannig et al. [73].

This lack of electron acceptors leads to a decrease in denitrification capacity of the ecosystem. In sedimentary environments with high organic loads, nitrate penetrates from the bottom water into the sediment where it is reduced at the depth where oxygen becomes limited. Even ammonia produced during remineralization will be oxidized within the sediment before it will be released as nitrate or denitrified to dinitrogen. In most pelagic redox zones, the lack of available organic material for heterotrophic denitrification is also the limiting factor for microbial heterotrophic activities. This might, at least in the central Baltic, explain why there are no drastic changes in bacterial numbers and growth rates over the whole redox zone, which should be expected by the drastic changes of energy yield in the use of different electron acceptors. It as well implies the importance of chemolithoautotrophy for life at pelagic redox zones.

Many organisms are known to oxidize manganese and in theory it should be sufficient to support chemolithoautotrophic growth. Real proof is lacking, but as genes for CO_2 fixation were found in a manganese oxidizing bacterium [74], this pathway seems very likely. The energy gain will, however, be relatively low. Under oxic conditions, these microorganisms should be outcompeted by others using oxygen more efficiently for growth, although the indicated lack of degradable organic matter (lacking heterotrophic denitrification) would impede both denitrifiers and other heterotrophic bacteria. There are other possible competitors

Table 3 Examples of redox reactions which could fuel chemolithoautotrophy within different layers of the redox zone

Condition	Redox reactions	ΔG^0 (kJ mol^{-1})	References
Oxygen available	(1) Ammonia oxidation $2NH_4^+ + 3O_2 \rightarrow 2NO_2^- + 4H^+ + 2H_2O$	−272	[75]
	(2) Nitrite oxidation $2NO_2^- + O_2 \rightarrow 2NO_3^-$	−75	[75]
	(3) Incomplete sulfide oxidation $2HS^- + O_2 \rightarrow 2S^0 + 2OH^-$	−145	[76]
	(4) Incomplete zero-valent sulfur oxidation $S^0 + O_2 + H_2O \rightarrow SO_3^{2-} + 2H^+$	−249	[76]
	(5) Manganese oxidation $2Mn_2^+ + O_2 + 2H_2O \rightarrow 2MnO_4 + 4H^+$	−81	[77]
	(6) Iron oxidation $4Fe^{2+} + O_2 + 10H_2O \rightarrow 4Fe(OH)_3 + 8H^+$	−88	[78]
Nitrite/nitrate available	(7) Anaerobic sulfide oxidation $5HS^- + 8NO_3^- + 3H^+ \rightarrow 5SO_4^{2-} + 4N_2 + 4H_2O$	−745	[79]
	(8) Anaerobic thiosulfate oxidation $5S_2O_3^{2-} + 8NO_3^- + H_2O \rightarrow 10SO_4^{2-} + 2H^+ + 4N_2$	−751	[76]
	(9) Anammox $NH_4^+ + NO_2^- \rightarrow N_2 + H_2O$	−360	[75]
Anoxic, without nitrite/nitrate	(10) Anaerobic sulfur oxidation $S^0 + 3MnO_2 + 4H^+ \rightarrow 3Mn^{2+} + 2H_2O + SO_4^{2-}$	−384	[80]
	(11) Anaerobic sulfide oxidation $HS^- + 4MnO_2 + 7H^+ \rightarrow SO_4^{2-} + 4Mn^{2+} + 4H_2O$	−525	[80]
	(12) Thiosulfate disproportionation $S_2O_3^{2-} + H_2O \rightarrow SO_4^{2-} + HS^- + H^+$	−6	[76]

for oxygen-nitrifying bacteria, manganese oxidizers, and other chemolithotrophs which oxidize reduced sulfur compounds, as they are not in need of organic substrates (Table 3). In Black Sea studies, a coexistence of reduced sulfur and oxygen is often negated [81]. In this case, there should be differences in manganese oxidation rates, as the concurrent process of sulfur oxidation is omitted. Rates of Mn oxidation should be higher in the Black Sea, as compared to the Baltic Sea and the Cariaco Basin, where the overlap between oxygen and reduced sulfur compounds is the standard situation, and therefore more favorable options for the exploitation of oxygen are present.

According to our present knowledge of chemolithoautotrophic bacteria and the distribution of electron acceptors, we would expect their main activity around the oxic–anoxic interface. Since oxidation pathways with nitrogen species provide nearly the same energy yield as oxygen-based processes and due to the fact that these compounds are also dissolved, they should be depleted within a relative short distance after the disappearance of oxygen. The only possible electron

acceptors which could enter deeper layers by sedimentation can be oxidized iron and manganese particles.

4 Observed Carbon Dioxide Fixation and Quantitative Explanation

The gradient system of oxidized and reduced inorganic compounds within redox zones seems to be a perfect place for chemolithotrophic organisms. Most of them use either oxygen or oxidized nitrogen compounds as terminal electron acceptors oxidizing reduced compounds. Therefore, we can expect their peak in activity at the oxic–anoxic interface until oxidized nitrogen compounds disappear. There are few reports from different pelagic redox zones that support this hypothesis [31, 61, 82]. But more often the maximum of the carbon dioxide fixation is located further down in the anoxic part of the redox zone [11, 12, 14, 83]. This vertical structure as well as the amount of carbon dioxide fixation was explained quite differently. At first, Jørgensen et al. [10] recognized the difficulty to explain the values of chemolithotrophic carbon dioxide fixation quantitatively. Although they mentioned the possible contribution of anoxygenic phototrophic bacteria, they ruled out that they could contribute a substantial part. Since in most of these pelagic redox zones light is of minor importance (except shallow fjords), we might rule out the importance of photosynthesis as an important process in the major marine pelagic redox zones of the Cariaco Basin, the Black Sea and the Baltic Sea. Even if there are some reports about photosynthetic activity of anaerobic bacteria at the chemocline of the Black Sea [84–86], their contribution to the measured carbon fixation (e.g., [10, 14, 37]) can only be of minor importance.

There are still two more options to explain dark CO_2 fixation. Heterotrophic bacteria might take up carbon dioxide by anaplerotic reactions. It is assumed that this could account for up to 8% of bacterial carbon fixation [87, 88]. Under anaerobic conditions, this percentage seems even to be slightly higher [89]. As in all pelagic redox zones, rates of dark CO_2 fixation are not coupled to heterotrophic bacterial production and often show comparatively low values in the suboxic part, where the heterotrophic bacterial production is higher than in the anoxic part of the redox zone, and anaplerotic CO_2 fixation cannot explain the observed rates.

The only remaining choice of probable agents for this process is then narrowed down to chemolithoautotrophic organisms. Isolation of chemolithoautotrophic bacteria from the respective layers can proof the presence of this type of organisms but not their quantitative role. First evidence for the importance of these bacteria came from the Baltic Sea. Jost et al. [44] demonstrated the existence of about 20–40% of chemolithoautotrophic bacteria within the redox zone fixing between 3.5 and more than 20 fg C per cell per day. According to their calculations, 0.8 fg C should be the upper limit, which could be fixed by heterotrophic bacteria within these samples. At least one group of chemolithoautotrophic bacteria could be easily discerned

from others by relatively high 90° light side scatter signals in their flow cytometric signature. This unique cluster of bacteria just appeared at the lower transition of the chemocline to sulfidic waters [44]. Casamayor et al. [90] observed such a shift in the flow cytometric signature of phototrophic bacteria when they accumulated internal elemental sulfur. Such a morphological signature may also explain the appearance of the optically active bacterial cluster below the chemoclines of the Baltic Sea, which was also observed in the Black Sea (unpublished results). The existence of chemolithoautotrophic bacteria was also detected by MICRO-CARD-FISH analyses at redox zones of the Baltic Sea and Black Sea [43]. This investigation verified not only the importance of chemolithoautotrophic bacteria, but also showed that their activity was nearly 100% restricted to *Eubacteria* below the chemoclines. As already suggested by Lin et al. [19], it could be proven that *Epsilonproteobacteria* play a major role in CO_2 fixation at pelagic redox zones. Between 70 and nearly 100% of the detected chemolithoautotrophic bacteria could be identified as *Epsilonproteobacteria* by MICRO-CARD-FISH probes [43]. Studies by Glaubitz et al. [82, 91] render it likely that the remaining chemolithoautotrophs belong to *Gammaproteobacteria* both in the Baltic and in the Black Sea. Although their contribution to the estimated CO_2 fixation was less than half of the amount fixed by *Epsilonproteobacteria*, the chemolithoautotrophic *Gammaproteobacteria* were more diverse than the *Epsilonproteobacteria* [82]. At least one group of these *Gammaproteobacteria* is closely related to a symbiont, and it is also known that sulfide-oxidizing bacteria appear as ectosymbionts of protozoa in sulfidic environments [92–95]. The observed transfer of the CO_2 fixation by bacteria to protozoa could be related not only to unspecified grazing but also to grazing of own ectosymbionts [91]. The closely related *Epsilonproteobacteria* belong to *Sulfurimonas* sp. and proved them to be versatile key players within pelagic redox zones by microdiversity analyses [5, 43, 82, 91]. These approaches for direct detection and identification of chemolithoautotrophic organisms were used in layers showing enhanced CO_2 fixation. For these layers, a clear dominance of the oxidation of reduced sulfur compounds to fuel chemolithoautotrophy could be demonstrated. Here, it can only be speculated, whether this is also the case for the upper suboxic part of the redox zone. In this environment, at least the presence of *Epsilonproteobacteria* was demonstrated [5], and according to Kamyshny et al. [67] the presence of reduced sulfur compounds is as well proven.

In the suboxic part of the redox zone, alternative reactions allow chemolithoautotrophy. The importance of nitrifying bacteria within suboxic environments is well known [96]. Ammonia oxidation is restricted to at least suboxic environments. In the Baltic Sea, this process is indicated by the appearance of a nitrate peak below the halocline [51, 97], which should be related to highest ammonia oxidation activities. In this layer, CO_2 fixation rates are, however, near the detection limit (Jost, unpublished results) and can be assigned only to the activity of chemolithoautotrophic ammonia oxidizers [12]. This view will probably be modified by new findings that *Crenarchaeota* are as well involved in the marine nitrogen cycle. It is assumed that the marine *Crenarchaeota* are also autotrophs [54, 98], and for the Black Sea it was suggested that both *Gammaproteobacteria* and *Crenarchaeota*

contribute to nitrification [6]. Because of different pathways of carbon fixation in bacterial and archaeal metabolism [99], their fixation rate per oxidation equivalent might slightly differ. Even if these organisms were just partly autotrophic or mixotrophic, as was assumed from crenarchaeotal uptake of amino acids [100, 101], their respective metabolism cannot change the overall budget within the suboxic layers of pelagic redox zones substantially, as CO_2 fixation rates are generally low. The calculated rates of carbon dioxide fixation by chemolithoautotrophic ammonia-oxidizing bacteria are not only in good agreement with the low rates measured in the suboxic part of the pelagic redox zone of the Baltic Sea, but can also explain the disappearance of ammonia around the chemocline [12].

The contribution of anammox bacteria (oxidation of NH_4 with NO_2 to N_2 and H_2O) to CO_2 fixation seems as well to be of minor importance, as their energy gain is in the same range as that of aerobic ammonia oxidizers [102]. Since these bacteria use nitrate or nitrite under anoxic conditions with an energy yield as low as nitrifying bacteria, they cannot contribute more to CO_2 fixation than the nitrifiers. Earlier, it was assumed that anammox would be restricted to anoxic and non-sulfidic environments, since it was completely inhibited already at oxygen concentrations as low as 2 μM [103]. But then it was found that anammox still proceeds under low oxygen concentrations [104], though under suboxic conditions anammox rates are lower than under anoxic conditions [105]. Lam et al. [6] postulated a short circuit between nitrification and anammox for the suboxic to upper anoxic layers of the redox zone of the Black Sea since they could not detect any denitrification. This implies that anammox bacteria could outcompete denitrifying bacteria. Since the energy yield of the anammox bacteria per mol nitrite/nitrate is about ten times less than that of heterotrophic denitrifiers or even chemolithoautotrophic denitrifiers using reduced sulfur compounds, this is not very probable in a concurrent situation. In case it occurs, it indicates a lack of suitable organic matter or reduced sulfur compounds. Under these conditions, the highest rates of CO_2 fixation should then be found in the deeper part of the suboxic layer and within the upper part of the anoxic layer. But here enhanced fixation rates of chemolithoautotrophic denitrifiers are not probable because of lacking nitrite/nitrate. Such a scenario seems, however, quite possible in an environment like the Black Sea, where an extended anoxic layer without detectable hydrogen sulfide seems to be existing at least temporarily [106].

In the Baltic Sea anammox could only be detected occasionally, rates were in the range of 0.05–0.005 μmol N L^{-1} day^{-1} [73]. This was attributed to higher Mn(IV) concentrations, which developed after intense salt water inflow led to a short period of fully oxygenated bottom water in the Gotland Basin. In a newly establishing pelagic redox zone extending from the sediment, relatively large amounts of sinking manganese oxide and its potential to oxidize sulfide seemed to be able to establish a temporarily zone, free of oxygen and H_2S. It should, however, be noted that these anammox measurements are based on the addition of nitrate to anoxic water samples without detectable in situ nitrate concentrations. Therefore, induction or at least an enhancement of the measured rates must be assumed.

The basic process that fuels all chemolithoautotrophic activities is basically driven by the stepwise oxidation of sulfide with oxygen over the total redox

gradient. But all calculations to explain the measured carbon dioxide fixation by sulfide oxidation failed so far [10–12, 24]. First, there is a lack of sulfide reaching the zone of enhanced carbon dioxide fixation by upward transport in all of the investigated systems, and second, the peak of the fixation zone is often within the sulfidic part of the redox zone without detectable amounts of oxygen and oxidized nitrogen, which are the most important electron acceptors for chemolithoautotrophic sulfur-oxidizing bacteria.

Although even in suboxic parts of pelagic redox zones sulfate-reducing bacteria were detected in the Baltic Sea [51], the Black Sea [50, 107], and the Cariaco Basin [35, 50], it seems very unlikely that these bacteria supplied enough, if any, sulfide to produce the required amount of sulfide to fuel the process. Albert et al. [108] measured production rates of up to 3.5 nmol H_2S L^{-1} day^{-1} below the pelagic redox zone of the Black Sea, but also deeper than the zone of elevated carbon dioxide fixation. Within this zone, Jørgensen et al. [10] measured values between 3 and 36 nmol H_2S L^{-1} day^{-1}. Since these rates were two orders of magnitude lower than measured sulfide oxidation rates within the same layer, sulfate reduction cannot provide an important source for sulfide [10]. Jost et al. [12] suggested a recycling of sulfide from only partly oxidized sulfur compounds like elemental sulfur or thiosulfate. Although the calculated turnover time of the sulfide pool seems with about 1 day comparatively low, this still needs to be verified. The most critical point in this argumentation is to explain the origin of the organic matter for the heterotrophic bacteria using thiosulfate or elemental sulfur as electron acceptors, as the quality and amount of organic matter in layers only several meters above are not even sufficient to fuel heterotrophic denitrification.

Since oxidized nitrogen compounds can only explain a small part of the observed carbon dioxide fixation by sulfur oxidizers, the question for alternative electron acceptors within the sulfidic environment remains open. Most likely seems to be the involvement of particulate iron and manganese [10–12]. But the amount of oxidized metals which could reach these anoxic layers would also by far be not sufficient to explain the observed carbon dioxide fixation rates [12]. It is well known that humic substances could mediate the electron transfer between particulate metal oxides and bacteria [109]. It has also been shown that humic substances could be used as electron acceptors for the oxidation of organic substances [110]. It is, however, unknown whether these substances could also be used to oxidize reduced sulfur compounds by chemolithoautotrophic bacteria. But even if this would be possible, these electron acceptors would needed to be recycled, e.g., by metal oxides, as otherwise their capacity to accept electrons would degrade quickly.

At the moment, we cannot provide a satisfying explanation for the extent of the carbon dioxide fixation rates especially in the anoxic part of the redox zones. Lateral intrusions were often assumed to supply the redox gradients with additional oxygen [5, 11, 28]. But even if this amount would be large enough, the capacity of the dissolved metal inventory would not be sufficient to transport it as equivalents into the anoxic part, which is characterized by enhanced carbon dioxide fixation.

Although a suite of precautionary measures were taken to eliminate oxygen contamination of the incubation samples by all groups engaged in these

experiments, an ultimate guarantee cannot be given. Even the observed progression of the carbon dioxide fixation maximum in the anoxic layer could be explained by assuming that every sample might have been contaminated with about the same amount of oxygen. Then, depending on the amount of reduced sulfur compounds, an increasing amount of carbon dioxide may be fixed, as long as enough microbes capable of oxidizing reduced sulfur compounds are present. In deeper layers with higher sulfide concentrations, their cell numbers will either decline or the bacteria might need longer lag phases to reestablish their physiology. Due to the fact that intense care has been taken, to keep oxygen out of the experiments, this scenario is not very probable but cannot be ruled out completely.

All published results showing enhanced carbon dioxide fixation within anoxic environments without nitrite/nitrate are based on incubations of water samples which have been transferred through oxic environments before incubation with ^{14}C- or ^{13}C-bicarbonate solution. Incubation-independent measurements like the estimation of stable isotopes within fatty acids show significant changes only at the layer around the chemocline and not in the sulfidic part [91]. At present, the trade-off of these arguments leaves us to conclude that there is at least the capacity for anoxic carbon dioxide fixation. The rates might, however, be overestimated by contaminations during incubation procedures. We therefore advocate the improvement of techniques toward in situ rate measurements and the integration of in situ molecular approaches like metatranscriptomics or -proteomics regarding carbon dioxide fixing key enzymes.

Acknowledgment This research was supported by institutional funding of the IOW.

References

1. Diaz RJ, Rosenberg R (2008) Spreading dead zones and consequences for marine ecosystems. Science 321:926–929
2. Fenchel T, King GM, Blackburn TH (1998) Bacterial biogeochemistry: the ecophysiology of mineral cycling. Academic, London
3. Morse J, Thomson H, Finneran D (2007) Factors controlling sulfide geochemistry in subtropical estuarine and bay sediments. Aquat Geochem 13:143–156
4. Vetriani C, Tran HV, Kerkhof LJ (2003) Fingerprinting microbial assemblages from the oxic/anoxic chemocline of the black sea. Appl Environ Microbiol 69:6481–6488
5. Grote J, Labrenz M, Pfeiffer B et al (2007) Quantitative distributions of *Epsilonproteobacteria* and a *Sulfurimonas* subgroup in pelagic redoxclines of the central Baltic Sea. Appl Environ Microbiol 73:7155–7161
6. Lam P, Jensen MM, Lavik G et al (2007) Linking crenarchaeal and bacterial nitrification to anammox in the Black Sea. Proc Natl Acad Sci USA 104:7104–7109
7. Zubkov MV, Sazhin AF, Flint MV (1992) The microplankton organisms at the oxic-anoxic interface in the pelagial of the Black Sea. FEMS Microbiol Ecol 101:245–250
8. Murray JW, Stewart K, Kassakian S et al (2005) Oxic, suboxic and anoxic conditions in the Black Sea. In: Gilbert A, Yanko-Hombach V, Panin N (eds) Climate change and coastline migrationas factors in human adaptation to the Circum-Pontic region: from past to forecast. Kluwer, New York, pp 437–452

9. Canfield DE, Thamdrup B (2009) Towards a consistent classification scheme for geochemical environments, or, why we wish the term 'suboxic' would go away. Geobiology 7:385–392
10. Jørgensen BB, Fossing H, Wirsen CO et al (1991) Sulfide oxidation in the anoxic Black Sea chemocline. Deep Sea Res 38:S1083–S1103
11. Taylor GT, Iabichella M, Ho T-Y et al (2001) Chemoautotrophy in the redox transition zone of the Cariaco Basin: a significant midwater source of organic carbon production. Limnol Oceanogr 46:148–163
12. Jost G, Martens-Habbena W, Pollehne F et al (2010) Anaerobic sulfur oxidation in the absence of nitrate dominates microbial chemoautotrophy beneath the pelagic chemocline of the eastern Gotland Basin, Baltic Sea. FEMS Microbiol Ecol 71:226–236
13. Rabouille C, Conley DJ, Dai MH et al (2008) Comparison of hypoxia among four river-dominated ocean margins: the Changjiang (Yangtze), Mississippi, Pearl, and Rhône rivers. Cont Shelf Res 28:1527–1537
14. Sorokin JI (1964) On the primary production and bacterial activities in the Black Sea. J Cons Int Explor Mer 29:41–60
15. Repeta D (1993) Chemocline of the Black Sea. Nature 366:415–416
16. Wakeham SG, Amann R, Freeman KH et al (2007) Microbial ecology of the stratified water column of the Black Sea as revealed by a comprehensive biomarker study. Org Geochem 38:2070–2097
17. Deuser WG (1973) Cariaco Trench: oxidation of organic matter and residence time of anoxic water. Nature 242:601–603
18. Zhang J-Z, Millero FJ (1993) The chemistry of the anoxic waters in the Cariaco Trench. Deep Sea Res I 40:1023–1041
19. Lin X, Scranton MI, Varela R et al (2007) Compositional responses of bacterial communities to redox gradients and grazing in the anoxic Cariaco Basin. Aquat Microb Ecol 47:57–72
20. Fonselius S (1981) Oxygen and hydrogen sulphide conditions in the Baltic Sea. Mar Pollut Bull 12:187–194
21. Brettar I, Rheinheimer G (1991) Denitrification in the central Baltic: evidence for H_2S-oxidation as motor of denitrification at the oxic-anoxic interface. Mar Ecol Prog Ser 77: 157–169
22. Neretin LN, Pohl C, Jost G et al (2003) Manganese cycling in the Gotland Deep, Baltic Sea. Mar Chem 82:125–143
23. Millero FJ (1991) The oxidation of H_2S in Framvaren Fjord. Limnol Oceanogr 36:1007–1014
24. Zopfi J, Ferdelman TG, Jørgensen BB et al (2001) Influence of water column dynamics on sulfide oxidation and other major biogeochemical processes in the chemocline of Mariager Fjord (Denmark). Mar Chem 74:29–51
25. Conley DJ, Humborg C, Rahm L et al (2002) Hypoxia in the Baltic Sea and basin-scale changes in phosphorus biogeochemistry. Environ Sci Technol 36:5315–5320
26. Conley DJ, Björck S, Bonsdorff E et al (2009) Hypoxia-related processes in the Baltic Sea. Environ Sci Technol 43:3412–3420
27. Özsoy E, Rank D, Salihoglu I (2002) Pycnocline and deep mixing in the Black Sea: stable isotope and transient tracer measurements. Estuar Coast Shelf Sci 54:621–629
28. Konovalov SK, Luther GW, Friederich GE et al (2003) Lateral injection of oxygen with the Bosporus plume – fingers of oxidizing potential in the Black Sea. Limnol Oceanogr 48: 2369–2376
29. Jost G, Clement B, Pakhomova S et al (2007) Field studies of anoxic conditions in the Baltic Sea during the cruise of R/V *Professor Albrecht Penck* in July 2006. Oceanology 47: 590–593
30. Astor Y, Muller-Karger F, Scranton MI (2003) Seasonal and interannual variation in the hydrography of the Cariaco Basin: implications for basin ventilation. Cont Shelf Res 23: 125–144
31. Tuttle JH, Jannasch HW (1979) Microbial dark assimilation of CO_2 in the Cariaco Trench. Limnol Oceanogr 24:746–753

32. Tuttle JH, Jannasch HW (1973) Sulfide and thiosulfate-oxidizing bacteria in anoxic marine basins. Mar Biol 20:64–70
33. Ho TY, Scranton MI, Taylor GT et al (2002) Acetate cycling in the water column of the Cariaco Basin: seasonal and vertical variability and implication for carbon cycling. Limnol Oceanogr 47:1119–1128
34. Taylor GT, Hein C, Iabichella M (2003) Temporal variations in viral distributions in the anoxic Cariaco basin. Aquat Microb Ecol 30:103–116
35. Lin X, Scranton MI, Chistoserdov AY et al (2008) Spatiotemporal dynamics of bacterial populations in the anoxic Cariaco Basin. Limnol Oceanogr 53:37–51
36. Bird DF, Karl DM (1991) Microbial biomass and population diversity in the upper water column of the Black Sea. Deep Sea Res 38:S1069–S1082
37. Sorokin YI, Sorokin PY, Avdeev VA et al (1995) Biomass, production and activity of bacteria in the Black Sea, with special reference to chemosynthesis and the sulfur cycle. Hydrobiologia 308:61–76
38. Gorlenko VM, Mikheev PV, Rusanov II et al (2005) Ecophysiological properties of photosynthetic bacteria from the Black Sea chemocline zone. Microbiology 74:201–209
39. Morgan JA, Quinby HL, Ducklow HW (2006) Bacterial abundance and production in the western Black Sea. Deep Sea Res II 53:1945–1960
40. Mosharova I, Sazhin A (2007) Bacterioplankton in the northeastern part of the Black Sea during the summer and autumn of 2005. Oceanology 47:671–678
41. Gast V, Gocke K (1988) Vertical distribution of number, biomass and size-class spectrum of bacteria in relation to oxic/anoxic conditions in the Central Baltic Sea. Mar Ecol Prog Ser 45:179–186
42. Brettar I, Höfle MG (1993) Nitrous oxide producing heterotrophic bacteria from the water column of the central Baltic: abundance and molecular identification. Mar Ecol Prog Ser 94:253–265
43. Grote J, Jost G, Labrenz M et al (2008) *Epsilonproteobacteria* represent the major portion of chemoautotrophic bacteria in sulfidic waters of pelagic redoxclines of the Baltic and Black Seas. Appl Environ Microbiol 74:7546–7551
44. Jost G, Zubkov MV, Yakushev E et al (2008) High abundance and dark CO_2 fixation of chemolithoautotrophic prokaryotes in anoxic waters of the Baltic Sea. Limnol Oceanogr 53: 14–22
45. Kriss AE (1959) The role of microorganisms in the primary production of the Black Sea. J Cons Int Explor Mer 24:221–230
46. Weinbauer MG, Brettar I, Höfle MG (2003) Lysogeny and virus-induced mortality of bacterioplankton in surface, deep, and anoxic marine waters. Limnol Oceanogr 48:1457–1465
47. Karl DM, Knauer GA (1991) Microbial production and particle flux in the upper 350 m of the Black Sea. Deep Sea Res 38:S921–S942
48. Ducklow HW, Hansell DA, Morgan JA (2007) Dissolved organic carbon and nitrogen in the Western Black Sea. Mar Chem 105:140–150
49. Schneider B, Nagel K, Struck U (2000) Carbon fluxes across the halocline in the eastern Gotland Sea. J Mar Syst 25:261–268
50. Lin X, Wakeham SG, Putnam IF et al (2006) Comparison of vertical distributions of prokaryotic assemblages in the anoxic Cariaco Basin and Black Sea by use of fluorescence in situ hybridization. Appl Environ Microbiol 72:2679–2690
51. Labrenz M, Jost G, Jürgens K (2007) Distribution of abundant prokaryotic organisms in the water column of the central Baltic Sea with an oxic-anoxic interface. Aquat Microb Ecol 46: 177–190
52. Coolen MJL, Abbas B, van Bleijswijk J et al (2007) Putative ammonia-oxidizing Crenarchaeota in suboxic waters of the Black Sea: a basin-wide ecological study using 16S ribosomal and functional genes and membrane lipids. Environ Microbiol 9:1001–1016
53. Labrenz M, Sintes E, Toetzke F et al (2010) Relevance of a crenarchaeotal subcluster related to *Candidatus* Nitrosopumilus maritimus to ammonia oxidation in the suboxic zone of the central Baltic Sea. ISME J 4:1496–1508

54. Kuypers MM, Blokker P, Erbacher J et al (2001) Massive expansion of marine archaea during a mid-Cretaceous oceanic anoxic event. Science 293:92–95
55. Woebken D, Fuchs BM, Kuypers MMM et al (2007) Potential interactions of particle-associated anammox bacteria with bacterial and archaeal partners in the Namibian upwelling system. Appl Environ Microbiol 73:4648–4657
56. Walker CB, de la Torre JR, Klotz MG et al (2010) *Nitrosopumilus maritimus* genome reveals unique mechanisms for nitrification and autotrophy in globally distributed marine crenarchaea. Proc Natl Acad Sci USA 107:8818–8823
57. Francis CA, Roberts KJ, Beman JM et al (2005) Ubiquity and diversity of ammonia-oxidizing archaea in water columns and sediments of the ocean. Proc Natl Acad Sci USA 102:14683–14688
58. Beman JM, Popp BN, Francis CA (2008) Molecular and biogeochemical evidence for ammonia oxidation by marine Crenarchaeota in the Gulf of California. ISME J 2:429–441
59. Tuttle JH, Jannasch HW (1972) Occurrence and types of thiobacillus-like bacteria in the sea. Limnol Oceanogr 17:532–543
60. Gocke K (1989) Bakterielle Stoffaufnahme im aeroben und anaeroben Milieu der Ostsee. Ber Inst Meeresforsch 188:40–47
61. Detmer AE, Giesenhagen HC, Trenkel VM et al (1993) Phototrophic and heterotrophic pico- and nanoplankton in anoxic depths of the central Baltic Sea. Mar Ecol Prog Ser 99:197–203
62. Labrenz M, Jost G, Pohl C et al (2005) Impact of different in vitro electron donor/acceptor conditions on potential chemolithoautotrophic communities from marine pelagic redoxclines. Appl Environ Microbiol 71:6664–6672
63. Anderson R, Weber F, Wylezich C et al. (2011) Protist diversity, distribution and bacterivory in Baltic Sea pelagic redoxclines. ASLO 2011 Aquatic Sciences Meeting, San Juan, Puerto Rico
64. Shively JM, van Keulen G, Meijer WG (1998) Something from almost nothing: carbon dioxide fixation in chemoautotrophs. Annu Rev Microbiol 52:191–230
65. Yakushev EV, Debolskaya EI (2000) Particulate manganese as a main factor of oxidation of hydrogen sulfide in redox zone of the Black Sea. In: Oceanic fronts and related phenomena. Konstantin Fedorov memorial symposium, Pushkin, Saint-Petersburg, Russia, 18–22 May 1998, Proceedings, IOC Workshop Report No 159. Kluwer Academic Publishers, pp 592–597
66. Schmale O, Schneider von Deimling J, Gülzow W et al (2010) Distribution of methane in the water column of the Baltic Sea. Geophys Res Let 37:L12604
67. Kamyshny A Jr, Yakushev EV, Jost G et al (2011) Role of sulfide oxidation intermediates in the redox balance of the oxic-anoxic interface of the Gotland Deep, Baltic Sea. In: Yakushev EV (ed) Chemical structure of pelagic redox interfaces: Observation and modeling. Springer, Berlin/Heidelberg, doi 698_2010_83
68. Hayes MK, Taylor GT, Astor Y et al (2006) Vertical distributions of thiosulfate and sulfite in the Cariaco Basin. Limnol Oceanogr 51:280–287
69. Cline JD, Richards FA (1972) Oxygen deficient conditions and nitrate reduction in the eastern tropical North Pacific Ocean. Limnol Oceanogr 17:885–900
70. Devol AH (1978) Bacterial oxygen uptake kinetics as related to biological processes in oxygen deficient zones of the oceans. Deep Sea Res 25:137–146
71. Rönner U, Sörensson F (1985) Denitrification rates in the low-oxygen waters of the stratified Baltic proper. Appl Environ Microbiol 50:801–806
72. Brettar I, Rheinheimer G (1992) Influence of carbon availability on denitrification in the central Baltic Sea. Limnol Oceanogr 37:1146–1163
73. Hannig M, Lavik G, Kuypers MMM et al (2007) Shift from denitrification to anammox after inflow events in the central Baltic Sea. Limnol Oceanogr 52:1336–1345
74. Caspi R, Haygood MG, Tebo BM (1996) Unusual ribulose-1,5-bisphosphate carboxylase/oxygenase genes from a marine manganese-oxidizing bacterium. Microbiology 142: 2549–2559
75. Broda E (1977) Two kinds of lithotrophs missing in nature. Z Allg Mikrobiol 17:491–493
76. Kelly DP (1999) Thermodynamic aspects of energy conservation by chemolithotrophic sulfur bacteria in relation to the sulfur oxidation pathways. Arch Microbiol 171:219–229

77. De Schamphelaire L, Rabaey K, Boon N et al (2007) The potential of enhanced manganese redox cycling for sediment oxidation. Geomicrobiol J 24:547–558
78. Sobolev D, Roden EE (2004) Characterization of a neutrophilic, chemolithoautotrophic Fe(II)-oxidizing β-proteobacterium from freshwater wetland sediments. Geomicrobiol J 21:1–10
79. Megonigal JP, Hines ME, Visscher PT (2004) Anaerobic metabolism: linkages to trace gases and aerobic processes. In: Schlesinger WH (ed) Biogeochemistry. Elsevier-Pergamon, Oxford, pp 317–424
80. Aller RC, Rude PD (1988) Complete oxidation of solid phase sulfides by manganese and bacteria in anoxic marine sediments. Geochim Cosmochim Acta 52:751–765
81. Murray JW, Jannasch HW, Honjo S et al (1989) Unexpected changes in the oxic/anoxic interface in the Black Sea. Nature 338:411–413
82. Glaubitz S, Labrenz M, Jost G et al (2010) Diversity of active chemolithoautotrophic prokaryotes in the sulfidic zone of a Black Sea pelagic redoxcline as determined by rRNA-based stable isotope probing. FEMS Microbiol Ecol 74:32–41
83. Pimenov NV, Neretin LN (2006) Composition and activities of microbial communities involved in carbon, sulfur, nitrogen and manganese cycling in the oxic/anoxic interface of the Black Sea. In: Neretin LN (ed) Past and present marine water column anoxia, vol 64. Springer, Dordrecht, pp 501–521
84. Overmann J, Cypionka H, Pfennig N (1992) An extremely low-light-adapted phototrophic sulfur bacterium from the Black Sea. Limnol Oceanogr 37:150–155
85. Overmann J, Manske AK (2006) Anoxygenic phototrophic bacteria in the Black Sea chemocline. In: Neretin LN (ed) Past and present marine water column anoxia, vol 64. Springer, Dordrecht, pp 523–541
86. Marschall E, Jogler M, Henßge U et al (2010) Large-scale distribution and activity patterns of an extremely low-light-adapted population of green sulfur bacteria in the Black Sea. Environ Microbiol 12:1348–1362
87. Romanenko VI (1964) Heterotrophic assimilation of CO_2 by bacterial flora of water. Microbiologiya 33:610–614
88. Roslev P, Larsen MB, Jørgensen D et al (2004) Use of heterotrophic CO_2 assimilation as a measure of metabolic activity in planktonic and sessile bacteria. J Microbiol Meth 59: 381–393
89. Hesselsoe M, Nielsen JL, Roslev P et al (2005) Isotope labeling and microautoradiography of active heterotrophic bacteria on the basis of assimilation of $^{14}CO_2$. Appl Environ Microbiol 71:646–655
90. Casamayor EO, Ferrera I, Cristina X et al (2007) Flow cytometric identification and enumeration of photosynthetic sulfur bacteria and potential for ecophysiological studies at the single-cell level. Environ Microbiol 9:1969–1985
91. Glaubitz S, Lueders T, Abraham W-R et al (2009) ^{13}C-isotope analyses reveal that chemolithoautotrophic *Gamma-* and *Epsilonproteobacteria* feed a microbial food web in a pelagic redoxcline of the central Baltic Sea. Environ Microbiol 11:326–337
92. Bernhard JM, Buck KR, Farmer MA et al (2000) The Santa Barbara Basin is a symbiosis oasis. Nature 403:77–80
93. Vopel K, Thistle D, Ott J et al (2005) Wave-induced H_2S flux sustains a chemoautotrophic symbiosis. Limnol Oceanogr 50:128–133
94. Rinke C, Schmitz-Esser S, Stoecker K et al (2006) "*Candidatus* Thiobios zoothamnicoli," an ectosymbiotic bacterium covering the giant marine ciliate *Zoothamnium niveum*. Appl Environ Microbiol 72:2014–2021
95. Rinke C, Lee R, Katz S et al (2007) The effects of sulphide on growth and behaviour of the thiotrophic *Zoothamnium niveum* symbiosis. Proc R Soc B 274:2259–2269
96. Ward BB (2008) Nitrification in marine systems. In: Capone DG, Bronk DA, Mulholland MR, Carpenter EJ (eds) Nitrogen in the marine environment. Academic, Amsterdam, pp 199–261

97. Brettar I, Moore ERB, Höfle MG (2001) Phylogeny and abundance of novel denitrifying bacteria isolated from the water column of the central Baltic Sea. Microb Ecol 42:295–305
98. Wuchter C, Schouten S, Boschker HTS et al (2003) Bicarbonate uptake by marine Crenarchaeota. FEMS Microbiol Lett 219:203–207
99. Berg IA, Kockelkorn D, Ramos-Vera WH et al (2010) Autotrophic carbon fixation in archaea. Nat Rev Microbiol 8:447–460
100. Herndl GJ, Reinthaler T, Teira E et al (2005) Contribution of Archaea to total prokaryotic production in the deep Atlantic ocean. Appl Environ Microbiol 71:2303–2309
101. Teira E, Lebaron P, van Aken H et al (2006) Distribution and activity of Bacteria and Archaea in the deep water masses of the North Atlantic. Limnol Oceanogr 51:2131–2144
102. Enrich-Prast A, Bastviken D, Crill P (2009) Chemosynthesis. In: Likens GE (ed) Encyclopedia of inland waters. Academic, Oxford, pp 211–225
103. Jetten MSM, Strous M, van de Pas-Schoonen KT et al (1999) The anaerobic oxidation of ammonium. FEMS Microbiol Rev 22:421–437
104. Kuypers MMM, Lavik G, Woebken D et al (2005) Massive nitrogen loss from the Benguela upwelling system through anaerobic ammonium oxidation. Proc Natl Acad Sci USA 102: 6478–6483
105. Jensen MM, Kuypers MMM, Lavik G et al (2008) Rates and regulation of anaerobic ammonium oxidation and denitrification in the Black Sea. Limnol Oceanogr 53:23–36
106. Murray JW, Yakushev E (2006) The suboxic transition zone in the Black Sea. In: Neretin LN (ed) Past and present marine water column anoxia, vol 64. Springer, Dordrecht, pp 105–138
107. Neretin LN, Abed RMM, Schippers A et al (2007) Inorganic carbon fixation by sulfate-reducing bacteria in the Black Sea water column. Environ Microbiol 9:3019–3024
108. Albert DB, Taylor C, Martens CS (1995) Sulfate reduction rates and low molecular weight fatty acid concentrations in the water column and surficial sediments of the Black Sea. Deep Sea Res I 42:1239–1260
109. Lovley DR, Coates JD, BluntHarris EL et al (1996) Humic substances as electron acceptors for microbial respiration. Nature 382:445–448
110. Bradley PM, Chapelle FH, Lovley DR (1998) Humic acids as electron acceptors for anaerobic microbial oxidation of vinyl chloride and dichloroethene. Appl Environ Microbiol 64:3102–3105

Manganese and Iron at the Redox Interfaces in the Black Sea, the Baltic Sea, and the Oslo Fjord

S. Pakhomova and E.V. Yakushev

Abstract The joint analysis of the data of manganese and iron species distributions (dissolved Mn, dissolved bound Mn, dissolved Fe(II) and Fe(III), particulate Fe and Mn) obtained in the Black Sea, the Baltic Sea, and the Oslo Fjord allowed to reveal the common features that testify the similarity of the mechanism of the redox layer biogeochemical structure formation in these regions. Our investigations demonstrated that Mn bound in stable complexes with hypothetically organic matter or pyrophosphate is observed in the redox zones in significant concentrations (up to 2 μM), and is likely presented by Mn(III), an intermediate product of Mn(II) oxidation and Mn(IV) reduction. This bound Mn(III) can explain phosphate distribution in redox interfaces – formation of so-called phosphate dipole with a minimum above the sulfidic boundary and a maximum just below, and with a steep increase in the concentrations between these two. This dipole structure serves as a geochemical barrier that decreases the upward flux of phosphate from the anoxic layer. On the base of the recent data obtained in the 100th cruise of RV "Professor Shtokman" (March to April, 2009), it was found that the bound Mn could exist in two forms – colloidal (0.02–0.40 μm) and truly dissolved (<0.02 μm) that perhaps result from complexing with different types of ligands. The flushing events, river input, sporadically increased mixing, and anoxygenic photosynthesis affect the distributions of the redox zone parameters. Response time for changes in the microbial processes involved in reduction and/or reoxidation of Mn and Fe lags

S. Pakhomova (✉)
P.P.Shirshov Institute of Oceanology of the Russian Academy of Sciences (SIO RAS), 36, Nakhimovskiy Pr., 109017 Moscow, Russia
e-mail: s-pakhomova@yandex.ru

E.V. Yakushev
P.P.Shirshov Institute of Oceanology of the Russian Academy of Sciences (SIO RAS), 36, Nakhimovskiy Pr., 109017 Moscow, Russia
and
Norwegian Institute for Water Researches (NIVA), Gaustadalléen 21, 0349 Oslo, Norway

E.V. Yakushev (ed.), *Chemical Structure of Pelagic Redox Interfaces: Observation and Modeling*, Hdb Env Chem (2013) 22: 67–94, DOI 10.1007/698_2011_98,

behind that for oxygen injection into water. Concentrations of redox-sensitive species of Mn and Fe should thus be useful as a tracer to inter prior hypoxic/anoxic conditions not apparent from oxygen levels at the time of sampling. Modeling results showed that the manganese cycle [formation of sinking down Mn(IV) and presence of dissolved Mn(III)] is the main reason of oxygen and hydrogen sulfide direct contact absence. Modeling allowed to study the role of affecting factors in the formation of the observed distributions.

Keywords Baltic Sea, Black Sea, Iron, Manganese, Oslo fjord, Redox zone

Contents

Abbreviations

B-Chl-e	Bacterial chlorophyll-e
DO	Dissolved oxygen
Fe(II)	Dissolved bivalent iron
Fe(III)	Dissolved trivalent iron
Mn-bou	Dissolved bound trivalent manganese Mn(III)
Mn-diss	Dissolved manganese Mn(II)
Mn-part	Particulate manganese Mn(IV)
NRL	Nepheloid redox layer
OM	Organic matter
SPM	Suspended particulate matter

1 Introduction

The cycles of manganese and iron in the changeable oxic/anoxic conditions are similar. Reduced forms of these compounds are dissolved. They diffuse upward where they oxidize and transfer to oxidized particulate forms that sink down and

reduce in hydrogen sulfide zone. The oxidation–reduction potentials and constants of reaction of oxidation of iron and manganese differ, and these reactions can occur in different amount of oxygen. Due to this, the depth of appearance of particulate manganese is located shallower than of particulate iron [1]. Bacteria have been shown to oxidize manganese [2], whereas iron oxidation is possible without bacteria but can be carried out with bacteria [3]. Reduced iron can be oxidized by particulate manganese, forming complex compounds [4].

According to the recent estimates, the biogeochemical structure of the water column redox layer is characterized by an absence of overlap between dissolved oxygen and hydrogen sulfide and presence of a suboxic zone, where both oxygen and hydrogen sulfide are below detection limits [5]. Oxygen disappears at a depth where the onset of ammonia and dissolved manganese is observed, while hydrogen sulfide appears in the Black Sea water column approximately 5–10 m deeper. In this layer, reduced and oxidized forms of several elements (N, S, C, Mn, Fe) can be observed, which reflects the complexity of processes occurring in this zone.

The role of cycles of different elements in the formation and support of the redox layer balance and biogeochemical structure is still not clear, particularly the reasons for the phenomenon of the suboxic zone existence [5]. One of the possible explanations can be connected with the manganese cycle [6]. The general scheme invoked to explain this phenomenon is the diffusion of reduced, dissolved Mn(II) up from the anoxic zone into the suboxic zone where it is oxidized biologically to solid phase Mn(IV) oxides. This promotes a sinking flux of Mn oxides that is reduced chemically by sulfide.

Recently Mn(III) was observed in the marine environment [7], an important intermediate product of the Mn cycle that could be formed both at Mn(II) oxidation [8, 9] and at Mn(IV) reduction [10, 11]. This dissolved oxidized Mn(III) could explain distribution of other elements in redox interfaces such as phosphate because of possibility forming P-containing complexes [9]. This oxidized and dissolved phase has only been revealed in recent years, and it became necessary to investigate its distributions in the natural systems to estimate its role on the redox zone structure formations. This form was not represented in suboxic zone models that seek to describe the flow of primary nutrients such as nitrogen, phosphate, and carbon as well as heavy metals through the oxic/anoxic boundary.

Iron concentrations in the water column are much smaller than the Mn ones, but nevertheless iron can probably also affect the structure of the redox zones; for example, there was proposed recently a mechanism of the coupling of the Mn and Fe cycling in the particles formed at the redox boundaries [12]. But there are still not enough accurate data on the iron forms distributions at the redox interface.

We suppose that the comparison of the biogeochemical structures of the redox interfaces from the different regions can give unique information necessary for understanding the processes occurring there. A numerical model can be a useful tool for analyzing these processes. This chapter is aimed for summarizing a new data received during the last years in the field of Mn and Fe biogeochemical cycling at the water column redox interfaces.

2 Methods

2.1 Study Site

Distributions of chemical parameters in the redox zone were studied in the north-eastern and the central Black Sea, the Baltic Sea (Gotland and Landsort Deeps), and the Oslo Fjord on board of RV "Akvanavt," "Ashamba," RV "Professor Shtokman"; RV "Professor Albrecht Penck"; RV "Poseidon" and RV "Uttern," respectively, during July 2004 to August 2009. The geographic locations of the study areas are given in Fig. 1.

The Black Sea redox interface is characterized by the most stable biogeochemical structure among comparable interfaces (i.e., Cariaco trench, Baltic Sea's anoxic deeps). In the whole Black Sea area, with an exception of the Bosphorus region, the chemical features are connected with the density structure and the vertical fluxes of main reductants and oxidants seem to be in balance, while the horizontal exchange is negligible.

The redox zones of the Gotland and Landsort Deeps of the Baltic Sea (240 and 450 m deep, respectively) are subjected to the influence of intrusions virtually throughout the whole year and observed features are usually complex due to a lack of equilibrium.

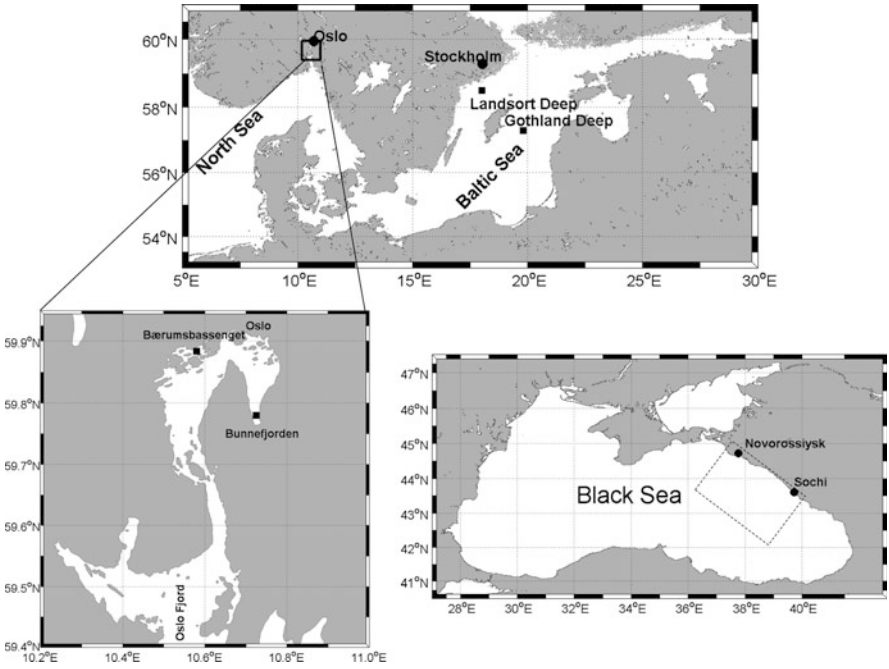

Fig. 1 Sampling locations in the Baltic Sea (**a**), the Oslo Fjord (**b**) and the Black Sea (**c**)

The Baerumsbassenget is a small part of the Oslo Fjord with an approximate area of 5 km^2 and a maximum depth of 31 m. It is separated from the main fjord through a series of islands with a maximum sill depth of 15 m. The inflow into the Baerumsbassenget, the Sandvika River, is responsible for the formation of its permanent meromictic structure with redox interface positioned in the euphotic zone (15–20 m). Bunnefjorden is a 160-m deep anoxic basin, with flushing ones per several years, redox interface at about 90 m.

2.2 Sampling

Water samples for chemical measurements were collected using a Rosette equipped with 5-L Niskin bottles and using pump systems. The used pump system was based on an onboard 12 V peristaltic pumps, with a 11-mm hose attached to the CTD probe. The time of the hose flushing was about 10 min for 170-m hose used in the Black Sea and about 1 min for 20-m hose used in the Oslo Fjord. These pump systems allowed to sample water protected from contamination with the atmospheric oxygen that is essentially for the suboxic systems studies. In our studies, we used the AANDERAA Optode 3835 sensor to measure oxygen concentrations in the hose during the sampling. In the Baltic Sea cruise, the Institute for the Baltic Sea Research's Warnemuende pump system with a pump established at the CTD probe [13] was used.

Sampling in the suboxic zone was performed at 2–3 m intervals in the Black and Baltic Seas and at 0.5–1 m intervals in the Oslo Fjord, aiming to obtain detailed data of the distribution of chemical parameters.

2.3 Chemical Measurements

Dissolved oxygen (Winkler), hydrogen sulfide, phosphate, polyphosphate, nitrate, nitrite, ammonia, and hydrogen sulfide were measured using the standard methods [14–18].

Water samples for dissolved metal analysis were filtered through 0.4-μm Nuclepore filters immediately after sampling. Dissolved manganese and dissolved iron (II), iron (III) concentrations were determined spectrophotometrically using the formaldoxime and ferrozine procedures, respectively [15, 19]. Dissolved organic matter was decomposed using UV irradiation with an addition of hydrogen peroxide (50 μL of 30% H_2O_2 per 20 mL of sample) at pH 2 during 1 h. An 80-W high-pressure Hg lamp was used as a source of UV radiation. Then total dissolvable metals concentration was determined spectrophotometrically. We called the difference between total dissolvable and dissolved metal bound manganese (Mn-bou) and iron (Fe-bou). Precision of dissolved metal analysis was typically 3%. Detection limits were 20 and 100 nM for iron and manganese, respectively.

Water samples for particulate iron and particulate manganese analyses were collected in 2-L plastic bottles. Filtration of water was undertaken no later than several hours after sampling using a Millipore filtration system and thoroughly washed and weighed 0.4 μm filters. Analyses of particulate metals were carried out by AAS following wet acid dissolution of the filters. Particulate Mn concentrations were also estimated as a difference between the spectrophotometric measurements of dissolved manganese in the filtered (0.4 μm) and unfiltered samples [Mn-part(ded)].

2.4 Modeling

For the analysis of the distribution of parameters, we used a coupled hydrophysical-biogeochemical one-dimensional O–N–S–P–Mn–Fe model based on RedOx Layer Model (ROLM) [20] and one-dimensional General Ocean Turbulent Model (GOTM) [21]. Processes of organic matter (OM) formation and decay, the reduction and oxidation of species of nitrogen, sulfur, manganese, iron, as well as transformation of phosphorus species are parameterized in ROLM. The model equations and parameters used and a detailed description are presented in [22]. ROLM was coupled with GOTM, and we used GOTM software to perform numerical calculations.

3 Results

3.1 Manganese

The data on dissolved inorganic manganese, Mn(II), obtained in *the Black Sea* (Figs. 2–5), are in agreement with the previous studies [1, 23, 24]. The characteristic features of the Mn(II) distribution are: (1) a low (nanomolar) content in the surface waters; (2) an intensive increase at the boundary of the sulfidic zone reaching maximum values of 8–10 μM in the first tens meters of the sulfidic zone; (3) a decrease to 4–5 μM and a relative stability of concentrations in the deep water.

The lack of Mn(II) in the upper layer can be explained by a formation under the oxic conditions of insoluble oxides [25, 26] that precipitate and therefore remove Mn from the upper layer.

In the suboxic zone and in the upper part of the anoxic zone, the concentrations of Mn(II) increase and reach its maximum values about 30–40 m below the sulfide boundary (Fig. 2). The vertical gradient of Mn(II) is maximal in the vicinity of the sulfide boundary (up to 0.55 μM/m). It decreases in the anoxic zone, while the concentration of dissolved manganese reaches its maximum (8–10 μM). Below this level, the Mn(II) concentrations decreases and remains in the limits 4–5 μM from ~1,000 m to the bottom [27, 28].

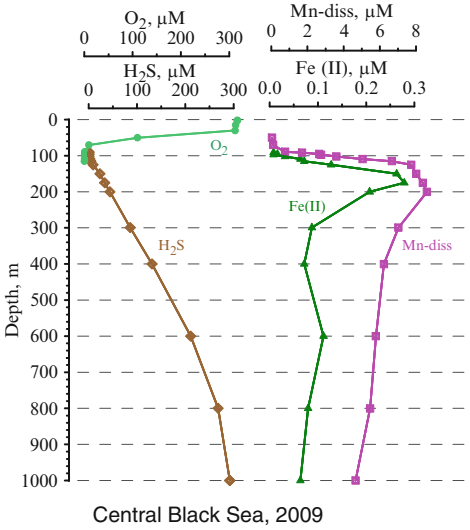

Fig. 2 Vertical distribution of dissolved oxygen (O_2), hydrogen sulfide (H_2S), dissolved Mn (Mn-diss) and dissolved Fe(II) in the central Black Sea, 2009

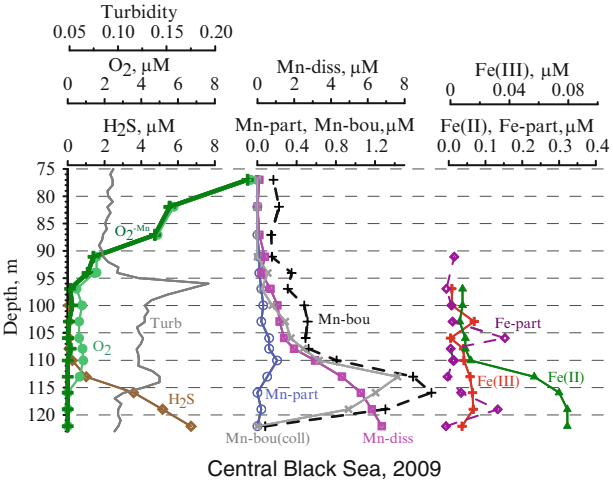

Fig. 3 Vertical distribution of dissolved oxygen measured with Winkler technique (O_2) and after deduction of oxidized Mn forms (O_2^{-Mn}), hydrogen sulfide (H_2S), dissolved Mn (Mn-diss), particulate Mn (Mn-part), bound Mn (Mn-bou), bound Mn in colloidal form (Mn-bou-coll), dissolved Fe(II), dissolved Fe(III), particulate Fe (Fe-part), and turbidity measured with the hydrophysical probe (Turb) in the central Black Sea, 2009

The described structure corresponds to the stable hydrophysical conditions when the upward oxidant and downward reductant fluxes are balanced, and the manganese onset takes place in the layers where the oxygen concentration drops down

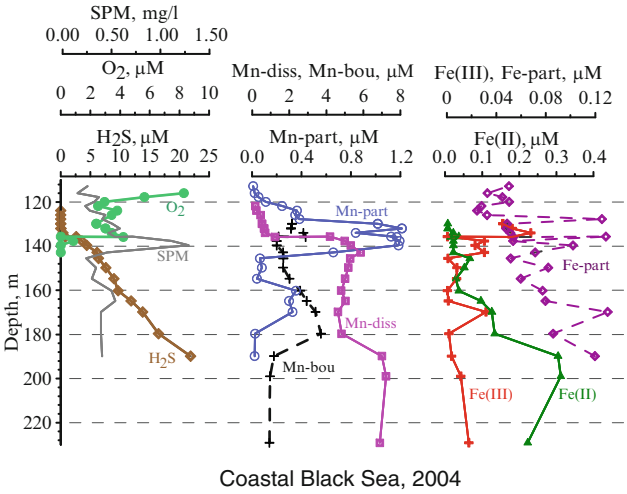

Fig. 4 Vertical distribution of dissolved oxygen (O_2), hydrogen sulfide (H_2S), dissolved Mn (Mn-diss), particulate Mn (Mn-part), bound Mn (Mn-bou), dissolved Fe(II), dissolved Fe(III), particulate Fe (Fe-part), and SPM in the coastal Black Sea, 2004

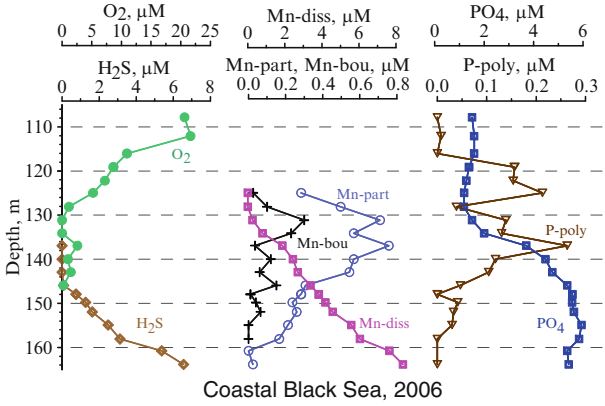

Fig. 5 Vertical distribution of dissolved oxygen (O_2), hydrogen sulfide (H_2S), dissolved Mn (Mn-diss), particulate Mn (Mn-part), bound Mn (Mn-bou), phosphate (PO_4), and polyphosphate (P-poly) in the coastal Black Sea, 2006

below the detection limit [29]. Under certain disturbances, i.e., interaction of the Rim Current and internal waves with the slope, causing vertical displacements of the waters with different densities, or due to the near-slope downwelling [29, 30], oxygen-rich waters can penetrate into sulfide zone. In this case, the stability of the biogeochemical structure disturbs and a messy distribution of elements can be observed. Such changes are registered in the areas affected by the Bosporus current [2, 8, 31] and in the coastal zone near Gelendzhik (Fig. 4) [28, 30].

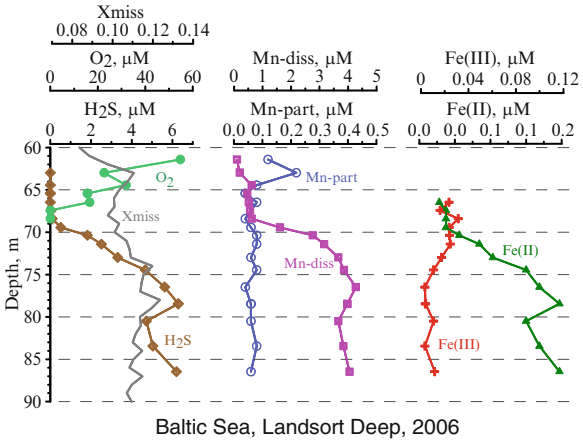

Fig. 6 Vertical distribution of dissolved oxygen (O_2), hydrogen sulfide (H_2S), dissolved Mn (Mn-diss), particulate Mn (Mn-part), dissolved Fe(II), dissolved Fe(III), and transmission measured with the hydrophysical probe (Xmiss) in the Baltic Sea, Landsort Deep, 2006

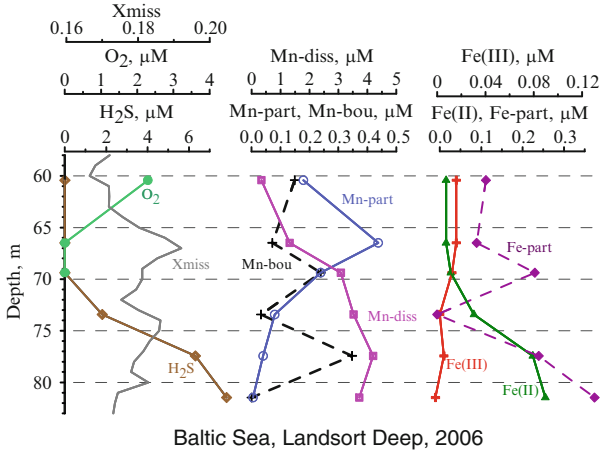

Fig. 7 Vertical distribution of dissolved oxygen (O_2), hydrogen sulfide (H_2S), dissolved Mn (Mn-diss), particulate Mn (Mn-part), bound Mn (Mn-bou), dissolved Fe(II), dissolved Fe(III), particulate Fe (Fe-part), and transmission measured with the hydrophysical probe (Xmiss) in the Baltic Sea, Landsort Deep, 2006

In *the Landsort Deep, Baltic Sea*, the Mn(II) distribution is close to the Black Sea one with an exception of a formation of well-pronounced maximum closer to the sulfidic boundary (usually the first meters) (Figs. 6 and 7). Mn(II) concentration reaches 4–5 μM and remains in the deeper layers practically constant. The maximal vertical gradient is the same as in the Black Sea.

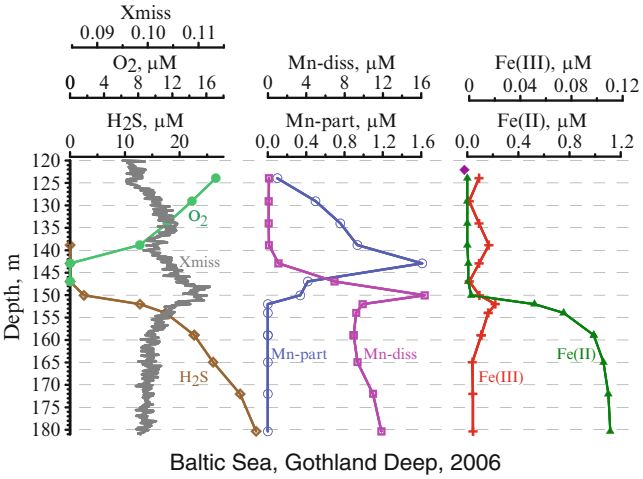

Fig. 8 Vertical distribution of dissolved oxygen (O_2), hydrogen sulfide (H_2S), dissolved Mn (Mn-diss), particulate Mn (Mn-part), dissolved Fe(II), dissolved Fe(III), and transmission measured with the hydrophysical probe (Xmiss) in the Baltic Sea, Gotland Deep, 2006

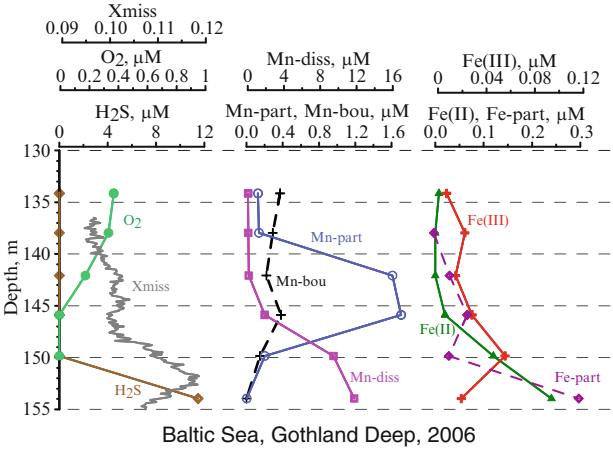

Fig. 9 Vertical distribution of dissolved oxygen (O_2), hydrogen sulfide (H_2S), dissolved Mn (Mn-diss), particulate Mn (Mn-part), bound Mn (Mn-bou), dissolved Fe(II), dissolved Fe(III), particulate Fe (Fe-part), and transmission measured with the hydrophysical probe (Xmiss) in the Baltic Sea, Gotland Deep, 2006

Distribution of dissolved manganese in *the Gotland Deep* is generally characterized by an increase in Mn(II) content with depth in all the sulfidic zone down to the bottom (Figs. 8 and 9). The periodic (ones per several years) oxygenated inflows lead to oxidation and complete vanishing of Mn(II) from the water column. During reestablishment of anoxic conditions, Mn(II) concentrations increase. According to

Table 1 Dissolved manganese near sea bottom concentration in the Gotland Deep

Dissolved Mn, μM	Year	Reference
15–18	1999–2001	Neretin et al. [32]
4	2003	Martens-Habbena, p.c.
30	2005	Our data, RV "Prof. A.Penck"
22	2006	Our data, RV "Prof. A.Penck"
10	2008	Our data, RV "Poseidon"
> 8	2010	Our data, RV "Skagerak"

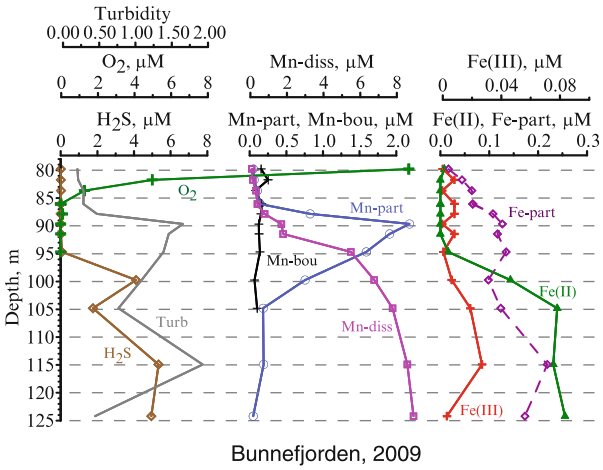

Fig. 10 Vertical distribution of dissolved oxygen (O_2), hydrogen sulfide (H_2S), dissolved Mn (Mn-diss), particulate Mn (Mn-part), bound Mn (Mn-bou), dissolved Fe(II), dissolved Fe(III), particulate Fe (Fe-part), and turbidity measured with the hydrophysical probe (Turb) in the Oslo Fjord, Bunnefjorden, 2009

the observations, the concentrations in the bottom layer can vary from 4 to 30 μM (Table 1). Frequent oxygen intrusion in the redox zone depth also leads to irregular distribution of Mn(II) there, for example, formation of Mn(II) maximum in the first meters of anoxic zone (Fig. 8). The vertical gradient of Mn(II) is also very changeable and can reach much higher values than in the Black Sea (up to 5.2 μM/m).

In *the Bunnefjorden*, the dissolved manganese reaches its maximal concentration of 8–10 μM in first meters of sulfidic zone, and then its concentrations are practically constant with depth (Fig. 10). Its maximal vertical gradient is about two times higher than in the Black Sea (about 1.1 μM/m).

Dissolved manganese distribution in *the Baerumsbassenget* is distinguished by high variability and has nonuniform character (Figs. 11 and 12). Even manganese concentration is not so high, about 4.5 μM, and the vertical gradient is maximal for the studied regions (5.5 μM/m). The specific feature of manganese distribution in Baerumsbassenget is that the onset of dissolved manganese is observed in more oxic conditions than in other regions, at oxygen concentration about 18 μM.

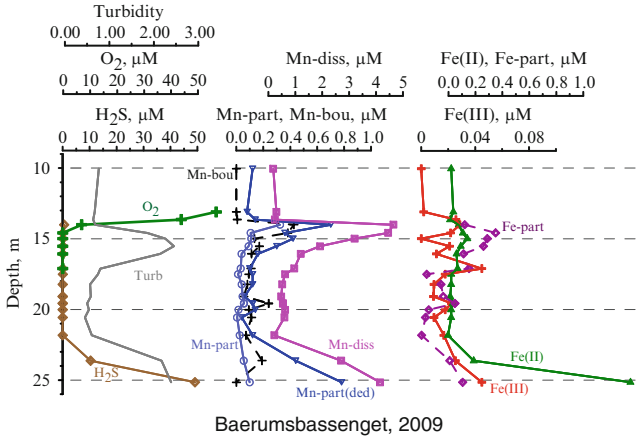

Fig. 11 Vertical distribution of dissolved oxygen (O_2), hydrogen sulfide (H_2S), dissolved Mn (Mn-diss), particulate Mn (Mn-part), particulate Mn determined by deduction of content of Mn in unfiltered sample relative to filtered through 0.4 µm Nuclepore filter immediately after sampling [Mn-part(ded)], bound Mn (Mn-bou), dissolved Fe(II), dissolved Fe(III), particulate Fe (Fe-part), and turbidity measured with the hydrophysical probe (Turb) in the Oslo Fjord, Baerumsbassenget, 2009

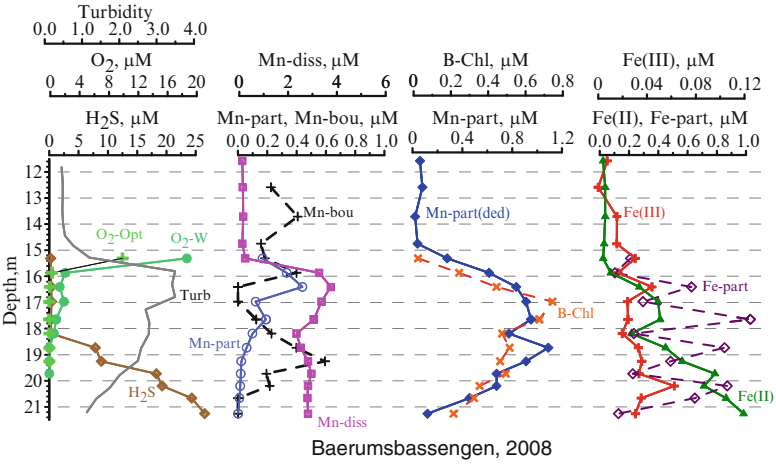

Fig. 12 Vertical distribution of dissolved oxygen measured with Winkler technique (O_2-W) and with Optode (O_2-Opt), hydrogen sulfide (H_2S), dissolved Mn (Mn-diss), particulate Mn (Mn-part), particulate Mn determined by deduction of content of Mn in unfiltered sample relative to filtered through 0.4 µm Nuclepore filter immediately after sampling [Mn-part(ded)], bound Mn (Mn-bou), dissolved Fe(II), dissolved Fe(III) and particulate Fe (Fe-part), turbidity measured with the hydrophysical probe (Turb), and bacteria-Chl-e (B-Chl), in the Oslo Fjord, Baerumsbassenget, 2008

The distribution of the particulate manganese, Mn(IV), in all the regions is characterized by a layer of increased concentration in suboxic zone with a maximum at the hydrogen sulfide boundary (Figs. 3–5, 7, and 9–12). As a rule,

an increase of the concentrations in the oxic zone is enough steep while a decrease in the hydrosulfide zone is more gradual. At the studied regions, the maximum concentration of particulate manganese amounted to 0.2–2.1 μM. The lower content was found in the central Black Sea, and the highest in the coastal Black Sea and the Bunnefjorden.

Dissolved bound manganese, Mn(III), may have several maxima of concentrations located between the particulate manganese and dissolved manganese maxima or can coincide with the Mn(IV) maximum. The concentration of Mn(III) in its maxima amounts in the Black Sea to 0.1–2 μM. In other regions, its concentration does not exceed 0.75 μM (0.5 μM in average). In the Black Sea, bound manganese exists both in colloidal form (0.02–0.40 μm) and truly dissolved (<0.02 μm). Colloidal form could amount up to 90% of bound manganese (Fig. 3).

It is necessary to note that the layers of maxima of both Mn(III) and Mn(IV) are very narrow compared with the possible sampling resolution; therefore the real maximum concentrations and the vertical gradients values can be higher than we can measure.

3.2 Iron

The distribution of dissolved Fe(II) in *the Black Sea* is similar to the manganese one (Figs. 2–4). It is characterized by an increase in the redox zone and the formation of an intermediate maximum within the limits of the dissolved manganese maximum. However, a drastic decrease of the iron (II) concentration takes place deeper as the result of the formation of insoluble iron sulfides.

Under the oxic conditions, Fe(II) rapidly oxidizes to transform into iron (III) represented under these conditions by oxides and hydroxides of low solubility. An increase in the dissolved Fe(II) concentrations occurs at more reduced condition than for dissolved Mn(II) and starts at the sulfidic boundary with a vertical gradient increasing toward the Fe(II) maximum. This maximum of Fe(II) (0.25–0.3 μM on average) is reached at the same depth as the dissolved manganese one. In the deeper layers, Fe(II) decreases to 0.05–0.07 μM, which is controlled by the iron sulfide solubility.

The distribution of Fe(II), as that of Mn(II), is affected by the intrusions of oxic water, which causes its concentration decrease resulting from oxidation.

In *the Landsort Deep* and the *Bunnefjorden*, the distribution of dissolved Fe(II) is quite similar to the Black Sea both by the position of its onset and by the concentration (Figs. 6, 7, and 10). The difference in these regions is that the concentration of Fe(II) does not decrease with depth in sulfidic zone and is practically constant there (0.3 μM) toward the bottom.

Distributions of dissolved Fe(II) for *the Gotland Deep* and the *Baerumsbassenget* differ from those in the Landsort deep and the Black Sea. In most cases, Fe(II) concentration increases toward the bottom and reach up to 1.5 μM in both regions (Figs. 8, 9, 11, and 12). In the Baerumsbassenget, an onset of Fe(II) is located not at

the sulfidic boundary as in other regions but at more oxidized condition at the depth where oxygen goes down below the detection limit.

The distribution of dissolved Fe(III) at all the studied regions is characterized by two maxima of 0.03–0.1 μM. One must note that all the peaks of the dissolved Fe(III) are situated either at the same depths as those of the particulate iron or just below them. The first maximum of Fe(III) coincides with the maxima of dissolved inorganic phosphorus and of particulate manganese. The second maximum of Fe(III) either coincides or is situated a little above the maximum of dissolved Fe(II).

The distribution of particulate iron is characterized by more nonuniformity than that of the particulate manganese, and at most of the stations, the maximum of the particulate iron coincides with that of the particulate manganese. The concentrations of particulate iron in the redox zone of the *Black Sea* amount to 0.04–0.3 μM, excluding the stations affected by the riverine runoff, at which the content of particulate iron may be as high as 2 μM. In the *Gotland*, *Landsort Deeps*, and *Bunnefjorden*, concentration of particulate iron reaches 0.2–0.5 μM, and in the *Baerumsbassenget* it reaches 0.85 μM.

In case of large concentrations, particulate iron may considerably affect the value of turbidity.

4 Discussion

The specific features of the hydrochemical structure observed in the studied objects are summarized in Table 2.

The thickness of the suboxic zone is the largest in the central Black Sea and in the Bunnefjorden. Suboxic zone can be absent in case of such factors as oxygen intrusions, river input, and currents. This was observed in coastal Black Sea, Baltic Deeps, and Baerumsbassenget.

Distribution of dissolved Mn(II) and bound Mn is quite different in the studied regions, while particulate manganese behavior is most similar.

The particulate manganese maximum often coincides with an increased turbidity and a so-called nepheloid redox layer (NRL) can be distinguished there [33]. Besides Mn(IV), a zero-valent sulfur [34], detritus, and bacteria can contribute to a decrease of transparency there. NRL is a usual feature of the Black Sea [28]. In the fjords, NRL usually coincides with maximum of particulate manganese. Only in the Baltic Sea, NRL is located just above the maximum of particulate manganese. Suspended particulate matter (SPM) in the Baerumsbassenget can include together with the manganese oxide, the higher amounts of organic matter and photosynthetic bacteria and has very intensive deep-brown color. Content of SPM in NRL is maximal in Baerumsbassenget (2.5–3.6 mg/l). In other regions it does not exceed 1 mg/l. But manganese content in NRL is minimal in Baerumsbassenget (1.3–1.8%). In the Black Sea its amount is varied from 5% to 15%, in the Bunnefjorden and Gotland Deep is maximal – about 25%.

Table 2 Characteristics of redox zones and Mn, Fe distributions in the Black Sea, the Baltic Sea and Oslo Fjord

	Black Sea		Baltic Sea		Oslo Fjord	
	Center	Periphery	Gotland deep	Landsort deep	Bunnefjorden	Baerumsbassenget
Main features	Stable hydrophysical structure	Enhanced mixing due to RIM current	Oxygen intrusions into suboxic zone	Oxygen intrusions into suboxic zone	Flushing ones per several years	Anoxygenic photosynthesis and river inflow
Depth, m max/redox interface	2,100/70–90	500/140–180	240/115–135	450/60–85	160/80–90	31/16–23
Thickness of suboxic zone, m	10–17	0–12	0–10	0–3	14	1–6
SPMmax, mg/l	0.16–1	1.2–2.4	0.43	0.65	0.5–0.66	2.5–3.6
c(Mn-diss)max, μM	8–10	7–9	16–20	4–4.8	8–10	4–4.6
Grad(Mn-diss) max, μM/m	0.55	0.4	5.2	0.7	1.1	5.5
c(Mn-part)max, μM	0.2–1	1–2	0.5–1.6	0.3–1.5	1.3–2.1	0.7–1
Mn-part, % in SPM	5.5	15	25	2–4	24	1.3–1.8
c(Mn-bou)max, μM	1.8	0.5	0.75	0.4	0.25	0.4–0.6
c(Fe(II))max, μM	0.34	0.45	1–1.5	0.32	0.33	0.4–1.4
c(Fe(III)-diss) max, μM	0.08	0.05	0.03	0.05	0.03	0.04
c(Fe-part)max, μM	0.15–0.29	0.22–0.48	0.36	0.54	0.18–0.22	0.60–0.85
Grad(Fe(II))max, nM/m	5–10	5	30–600	3–25	19	500

A shallow position of the redox interface at Baerumsbassenget can lead to intensive anoxygenic photosynthesis. The whole cell absorption spectra of the samples show a characteristic absorption peak at 715 nm, indicating the presence of bacterial chlorophyll-e (B-Chl-e) and the photosynthetic bacteria type *Chlorobium* sp. [35]. The vertical distribution of the B-Chl-e in the Baerumsbassenget was characterized by a maximum at 17 m, in the middle of the suboxic zone between the onsets of H_2S and O_2 [36]. The B-Chl-e concentrations decrease rapidly until the appearance of H_2S where this decreases slowed down. A similar structure was observed previously at Framvaren Fjord [37]. The B-Chl-e maximum did not correspond to any minimum in the phosphate curve; however, a strong relationship between the vertical distribution of B-Chl-e and SPM (Fig. 12) was shown.

The content of particulate Mn is a subject to seasonal variability [28, 38, 39]. In the Black Sea, particulate Mn concentrations were approximately 0.35 μM in summer and more than 2 μM in winter–spring, and its portion in SPM varied from 6–12% in summer to 35% in winter [28]. This is due to an increase in organic matter content in SPM during the summer and more intensive vertical mixing in the winter. Pohl et al. [39] showed that in the Baltic Sea (Gotland Deep) the seasonal variability of particulate Mn content in SPM (1–5.5%) occurred, with an increase in winter and a decrease in summer, in addition to a high interannual variability, connected to the Baltic Sea oxygenated flushing events. The data received during 2008 correspond to summer values in the Black Sea, significantly greater than values observed in Landsort Deep during 2006 (0.15–0.4 μM of Mn-part, 2% of SPM, [40]). The latter can be linked with the oxygenated intrusions taking place in Landsort Deep before and during the studies.

Particulate Mn variability in the fjord systems could be higher than in the Baltic Sea due to a larger number of the affecting processes (i.e., river input, tides, storm weather, anoxygenic photosynthesis, etc.). The redox zones in the fjords have more "reduced" character. Suspended Mn practically disappeared from the samples, being measured next day. This never was observed for the Black Sea or Baltic Sea.

Our data demonstrate the presence of the dissolved bound Mn(III) in the vicinity of the redox interface at all the studied redox interfaces. The question is what oxidation state of manganese forms complexes and what type of ligands (organic matter?) are involved in. It is known that stable complexes with OM are not typical for the bivalent manganese. Tebo et al. [8] demonstrated the existence of Mn(III) in complexes with high-stability constant (siderophores, $\log K = 47.5$). Trouwborst et al. [7] studied the distribution of Mn(III) in the southwestern Black Sea water in the RV "Knorr" Black Sea cruise 173–7. According to their data, Mn(III) forms a layer with increased content between the particulate Mn maximum and dissolved Mn(II) maximum. As noted above, our data on the bound Mn correspond well with the values and position of the maximum layer; thus we can assume that this bound Mn is Mn(III) complexes [28].

Mn(III) is an intermediate product of Mn(II) oxidation, and it is in unstable form that has to be complexed to exist in marine conditions. Reduction of Mn(IV) to Mn(II) with hydrogen sulfide can also be provided through an intermediate stage of Mn(III) [10, 11] leading to the additional increase of the Mn(III) pool. Many factors

could influence on Mn(III) presence and its content in the redox zone, i.e., the rate of Mn(II) oxidation and Mn(IV) reduction, presence of Mn-oxidizing bacteria, complexing agents for binging Mn(III) with different stability of formed complexes, the rate of vertical diffusion, etc. In the studied regions, the most favorable conditions for existing of the bound Mn(III) are in the Black Sea, where this form of Mn was found at all the studied station with concentration up to 2 μM. In the Baltic Deeps, the presence of bound Mn(III) in the redox zone is not a usual feature.

The occurrence of trivalent manganese in the redox zone of the Black Sea is of great importance.

First, this is one more oxidant that helps to explain the phenomenon of the suboxic zone and an absence of a layer of coexistence of hydrogen sulfide and oxygen. Dissolved oxygen is measured by Winkler method with adding of manganese compounds. Oxidized manganese forms [particulate Mn(IV) and dissolved Mn (III)] presented in sea water above the hydrogen sulfide zone overstate the results of oxygen determination. For example in the 100th cruise of RV "Professor Shtokman," a total concentration of particulate and bound Mn at the sulfidic boundary was to 0.2–0.5 μM with maximum 1.5 μM. After deduction of these values from dissolved oxygen results obtained by the Winkler titration, a 10-m suboxic layer was distinguished where both oxygen and hydrogen sulfide were absent (Fig. 3) [41]. The presence of this layer conforms to modern theoretical conceptions and experimental investigations (e.g., by measurements with oxygen Optode, Fig. 12).

Second, the properties of the trivalent manganese are similar to those of trivalent iron. For example, these compounds form identical complexes with organic matter of seawater [8, 42], which causes concurrent reactions between them. This is of importance for the distribution and biological availability of dissolved iron.

Third, the presence of large amounts of trivalent manganese in the redox zone may affect the distribution of other elements capable of forming compounds with manganese (e.g., phosphorus). Manganese (III)–pyrophosphate complexes are characterized by the ratio Mn/P = 0.52 for $Mn(HP_2O_7)_2^{3-}$, or Mn/P = 0.17 for $Mn(H_2P_2O_7)_3^{3-}$ [9]. As we think, the possible formation of Mn(III) complexes with pyrophosphates might explain the structure observed for the distribution of phosphates. The upper phosphate minimum is located at the depth where Mn(II) disappears due to the oxidation by oxygen, and the lower minimum of phosphates is located a little below the hydrosulfide interface. On the base of our data received in the autumn 2006 near Gelendzhik (Fig. 5), a polyphosphates maximum can be distinguished between the upper minimum and lower maximum of phosphates, with the location depth conforming to the maximum of the Mn-containing dissolved complexes.

A correlation between the Mn-bou and P-poly concentrations was revealed in the redox zone in the Black Sea and the Landsort Deep with the ratios 1.25 and 0.53, respectively [36]. Virtually no correlation between the Mn-bou and P-poly was found in the Oslo Fjord. It can be explained by the fact that in the Baerumsbassenget the redox interface is located very shallow, and the phosphorus cycle (and P-poly

formation) it affected by the biological activity and the river input. In the Bunnefjorden, the upper phosphate minimum was not pronounced and Mn-bou content in the redox layer was very low (0.1 μM). In addition, Mn(III) can form complexes not only with the phosphorus compounds but also with other organic compounds. The composition of organic matter varies in each basin that leads to the formation of different Mn(III) complexes with a different stability constant able to compete with P-containing ligands. This can therefore result in a variable P/Mn ratio for different regions [36]. On the base of the recent data obtained in the 100th cruise of RV "Professor Shtokman" (March to April, 2009), it was found that the bound Mn could exist in two forms – colloidal (0.02–0.40 μm) and truly dissolved (<0.02 μm) that also testify about Mn(III) complexing with different types of ligands.

A different behavior of dissolved manganese below the hydrogen sulfide boundary was noted for studied regions. In the most of the stations in the Baltic Sea and in the fjords, the concentration of dissolved manganese practically does not change with depth in anoxic zone. In the Black Sea, maximum of dissolved Mn is observed in the first tens of meters of sulfidic zone. After that its concentration decreases to about 4 μM and remains constant till the bottom. The mechanism of this maximum formation is not clear as well why it does not exist in other regions. In general, the manganese transformation in the redox zone is characterized by a cyclic character. Being diffused from the sulfidic zone upward to the oxic zone, dissolved manganese is oxidized to transform into particulate form. These high dense particles precipitate down into the sulfidic zone where it is dissolved. The appearance of colloidal manganese foregoes the beginning of the particulate manganese formation. The bound into complexes Mn(III), as an intermediate of Mn reduction and oxidation, is observed between the maxima of dissolved Mn(II) and particulate Mn(IV). In this case, the dissolution of particulate and colloidal manganese and, probably, the decomposition of manganese complexes enlarge the intermediate maximum of dissolved maximum in the Black Sea. In the other regions, this maximum cannot be formed, because the affecting processes are of different intensity as in the Black Sea, i.e., the rates of Mn oxidation/reduction and dissolution; the rates of Mn(IV) particles sinking; the size of these particles; vertical mixing; formation of solid sulfides and carbonates. According to the model calculations, these solid sulfides and carbonates could exist in the Black Sea anoxic waters [1, 43, 44], but they were never found as in the SPM and in the sediment there. Furthermore, these forms were observed in the Baltic Sea where formation of Mn maximum is not a usual feature. The above-mentioned factors affect also the formation and stability of oxidized Mn(III). We tried to estimate its influence on the redox zone structure using modeling.

In the Baerumsbassenget, it was noted that dissolved Mn concentration started to increase at 18 μM of O_2, 15 m depth, and that manganese reduction in this zone must be an aerobic process. The same situation was observed in the Framvaren Fjord, where the highly organic nature of the water column in fjords suggests that the breakdown of humic acids may be critical in the early redox cycling of manganese [45].

At several stations in all the studied regions, some irregularities in the redox zone manganese species distribution [i.e., secondary maxima of Mn(III, IV), changeable gradient of Mn(II)] were observed, while the distributions of O_2 and H_2S were typical (Fig. 4) (for details, see [28]). Under coastal runoffs, currents, etc., the oxic water may be supplied into the anoxic zone. In this case, the stationary conditions of the system are broken and a nonuniform distribution of elements can occur. It is known that different time periods are needed for different elements to return to a stable equilibrium state. Response time for changes in the microbial processes involved in the reduction and/or reoxidation of Mn lags behind that for oxygen injection into water [46]. Concentrations of redox-sensitive species of Mn should thus be useful as a tracer to inter prior hypoxic/anoxic conditions not apparent from redox conditions at the time of sampling.

The above discussion will also impact upon the iron cycle. Distributions of the iron species depend on redox conditions much stronger than the manganese ones, and it seems that the reactions of iron oxidation/reduction occur very fast. Fe(II) was never observed at oxic conditions in contrast to Mn(II). So, the presence of Fe (II) in the absence of detectable oxygen and hydrogen sulfide could indicate to the reduced condition of the system (Fig. 11).

The iron content within the composition of the NRL suspended matter is as high as 1–5.6% in all the studied regions (about 2% in average). In the Gotland Deep and Bunnefjorden, content of Mn-part in the NRL is much higher than that of Fe-part. In the Landsort Deep, their concentrations are comparable. In the Black Sea, both cases were observed. Only in the Baerumsbassenget, Fe-part content exceeds Mn-part content up to ten times practically in all samples. It could be caused by an intensive iron supply with a river and a release from the sediment settled 10–20 m deeper the redox zone. Difference in dissolved Mn(II) and Fe(II) concentrations is also minimal in this basin among the studied regions.

One can conclude that because of its low content in the redox zones, iron does not play any significant role in the formation of the redox interface structure in studied regions with the exception of Baerumsbassenget.

At several stations in the Black Sea, we tried to measure iron bound in stable complexes. Our data show that iron bound into stable, evidently organic, complexes in the water amounts to 0.1–0.5 μM (not shown, see details in [28]). The distribution of bound iron is characterized by two layers of increased iron content: in the oxygenated intermediate water and just under hydrogen sulfide boundary [28]. The first one could coincide with either the upper maximum of the nitrite or positions just above it, and is related probably to the organic matter, which is revealed by fluorescence. The decomposition of plankton organic matter may cause an increase in nitrate and organic iron forms. The second, deep maximum is usually several times lower than to the shallow one. We may suppose that the high concentrations of dissolved bound iron in the layers of maximum can be related to the terrigenous supply of iron and to the biogeochemical transformation to dissolved complexes of OM in the photic layer and below. As a result, a considerable fraction of iron remains dissolved [42, 47–49]. These organic iron complexes are inert; the logarithm of their stability constants may be as high as 45 [42] and they could exist in the colloidal state

[49]. It seems that due to low concentrations of iron bound into the complexes, this compound does not play any important role in the redox processes.

The data we received confirm the existing theories about the functioning of biogeochemical cycles of Mn and Fe. The reduced forms of these metals are soluble compounds supplied by diffusion from the hydrosulfide zone upward, where they are oxidized to transform into the oxidized particulate forms. These forms, due to their higher density, go downward where they are into dissolved forms. This is superposed by the processes of sulfidization and formation of insoluble iron sulfides. The reduced forms of both iron and manganese interact with oxygen. However, the redox potentials and the rate constants of these reactions are different, and the proper reactions may proceed at different contents of oxygen. Manganese is oxidized under the action of bacteria; iron oxidation is possible without bacteria. The reduced iron may be oxidized by particulate manganese to form complex compounds. The layers of particulate iron formation are located lower and those of manganese are higher, which, in general, conforms to the thermodynamics of these processes. The locations of the layers of the maxima of the dissolved manganese and iron in the upper part of the hydrogen sulfide zone also agree with this sequence.

5 Modeling

The redox-interface chemical structure and the abnormality of the distributions of certain parameters are subject to a number of factors. An effective method of analyzing the roles of these factors is the mathematical modeling. In general, the data obtained on the distribution of the different forms of manganese and iron, their seasonal variability, and their influence on the processes occurring in the redox zone are in agreement with the modeling we performed, which are described in detail in [20, 22, 36].

The modeling studies showed that the formation of tetravalent manganese might considerably affect the distribution of the suspended matter and the formation of the layer of turbidity [6]. The particulate manganese may be a primary oxidant of hydrogen sulfide into elementary sulfur. The intense vertical transfer of detritus grains with the heavy particles of Mn (IV) oxide is a cause of the existence of the zone with no detectable oxygen concentrations (Fig. 13).

This makes possible the processes of anoxic oxidation of reduced compounds, such as methane, reduced iron, and ammonium [20].

The theoretical requirement of the occurrence of seasonal variations of the particulate manganese concentrations was also confirmed by means of the model [20] that treated this phenomenon according to the competition for dissolved oxygen between the organic matter supplied from the upper layers and the reduced compounds supplied from the hydrosulfide zone. This competition results in a fact that the processes of the organic matter mineralization become more intense in the summer; hence, less oxygen is available for the oxidation of the reduced forms of

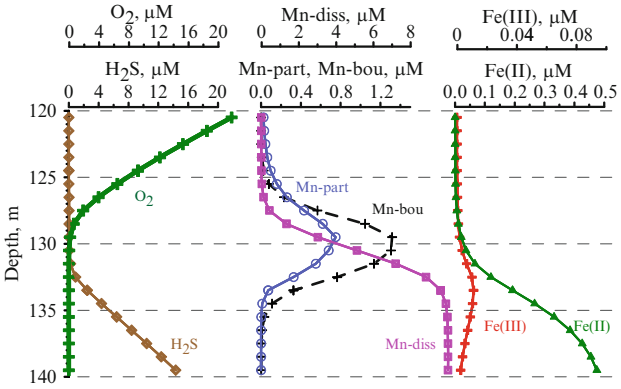

Fig. 13 Vertical distribution of dissolved oxygen (O_2), hydrogen sulfide (H_2S), dissolved Mn (Mn-diss), particulate Mn (Mn-part), bound Mn (Mn-bou), dissolved Fe(II), and dissolved Fe(III) calculated in the model

manganese, iron, and sulfur. At the same time, more oxygen is available for the formation of particulate manganese and iron.

The modeling calculations [20] considering Mn(III) as an independent parameter showed that Mn(III) might oxidize 43% of the sulfides against 50% for Mn(IV). Thus, the total amount of sulfides oxidized into elementary sulfur by oxidized Mn compounds amounts to 93%.

By means of this model, a numerical experiment was performed on the effect of the different processes on the formation of the phosphate distribution profiles. These factors may be (1) chemosynthesis, (2) coprecipitation with metal oxides, and (3) the formation of pyrophosphate complexes with Mn(III). As seen from Fig. 14, at the absence of all three factors listed, the phosphates behave conservatively at the interface area (Fig. 14a). The addition of the chemosynthesis process (Fig. 14b) or of coprecipitation with iron hydroxides (Fig. 14c) causes no pronounced changes. However, the involvement of the process of complexation with Mn(III) allows one to obtain a distribution close to that observed and clearly reproducing the distribution minimum above the hydrosulfide interface and a drastic decrease of the phosphates down to the appearance of hydrogen sulfide (Fig. 14d). According to [9], the Mn:P ratio in the Mn(III)–pyrophosphate complexes may be equal to 0.25 for $Mn(HP_2O_7)_2^{3-}$, or 0.17 for $Mn(H_2P_2O_7)_3^{3-}$. In this model [20], the Mn:P value was 0.66, i.e., even higher by a factor of 2.5–4 than according to [9]. With this ratio, only about 25% of the total Mn(III) should form complexes with pyrophosphates, whereas the remaining fraction may be bound to other ligands. The concentrations of Mn(III) calculated by the model amount to 0.2 μM, which is lower than those usually observed (see above). However, the "phosphate dipole" can be explained even if a part of this Mn(III) forms complexes with phosphorus.

The parameterization of the difference of the rates of the iron and manganese transformation in the model [20] allowed us to reproduce the distribution of the iron

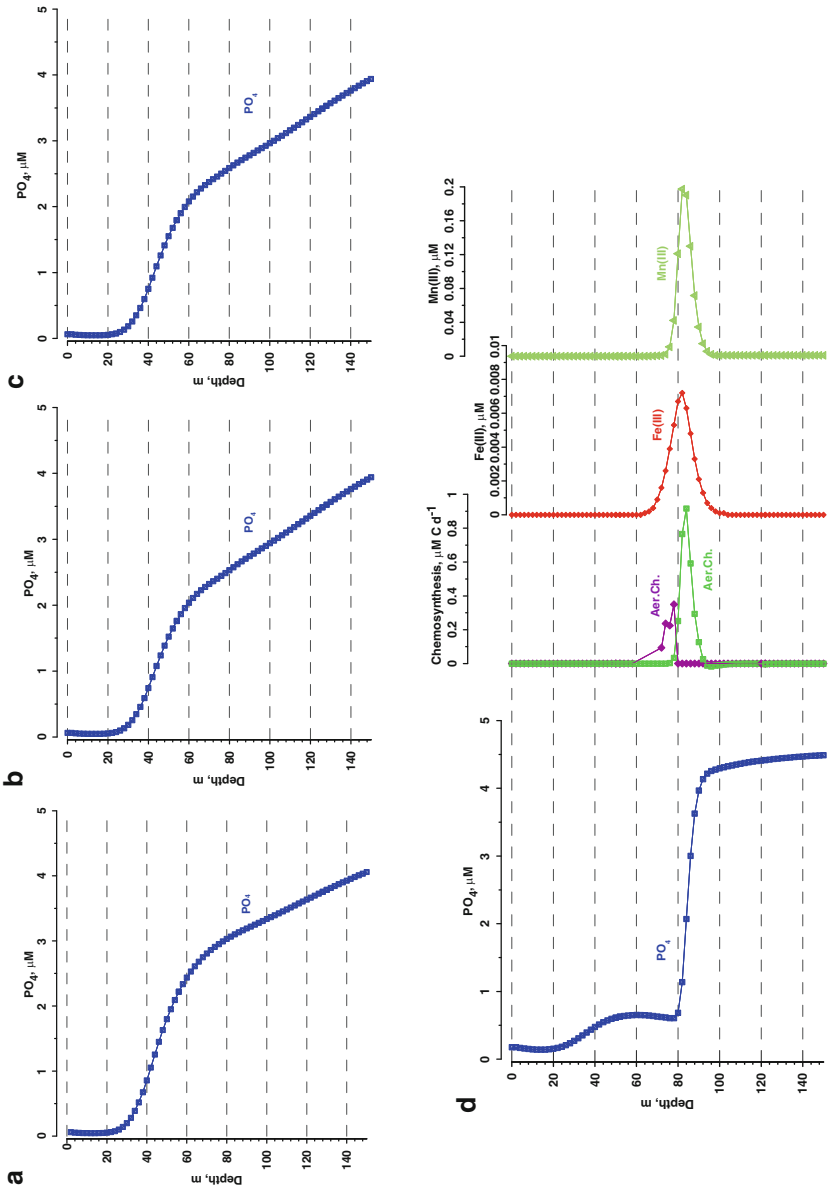

Fig. 14 Model experiments on phosphate minimum formation: (**a**) without influence of Fe(III), chemosynthesis and Mn(III); (**b**) with influence of Fe(III); (**c**) with influence of Fe(III) and chemosynthesis; (**d**) with influence of Fe(III), chemosynthesis and Mn(III), and distributions of chemosynthesis rate, Fe(III), and Mn(III)

forms qualitatively similar to that observed (Fig. 13). The model experiments allow one to conclude that, because of the small concentrations, the role of the iron cycle is insignificant in the formation of the main features of the boundary layer structure between the hydrosulfide and oxic waters.

We used our model to consider the influence of vertical mixing, rate of Mn particles sinking, dissolved Mn content and anoxygenic photosynthesis on the oxidized Mn species, phosphate distributions, and on the suboxic zone wide. Some results of these simulations are presented in Table 3 (in detail, it is described in [36]). One can see that the changes of all studied factors separately could be of great importance for the redox zone structure. In nature, all mentioned factors are not constant and can vary from region to region and from time to time. Their exact combination results in the shape of the distribution of observed parameters.

6 Conclusions

The joint analysis of manganese and iron species distributions (dissolved Mn, dissolved bound Mn, dissolved Fe(II) and Fe(III), particulate Fe and Mn) data obtained in the northeastern Black Sea, the Gotland, and Landsort Deeps of the Baltic Sea and the Oslo Fjord enabled common features to be revealed that demonstrate the similarity of the redox layer formation mechanism in these geographical regions.

Our investigations demonstrate that Mn bound in stable complexes with hypothetical organic matter or pyrophosphate is observed in the redox zones at significant concentrations (up to 2 μM), and is likely present as Mn(III), an intermediate product of the oxidation of Mn(II) and reduction of Mn(IV). This bound Mn plays an important role in the cycle of Mn, and in the cycles of other elements in the redox zone both as oxidizer and complexing agent. It was found that the bound Mn could exist in two forms – colloidal (0.02–0.40 μm) and truly dissolved (<0.02 μm) that perhaps results from complexing with different types of ligands.

Redox interfaces are characterized by the formation of a so-called phosphate dipole with a minimum above the sulfidic boundary and a maximum just below, with a steep increase in concentrations between the two. The hypothesis that P and Mn cycles are interconnected by the formation of complexes between Mn(III) and P-containing ligands can explain the presence of the shallow phosphate minimum above the sulfide interface. The presence of the deep phosphate minimum (below the H_2S boundary) is probably due to the formation of P-containing iron particles [12].

Further studies of the relation between the Mn(III), pyrophosphates, and polyphosphates are of importance to better understand the ecology of seas with anoxic conditions, because the flux of phosphates to the anoxic zone affects the processes of OM production.

Table 3 Simulated by modeling changes in the redox zone structure under different factors. Initial structure parameters: $K_z = 3.5 \times 10^{-5}$ m^2 s^{-1}, W-Mn (IV) = 7.5 md^{-1}, Mn(II)max = 10 μM, Mn-part≈Mn-bou = 0.8 μM, suboxic zone wide – 3 m

Factors		Suboxic zone wide	Oxidized Mn species	Mn-part/Mn-bou	Example of existence
Vertical mixing	High, $K_z = 3.5 \times 10^{-5}$	Absent, C-layer formed	Increase	>	Black Sea near Bosphorus or RIM current
	Low, $K_z = 1 \times 10^{-6}$	Increase, > 5 m	Decrease	≈ <	Central and Coastal Black Sea
Mn particles sinking rate	High, W = 40 md^{-1}	Increase, ≈ 5 m	Decrease	<	Central Black Sea
	Low, W = 0.5 md^{-1}	Present, no changes	Increase	>>	Coastal Black Sea, Gotland Deep, Bunnefjorden
Maximal Mn(II) concentration	High, 30 μM	Increase, >20 m	Increase	≈ <	–
	Low, 5 μM	Disappear, O_2 & H_2S depleted in the same level	No changes	≈	Landsort Deep
Anoxygenic photosynthesis		Increase, >20 m	Decrease	≈	Baerumsbassenget

The flushing events, river input, and sporadically increased mixing and anoxygenic photosynthesis play an important role in the formation of redox zones. Response time for changes in the microbial processes involved in reduction and/or reoxidation of Mn and Fe lags behind that for oxygen injection into water. Concentrations of redox-sensitive species of Mn and Fe should thus be useful as a tracer to inter prior hypoxic/anoxic conditions not apparent from oxygen levels at the time of sampling.

Modeling results confirm that exactly manganese cycle [formation of sinking down Mn(IV) and presence of dissolved Mn(III)] is the main reason of oxygen and hydrogen sulfide direct contact absence. Because of the small concentrations, the role of the iron cycle is insignificant in the formation of the main features of the boundary layer structure between the hydrosulfide and oxic waters. The model experiments enabled the role of a number of factors to be assessed. We suggest that in nature all the factors analyzed (amount of Mn, intensity of mixing, sinking rate) are not constant and can vary from region to region and from time to time. Their exact combination results in the shape of the distributions of the observed parameters.

The further studies of the manganese and iron cycling at the changeable redox conditions are necessary to understand the consequences of oxygen depletion development, i.e., effects for transformation of nutrient and hazardous substances.

References

1. Lewis BL, Landing WM (1991) The biochemistry of manganese and iron in the Black Sea. Deep-Sea Res II 38:S773–S803
2. Tebo BM (1991) Manganese(II) oxidation in the suboxic zone of the Black Sea. Deep-Sea Res II 38:S883–S905
3. Canfield DE, Thamdrup B, Kristensen E (2005) Aquatic geomicrobiology. In: Southward AJ, Tyler PA, Young CM, Fuiman LA (eds) Advances in marine biology, 48. Elsevier Academic Press, Amsterdam – Tokio, p 640
4. Dubinin AV (2005) Geochimiya redkozemelnykh elementov v okeane (Geochemistry of the rare earth elements in the ocean). Naukja, Moscow
5. Murray JW, Codispoti LA, Friederich GE (1995) Oxidation–reduction environments. The suboxic zone in the Black Sea. In: Huang CP et al (eds) Aquatic chemistry: interfacial and interspecies processes, ACS advances in chemistry series 244, pp 157–176
6. Yakushev EV, Debolskaya EI (2000) Particulate manganese as a main factor of oxidation of hydrogen sulfide in redox zone of the Black Sea. In: Oceanic fronts and related phenomena. Konstantin Fedorov Memorial Symposium. Pushkin, Saint-Petersburg, Russia. 18–22 May 1998. Proceedings. IOC Workshop Report No. 159. Kluwer Acad. Publ., 2000, pp 592–597
7. Trouwborst RE, Brian GC, Tebo BM, Glazer BT, Luther GW III (2006) Soluble Mn(III) in Suboxic Zones. Science 313:1955–1957
8. Tebo BM, Clement BG, Luther GW III, Trouwborst RE, Webb SM, Bargar JR, Parker DL, Sposito G (2005) The mechanism of bacterial manganese(II) oxidation and its implication for maintenance of the suboxic zone in the Black Sea. In: Program and abstracts of international ocean research conference, Paris, France, p 154, 5–10 June 2005

9. Webb SM, Dick GJ, Bargar JR, Tebo BM (2005) Evidence for the presence of Mn(III) intermediates in the bacterial oxidation of Mn(II). PNAS 102:5558–5563
10. Kostka JE, Luther GW III, Nealson KH (1995) Chemical and biological reduction of Mn(III)-pyrophosphate complexes: potential importance of dissolved Mn(III) as an environmental oxidant. Geochim et Cosmochim Acta 59:885–894
11. Ali K, Ashiq U (2004) Study of the kinetics and activation parameters of reduction of Mn (III) to Mn(II) by SO_3^{2-} ion in $(MnSiW_{11}O_{40}H_2)_5$- heteropoly ion. J Iran Chem Soc 1:122–127
12. Dellwig O, Leipe T, Glockzin M, Marz C, Pollehne F, Schnetger B, Yakushev EV, Brumsack H-J, Böttcher ME (2010) A new particulate Mn-Fe-P-shuttle in the water column of anoxic basins. Geochim Cosmochim Acta. doi:10.1016/j.gca.2010.09.017
13. Krueger S (2004) Operating manual, integrated IOW/MPI PUMP CTD System, IOW, Warnemuende Germany; <Siegfried.Krueger@iowarnemuende.de>
14. Bordovskiy OK, Chernyakova AM (eds) (1992) Modern methods of the ocean hydrochemical investigations. P.P.Shirshov Institute of Oceanology, Moscow, p 200 (in Russian)
15. Grashoff K, Kremling K, Ehrhard M (1999) Methods of seawater analysis, 3rd completely revised and extended edition. WILEY-VCH, Weinheim
16. Hansen HP (1999) Determination of oxygen. In: Grashoff K, Kremling K, Ehrhard M (eds) Methods of seawater analysis 3rd completely revised and extended edition. WILEY-VCH, Weinheim, pp 75–90
17. Hansen HP, Koroleff F (1999) Determination of nutrients. In: Grashoff K et al (eds) Methods of seawater analysis, 3rd completely revised and extended edition. WILEY-VC, Weinheim, p 149–228
18. Koroleff F, Kremling K (1999) Analysis by spectrophotometry. In: Grashoff K, Kremling K, Ehrhard M (eds) Methods of seawater analysis, 3rd completely revised and extended edition. WILEY-VCH, Weinheim, pp 341–344
19. Kononets MYu, Pakhomova SV, Rozanov AG, Proskurnin MA (2002) Determination of soluble iron species in seawater using ferrozine. J Anal Chem 57:704–708
20. Yakushev EV, Pollehne F, Jost G, Umlauf L, Kuznetsov I, Schneider B (2007) Analysis of the water column oxic/anoxic interface in the Black and Baltic seas with a Redox-Layer Model. Mar Chem 107:388–410
21. Burchard H, Bolding K, Kuhn W, Meister A, Neumann T, Umlauf L (2006) Description of flexible and extendable physical-biogeochemical model system for the water column. J Mar Syst 61:180–211
22. Yakushev EV (2011) RedOx layer model. The Handbook of Environmental Chemistry (this volume)
23. Rozanov AG, Volkov II (2002) Manganese in the Black Sea. In: Complex investigations of the northeastern part of the Black Sea. Nauka, Moscow, p 190–200 (in Russian)
24. Yemenicioglu S, Erdogan S, Tugrul S (2006) Distribution of dissolved forms of iron and manganese in the Black Sea. Deep-Sea Res II 53:1842–1855
25. Skopintsev BA (1975) Forming of the modern chemical composition of water in the Black Sea. Hydrometizdat, Leningrad (in Russian)
26. Stumm W, Morgan JJ (1981) Aquatic chemistry. Wiley, New York
27. Yakushev EV, Chasovnikov VK, Murray JW, Pakhomova SV, Podymov OI, Stunzhas PA (2008) Vertical hydrochemical structure of the Black Sea. In: Kostyanoy AG, Kosarev AN (eds) The Black Sea environment, vol 5, The handbook of environmental chemistry. Springer, Berlin, pp 277–307
28. Pakhomova SV, Rozanov AG, Yakushev EV (2009) Dissolved and particulate forms of iron and manganese in the redox zone of the Black Sea. Oceanology 49:773–787
29. Stunzhas PA, Yakushev EV (2006) Fine hydrochemical structure of the redox zone in the Black Sea according to the results of measurements with an open oxygen sensor and with bottle samplers. Oceanology 46:629–641

30. Stunzhas PA (2000) On the structure of the interaction zone of aerobic and anaerobic water in the Black Sea on the base of measurements by membrane-free oxygen sensor. Oceanology 40:503–509
31. Bashturk O, Volkov II, Gekman S, Gungor H, Romanov AS, Yakushev EV (1998) International expedition on R/V Bilim in July 1997 in the Black sea. Oceanology 38:473–476
32. Neretin L, Pohl C, Jost G, Leipe T, Pollehne F (2003) Manganese cycling at the oxic/anoxic interface in the Gotland deep, Baltic Sea. Mar Chem 82:125–143
33. Volkov II, Kontar EA, Lukashev YuF, Neretin LN, Niffeler F, Rozanov AG (1997) The upper boundary of hydrogen sulfide and redox nefeloid layer in water of the Caucasian slope in the Black Sea. Geochemistry 7:540–550
34. Kamyshny A Jr, Yakushev EV, Jost G, Podymov OI (2011) Role of Sulfide Oxidation Intermediates in the Redox Balance of the Oxic-Anoxic Interface of the Gotland Deep, Baltic Sea. The Handbook of Environmental Chemistry. doi:10.1007/698_2010_83
35. Gloe A, Pfennig N, Brockmann H, Trowitzsch W (1975) A new bacteriochlorophyll from brown-colored Chlorobiaceae. Arch Microbiol 102:103–109
36. Yakushev E, Pakhomova S, Sørenson K, Skei J (2009) Importance of the different manganese species in the formation of water column redox zones: observations and modeling. Mar Chem 117:59–70
37. Sørensen K (1988) The distribution and biomass of phytoplankton and phototrophic bacteria in Framvaren, a permanently anoxic fjord in Norway. Mar Chem 23:229–241
38. Ozturk M (1995) Trends of trace metal (Mn, Fe, Co, Ni, Cu, Zn, Cd and Pb) distributions at the oxic-anoxic interface and in sulfidic water of the Drammensfjord. Mar Chem 48:329–342
39. Pohl C, Loffler A, Hennings U (2004) A sediment trap study for trace metals under seasonal aspects in the stratified Baltic Sea (Gotland Basin; 57º19.20'N; 20º03.00'E). Mar Chem 84:143–160
40. Jost G, Clement B, Pakhomova SV, Yakushev EV (2007) Field studies of anoxic conditions in the Baltic Sea during the cruise of R/V Professor Albrecht Penck in July 2006. Oceanology 47:590–593
41. Yakushev EV, Vinogradova EL, Dubinin AV, Kostyleva AV, Pakhomova SV (2011) On the determination of low oxygen concentrations with Winkler technique. Oceanology (in press)
42. Lewis BL, Holt PD, Taylor SW, Wilhelm SW, Trick CG, Butler A, Luther GW III (1995) Voltammetric estimation of iron(III) thermodynamic stability constants for catecholate siderophores isolated from marine bacteria and cyanobacteria. Mar Chem 50:176–188
43. Spenser DW, Brewer PG (1972) Aspect of the distribution and trace element composition of suspended matter in the Black Sea. Geochim Cosmochim Acta 36:71–86
44. Haraldsson C, Westerlund S (1988) Trace metals in the water columns of the Black Sea and Framvaren Fjord. Mar Chem 23:417–424
45. Swarzenski PW, McKee BA, Sørensen K, Todd JF (1999) ^{210}Pb and ^{210}Po, manganese and iron cycling across the O_2/H_2S interface of a permanently anoxic fjord: Framvaren, Norway. Mar Chem 67:199–217
46. Lewis BL, Glazer BT, Montbriand PJ, Luther GW, Nuzzio DB, Deering T, Ma S, Theberge S (2007) Short-term and interannual variability of redox-sensitive chemical parameters in hypoxic/anoxic bottom waters of the Chesapeake Bay. Mar Chem 105:296–308
47. Rue EL, Bruland KW (1995) Complexation of iron(III) by natural organic ligands in the Central North Pacific as determined by a new competitive ligand equilibration/adsorptive cathodic stripping voltammetric method. Mar Chem 50:117–138
48. Van den Berg CMG (1995) Evidence for organic complexation of iron in seawater. Mar Chem 50:139–157
49. Powell RT, Landing WM, Bauer JE (1996) Colloidal trace metals, organic carbon and nitrogen in a southeastern U.S. estuary. Mar Chem 55:165–176

Role of Sulfide Oxidation Intermediates in the Redox Balance of the Oxic–Anoxic Interface of the Gotland Deep, Baltic Sea

A. Kamyshny, Jr., E.V. Yakushev, G. Jost, and O.I. Podymov

Abstract Depth profiles of sulfur species, including sulfide oxidation intermediates (zero-valent sulfur and thiosulfate), nutrients, metals (Mn, Fe), oxygen, temperature, salinity, and turbidity, were measured in the Gotland Deep, at the eastern Gotland Basin, in July 2007. We found that the highest concentrations of more oxidized sulfide oxidation intermediate, thiosulfate, were located below the highest concentrations of zero-valent sulfur. We explain this paradox by bacterial nitrate reduction coupled with thiosulfate oxidation. The same process using zero-valent sulfur is less effective due to particulate form of the latter. Oxic water intrusions were traced in both the redox transition zone (RTZ) and deep water column by decrease in concentrations of reduced nitrogen and sulfur species (sulfide, zero-valent sulfur, and thiosulfate) as well as by increase in nitrate concentration. Two turbidity maxima were found in the RTZ. Turbidity maximum, which coincides with past oxic water intrusion, was found in the deep sulfide-rich water layer. Profiles of metals and nutrients in most of the profiles indicate as well unstability of the redoxcline and oxic water intrusions at and below the redoxcline.

A. Kamyshny Jr. (✉)
Leibniz Institute for Baltic Sea Research Warnemünde, Seestrasse 15, 18119 Rostock, Germany
Department of Biogeochemistry, Max Planck Institute for Marine Microbiology, Celsuisstrasse 1, 28359 Bremen, Germany
Department of Geology, University of Maryland, College Park 20742, MD, USA
e-mail: alexey93@gmail.com
E.V. Yakushev
Norwegian Institute for Water Research, Gaustadalleen 21, NO-0349 Oslo, Norway
Southern Branch of P.P. Shirshov Institute of Oceanology, Russian Academy of Sciences, Okeanologiya, Gelendzhik – 7, 353470 Krasnodarsky Kray, Russia
G. Jost
Leibniz Institute for Baltic Sea Research Warnemünde, Seestrasse 15, 18119 Rostock, Germany
O.I. Podymov
Southern Branch of P.P. Shirshov Institute of Oceanology, Russian Academy of Sciences, Okeanologiya, Gelendzhik – 7, 353470 Krasnodarsky Kray, Russia

E.V. Yakushev (ed.), *Chemical Structure of Pelagic Redox Interfaces: Observation and Modeling*, Hdb Env Chem (2013) 22: 95–120, DOI 10.1007/698_2010_83,

Keywords Baltic Sea, Gotland Deep, Hydrogen sulfide, Stratified basin, Sulfide oxidation, Thiosulfate, Zero-valent sulfur

Contents

Abbreviations

BBL Bottom boundary layer
RTZ Redox transition zone

1 Introduction

Anoxic conditions in the water column are abundant in upwelling areas [1] and in aquatic systems with restricted circulation, such as Black Sea [2], central parts of Baltic Sea [3], Cariaco Basin [4], some fjords [5, 6], meromictic [7], and monomictic lakes [8]. Bacterial sulfate reduction in the water column and especially in the sediments of stratified basins leads to the buildup of significant concentrations of hydrogen sulfide in the anoxic waters. The water column redox transition zone (RTZ), where both oxygen and sulfide are absent [9], present in insignificant concentrations [6], or coexist at low concentrations [10], is characterized by a complex system of chemical and bacterially driven redox reactions including elements such as oxygen, sulfur, nitrogen, iron, manganese, and trace elements.

Sulfur cycle in the RTZs of stratified basins is complex due to a variety of sulfur-containing compounds with different oxidation states of this element. Sulfate, the most abundant sulfur species in oxic seawater (28.2 mmol l^{-1} at salinity equal to 35), is transformed by bacterial sulfate reduction to sulfide (1).

$$2CH_2O + SO_4^{2-} \rightarrow H_2S + 2HCO_3^- \quad (1)$$

Hydrogen sulfide can be oxidized by oxygen (2) [11, 12], Fe (III) hydroxides (3) ([13–15] and references therein), MnO_2 (4) ([16, 17] and references therein), and Mn(III) complexes [10, 18] to polysulfides (S_n^{2-}), elemental sulfur (S^0), thiosulfate ($S_2O_3^{2-}$), sulfite (SO_3^{2-}), or sulfate (SO_4^{2-}). Microbial processes use these electron acceptors as well as nitrate (NO_3^-) (5) ([19] and references therein) and carbon dioxide (CO_2) [20] (6) for sulfide oxidation. Complexity of the sulfur cycle in anoxic environments increases by bacterial disproportionation of sulfur to sulfide and sulfate (7) ([19] and references therein) and thiosulfate to sulfide and sulfate (8) ([19, 21–23] and references therein).

$$H_2S + O_2 \rightarrow S_n^{2-},\ S^0,\ S_2O_3^{2-},\ SO_3^{2-},\ SO_4^{2-} \quad (2)$$

$$H_2S + Fe(O)OH \rightarrow S_n^{2-},\ S^0,\ S_2O_3^{2-},\ SO_3^{2-} \quad (3)$$

$$H_2S + MnO_2, Mn(III) \rightarrow S_n^{2-},\ S^0,\ S_2O_3^{2-},\ SO_3^{2-},\ SO_4^{2-} \quad (4)$$

$$H_2S + NO_3^- \rightarrow SO_4^{2-} + N_2,\ NH_4^+ \quad (5)$$

$$2H_2S + CO_2 \rightarrow CH_2O + 2S^0 + H_2O \quad (6)$$

$$4S^0 + 4H_2O \rightarrow 3H_2S + SO_4^{2-} + 2H^+ \quad (7)$$

$$S_2O_3^{2-} + H_2O \rightarrow H_2S + SO_4^{2-} \quad (8)$$

As seen from reactions (2–4), different oxidants can convert sulfide to the same sulfide oxidation intermediates. They can oxidize sulfide oxidation intermediates further to sulfate. Production of sulfate by oxidation of sulfide, elemental sulfur, and thiosulfate coupled with bacterial denitrification or nitrate ammonification processes (5, 9, 10) are well studied in bacterial cultures and shown to exist in natural aquatic systems ([19] and references therein; [24–27]). Iron sulfide was also found to be a potential electron donor for microbial nitrate reduction in freshwater wetlands [28]. Sulfide and thiosulfate oxidation coupled with denitrification was proposed to be important in the Gotland Deep RTZ [24, 29]. Production of thiosulfate by culture of *Thioploca* was also shown [30].

$$S^0 + NO_3^- \rightarrow SO_4^{2-} + N_2,\ NH_4^+ \quad (9)$$

$$S_2O_3^{2-} + NO_3^- \rightarrow SO_4^{2-} + N_2,\ NH_4^+ \quad (10)$$

FeOOH and Mn(IV) are possible electron acceptors responsible for sulfide oxidation intermediates formation and consumption in the Cariaco Basin RTZ (4, 11) [31].

$$S_2O_3^{2-} + FeOOH + 14H^+ \rightarrow 2SO_4^{2-} + 8Fe^{2+} + 11H_2O \quad (11)$$

Recent development of sensitive and robust method for detection of polysulfides [32–34], thiosulfate, and sulfite [35–37] allowed quantitative determination of these compounds in the natural water columns, where they present at low-micromolar and sub-micromolar concentrations [6, 38–42]. Measurements of concentration of sulfide oxidation intermediates in marine water columns are still scarce, and their biogeochemistry in such systems is still less understood.

In the Black Sea, total zero-valent sulfur concentrations are up to 5.4 μM at 115–150 m range [2], forming a maximum at the vicinity (±5 m) of the hydrogen sulfide onset [43]. The concentration of zero-valent sulfur retained on 0.2 μm filter shows maximum at about 120 m depth with concentrations not more than 60 nM [44].

In the Cariaco Basin, Hayes et al. [40] report 1–5 μM of $S_2O_3^{2-}$ above the chemocline, defined as the depth of the first appearance of H_2S, 1–5 μM of $S_2O_3^{2-}$ at the chemocline, and up to 6 μM of $S_2O_3^{2-}$ below the chemocline. Concentrations of sulfite are even higher: 1–9 μM, 1–7 μM, and up to 17 μM above, at the chemocline, and below, respectively. Profiles presented in this work show minimum of thiosulfate and sulfite concentrations at the chemocline. The same shape of profiles was reported for Cariaco Basin by Percy et al. [31]. Zhang and Millero [45] showed an increase in both species in Cariaco Basin with depth to 1 μM of thiosulfate and 1.5 μM of sulfite. Tuttle and Jannasch [46] and Li et al. [42] also reported distinct maximum in thiosulfate concentration at dozens meters below the chemocline. Li et al [42] detected zero-valent sulfur concentrations at the RTZ of the Cariaco Basin. Particulate zero-valent sulfur content usually reaches the highest values at or just below the chemocline, above thiosulfate concentration maximum, with typical concentrations between 0.5 and 1 μM. Total zero-valent sulfur concentration reaches more than 1.2 μM. At the depths significantly deeper than the chemocline, all zero-valent sulfur (ca. 0.4 μM) passes through 0.2 μm filter, showing prevalence of dissolved zero-valent sulfur (dissolved cyclooctasulfur and inorganic polysulfides).

In the stratified Mariager Fjord (Denmark), up to 17.8 μM of S^0 and 5.2 μM of thiosulfate were detected at the chemocline, with sharp decrease in the concentrations of these species below and above the chemocline [6]. Peak of S^0 concentrations was found below oxygen–hydrogen sulfide interface. Offset of thiosulfate and sulfite concentrations was found at the same depth as S^0 concentration maximum.

In the Baltic Sea, anoxic water conditions prevail in the deep water of Gotland Deep and Landsort Deep. The central Baltic Sea is intruded sporadically with oxic and saline water from the North Sea. In the periods between oxic water intrusion events, chemocline in the Gotland Deep stabilizes at the depths between 115 m [39] and 135 m (this work). Volkov and Demidova [39] reported zero-valent sulfur and

thiosulfate profiles in the Gotland Deep. Small local maximum of zero-valent sulfur (1.13 μmol l^{-1}) was found at 120 m, the shallowest sample with sulfide concentration >1 μmol l^{-1}. Small local maximum of thiosulfate (1.16 μmol l^{-1}) was found at 125 m depth. After the local minimum at 130–140 m, both species showed higher concentration in sulfidic water layer with maximum concentrations of 2.72 μmol l^{-1} for zero-valent sulfur at 170 m depth and 2.46 μmol l^{-1} for thiosulfate at 210 m depth.

The vertical structure of the reduced sulfur compounds (sulfide, thiosulfate, and zero-valent sulfur) at the redox interface was simulated with a 1D RedOx Layer Model, ROLM [47]. This model considered the processes of oxidation of sulfide with oxygen, manganese (III)/manganese(IV), iron, and nitrate/nitrite to zero-valent sulfur, the further oxidation of S^0 to thiosulfate and sulfate with oxygen and disproportionation of S^0. The calculated distributions under these assumption reproduced a narrow maximum of thiosulfate with concentration of 0.25 μmol l^{-1} just above the sulfide onset, and a maximum of S^0 (1.4 μmol l^{-1}) at the sulfide onset. Then the concentrations of S^0 gradually decreased to 0.2–0.4 μmol l^{-1} about 100 m below the RTZ.

Contrary to calculations published by Yakushev et al. [47], Volkov and Demidova [39] found in RTZ of Gotland Deep the local maximum of S^0 concentrations to be 5 m above the local maximum of thiosulfate concentrations. Thiosulfate maximum below zero-valent sulfur maximum was detected as well by Zopfi et al. [6] in Mariager Fjord and by Li et al. [42] in Cariaco Basin. The data of Li et al. [42] are confirmed by thiosulfate profiles from Percy et al. [31] and elemental sulfur profiles from Hastings and Emerson [48].

One of the main goals of this research was thorough study of location of thiosulfate maximum vs. zero-valent sulfur maximum in the Gotland Deep and explanation of observed trends on the basis of detailed study of nutrients, dissolved and particulate metals concentrations, and to refine the model so that it fitted to observed sulfur intermediates speciation. Another goal was to study an effect of concentrations of nutrients and metals (Fe and Mn) on sulfide oxidation intermediates distribution and speciation in the RTZ.

2 Materials and Methods

2.1 Sampling

Sampling was performed in the eastern Gotland Basin at the Gotland Deep (57°19.2 N; 20°03 E) in July 7–11, 2007. Water samples from different depths around the chemocline, defined as the shallowest appearance of sulfide, were collected by 5l-Free-Flow bottles (Hydrobios) attached to a rosette. The physical structure of the water column was recorded by a conductivity-temperature-depth (CTD) unit (Seabird 911 plus) equipped with a SBE oxygen sensor (Seabird Electronics) and a device for measuring turbidity backscatter signals (Dr. Haardt, Kiel).

2.2 Analytical Techniques

2.2.1 Sulfide and Sulfide Oxidation Intermediates

Hydrogen sulfide was determined photometrically with paraphenilendiaminaccording to Fonselius et al. [49].

Thiosulfate was detected by the monobromobimane method [35]. Fifty microliters of 48 mM solution of monobromobimane in acetonitrile was added to 500 µl of sample in a septa closed 2 ml HPLC vial, immediately followed by addition of 50 µl of buffer (500 mM HEPES, 50 mM EDTA, pH 8). After 30 min, 50 µl of 324 mM methaneulfonic acid was added to stop the derivatization, and the samples were immediately frozen at −20°C and analyzed in less than 1 month. All reagents were added from gas tight syringes through the septa. A Sykam gradient controller S2000, Lichrosphere 60RP select B column (125 × 4 mm, 5 µm, Merck), and a Waters 470 Scanning fluorescent detector (excitation at 380 nm, detection at 480 nm) were used for HPLC analysis. The gradient program used two eluents: Eluent A was 0.25 (v/v) acetic acid, pH adjusted to 3.5 with 5 mol/l NaOH, and eluent B was HPLC grade methanol. The following gradient was used: 0 min – 10% B, 7 min – 12% B, 15–19 min – 30% B, 23 min – 50% B, 30 min – 100% B, 34–39 min – 10% B. Mobile phase flow rate was 1 ml min^{-1}. Detection limit for thiosulfate was 20–30 nM.

Zero-valent sulfur was detected on $ZnCl_2$ preserved samples by chloroform extraction according to Kamyshny et al. [33] with minor changes. To 25 ml of sample, 12.5 ml of 5% $ZnCl_2$ solution was added and the sample was frozen immediately and stored at −20°C before analysis. After sawing, 100 µl of internal standard (400 ppm 4,4′-dibromobiphenyl solution in methanol) was added and the sample was extracted with 2 × 0.5 ml of chloroform. Extracts were combined and analyzed by HPLC. Sulfur was separated on Supelco Discovery C18 reverse phase column (250 mm × 4.6 mm × 5 µm). Dionex GP50 Gradient Pump was used for pumping the mobile phase (methanol) at 1 ml min^{-1}. Dionex UVD340S Diode Array Detector was used for HPLC analysis at 265 nm wavelength. Injection volume was 100 µl. Detection limit was 250–400 nM.

2.2.2 Oxygen, Nutrients, and Metals

Oxygen concentrations were determined by Winkler titration in 100 ml glass bottles [50] using a Metrohm potentiometric titrator. Nutrients were measured photometrically according to [51].

For analysis of metals, 50 ml of water samples were pumped directly into a syringe and filtered through 25 mm Whatman GF/F glass fiber filters. The analyses were performed in the total and filtered fractions according to [52, 53].

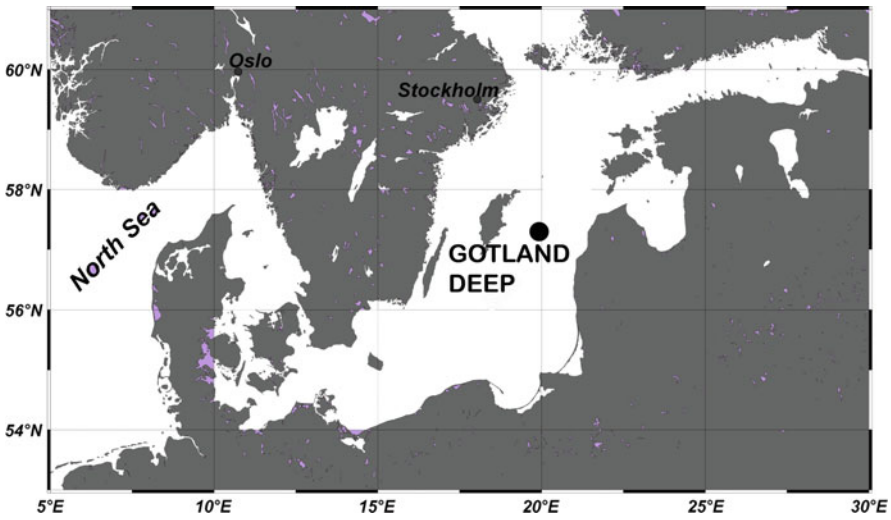

Fig. 1 Location of sampling site, Gotland Deep, Baltic Sea

3 Results

The studies were performed during the RV "Professor Penck" 2007 cruise to the Gotland Deep in the central Baltic Sea (Fig. 1). We had an opportunity to study the structure of RTZ in the stable conditions (absence of intrusions) and unstable conditions (after an intrusion) and the distribution of redox sensitive species in the bottom layer.

3.1 Redox Transition Zone

Profile I (Fig. 2) was taken in July 7, 2007. This profile consists of 12 points with 2 m interval between the points (Profile 1.02). Three depths were sampled above the sulfidic water layer ([total S(II)] < 1 μmol l^{-1}) and nine points at sulfide-rich ([total S(II)] > 1 μmol l^{-1}) water layer. Offset of high sulfide concentration was found at 135 m depth.

In situ temperature decreased from 6.43°C at 128.7 m depth to 6.13°C at 135.4 m depth. At the depth interval, 135.4–151.2 m in situ temperature was in the range 6.10–6.15°C. Salinity increased with depth. Increase was sharp in the depth range 128.7–137.5 m (0.0142 m^{-1}) and slow (0.0066 m^{-1}) in the depth range 137.5–151.2 m (Fig. 2a). In Profile I, two turbidity maxima were recorded: 0.395 Haardt-T at 132.75 m and 0.312 Haardt-T at 138.75 m (Fig. 2b).

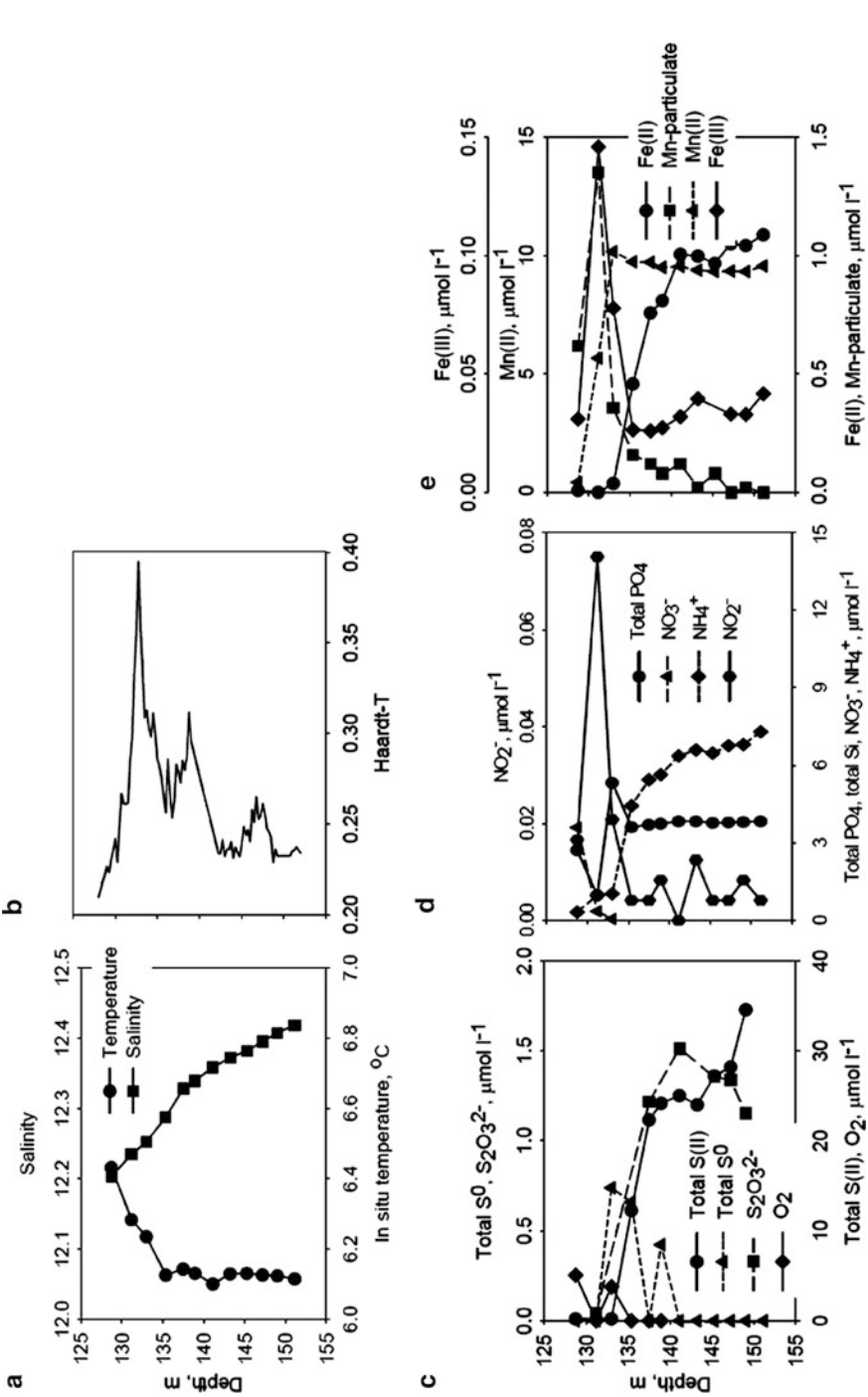

Fig. 2 Profile 1.02. Turbidity (**a**); in situ temperature and salinity (**b**); dissolved oxygen, total S(II), total zero-valent sulfur and thiosulfate (**c**); total phosphate, nitrate, nitrite, and ammonium (**d**); and particulate manganese, Mn(II), Fe(III), and Fe(II) (**e**) profiles

Dissolved oxygen was detected at $\leq$133.0 m depth and sulfide at $\geq$135.4 m depth. S^0 reached a concentration of 0.74 μM at 133.0 m depth. No S^0 was detected below 138.9 m depth. An offset of thiosulfate concentrations was below the peak of S^0, at 137.5 m. Peak of thiosulfate concentrations was detected at 141.1 m (1.51 μmol l^{-1}) followed by slow decrease to 1.15 μmol l^{-1} at 149.0 m (Fig. 2c).

Nitrate sharply decreased to $\leq$0.5 μmol l^{-1} at 131.2 m depth. At this depth, sharp peak of nitrite (0.075 μmol l^{-1}) was detected. Ammonia concentration sharply increased to 4.44 μmol l^{-1} at 135.4 m with further slow increase to 7.30 μmol l^{-1} at 151.2 m depth. Phosphate concentration peak was found at 133.0 m (5.33 μmol l^{-1}) and silicate concentration increased from 9.38 μmol l^{-1} at 128.7 m to 11.15 μmol l^{-1} at 133.0 m (Fig. 2d).

The highest concentration of particulate manganese (1.35 μmol l^{-1}) was detected at 4.2 m above the offset of hydrogen sulfide, at 131.2 m depth, followed by sharp decrease in concentration to 0.16 μmol l^{-1} at the sulfide concentration offset depth and to $\leq$0.1 μmol l^{-1} at 143.2 m depth and deeper samples. Mn(II) concentrations sharply increased from 0.42 μmol l^{-1} at 128.7 m depth to 10.16 μmol l^{-1} at 133.0 m depth. All deeper samples had concentrations of Mn(II) in the range 9.3–9.8 μmol l^{-1}. Fe (III) concentrations showed the pattern, which is very similar to the one of particulate manganese with sharp peak at 131.2 m depth (0.15 μmol l^{-1}), followed by sharp decrease to 0.026–0.042 μmol l^{-1} at 135.4–151.2 m depth. Fe(II) concentrations showed an increase, which started at 133 m depth and continued to 141.1 m depth, where it reached 1.01 μmol l^{-1} concentration. At greater depths, Fe(II) concentration stayed in the range of 0.96–1.09 μmol l^{-1} (Fig. 2e).

Profile II (Fig. 3) was taken in July 11, 2007. This profile consists of 13 points with 1 m interval between the points (sample 5.03). All the samples with depth $\geq$127 m show [total S(II)] $>$ 1 μmol l^{-1}.

In situ temperature showed minimum at 132.2 m (6.10°C) with further slight increase to 6.12°C at 138.2 m depth. Salinity increased with depth. Increase was sharp in the depth range 126.1–132.2 m (0.0152 m^{-1}) and slow (0.0097 m^{-1}) in the depth range 132.2–138.2 m (Fig. 3a). In Profile II, two turbidity maxima were recorded: 0.261 Haardt-T at 129.5 m and 0.313 Haardt-T at 137.0 m (Fig. 3b).

Dissolved oxygen was detected only at 126 m depth. Sulfide was present at this depth as well. Concentrations of total S(II) and dissolved oxygen at 127.1 m depth were 1.44 and 0.33 μmol l^{-1}, respectively. An offset of S^0 concentrations was detected at 128.1 m depth and reached a concentration of 1.10 μM at 129.1 m depth. An offset of thiosulfate concentrations ($[S_2O_3^{2-}] > 0.1$ μmol l^{-1}) coincided with an offset of S^0. Although concentrations of thiosulfate varied significantly, overall increase with depth was observed and the highest concentration was detected in the deepest sample, 1.30 μmol l^{-1} at 138.2 m (1.51 μmol l^{-1}; Fig. 3c).

Nitrate concentrations were $\leq$0.1 μmol l^{-1} at all the depths. Two peaks of nitrite concentrations were detected: 0.033 μmol l^{-1} at 126.1 m and 0.046 μmol l^{-1} at 129.1 m. Ammonia concentration increased from 1.44 μmol l^{-1} at 126.1 m to 5.33 μmol l^{-1} at 138.2 m. Phosphate concentration slowly decreased with depth and had small local maximum at 130.1 m depth. Silicate concentration increased from 10.49 μmol l^{-1} at 126.1 m to 11.24 μmol l^{-1} at 138.2 m (Fig. 3d).

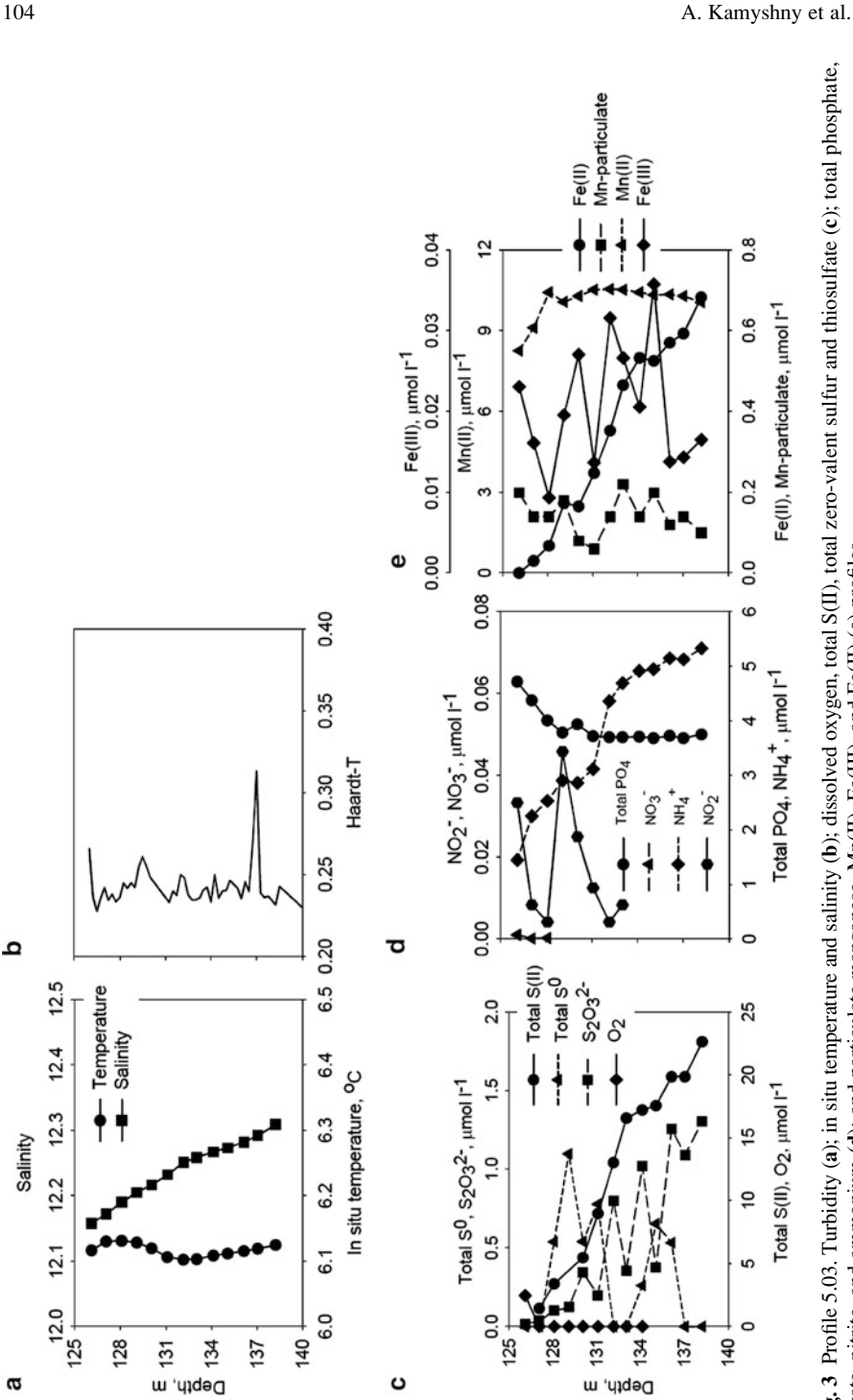

Fig. 3 Profile 5.03. Turbidity (**a**); in situ temperature and salinity (**b**); dissolved oxygen, total S(II), total zero-valent sulfur and thiosulfate (**c**); total phosphate, nitrate, nitrite, and ammonium (**d**); and particulate manganese, Mn(II), Fe(III), and Fe(II) (**e**) profiles

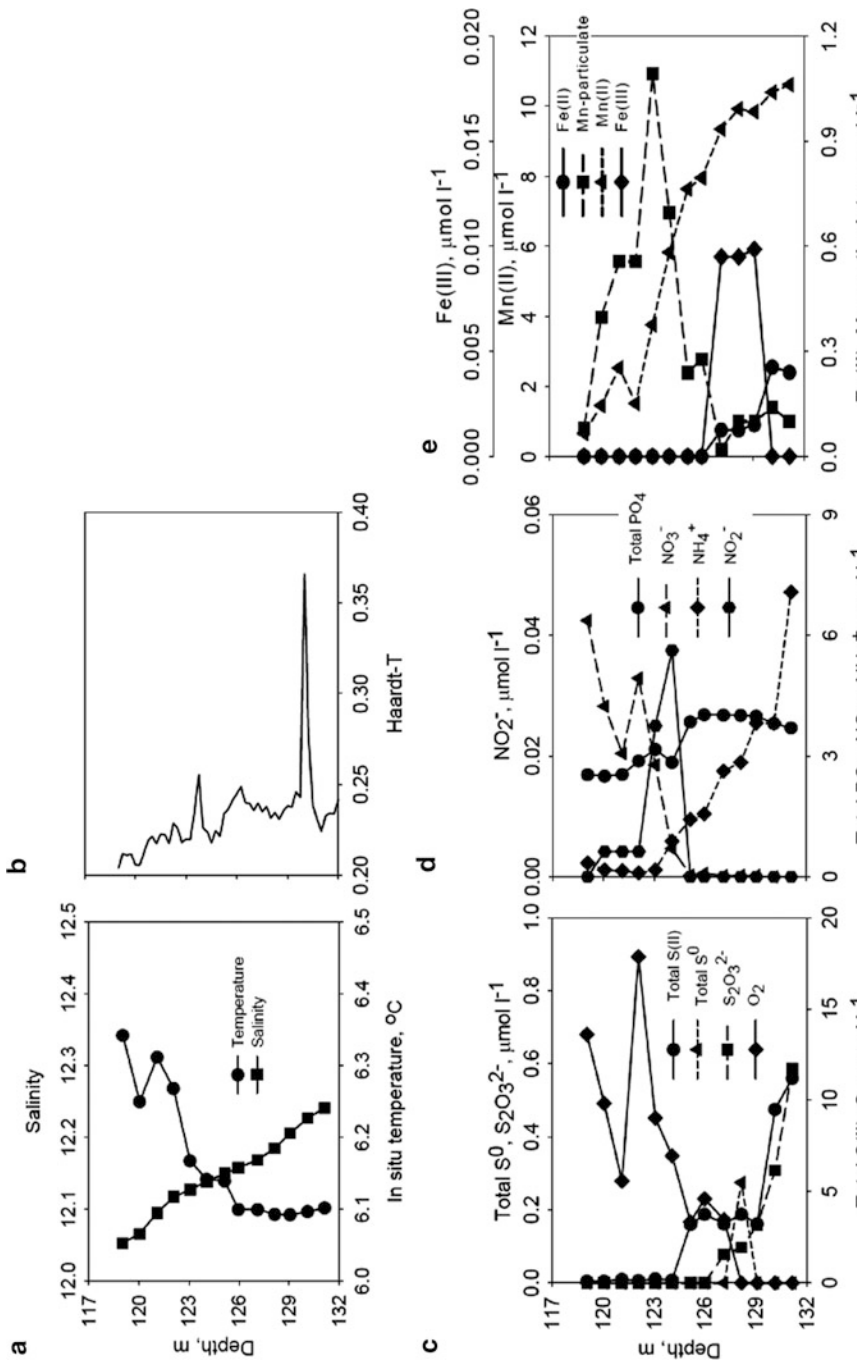

Fig. 4 Profile 5.05. Turbidity (**a**); in situ temperature and salinity (**b**); dissolved oxygen, total S(II), total zero-valent sulfur, and thiosulfate (**c**); total phosphate, nitrate, nitrite, and ammonium (**d**); and particulate manganese, Mn(II), Fe(III), and Fe(II) (**e**) profiles

Concentrations of particulate manganese were low at all sampled depths (0.06–0.22 μmol l^{-1}) and showed no depths dependence. Mn (II) concentrations increased from 8.25 μmol l^{-1} at 126.1 m depth to 10.42 μmol l^{-1} at 128.1 m depth. All deeper samples contained Mn(II) in concentrations 10.0–10.6 μmol l^{-1}. Fe (III) concentrations, like particulate manganese concentrations, showed no depth dependence and were in the range 0.009–0.036 μmol l^{-1} at all the depths. Fe(II) concentrations showed an increase from zero value at 126.1 m to 0.68 μmol l^{-1} at 138.2 m (Fig. 3e).

Profile III (Fig. 4) was taken on July 11, 2007. This profile consists of 13 points with 1 m interval between the points (sample 5.05). Six depths were sampled above the sulfidic water layer ([total S(II)] $<$ 1 μmol l^{-1}) and seven points at sulfide-rich ([total S(II)] $>$ 1 μmol l^{-1}) water layer. Offset of high sulfide concentration was found at 125 m depth.

In situ temperature decreased from 6.34°C at 119.1 m depth to 6.10°C at 126.0 m depth with local maximum of 6.31°C at 121.1 m. At the depth interval 126.0 m–131.1 m, in situ temperature was in the range 6.09–6.11°C. Salinity increased with depth from 12.05 at 119.1 m depth to 12.24 at 131.1 m depth (0.0157 m^{-1}; Fig. 4a). Two turbidity maxima were recorded: 0.255 Haardt-T at 123.75 m and 0.366 Haardt-T at 130.0 m (Fig. 4b).

Dissolved oxygen was detected at $\leq$127 m depth and sulfide at $\geq$125 m depth. At the depth interval 125–128 m, sulfide and dissolved oxygen coexisted. At 126.0 m depth, concentration of total S(II) was 3.76 μmol l^{-1} and concentration of dissolved oxygen was 4.60 μmol l^{-1}. S^0 was detected only at 128.1 m depth, and its concentration was 0.27 μmol l^{-1}. Thiosulfate was detectable at depths $\geq$127.1 m and its concentrations increased to 0.59 μmol l^{-1} at 131.1 m (Fig. 4c).

Nitrate concentrations dropped to below 0.1 μmol l^{-1} at $\geq$125.2 m depths. Nitrite concentrations were $\geq$0.02 μmol l^{-1} at 123.1–124.1 m depth. Ammonia concentration sharply increased from 0.17 μmol l^{-1} at 123.1 m depth to 7.07 μmol l^{-1} at 131.1 m depth. Phosphate concentration showed a slow increase in the RTZ with one local minimum value at 124.1 m, and silicate concentration increased from 9.57 μmol l^{-1} at 119.1 m to 10.97 μmol l^{-1} at 131.1 m (Fig. 4d).

Particulate manganese concentrations had a peak at 120.1–126.0 m depth with maximum at 123.1 m depth (1.09 μmol l^{-1}). Mn(II) concentrations increased with depth from 0.66 μmol l^{-1} at 119.1 m to 10.62 μmol l^{-1}at 131.1 m. Fe (III) was detectable only at 128.1–130.1 m, and detected concentrations were in 0.009–0.010 μmol l^{-1} range.

Fe(II) concentrations increased with depth with offset at 127.1 m. The highest concentration of Fe(II) was detected at 130.1 m depth (0.26 μmol l^{-1}) (Fig. 4e).

On July 12, 2007, Profile IV (Fig. 5) was taken at and above the RTZ. It refers to the system with intrusions of oxic water below the primary offset of high sulfide concentrations. This profile consists of 13 points with 1 m interval between the points (sample 6.02). Concentration of total S(II) at 120–122 and $\geq$127 m is higher than 1 μmol l^{-1}.

In situ temperature profile showed two peaks at 124.0 m depth (6.25°C) and 129.1 m depth (6.20°C) with a minimum (126.2 m, 6.14°C) between them. Salinity

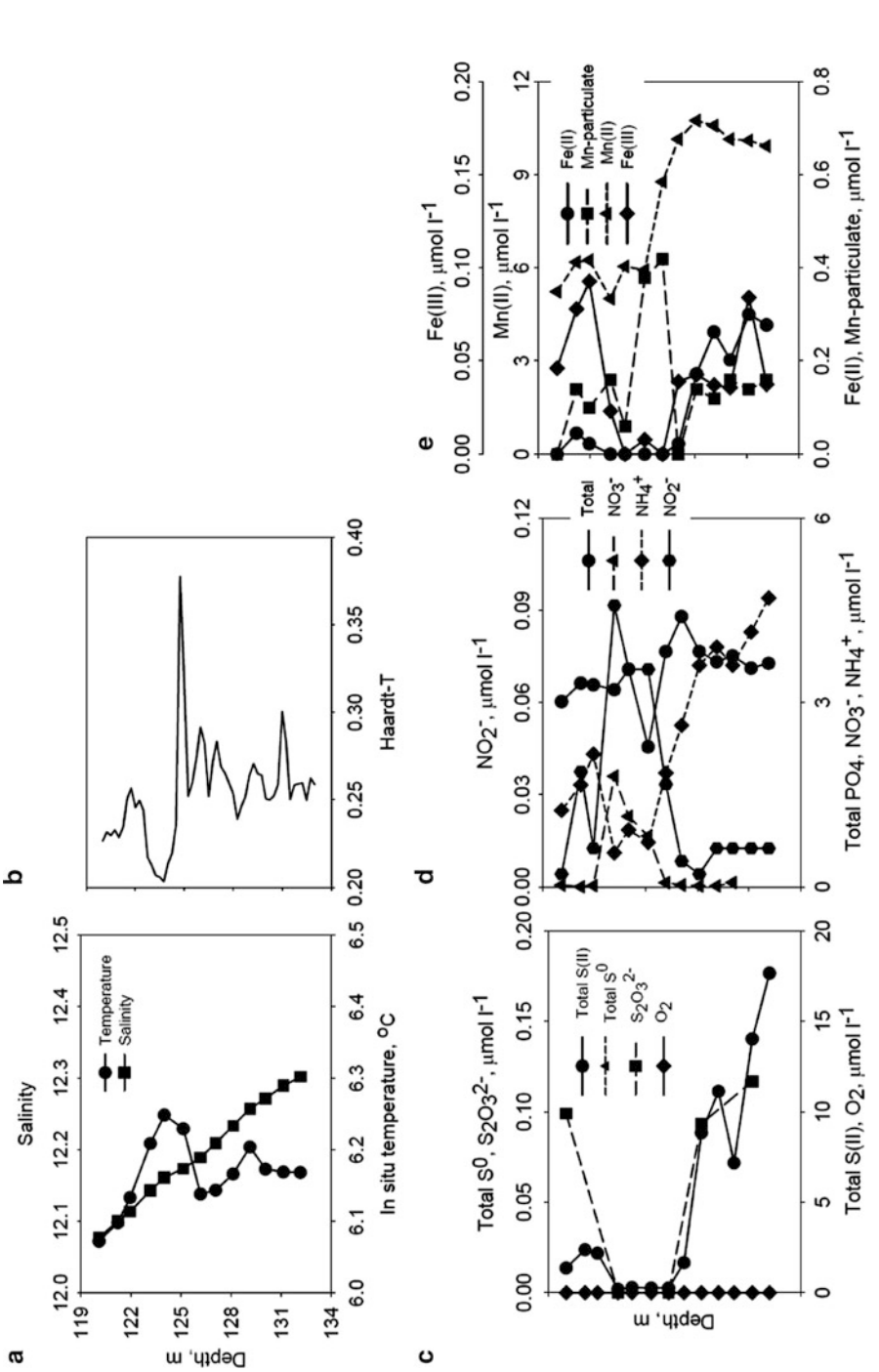

Fig. 5 Profile 6.02. Turbidity (**a**); in situ temperature and salinity (**b**); dissolved oxygen, total S(II), total zero-valent sulfur, and thiosulfate (**c**); total phosphate, nitrate, nitrite, and ammonium (**d**); and particulate manganese, Mn(II), Fe(III), and Fe(II) (**e**) profiles

increased with depth from 12.08 at 121.1 m depth to 12.30 at 132.2 m depth (0.0186 m^{-1}; Fig. 5a). Two turbidity maxima were recorded: 0.378 Haardt-T at 124.75 m and 0.301Haardt-T at 131.0 m (Fig. 5b).

Dissolved oxygen was below the detection limit (2 μmol l^{-1}) at all the depths. Profile of sulfide concentrations vs. depth is a mirror image of dissolved oxygen concentrations profile. Sulfide concentrations rose to 2.1–2.4 μmol l^{-1} at 121.2–121.9 m depth interval and then dropped to <0.3 μmol l^{-1} at 123.2–126.2 m depth. Below 126.2 m depth, sulfide was always present, though at 130.1 m depth sulfide concentration profile had local minimum. S^0 concentrations were below the detection at any depth. Low thiosulfate concentrations were detected only at 120.1 and 128.1–131.1 m depths with maximum of 0.12 μmol l^{-1} at 131.1 m (Fig. 5c).

Peak of nitrate concentrations was detected at 123.2–125.1 m depth. At these depths, concentrations of nitrate were in the range 0.8–1.8 μmol l^{-1}. At all other depths, nitrate was 0.07 μmol l^{-1}. Depth of the highest concentrations of nitrite and nitrate coincided. At 123.2 m depth, 0.092 μmol l^{-1} concentration was detected. Ammonia concentration was 0.7–2.2 μmol l^{-1} at 120.1–125.1 m depths and increased to 4.70 μmol l^{-1} at 132.2 m depth. Phosphate concentration profile showed minimum at 125.1 m depth (2.28 μmol l^{-1}) and maximum at 127.1 m depth (4.40 μmol l^{-1}). Silicate concentration had local maximum at 121.9 m (10.53 μmol l^{-1}), and in the range 125.1–132.2 m silicate concentrations increased from 10.29 to 11.09 μmol l^{-1} (Fig. 5d).

The highest concentration of particulate manganese (0.38–0.42 μmol l^{-1}) was detected between two peaks of hydrogen sulfide concentration, at 125.1–126.2 m depths, followed by sharp decrease in concentration to <0.16 μmol l^{-1}. Significant Mn(II) concentrations were detected at all the depths. In the upper sulfidic waters and underlying non-sulfidic oxic water, Mn(II) concentrations were 5.2–6.3 μmol l^{-1}. At greater depth, Mn (II) concentration increased to 9.9–10.8 μmol l^{-1} (127.1–132.2 m depth). Fe (III) concentrations showed two distinct peaks. The first was at 121.9 m depth (0.093 μmol l^{-1}) just above the oxic layer, located between two sulfide-rich water layers, and the second was at 131.1 m depth (0.084 μmol l^{-1}). Fe(II) showed two maxima as well, the first coinciding with upper sulfidic layer at 121.2 m depth (0.045 μmol l^{-1}), and the second at 131.1 m depth (0.300 μmol l^{-1}; Fig. 5e).

3.2 Bottom Layer

Profile V (Fig. 6) was taken on July 10, 2007. It was dedicated to the study of the conditions below the RTZ with emphasis on the sulfidic deep water column of the Gotland Deep. It consists of nine points taken at different depth intervals between 150 and 233 m water depth (sample 4.03).

In Profile V, wide peak of turbidity with Haardt-T values >0.26 was recorded in 185–212 m depth interval. In situ temperature profile showed minimum (6.10°C) at

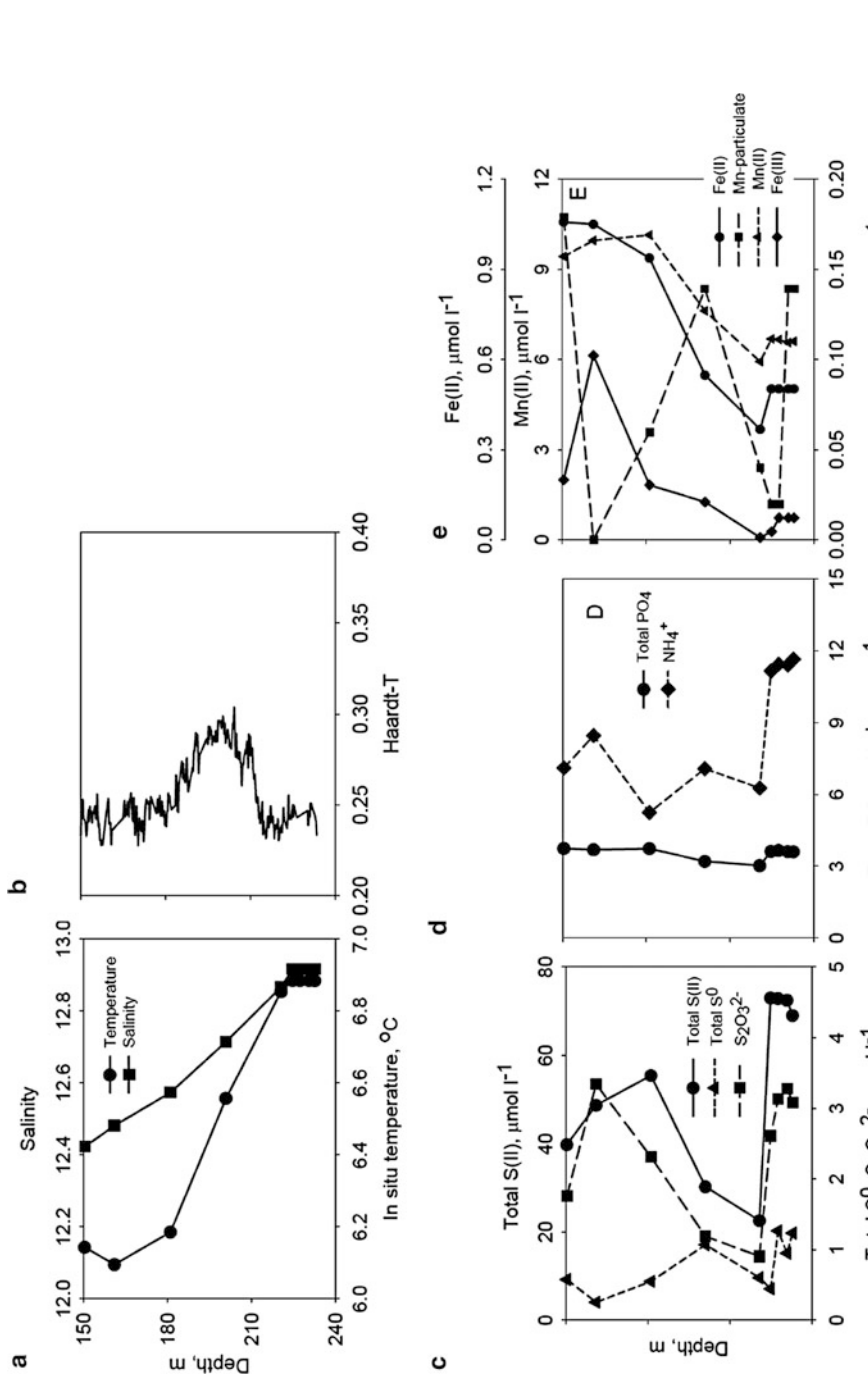

Fig. 6 Profile 4.03. Turbidity (**a**); in situ temperature and salinity (**b**); total S(II), total zero-valent sulfur, and thiosulfate (**c**); total phosphate and ammonium (**d**); and particulate manganese, Mn(II), Fe(III), and Fe(II) (**e**) profiles

161.1 m depth followed by increase with depth to 6.88°C at 224.8 m. Temperature showed no trend with depth (6.88–6.89°C in the 224.8–232.8 m depth interval) near the bottom. Salinity increased with depth from 12.42 at 150.5 m depth to 12.92 at 224.8 m depth (0.0066 m^{-1}). Salinity remained constant at 224.8–232.8 m depth interval (Fig. 6a).

Wide turbidity maximum was found at 180–210 m depth interval (Fig. 6b).

Sulfide concentrations increased with depth in the range 150.5–181.1 m from 39.8 to 55.4 μmol l^{-1}. Two deeper samples (201.0 and 220.7 m depths) showed sharp decrease in sulfide concentrations (30.2 and 22.6 μmol l^{-1}, respectively). At 224.8 m depth, sulfide concentration reached maximum (73.0 μmol l^{-1}) and then decreased reaching again 69.0 μmol l^{-1} near the bottom (232.8 m depth). Total S^0 showed maxima at 201.0 m (1.07 μmol l^{-1}) and near the bottom: 0.95–1.27 μmol l^{-1} at 227.5–232.8 m depths. Thiosulfate showed two concentration maxima as well: 3.34 μmol l^{-1} at 161.1 m depth and near the bottom: 2.61–3.28 at 224.8–232.8 m depths (Fig. 6c).

Nitrate and nitrite were not detected at any depth at Profile V. Ammonia concentration had two maxima: 8.46 μmol l^{-1} at 161.1 m and 11.1–11.7 μmol l^{-1} near the bottom (224.8–232.8 m). Phosphate concentrations were in the range 3.0–3.8 μmol l^{-1} with minimum at 220.7 m depth. Silicate concentration profile showed minimum (11.1–11.3 μmol l^{-1}) at 201.0–220.7 m depths with sharp increase to 13.1–13.2 μmol l^{-1} at 224.8–232.8 m depths (Fig. 6d). Particulate manganese concentrations varied from 0 to 0.18 μmol l^{-1}. Mn (II) showed a minimum (5.93 μmol l^{-1}) at 220.7 m depth with slight increase near the bottom (6.5–6.7 μmol l^{-1}) at 224.8–232.8 m depths. Fe (III) concentrations were the highest (0.102 μmol l^{-1}) at 161.1 m depth. Near the bottom concentrations of Fe (III) are much lower: 0.001–0.012 μmol l^{-1} at 220.7–223.8 m depths. Profile of Fe (II) was similar to that of Fe(III). Fe(II) minimum (concentration 0.368 μmol l^{-1}) coincided with Fe(III) minimum (Fig. 6e).

4 Discussion

Five water profiles presented in this work show three different systems. Profiles I, II, and III represent relatively stable chemocline without intrusions. Profile IV represents chemocline with recent intrusion of oxic water at 123–126 m depth. Although oxygen concentration is already below the detection limit (2 μmol l^{-1}) between 120 and 132 m depths, sulfide and ammonia profiles with minimum in the 123–126 m interval still record this intrusion. Profile V shows distribution of sulfide oxidation intermediates, nutrients, and metals below the chemocline. This profile records as well past oxygen-rich waters intrusion at 200–220 m depth as minimum in sulfide and phosphate concentrations as well as relatively low ammonia concentrations.

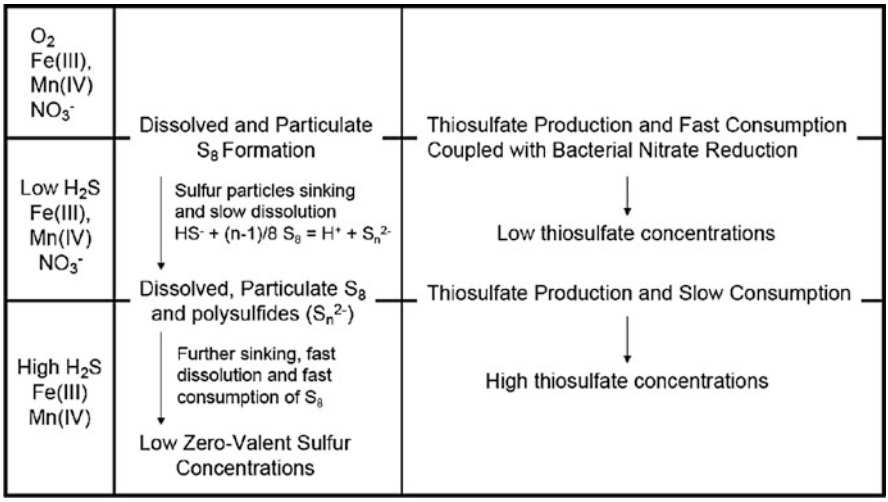

Fig. 7 Scheme of sulfide oxidation intermediates formation and distribution in the RTZ

4.1 Zero-Valent Sulfur–Thiosulfate Distribution Paradox

In all three profiles representing stable chemocline conditions (Profiles I–III), an onset of zero-valent sulfur concentrations (detection limit 400 nmol l^{-1}) occurs above or at same depth as onset of thiosulfate concentrations ($[S_2O_3^{2-}] > 100$ nmol l^{-1}. Maximum of thiosulfate concentrations was always found deeper (3–9 m) than the maximum of zero-valent sulfur concentrations.

Metals such as Fe(III) and/or Mn(IV), which can oxidize sulfide to produce sulfide oxidation intermediates, were detected at the depth of peaking zero-valent sulfur concentrations as well as in the zone of peaking thiosulfate concentrations, and thus cannot account for the measured differences in distribution of these species.

On the other hand, distribution of nitrate in water column negatively correlates with $S_2O_3^{2-}$ concentration profile. Thiosulfate concentrations greater than 50 nmol l^{-1} were always detected at the same depth, where nitrate concentrations declined below 70 nmol l^{-1}. Onset of zero-valent sulfur concentrations has no dependence on nitrate concentrations and rather coincides with oxygen–hydrogen sulfide interface.

We explain the observed distribution of sulfide oxidation intermediates by the following scheme (Fig. 7).

At the interface of oxic and sulfidic waters, both zero-valent sulfur and thiosulfate are produced. Main oxidants here are oxygen and particulate iron and manganese. Zero-valent sulfur at this depth exists as particulate (rhombic and colloidal S_8) and dissolved S_8. Solubility of rhombic cyclooctasulfur in seawater at 12°C is only 7.2 nmol l^{-1}. Most of the produced sulfur exists in the particulate form and thus less bioavailable than dissolved thiosulfate. Bacterial oxidation of thiosulfate coupled with nitrate reduction (10) is much faster than sulfur oxidation by the same

process (9) and even faster than sulfide oxidation with nitrate, effectively suppressing buildup of thiosulfate concentrations.

At greater depth, oxygen is depleted and bacterial nitrate reduction depletes nitrate in the water column. Thiosulfate is produced by oxidation of sulfide with particulate iron and manganese. Bacterial consumption of thiosulfate is much lower at this depth, so thiosulfate concentrations increase. Due to increasing sulfide concentrations, sinking sulfur particles are dissolved according to the reaction (12).

$$HS^- + \frac{n-1}{8} S_8 = H^+ + S_n^{2-} \tag{12}$$

This process increases bioavailability and reactivity of zero-valent sulfur and depletes its concentration in the water column. A part of elemental sulfur may be

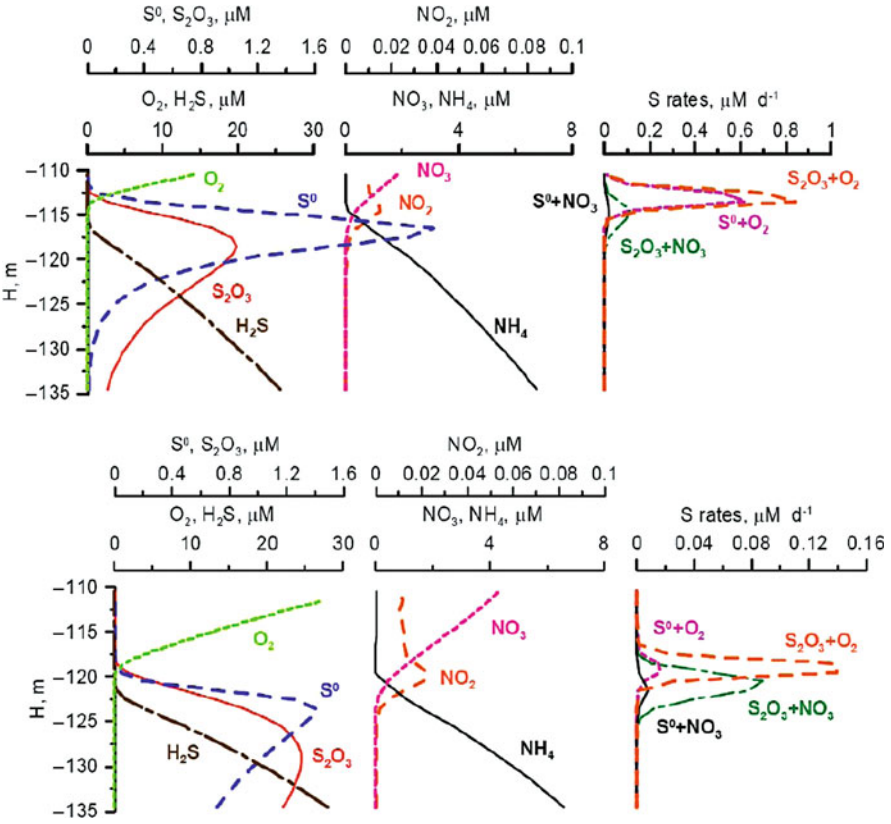

Fig. 8 (**a**) Modeling results taking into account thiosulfate and elemental sulfur oxidation coupled with nitrate reduction. (**b**) Modeling results taking into account thiosulfate and elemental sulfur oxidation coupled with nitrate reduction and sinking of particulate elemental sulfur. S-rates stands for rates of sulfur compound transformation, µmol l^{-1} d^{-1}

oxidized or disproportionated producing thiosulfate as intermediate further increasing concentration of the latter.

Modeling of concentrations of sulfide oxidation intermediates in the chemocline without taking into account sinking of particulate sulfur and processes depicted by (9) and (10) [47] predicted peaking of zero-valent sulfur concentrations below peaking of thiosulfate concentrations. In this work, we changed the model to include these processes. Results of calculations taking into account (1) bacterial oxidation of sulfur and thiosulfate coupled with nitrate reduction (Fig. 8a) and (2) bacterial oxidation of sulfur and thiosulfate coupled with nitrate reduction plus sinking of sulfur particles (Fig. 8b) show that both processes are required to comprehensively explain measured profiles of zero-valent sulfur and thiosulfate.

Another possible explanation of the observed trend considers a possible production of thiosulfate at low electron donor concentrations [54, 55] with sulfate reducers. Thiosulfate concentration rose above 90 nmol l^{-1} only at the depth, where $[O_2] < 1$ μmol l^{-1} and $[H_2S] < 6$ μmol l^{-1}. Maximum thiosulfate concentrations were found at the depths, where $[H_2S] = 0.23–28.2$ μmol l^{-1}. We do not regard this explanation with favor due to the possible extremely low bacterial sulfate reduction rates near the RTZ.

4.2 Nutrients Distribution

Vertical distribution of nutrients was typical for the Gotland Deep RTZ in summer period, which is subjected to the influence of intrusions that erode the upper part of the sulfidic layer. Even in the relatively stable situation (Profiles I–III), the distribution was not "classical" stable structure, where phosphate is characterized by a well-pronounced minimum above the sulfide onset and a maximum at the depth of sulfide appearance. But nevertheless in all of the three first profiles, there was observed well-pronounced maximum of nitrite that marked out a boundary between the upper layer where the concentrations of nitrate started to increase, and the layer below, where the ammonia increase took place. Compared to the balanced RTZ chemical structure that is observed in the Black Sea [56], the non-uniformity of all the nutrient distributions testifies for the presence of intrusions before the observations took place.

The distributions in the period of intrusion are characterized by complicated profiles. A thick layer of increased concentrations of nitrite can testify to redox reactions where this compound forms as a mediator.

The distributions near the bottom allowed to distinguish a 15 m bottom boundary layer (BBL) with uniform distributions of phosphate and ammonia, which was marked out in the Gotland Deep in 2006 [57] and in the Black Sea [58].

4.3 Distribution of Metals

The distributions of metals also allowed distinguishing between the stable balanced structure and a structure subjected to intrusions. The more stable situation was observed in Profile I, where maximum of Mn(IV) was found above the layer of maximum and constant values of Mn(II), and the Fe(III) maximum could be seen above the layer of maximum values of Fe(II). The maximum of Fe(III) was positioned practically at the same depth as the Mn(IV) maximum (±2 m), while an increase in Mn(II) started shallower than an increase in Fe(II) (Fig. 2e). The distributions found in Profiles II and IV were complicated with a changeable concentrations of the metal species at every sampled depth. That might be explained by oxygen rich water intrusions (Figs. 3e and 5e). Profile III demonstrates an intermediate structure, probably the intrusions that took place in the past and the system returns to the steady state situation (Fig. 4e). The distribution of metals in the deep water allows to distinguish the BBL with uniform distribution of the species studied.

4.4 Oxic Water Intrusions at and Below RTZ

Water column of Gotland Deep is not permanently anoxic. Periodic oxygenated salt-rich water intrusions from the North Sea ventilate Baltic Sea deep waters [59]. Oxygen concentrations decrease and sulfide concentrations are built up during stagnation periods. Even during stagnation periods, chemocline is not very stable and periodical intrusions of oxygen-rich waters can be traced below the RTZ. An example of a lens formed by such an intrusion can be clearly seen in Profile IV. Relatively warm, nitrate-rich water layer depleted in ammonia, sulfide, and thiosulfate can be clearly seen at 123–125 m depth. Although oxygen is not detectable at these depths, intrusion of oxic water can still be traced by the depletion in reduced sulfur and nitrogen species.

Another example for such a lens can be seen on the deep water profile (Profile V). Decrease in ammonia, sulfide, and thiosulfate concentrations at 200–220 m depth and increase in temperature, salinity, and wide turbidity peak at 180–210 m are remnant tracers of oxic water intrusion. Between 220 and 224 m depths, the concentrations of all dissolved sulfur, nitrogen, phosphorus, iron, and manganese species as well as salinity and temperature are more homogeneous (Fig. 5). Concentrations of thiosulfate and total zero-valent sulfur reach 3.28 and 1.27 μmol l^{-1}, respectively, probably due to sulfide oxidation at the boundary of past oxic water intrusion. This explanation is supported by relatively high concentration of thiosulfate (3.34 μmol l^{-1}) above the upper boundary of past oxic water intrusion.

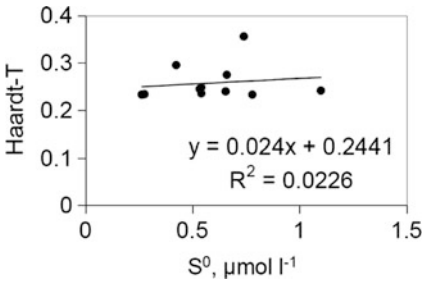

Fig. 9 Turbidity vs. zero-valent sulfur concentration in RTZ of Gotland Deep

4.5 Origin of the Turbidity Maxima

A well-defined first turbidity peak is often found at that depth where measurements of oxygen and H_2S both were at the detection limit. This fine particle layer (FPL) is associated with the RTZ, and the light transmission minimum is observed near the hydrogen sulfide boundary [60].

Until now, all attempts to identify the background of this backscatter signal did not succeed. This signal coincided well with observations done by a camera with a light source attached to the rosette. At the depth of the upper backscatter peak, the camera showed the starting of milky water clouds, sometimes containing even very distinct milky bands (S. Krueger, personal communication).

Turbidity maxima were detected in all profiles. At RTZ, two turbidity maxima were detected with 6.5 $\pm$ 0.7 m difference. In Profiles I and II, upper turbidity peak coincided with zero-valent sulfur peak, but in other profiles no coincidence was found. From Fig. 9, which shows turbidity vs. total zero-valent sulfur concentrations for all RTZ profiles with detectable zero-valent sulfur concentrations ($[S^0] > 250$ nmol l^{-1}), no clear correlation between zero-valent sulfur concentration and turbidity can be seen. In two profiles, upper turbidity peak correlates with nitrite concentration maximum, but there is no clear correlation between nitrate concentration and turbidity as well. We may propose that zero-valent sulfur can be one of the factors that contribute to the FPL formation. The other factors might be the particles of particulate metals and the bacteria.

5 Conclusions

Detailed study of RTZ and water profiles of water column of Gotland Deep (Baltic Sea) revealed that RTZ in this system can be relatively stable (Profiles I–III) and dominated by oxic water intrusions below the oxic–anoxic water boundary (Profile IV). Oxygen intrusion in the deep water was documented as well (Profile V). Although no oxygen was detected below the RTZ, decrease in ammonia, sulfide, and thiosulfate concentrations and increase in temperature, salinity, and

turbidity at 180–220 m depth are the result of recent oxic water intrusion. Even in the profiles with relatively stable RTZ, no phosphate minimum above the sulfide onset and no maximum at sulfide appearance depths were found.

Concentrations of sulfide oxidation intermediates were relatively low. At the RTZ, the highest concentrations of zero-valent sulfur and thiosulfate were 1.10 and 1.51 μmol l^{-1}, respectively. In deep water below RTZ, the highest concentrations of zero-valent sulfur and thiosulfate were found to be 1.27 and 3.34 μmol l^{-1}, respectively. Similar concentrations for thiosulfate and zero-valent sulfur were reported in the RTZ of Gotland Deep by Volkov and Demidova [39] and in RTZ of Cariaco basin by Li et al. [42]. Oxygen is the main electron acceptor for sulfide oxidation at RTZ. Below RTZ, Fe(III) and Mn(IV) are responsible for sulfide oxidation and production of sulfide oxidation intermediates in the deep water column. In profiles with relatively stable redoxcline (Profiles I–III), the maximum thiosulfate concentrations was found at the level, which is 3–9 m deeper than that for the maximum of zero-valent sulfur concentrations. Onset of thiosulfate concentration coincides with depth of nitrate depletion. We propose that thiosulfate oxidation coupled with nitrate reduction is the reason for thiosulfate depletion in the chemocline. Zero-valent sulfur is not removed by this mechanism due to its low solubility in non-sulfidic waters that makes zero-valent sulfur less bioavailable.

Acknowledgments This research was supported by the IOW, Norwegian Institute for Water Research project 29083. A.K. gratefully acknowledges support from the MPG Minerva Program and Max Planck-Society.

References

1. Brüchert V, Jørgensen BB, Neumann K, Riechmann D, Schlösser M, Schulz H (2003) Regulation of bacterial sulfate reduction and hydrogen sulfide fluxes in the central namibian coastal upwelling zone. Geochim Cosmochim Acta 67:4505–4518
2. Neretin LN, Volkov II, Rozanov AG, Demidova TP, Falina AS (2006) Biogeochemistry of the Black Sea anoxic zone with areference to sulphur cycle. In: Neretin LN (ed) Past and present water column anoxia. Springer, Dordrecht, pp 69–104
3. Gustafsson BG, Stigebrandt A (2007) Dynamics of nutrients and oxygen/hydrogen sulfide in the Baltic Sea deep water. J Geophys Res 112:G02023
4. Scranton MI, Astor Y, Bohrer R, Ho T-Y, Muller-Karger F (2001) Controls on temporal variability of the geochemistry of the deep Cariaco Basin. Deep Sea Res Part I Oceanogr Res Pap 48:1605–1625
5. Skei JM, Dyrssen D (eds) (1988) Processes in anoxic basins – with special reference to Framvaren, South Norway. Mar Chem (special volume) 23:209–461
6. Zopfi J, Ferdelman TG, Jørgensen BB, Teske A, Thamdrup B (2001) Influence of water column dynamics on sulfide oxidation and other major biogeochemical processes in the chemocline of Mariager Fjord (Denmark). Mar Chem 74:29–51
7. Overmann J, Beatty JT, Hall KJ, Pfennig N, Northcote TG (1991) Characterization of a dense, purple sulfur bacterial layer in a meromictic salt lake. Limnol Oceanogr 36:846–859
8. Eckert W, Conrad R (2007) Sulfide and methane evolution in the hypolimnion of a subtropical lake: a three-year study. Biogeochemistry 82:67–76

9. Murray JW, Codispoti LA, Friederich GE (1995) In: Huang CP, O'Melia CR, Morgan JJ (eds) Aquatic chemistry: interfacial and interspecies processes. ACS advances in chemistry series. No. 224. American Chemical Society, Washington, DC, pp 157–176
10. Trouwborst RE, Clement BG, Tebo BM, Glazer BT, Luther GW (2006) Soluble Mn(III) in suboxic zones. Science 313:1955–1957
11. Chen KY, Morris JC (1972) Kinetics of oxidation of aqueous sulfide by O_2. Environ Sci Technol 6:529–537
12. Zhang J, Millero FJ (1993) The products from the oxidation of H_2S in seawater. Geochim Cosmochim Acta 57:1705–1718
13. Pyzik AJ, Sommer SE (1981) Sedimentary iron monosulfides – kinetics and mechanism of formation. Geochim Cosmochim Acta 45:687–698
14. dos Santos Afonso M, Stumm W (1992) Reductive dissolution of iron(III) hydr(oxides) by hydrogen sulfide. Langmuir 8:1671–1675
15. Yao W, Millero FJ (1996) Oxidation of hydrogen sulfide by hydrous Fe(III) oxides in seawater. Mar Chem 52:1–16
16. Burdige DJ, Nealson KH (1986) Chemical and microbiological studies of sulfide-mediated manganese reduction. Geomicrobiol J 4:361–387
17. Yao W, Millero FJ (1993) The rate of sulfide oxidation by δMnO2 in seawater. Geochim Cosmochim Acta 57:3359–3365
18. Kostka JE, Luther GW III, Nealson KH (1995) Chemical and biological reduction of Mn (III)-pyrophosphate complexes: potential importance of dissolved Mn (III) as an environmental oxidant. Geochim Cosmochim Acta 59:885–894
19. Jørgensen BB (2000) Bacteria and marine biogeochemistry. In: Schulz HD, Zabel M (eds) Marine geochemistry. Springer, Berlin, pp 173–207
20. Cohen Y, Jørgensen BB, Padan E, Shilo M (1975) Sulphide-dependent anoxygenic photosynthesis in the cyanobacterium *Oscillatoria limnetica*. Nature 257:489–492
21. Jørgensen BB (1990) A thiosulfate shunt in the sulfur cycle of marine sediments. Science 249:152–154
22. Jørgensen BB (1990) The sulfur cycle of freshwater sediments: role of thiosulfate. Limnol Oceanogr 35:1329–1342
23. Jørgensen BB, Bak F (1991) Pathways and microbiology of thiosulfate transformations and sulfate reduction in a marine sediment (Kattegat, Denmark). Appl Environ Microbiol 57:847–856
24. Brettar I, Rheinheimer G (1991) Denitrification in the Central Baltic: evidence for H_2S-oxidation as motor of denitrification at the oxic-anoxic interface. Mar Ecol Prog Ser 77: 157–169
25. Dannenberg S, Kroder M, Dilling W, Cypionka H (1992) Oxidation of H_2, organic compounds and inorganic sulfur compounds coupled to reduction of O_2 or nitrate by sulfate-reducing bacteria. Arch Microbiol 158:93–99
26. Taylor GT, Iabichella M, Ho T-Y, Scranton MI, Thunell RC, Muller-Karger F, Varela R (2001) Chemoautotrophy in the redox transition zone of the Cariaco Basin: a significant midwater source of organic carbon production. Limnol Oceanogr 46:148–163
27. Soares MIM (2002) Denitrification of groundwater with elemental sulfur. Water Res 36: 1392–1395
28. Haajer SCM, Lamers LPM, Smolders AJP, Jetten MSM, Op den Camp HJM (2007) Iron sulfide and pyrite as potential electron donors for microbial nitrate reduction in freshwater wetlands. Geomicrobiol J 24:391–401
29. Brettar I, Labrenz M, Flavier S, Bötel J, Kuosa H, Christen R, Höfle MG (2006) Identification of a Thiomicrospora denitrificans-like Epsilonproteobacterium as a catalyst for autotrophic denitrification in the central Baltic Sea. Appl Environ Microbiol 72:1364–1372
30. Otte S, Kuenen JG, Nielsen LP, Paerl HW, Zopfi J, Schulz HN, Teske A, Strotmann B, Gallardo VA, Jørgensen BB (1999) Nitrogen, carbon, and sulfur metabolism in natural Thioploca samples. Appl Environ Microbiol 65:3148–3157

31. Percy D, Li X, Taylor GT, Astor Y, Scranton MI (2008) Controls on iron, manganese and intermediate oxidation state sulfur compounds in the Cariaco Basin. Mar Chem 111:47–62
32. Kamyshny A Jr, Ekeltchik I, Gun J, Lev O (2006) Method for the determination of inorganic polysulfide distribution in aquatic systems. Anal Chem 78:2631–2639
33. Kamyshny A Jr, Borkenstein CG, Ferdelman TG (2009) Protocol for quantitative detection of elemental sulfur and polysulfide zero-valent sulfur distribution in natural aquatic samples. Geostand Geoanal Res 33:415–435
34. Kamyshny A Jr (2009) Solubility of cyclooctasulfur in pure water and sea water at different temperatures. Geochim Cosmochim Acta 73:6022–6028
35. Fahey RC, Newton GL (1987) Determination of low-weight thiols using monobromobimane fluorescent labeling and high-performance liquid chromatography. Methods Enzymol 143: 85–96
36. Vairavamurthy A, Mopper K (1990) Determination of sulfite and thiosulfate in aqueous samples including anoxic seawater by liquid chromatography after derivatization with 2, 2′-Dithiobis(5-nitropyridine). Environ Sci Technol 24:333–337
37. Rethmeier J, Rabenstein A, Langer M, Fischer U (1997) Detection of traces of oxidized and reduced sulfur compounds in small samples by combination of different high-performance liquid chromatography methods. J Chromatogr A 760:295–302
38. Zopfi J, Böttcher M, Jørgensen BB (2008) Biogeochemistry of sulfur and iron in Thioploca-colonized surface sediments in the upwelling area off central Chile. Geochim Cosmochim Acta 72:827–843
39. Volkov II, Demidova TP (2003) Compounds of reduced inorganic sulfur in the waters of the Baltic Sea. Oceanology 43:805–810
40. Hayes MK, Taylor GT, Astor Y, Scranton MI (2006) Vertical distribution of thiosulfate and sulfite in the Cariaco Basin. Limnol Oceanogr 51:280–287
41. Kamyshny A Jr, Zilberbrand M, Ekeltchik I, Voitsekovski T, Gun J, Lev O (2008) Speciation of polysulfides and zero-valent sulfur in sulfide-rich water wells in southern and central Israel. Aquat Geochem 14:171–192
42. Li X, Taylor GT, Astor Y, Scranton MI (2008) Relationship of sulfur speciation to hydrographic conditions and chemoautotrophic production in the Cariaco Basin. Mar Chem 112: 53–64
43. Yakushev EV, Neretin LN (1997) One-dimensional modeling of nitrogen and sulfur cycles in the aphotic zones of the Black and Arabian Seas. Global Biogeochem Cycles 11:401–414
44. Luther GW III, Church TM, Powell D (1991) Sulfur speciation and sulfide oxidation in the water column of the Black Sea. Deep Sea Res 38(Suppl 2):S1121–S1137
45. Zhang J, Millero FJ (1993) The chemistry of the anoxic waters of the Cariaco Trench. Deep Sea Res I 40:1023–1041
46. Tuttle JH, Jannasch HW (1979) Microbial dark assimilation of CO_2 in the Cariaco Trench. Limnol Oceanogr 24:746–753
47. Yakushev EV, Pollehne F, Jost G, Kuznetsov I, Schneider B, Umlauf L (2007) Analysis of the water column oxic/anoxic interface in the Black and Baltic seas with a numerical model. Mar Chem 107:388–410
48. Hastings D, Emerson S (1988) Sulfate reduction in the presence of low oxygen levels in the water column of the Cariaco Trench. Limnol Oceanogr 33:391–396
49. Fonselius S, Dyrssen D, Yhlen B (1999) Determination hydrogen sulfide. In: Grashoff K, Kremling K, Ehrhard M (eds) Methods of seawater analysis. 3d, completely revised and extended edition. WILEY-VCH, Weinheim, pp 91–100
50. Hansen HP (1999) Determination of oxygen. In: Grashoff K, Kremling K, Ehrhard M (eds) Methods of seawater analysis. 3d, completely revised and extended edition. WILEY-VCH, Weinheim, pp 75–90

51. Hansen HP, Koroleff F (1999) Determination of nutrients. In: Grashoff K, Kremling K, Ehrhard M (eds) Methods of seawater analysis. 3d, completely revised and extended edition. WILEY-VCH, Weinheim, pp 149–228
52. Koroleff F, Kremling K (1999) Analysis by spectrophotometry. In: Grashoff K, Kremling K, Ehrhard M (eds) Methods of seawater analysis. 3d, completely revised and extended edition. WILEY-VCH, Weinheim, pp 341–344
53. Pakhomova SV (2005) Soluble forms of iron and manganese in the sea water, sediments, and on the water–bottom interface, Candidate's Dissertation in Geology and Mineralogy (IO RAN)
54. Fitz RM, Cypionka H (1990) Formation of thiosulfate and trithionate during sulfite reduction by washed cells of Desulfovibrio desulfuricans. Arch Microbiol 154:400–406
55. Sass H, Steuber J, Kroder M, Kroneck PMH, Cypionka H (1992) Formation of thionates by freshwater and marine strains of sulfate-reducing bacteria. Arch Microbiol 158:418–421
56. Yakushev EV, Chasovnikov VK, Debolskaya EI, Egorov AV, Makkaveev PN, Pakhomova SV, Podymov OI, Yakubenko VG (2006) The northeastern Black Sea redox zone: hydrochemical structure and its temporal variability. Deep Sea Res II 53:1764–1786
57. Jost G, Clement B, Pakhomova SV, Yakushev EV (2007) Field studies of anoxic conditions in the Baltic Sea during the cruise of R/V Professor Albrecht Penck in July 2006. Oceanology 47:590–593
58. Volkov II, Skirta AY, Makkaveev PN, Demidova TP, Rozanov AG, Yakushev EV (2002) On hydropphysical and hydrochemical uniformity of the deep waters of the Black Sea. In: Zatsepin AG, Flint MV (eds) Complex investigation of the Northeastern Black Sea. Nauka, Moscow, pp 119–133 (In Russian)
59. Kautsky L, Kautsky N (2000) The Baltic Sea, including Bothnian Sea and Bothnian Bay. In: Sheppard CRC (ed) Seas at the millenium: an environmental evaluation, vol 1, Regional Seas: Europe, The Americas and West Africa. Elsevier Science Ltd., Oxford (UK) and Pergamon Press, Amsterdam (Netherlands), pp 121–133
60. Volkov II, Kontar' EA, Lukashev YF, Neretin LN, Nyffeler F, Rozanov AG (1997) Upper boundary of the hydrogen sulfide and the nature of the Nepheloid Redox Layer in the waters of the Caucasian Slope of the Black Sea. Geochem Int 6:618–629

On Interannual Variability of Chemical Characteristics of Redox Layer and Cold Intermediate Layer of the Black Sea

O.I. Podymov, E.V. Yakushev, and A.V. Kostyleva

Abstract Based on the measurements on more than 1,700 stations during last three decades in the northeastern Black Sea, analysis of seasonal and interannual variability of chemical characteristics of Cold Intermediate Layer (CIL) and redox layer is given. Studied species include main nutrients, dissolved oxygen, hydrogen sulfide, and carbon system elements. Our studies showed that surface layers ventilation with dissolved oxygen down to the depth of the CIL occurs in winter. The intensity of ventilation is determined by climate forcing, which may be regulated by large-scale climate formations like the NAO. This ventilation sets the upper boundary conditions for the downward transport of O_2. The Black Sea hydrogen sulfide boundary oscillates in the density field with an amplitude of $\sigma_\theta = 0.05–0.15$ kg m^{-3} depending on the climate variability, which is well related to the NAO index. The position of the sulfide boundary indicates on the volume of the oxic layer in the Black Sea and plays a major role in the functioning of the Sea ecosystem. No clear trend of pH decrease in the Black Sea CIL, testifying to progressive acidification, was revealed. The CIL pH variability was significantly correlated with the CIL oxygen changes, which were logically consistent with the interannual variability of the winter vertical mixing intensity.

Keywords Black Sea, Cold intermediate layer, Interannual variability, North Atlantic oscillation, Redox zone, Sulfidic boundary

O.I. Podymov (✉) and A.V. Kostyleva
Southern Branch of P.P. Shirshov Institute of Oceanology, Russian Academy of Sciences, Okeanologiya, Gelendzhik – 7, 353470 Krasnodarsky Kray, Russia
e-mail: huravela@yahoo.com

E.V. Yakushev
Southern Branch of P.P. Shirshov Institute of Oceanology, Russian Academy of Sciences, Okeanologiya, Gelendzhik – 7, 353470 Krasnodarsky Kray, Russia

Norwegian Institute for Water Research, Gaustadalleen 21, Oslo 0349, Norway

E.V. Yakushev (ed.), *Chemical Structure of Pelagic Redox Interfaces: Observation and Modeling*, Hdb Env Chem (2013) 22: 121–136, DOI 10.1007/698_2011_122,

Contents

Abbreviations

CIL	Cold intermediate layer
EAWR	East Atlantic/West Russia
NAO	North Atlantic oscillation
NBS	National Bureau of Standards
NIST	National Institute of Standards and Technology
Nm	Nautical mile
OM	Organic matter
RAS	Russian Academy of Sciences
TIC	Total inorganic carbon

1 Introduction

While anoxic conditions are rather common feature in numerous areas of coastal and marginal seas, the case of the Black Sea is unique. The vertical structure of this world's deepest anoxic basin is subject to a permanent halocline (50–120 m), which separates the waters of riverine origin from the high salinity waters stemming from the Marmara Sea. Annual winter mixing occurs only down to the depth of 50–80 m ($\sigma_\theta \sim 14.45$–14.6 kg m^{-3}), where the Cold Intermediate Layer (CIL) is formed. The consequent strong vertical stratification results in permanent anoxic conditions of the deep layers of the Black Sea (from 60–180 m to bottom $\sigma_\theta \sim 17.23$–17.24 kg m^{-3} [1]). The suboxic zone with concentrations of both oxygen and hydrogen sulfide lower than the detection limit is formed between the oxic layer and anoxic deep layers [2].

Away from the SW region, influenced by the Bosphorus Plume, redox potential decreases gradually with increasing depth and water density. In the depth range where oxic conditions change to anoxic (the redox zone), oxidized and reduced chemical species interact. These processes occur in a predictable sequence depending on the changes in redox potential [2, 3]. Redox reactions involving species of Fe, Mn, N, S, C, and some other elements occur in the suboxic zone.

Also, the hydrophysical structure of the redox layer is very stable comparing with other redox regions, often affected by eddies or intrusions of oxygenated waters (i.e., the Gotland Deep, Cariaco Trench).

The sequence of reactions is characterized by diagnostic chemical parameters distributions. Certain features (maxima, minima, onset points) occur in narrow layers of water of similar density, and they are very stable in the density field. These distributions display *chemotropicity* – the correspondence of vertical chemical structure to specific density levels [4]. There are numerous estimates of typical density levels of the onset of chemical species, depths of extremes and depths of change of vertical gradients [2, 4–7].

The CIL, which is generally considered within the bounds of the 8°C isotherms [8], is usually located above $\sigma_\theta \sim 15.2–15.8$ kg m^{-3} with its core at $\sigma_\theta \sim 14.45–14.6$ kg m^{-3}. The main pycnocline lies between $\sigma_\theta \sim 14.5$ kg m^{-3} and $\sigma_\theta \sim 16.5$ kg m^{-3}. The oxycline is on the average located between $\sigma_\theta \sim 14.4–14.6$ kg m^{-3} and $\sigma_\theta \sim 15.6–15.9$ kg m^{-3}, i.e., between the core of the CIL and the upper boundary of the redox layer. The redox layer can be defined as the layer between the oxycline, where the nitrate maximum is located, and the upper part of the sulfidic zone, where the oxidized forms of manganese disappear ($\sigma_\theta \sim 16.1–16.3$ kg m^{-3}). Therefore, the suboxic layer with concentrations of oxygen and hydrogen sulfide lower than the detection limit (usually from $\sigma_\theta \sim 15.8–15.9$ kg m^{-3} to $\sigma_\theta \sim 16.1–16.2$ kg m^{-3}), is positioned within the bounds of the redox layer. A term oxic/anoxic interface is usually associated with the sulfidic boundary position. The anoxic layer occupies the water column from the sulfidic boundary to the bottom of the Black Sea.

All these layers' spatial distribution is characterized by a dome-like form with shallower depth in the center of the Sea and deeper near the coasts (e.g., the sulfidic boundary depth is about 80–100 m in the center and about 160–200 m near the coasts).

The surface water is the only source of cold water into the CIL since the Bosporus inflow is warmer (about 12°C), thus the variations in this layer determine variable ventilation of surface water into the CIL. The most common view is that the waters of the CIL are renewed from the surface every year [8, 9], and the intensity of the CIL formation varies from year to year depending mainly on the atmospheric forcing.

The chemical characteristics of seawater are inevitably subject to interannual changes. During the last years, the studies on ocean de-oxygenation [10, 11] and on ocean acidification [12] became very topical and worthy in connection to climate change consequences assessments. The Black Sea represents a separate from the World Ocean water body. However, it is influenced by the same climatic forcing, and the predictable global changes manifested elsewhere shall be reflected at the regional level of the Black Sea as well. Herewith, the goal of this work was to study the peculiarities of interannual variability of chemical characteristics in the redox layer and the CIL of the Black Sea and to relate then to climate forcing.

2 Materials and Methods

The analyzed data included results of measurements at more than 1,700 stations acquired mainly in the northeastern part of the Black Sea from 1984 up to present (Fig. 1).

It is worth mentioning that all the measurements in the compiled data set were performed in the expeditions of the Shirshov Institute of Oceanology of RAS applying the same modifications of analytical techniques (and compatible sets of standards); therefore, the chemical data throughout the whole period of investigations are comparable. A detailed inventory of these data is presented in [7, 13]. The studied area is far from the influence of the Bosporus input and Danube River inflow, thus chemical dynamics in the upper layers of this region should reflect "integrated" rather than local changes of the sea.

A standard set of analytical techniques described in [14, 15] was used. Dissolved oxygen (O_2) analyses were performed using Winkler technique. pH was determined on the NBS/NIST scale using standard buffer solutions produced in the USSR and Russia. Total alkalinity (Alk) was determined in the coastal laboratory by direct titration with hydrochloric acid, according to Bruevich's modification [15]. The process of titration with constant venting with CO_2-free air to a pH of 5.45 was monitored using a glass electrode. Hydrogen sulfide (H_2S) was determined photometrically with paraphenilendiamin, ammonium (NH_4) was determined by the phenol-hypochlorite reaction. Dissolved manganese (Mn(II)) was determined spectrophotometrically using the formaldoxime procedure [14].

Elements of the carbonate system (partial pressure of carbon dioxide, pCO_2; total inorganic carbon, TIC; bicarbonate, HCO_3^-; carbonate CO_3^{2-}; and aragonite saturation) were calculated as function of pH and Alk. according to Roy et al. [16] and verified with CO2SYS program [17], which produced the same results.

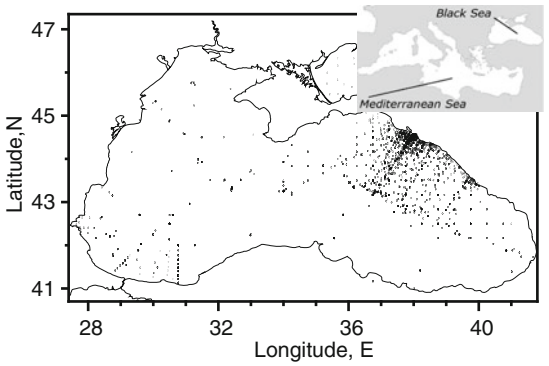

Fig. 1 Location of sampling stations, from 1984 to 2009

3 Results

3.1 Characteristic Vertical Biogeochemical Structure

The typical vertical biogeochemical structure of the Black Sea is demonstrated by a selected example in Fig. 2.

These particular distributions were observed in the coastal zone of the NE Black Sea at 10 nm offshore the city of Gelendzhik on the 21th of July, 2010. During the referred observations, the CIL was thicker and was situated deeper than its typical level, at $\sigma_\theta \sim 14.35–15.0$ kg m^{-3}.The halocline was observed below the CIL at $\sim 14.65–15.55$ kg m^{-3} (Fig. 2a).

Dissolved oxygen was depleted at $\sigma_\theta \sim 15.85$ kg m^{-3}. The nitrate maximum was located at around $\sigma_\theta \sim 15.3$ kg m^{-3} (Fig. 2b). The depletion point of hydrogen sulfide was found at $\sigma_\theta \sim 16.10$ kg m^{-3}. The deep ammonia and dissolved reduced manganese depletions were observed at $\sigma_\theta \sim 16.0$ kg m^{-3}.

The phosphate "dipole" [18] was clearly pronounced with the shallower maximum at $\sigma_\theta \sim 15.8–15.9$ kg m^{-3}, the deep maximum at $\sigma_\theta \sim 16.2–16.3$ kg m^{-3}, the shallow minimum at $\sigma_\theta \sim 15.96–16.00$ kg m^{-3} and the beginning of a phosphate decrease toward the deep minimum deeper than $\sigma_\theta \sim 16.3$ kg m^{-3}. Oxidized Mn (III) and Mn (IV) peaks corresponded to the shallow phosphate minimum (around $\sigma_\theta \sim 16.0$ kg m^{-3}) that confirmed their interconnection [19]. The oxidized manganese forms disappeared at $\sigma_\theta \sim 16.15$ kg m^{-3}.

The distribution of the carbonate system parameters were well in agreement with the existing conception. pH decreased from values of 8.2–8.3 (in situ, NBS units) at the surface to minimum values of about 7.83–7.85 in the redox layer (Fig. 2c). According to [20] in the upper layer, pH values vary from 7.8 to 8.6 with maximal values in winter. The vertical distribution of pH in the suboxic layer is remarkable for its minimal values (i.e., 7.80–7.90). This decrease of pH values is connected with the decomposition of OM to CO_2 and the oxidation of reduced forms of sulfur, nitrogen, carbon, manganese, and iron [20].

The distribution of alkalinity was characterized by a noisy pattern with a general increasing trend of concentrations from 3350–3400 μM in the surface layer to 3350–3500 μM in the redox layer (Fig. 2c). According to the existing estimates [21, 22], the Black Sea is characterized by elevated content of inorganic carbon. The carbonate alkalinity in the Black Sea surface waters (3,000 μM) is by 1.4 times higher than in the oceanic waters (2,150 μM). In the deep waters, it varies from over 1 μM up to 4250–4300 μM [21].

The vertical distributions of the calculated carbonate system components (TIC, HCO_3^-, CO_3^{2-} and Aragonite Saturation) are shown in Fig. 4. The distributions of TIC and HCO_3^- demonstrated a correlated increase of concentrations from 3200 μM and 3000 μM in the surface layer to 3450 μM and 3300 μM in the redox zone correspondingly, while CO_3^{2-} decreased from 180 μM in the surface layer to 80 μM in the redox zone. One can note that the aragonite saturation is close

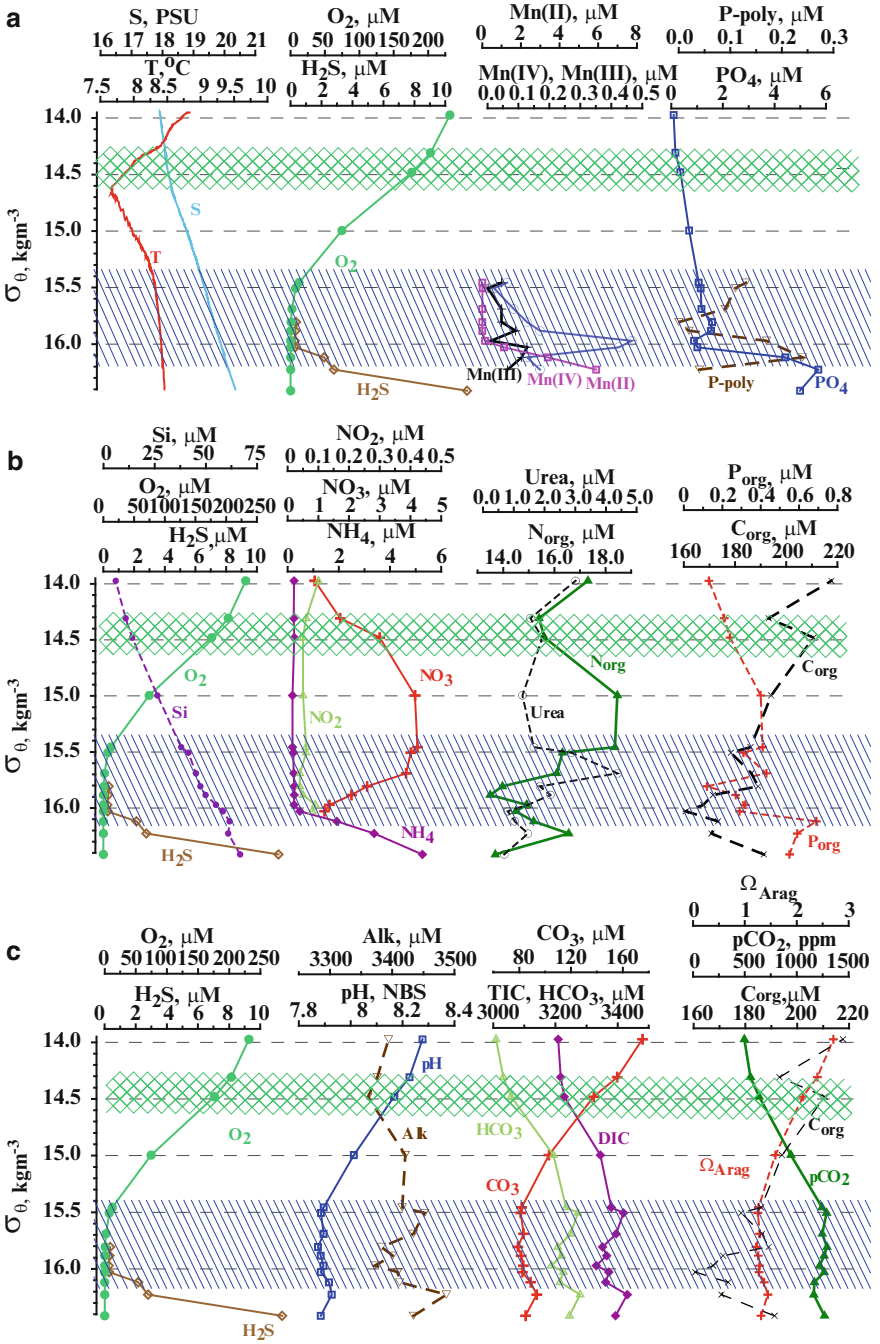

Fig. 2 Characteristic vertical structure of the Black Sea: distributions of temperature, *T*; salinity, *S*; dissolved oxygen, O_2; hydrogen sulfide, H_2S; dissolve manganese, *Mn(II)*; particulate manganese, *Mn(IV)*; dissolved bound manganese, *Mn(III)*; phosphate, PO_4; polyphosphate, *P-poly* (**a**);

to 1 in the redox zone compared with 2.5–3 at the surface. In the CIL aragonite saturation was about 2.

The vertical distributions of dissolved organic carbon, nitrogen, and phosphate shown in Fig. 2 reflect a general decreasing tendency of organic carbon and organic nitrogen values from the upper layer to the redox zone, while organic phosphorus is characterized by an increase of values at the sulfidic boundary, that was observed earlier [7]. The carbon present in dissolved organic form decreased from 200–220 μM in the surface layer to 160–180 μM in the redox layer, and in all the depth was higher than the carbon present as carbonate ion CO_3^{2-}.

The structure shown in Fig. 2 is typical for the northeastern Black Sea summer distributions, observed earlier as well [4, 23]. Overall, the density levels corresponded to those listed in Chelysheva et al. [24]. As proposed earlier [38], the nitrate maximum can be taken as the upper boundary of the redox layer ($\sigma_\theta \sim 15.3$ kg m^{-3}). For the lower boundary of this layer, it is reasonable to choose the level of disappearance of the oxidized manganese forms ($\sigma_\theta \sim 16.15$ kg m^{-3}). This layer is shown in Fig. 2 as diagonal-hatched area. For the calculations in this work, we identified CIL as the layer between isopycns of 14.45 and 14.60 kg m^{-3} (shown as cross-hatched area in Fig. 2).

3.2 *Interannual Variability of O_2, H_2S, NH_4 and Mn(II)*

Based on the available data, the variations of onsets in the density field of H_2S, NH_4, and Mn(II) and changes of the averaged concentrations of O_2 and carbonate system parameters for the CIL were evaluated.

Monthly averaged results of calculations for the months when any data were available are shown in Figs. 3 and 4. The data for the summer months (May–October) are shown as diamonds and for the winter months (November–April) as circles.

The Akima spline-based method was used to calculate the onset values [13]. The obtained values slightly differed from the estimates reported by other authors who used the visual or linear regression criteria for estimating the onset of hydrogen sulfide [2, 25]. We believe the Akima spline-based method is more accurate as it is nonlinear and based on the objective approach to every single station, which is appropriate in analysis of large data arrays.

Fig. 2 (continued) distributions of silicate, *Si*; nitrate, NO_3; nitrite, NO_2; ammonia, NH_4; dissolved organic nitrogen, N_{org}; Urea; dissolved organic carbon, C_{org}; dissolved organic phosphorus, P_{org} (**b**); distributions of pH; alkalinity, *Alk*; bicarbonate, HCO_3; carbonate, CO_3^{2-} total inorganic carbon, *TIC*; partical pressure of CO_2, pCO_2 and aragonite saturaion Ω_{Arag} (**c**). CIL is shown as cross-hatched area ($\sigma_\theta \sim 14.45$–14.60 kg m^{-3}), redox zone is shown as a diagonal-hatched area ($\sigma_\theta \sim 15.30$–16.15 kg m^{-3})

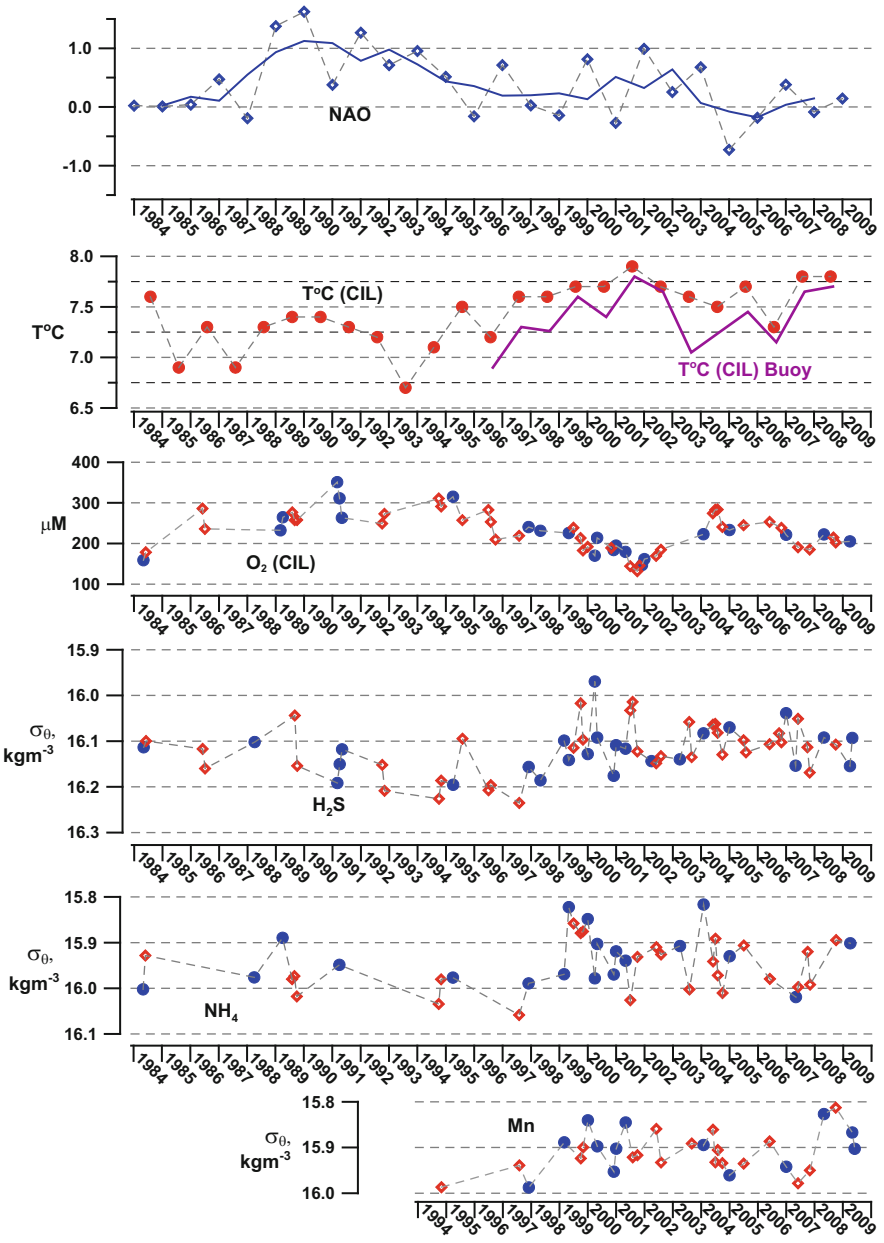

Fig. 3 Interannual variability of the winter NAO index (*diamonds* – averaged for February–April, *lines* – averaged for 3 successive years), *NAO*; temperature in CIL core in the Northeastern Black Sea (data of V.G. Krivosheya), *T°C(CIL)*; averaged temperature in the CIL core (data of the MHI oceanographic database and ARGO floats), *T°C(CIL)Buoy*; averaged concentration of oxygen in the CIL (in the layer $\sigma_\theta = 14.45$–14.60 kg m^{-3}), *O_2(CIL)*; onsets in the density field of hydrogen sulfide, *H_2S*; ammonia, *NH_4*; total manganese, *Mn*. The data for the summer months (May–October) are shown as *diamonds* and for the winter months (November–April) as *circles*

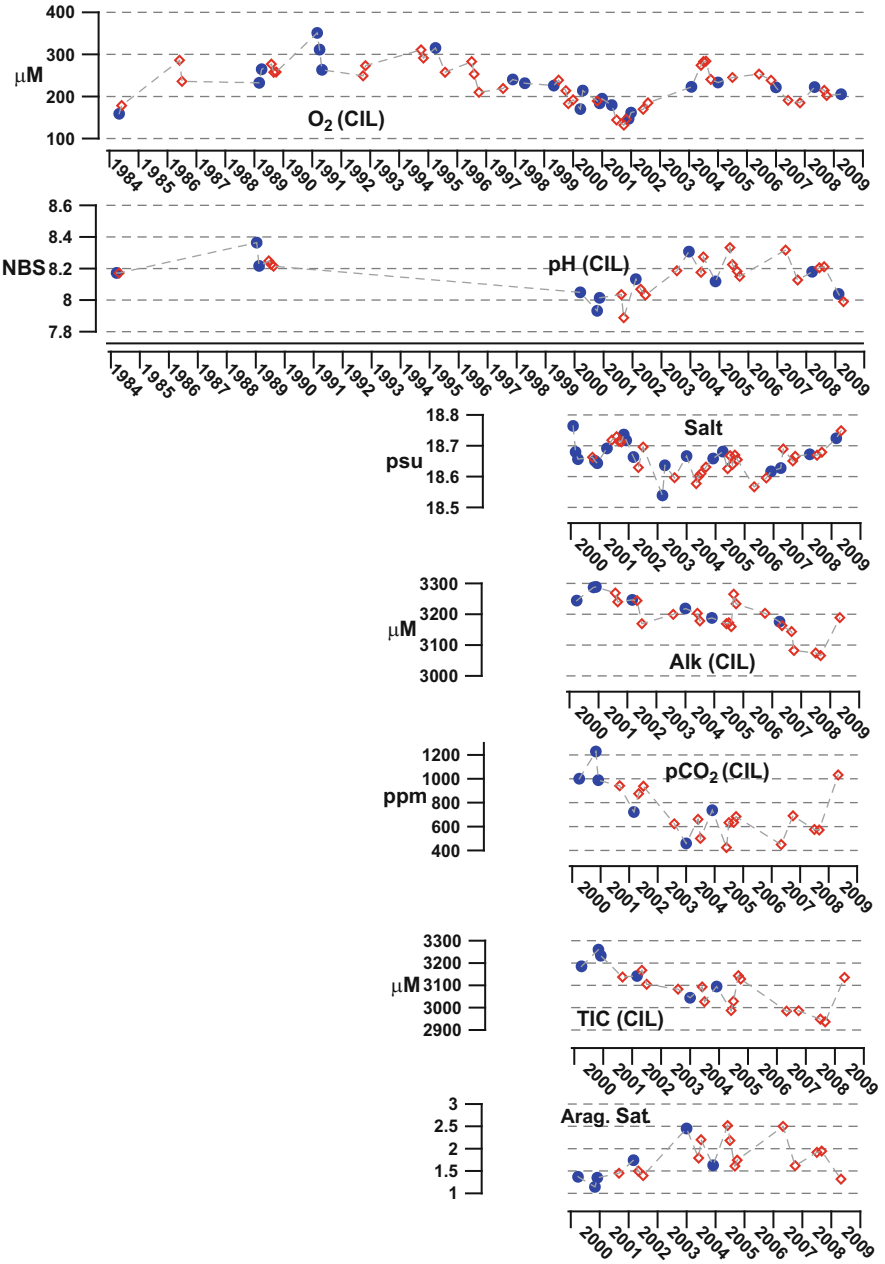

Fig. 4 Interannual variability of averaged concentration of oxygen in the CIL, O_2(CIL); averaged value of pH in the CIL, pH; averaged value of salinity in the CIL, Salt; averaged concentration of alkalinity in the CIL, Alk; averaged value of pCO_2 in the CIL, pCO_2; averaged concentration of TIC in the CIL, TIC; averaged value of aragonite saturation in the CIL, Arag. Sat. The data for the summer months (May–October) are shown as *diamonds* and for the winter months (November–April) as *circles*

The calculation results show that the depth of disappearance of hydrogen sulfide was characterized by maximum values of $\sigma_\theta = 16.15–16.25$ kg m^{-3} in 1991–1998 (Fig. 3). In 1999–2000, shoaling of this boundary was observed. The value of this shoaling was about $\sigma_\theta = 0.05–0.15$ kg m^{-3} (corresponding to about 5–15 m of upward movement at these depths). After 2000, the position of hydrogen sulfide stabilized and corresponded to the depth range of $\sigma_\theta = 16.05–16.15$ kg m^{-3}, as it was in 1984–1988.

The same tendency was observed in the vertical distributions of other studied reductants – NH_4 and Mn(II) (Fig. 3). Ammonia onset deepened from $\sigma_\theta = 15.85–16.00$ kg m^{-3} in 1984–1988 to $\sigma_\theta = 15.95–16.05$ kg m^{-3} in 1991–1998 and then after 2000 shallowed to $\sigma_\theta = 15.85–16.00$ kg m^{-3}. Mn(II) data are available since 1994, yet it was possible to reveal a tendency of shallowing from $\sigma_\theta = 15.90–16.00$ kg m^{-3} in 1994–1998 to $\sigma_\theta = 15.85–15.95$ kg m^{-3} after 2000.

For all discussed parameters, a tendency of slightly deepening onsets can be distinguished for the period 2003–2006 compared with 1999–2001 and 2006–2009 (Fig. 3).

No difference between the winter and summer data was found. The vertical gradients of hydrogen sulfide, ammonium and total manganese were stable in both periods [7].

The discussed variations of the onset positions of H_2S, NH_4 and Mn(II) could be well connected with the corresponding winter weather conditions. For example, the two warm winters of 1998–1999 could affect the winter formation of the oxygen-rich CIL. These years were remarkable for the increased sea surface temperature, increased temperature in the core of CIL (Fig. 3) [26–28], and corresponding shoaling of CIL in the density field [29]. The decrease of the CIL formation intensity should lead to increased temperature and decreased oxygen content in its core. To check these assumptions, we calculated the average concentrations of dissolved oxygen in CIL (for the layer $\sigma_\theta = 14.45–14.6$ kg m^{-3}, as mentioned above) (Fig. 3). The performed calculations should reflect both changes of concentrations in CIL and the vertical shifts of the CIL core in the density field. In 1999–2000, with the shoaling of reductants a decrease of oxygen content was observed as well. Minimal concentrations of oxygen were registered in 1984 and 2000–2001 (Fig. 3). Increase in oxygen content in the CIL layer was observed in 1989–1996 (to about 300 μM) and in 2003–2004 (to about 250 μM). The 2003–2004 increase followed the relatively cold winter of 2003. In 2008–2009, a decrease of oxygen concentrations to about 200 μM was recorded. According to [30], the dissolved oxygen concentration in the CIL corresponds to that in the surface layer before 1999 reflecting annual renovation of the upper part of the CIL. Since 2000 remarkable and stable difference between dissolved oxygen content in the surface layer and in the CIL has been observed evidencing the absence of full renovation of the CIL. One of the causes of this incomplete CIL renovation is the density gradient increase related to lower intensity of vertical mixing [30].

3.3 Interannual Variability of Carbonate System Parameters

Relatively regular observations of the carbonate system parameters (both pH and alkalinity) are available since 1999 (Fig. 4). According to some data on pH that are available since 1984, pH values in the CIL were about 8.1–8.2 in 1984, then increased to 8.2–8.4 in 1989, and decreased again to 7.9–8.1 in 1999–2001. There can be revealed an increase in pH from 8.1 to 8.4 in 2003–2006 and later decrease to about 8.0. Generally, the interannual variability of pH in the CIL is very close to that of oxygen (Fig. 4).

Concentrations of total alkalinity in the CIL slightly decreased from 3200–3250 μM in 1999–2001 to 3000–3100 μM in 2008–2009, while the variability of salinity followed that of the temperature in the CIL (Figs. 3 and 4) with lower values in 2002–2007 compared with 1999 and 2008. Variability of TIC followed Alk, decreasing from 3150–3250 μM in 1999–2001 to 2900–3000 μM in 2008–2009. A slight increase of concentration of both Alk and TIC was noticed in 2009. pCO_2 in the CIL changed from about 1,000 ppm in 1999–2001 to 400–800 ppm in 2003–2008 with a following increase to about 1,000 ppm in 2009. The oversaturation of CIL with aragonite changed in the range of 1.5–2.5 in 1999–2009 with higher values in 2002–2007.

4 Discussion

Conventionally, the changes in the oxygen and nutrient regime of the Black Sea and, in particular, its cold intermediate layer and the redox layer structures are determined by the physical forcing (thermal regime, mixing, or precipitation) and the anthropogenic forcing (i.e., supply of nutrient from the land-based sources), respectively.

The physical forcing is assumed to exhibit clearly the climatic signal. Temperature variations in the Black Sea appear to be governed by the North Atlantic Oscillation (NAO) and the East Atlantic/West Russia (EAWR) teleconnection patterns, comprising various combinations of the low and high surface pressure anomaly centers over the North Atlantic and Eurasia [26]. In the Black Sea relatively cold and dry winters occur during the positive phase of the NAO, and the milder and wetter winters during the negative NAO (Fig. 3). It is hypothesized that a clear connection between the NAO index and the Black Sea surface temperature is distinguished only at values of the NAO index considerably different from zero [31, 32].

The results obtained in this study illustrate the mechanism of reaction of the Black Sea biogeochemical systems to climate change as derived from the NAO variability. Correlated with the decadal NAO index behavior, changes in the winter weather condition result in larger or less intensive cooling of the upper layer waters [7, 26]. Changes in the sea surface temperature lead to changes of winter CIL

formation intensity [26, 32, 33] and predetermine the oxygen renovation there. A similar mechanism of dependence of dissolved oxygen variability upon climatic variations in the Swedish Fjord was reported by Erlandsson et al. [34], who demonstrated that about 40% of the observed oxygen depletion dynamics were determined by the physical factors connected to the NAO.

The oxygen inventory in the CIL acts as a specific accumulator that secures the consumption of oxygen for the organic matter decay and downward diffusive flux during all the year. The interannual variations of this oxygen renovation in CIL lead to changes of suboxic layer hydrochemical structure and in particular of position of the anoxic boundary in the density field.

Figure 4 clearly demonstrates that the oxygen changes are significantly correlated with the changes of pH. The similarity of their variability in the CIL (Fig. 4), with amplitudes of 200 μM for the oxygen and 0.4 for the pH, testifies the presence of significant changeability of the level of acidification well correlated with the interannual variability of the NAO index. Similar changes of pH with an amplitude of about 0.3 over a period of about 50 years were revealed by a 300 years reconstruction at the Flinders Reef, Australia, based on boron isotope (δ11B) data retrieved from a 300-year-old *Porites* coral [35]. These changes co-vary with the Interdecadal Pacific Oscillation which affects the lagoon flushing events there [35]. As in the World Ocean and in the Black Sea, the observed multiscale interdecadal and interannual oscillations of pH values could mask or amplify the possible trend of global decrease of the oceanic pH (the ocean acidification) correlated with the observed increase of carbon dioxide in the atmosphere [12].

Additional factor affecting the redox layer chemical features is the cultural eutrophication. The 1970s–1980s was a period of increased nutrient levels in the Black Sea [36] and this appeared to result in lower oxygen concentration in the CIL, which consequently affected the distributions of all other redox layer parameters [37]. It is not clear whether and when the physical forcing amplifies the anthropogenic forcing or acts to weaken (relieve) it.

It is necessary to stress that the direct result of the observed anoxic boundary oscillations by 5–10 m is the change of the volume of the oxic waters by approximately 5–10%, where the Black Sea oxic ecosystem exists [7]. Such oscillations are vitally significant and should be studied in detail.

5 Conclusions

The reported investigations showed that the biogeochemical system of the redox layer and the CIL of the Black Sea are subjects to visible interannual changes. Surface layers ventilation by dissolved oxygen down to the depth of the CIL occurs in winter. The intensity of ventilation is predetermined by climate forcing, which is possibly regulated by the large-scale climate formations like the NAO that affects the temperature of air and surface water, and they in turn set up the upper boundary conditions for the downward transport of O_2.

No clear trend of pH decrease in the Black Sea CIL testifying a progressive acidification was revealed. The CIL pH variability was significantly correlated with the CIL oxygen changes, which were logically consistent with the interannual variability of the winter vertical mixing intensity.

The position of the hydrogen sulfide boundary in the density field (and the volume of the Black Sea oxic layer) is connected with the climate variability, and related well to the NAO index. Therefore, the variations of chemical parameters distribution in the density field of the Black Sea redox layer shall be a good indicator of global climate change.

Acknowledgments The authors thanks Violeta Velikova for the discussions of this work results. We thank the staff of the Laboratory of Biohydrochemistry (Moscow) and the Laboratory of Marine Chemistry (Gelendzhik) of the Shirshov Institute of Oceanology RAS for the collected data. This research was supported by the Norvegian Research Council grant 211227/F11 and the Russian Foundation for Basic Research grant 10-05-00653.

References

1. Neretin LN, Volkov II, Rozanov AG, Demidova TP, Falina AS (2006) Biogeochemistry of the Black Sea anoxic zone with a reference to sulphur cycle. In: Neretin LN (ed) Past and present water column anoxia, NATO sciences series. Springer, Dordrecht, pp 105–138
2. Murray JW, Codispoti LA, Friederich GE (1995) Oxidation-reduction environments:the suboxic zone in the Black Sea. In: Huang CP, O'Melia CR, Morgan JJ (eds) Aquatic chemistry: interfacial and interspecies processes, Adv Chem Ser. ACS, Washington, DC, p 157
3. Rosanov AG (1995) Redox stratification of the Black Sea water. Oceanology 35:544–549 (in Russian)
4. Yakushev EV, Chasovnikov VK, Podymov OI (2005) Seasonal changes in the hydrochemical structure of the Black Sea redox zone. Oceanography 18:48–55
5. Vinogradov ME, Nalbandov YR (1990) Dependence of physical, chemical and biological parameters in pelagic ecosystem of the Black Sea upon the water density. Oceanology 30:769–777
6. Codispoti LA, Friederich GE, Murray JW, Sakamoto CM (1991) Chemical variability in the Black Sea: implications of continuous vertical profiles that penetrated the oxic/anoxic interface. Deep Sea Res 38:691–710
7. Yakushev EV, Chasovnikov VK, Debolskaya EI, Egorov AV, Makkaveev PN, Pakhomova SV, Podymov OI, Yakubenko VG (2006) The northeastern Black Sea redox zone: hydrochemical structure and its temporal variability. Deep Sea Res Part II 53:1764–1786
8. Ovchinnikov IM, Popov YI (1987) Evolution of the cold intermediate layer in the Black Sea. Oceanology 27:555–560 (in Russian)
9. Tolmazin D (1985) Changing coastal oceanography of the Black Sea. I: Northwestern shelf. Prog Oceanogr 15:217–276
10. Diaz RJ, Rosenberg R (2008) Spreading dead zones and consequences for marine ecosystems. Science 321:926–929
11. Stramma L, Johnson GC, Sprintall J, Mohrholz V (2008) Expanding oxygen-minimum zones in the tropical oceans. Science 320(5876):655–658
12. IPCC (2007) Climate Change 2007: The Physical Science Basis. Contribution of Working Group I to the Fourth Assessment Report of the Intergovernmental Panel on Climate Change. Solomon S, Qin D, Manning M, Chen Z, Marquis M, Averyt KB, Tignor M, Miller HL (eds.). Cambridge University Press, Cambridge, United Kingdom and New York, NY, USA, p 996

13. Podymov OI (2008) Use of a problem-oriented database for statistical analysis of the hydrochemical characteristics of the redox layer of the Black Sea. Oceanology 48(5):656–663
14. Grashoff K, Kremling K, Ehrhard M (1999) Methods of seawater analysis, 3rd completely revised and extended edition. WILEY-VCH, Weinheim
15. Bordovsky OK, Chernyakova AM (1992) Sovremenniye metody gydrokhimicheskikh issledovaniy okeana (Modern techniques of the hydrochemical studies of the Ocean). IO RAN, Moscow, p 200 (in Russian)
16. Roy RN, Roy LN, Vogel KM, Porter-Moore C, Pearson T, Good CE, Millero FJ, Campbell DM (1993) The dissociation constants of carbonic acid in seawater at salinities 5 to 45 and temperatures 0 to 45°C. Mar Chem 44:249–267
17. Lewis E, Wallace DWR (1998) Program developed for CO2 system calculations. ORNL/CDIAC-105. Carbon Dioxide Information Analysis Center, Oak Ridge National Laboratory, US Department of Energy, Oak Ridge, TN
18. Shaffer G (1986) Phosphate pumps and shuttles in the Black Sea. Nature 321:515–517
19. Pakhomova SV, Yakushev EV (2011) Manganese and iron at the redox interfaces in the Black Sea, the Baltic Sea, and the Oslo Fjord. In: Yakushev EV (ed) Chemical structure of pelagic redox interfaces: observation and modeling, Hdb Env Chem. Springer, Berlin. doi:10.1007/698_2011_98
20. Bezborodov AA, Eremeev VN (1993) Chernoe more. Zona vzaimodeistviya aerobnikh I anaerobnikh vod (Black Sea. The oxic/anoxic interface), MHI NASU, Sevastopol (in Russian)
21. Sorokin YI (2002) The Black Sea: ecology and oceanography. Backhuys, Leiden
22. Makkaveev PN (2002) Calculations of the component of the total titrated alkalinity in the Black Sea waters. In: Zatsepin AG, Flint MV (eds) Complex investigation of the northeastern Black Sea. Nauka, Moscow, p 447 (in Russian)
23. Yakushev EV, Chasovnikov VK, Murray JW, Pakhomova SV, Podymov OI, Stunzhas PA (2007) Vertical hydrochemical structure of the Black Sea. In: Kostyanoy AG, Kosarev AN (eds) The Black Sea environment. Springer, Berlin, pp 277–307
24. Chelysheva MV, Yakushev EV, Vinogradova EV, Chasovnikov VK (2011) Biogeochemical peculiarities of the vertical distributions of nutrients in the Black Sea. In: Yakushev EV (ed) Chemical structure of pelagic redox interfaces: observation and modeling, Hdb Env Chem. Springer, Berlin. doi:10.1007/698_2011_119
25. Volkov II, Kontar EA, Lukashev YF, Neretin LN, Nyffeler F, Rozanov AG (1997) Upper boundary of hydrogen sulfide: implications for the nepheloid redox layer in waters of Caucasian Slope of the Black Sea. Geochem Int 35(6):540–550
26. Oguz T, Dippner JW, Kaymaz Z (2006) Climate regulation of the Black Sea hydro-meteorological and ecological properties at interannual-to-decadal time scales. J Mar Syst 60:235–248
27. Ginzburg AI, Kostianoy AG, Sheremet NA (2004) Seasonal and interannual variability of the Black Sea surface temperature as revealed from satellite data (1982–2000). J Mar Syst 52(1–4):33–50
28. Krivosheya VG, Ovchinnikov IM, Skirta AY (2002) Intraannual variability of the cold intermediate layer of the Black Sea. In: Zatsepin AG, Flint MV (eds) Complex investigation of the northeastern Black Sea. Nauka, Moscow, p 27 (in Russian)
29. Murray JW, Konovalov SK, Tebo B, Oguz T, Besiktepe S, Tugrul S, Yakushev EV (2003) 2001 R/V Knorr cruise: new observations and variations in the structure of the suboxic zone. In: Proceedings "Oceanography of the eastern Mediterranean and Black Sea". Ankara, 545–557, October 2002
30. Pakhomova SV, Vinogradova EL, Yakushev EV, Zatsepin AG, Shtereva G, Chasovnikov VK, Podymov OI. Submitted. Black Sea biogeochemical regime recent decades variability. Mediterranian Marine Science Journal
31. Kazmin AS, Zatsepin AG (2007) Long-term variability of surface temperature in the Black Sea, and its connection with the large-scale atmospheric forcing. J Mar Syst 68:293–301
32. Kazmin AS, Zatsepin AG, Kontoyiannis H (2010) Comparative analysis of the long-term variability of winter surface temperature in the Black and Aegean Seas during 1982–2004 associated with the large-scale atmospheric forcing. Int J Climatol 30:1349–1359

33. Oguz T, Ediger D (2006) Comparison of in situ and satellite-derived chlorophyll pigment concentrations, and impact of phytoplankton bloom on the suboxic layer structure in the western Black Sea during May–June 2001. Deep Sea Res Part II 53:1923–1933
34. Erlandsson CP, Stigebrandt A, Arneborg L (2006) The sensitivity of minimum oxygen concentrations in a fjord to changes in biotic and abiotic external forcing. Limnol Oceanogr 51:631–638
35. Pelejero C, Calvo E, McCultoch T, Marshall JF, Gagan K, Louhj JM, Opdyke BN (2005) Preindustrial to modern interdecadal variability in coral reef pH. Science 309:2204–2207
36. Oguz T, Kideys A, Velikova V (2008) A overall assessment of the present state of the Black Sea ecosystem. In: BSC, 2008. State of the Environment of the Black Sea 2001–2006/7. Black Sea Commission Publications, Istanbul, Turkey, 417–446
37. Konovalov SK, Murray JW (2001) Variations in the chemistry of the Black Sea on a time scale of decades (1960–1995). J Mar Syst 31:217–243
38. Yakushev EV, Lukashev YF, Chasovnikov VK, Chzhu VP (2002) Modern notion of the vertical hydrochemical structure of the Black Sea redox zone. In: Zatsepin AG, Flint MV (eds) Complex investigation of the northeastern Black Sea. Nauka, Moscow, pp 119–132 (in Russian)

Large-Scale Dynamics of Hypoxia in the Baltic Sea

Oleg P. Savchuk

Abstract Large-scale hypoxia is an inherent natural property of the Baltic Sea caused by geographically and climatically determined insufficiency of oxygen supply to the deep water layers. During 1961–2005, the hypoxic zone covered by waters with oxygen concentration less than 2 mL L^{-1} extended on average over a huge area of about 50,000 km^2, albeit with large seasonal (a few thousand km^2) and, especially inter-annual (dozens of thousand km^2) variations, the later caused by an irregular ventilation with sporadic inflows of saline oxygen-enriched waters. The expansion of hypoxia induces a reduction of dissolved inorganic nitrogen pool due to denitrification and an increase of dissolved phosphate pool by internal loading, these changes reaching hundred thousand tonnes of N and P. The resulting excess of phosphate pool over the "Redfield" demand by phytoplankton is favourable for the dinitrogen fixation by cyanobacteria in amounts sufficient to compensate for denitrification and to counteract possible reductions of the nitrogen land loads.

Keywords Anoxia, Denitrification, Eutrophication, Hypoxic area, Internal phosphorus loading, Nitrogen fixation, Oxygen deficiency

Contents

O.P. Savchuk
Baltic Nest Institute, Stockholm University, Stockholm 10691, Sweden
e-mail: oleg@mbox.su.se

E.V. Yakushev (ed.), *Chemical Structure of Pelagic Redox Interfaces: Observation and Modeling*, Hdb Env Chem (2013) 22: 137–160, DOI 10.1007/698_2010_53,

Abbreviations

BED	Baltic environmental database
DAS	Data assimilation system
DIN	Dissolved inorganic nitrogen
DIP	Dissolved inorganic phosphorus
HELCOM	Helsinki commission
OM	Organic matter

1 Introduction

Occurrence, duration, extension, and intensity of hypoxia (oxygen deficiency) in natural waters are determined by an imbalance between oxygen consumption and supply. Oxygen is consumed for oxidation of organic matter (OM) and other reductants wherever they are present in the water column and bottom sediments, and the intensity of consumption is ultimately dependent on the input of OM and ambient temperature. Because of these positive feedbacks with eutrophication and global warming and because low oxygen concentration is detrimental for aerobic organisms, hypoxia is increasingly considered an important indicator of the environmental change and "ecosystem health" (e.g. [1–4]). Mechanisms of oxygen supply vary in relation to a location within the aquatic system. In the surface water layers, where dissolved oxygen is produced by photosynthetic organisms and its concentration is regulated by air–water gas exchange and intensive vertical mixing, hypoxia may occur only when such aeration is greatly suppressed, for instance, under ice cover or beneath thick green algal mats. In the deeper layers, oxygen transports are governed by multi-scale water movements and, consequently, are hampered by any restrictions to water exchange, especially by the water stratification and geomorphologic obstacles. Oxygen conditions in the surface sediments are primarily determined by oxygen concentration in the near-bottom waters. At a certain depth deeper in the sediments, where slow downward oxygen diffusion in pore waters is not sufficient to meet oxidative demand, oxygen becomes completely exhausted and anoxia (absence of oxygen) inevitably sets in.

These basic mechanisms of oxygen depletion as well as related effects on nutrients have been described since long-time ago (e.g. [5] and references therein). A lot of such understanding has been acquired in the Baltic Sea (Fig. 1, [6, 7]), one of the best sampled marine systems in the world (e.g. [8, 9]). Especially hypoxia prone at a large scale is the Baltic Proper, where a combination of bathygraphic peculiarities, limited and variable water exchange with the ocean, and permanent halocline generated by estuarine circulation hampers aeration of deep water layers (Fig. 2). Deep waters of the Gulf of Bothnia have not suffered from hypoxia in the modern history both because of relatively low rates of primary production and subsequent degradation of OM and because of better ventilation due to lower

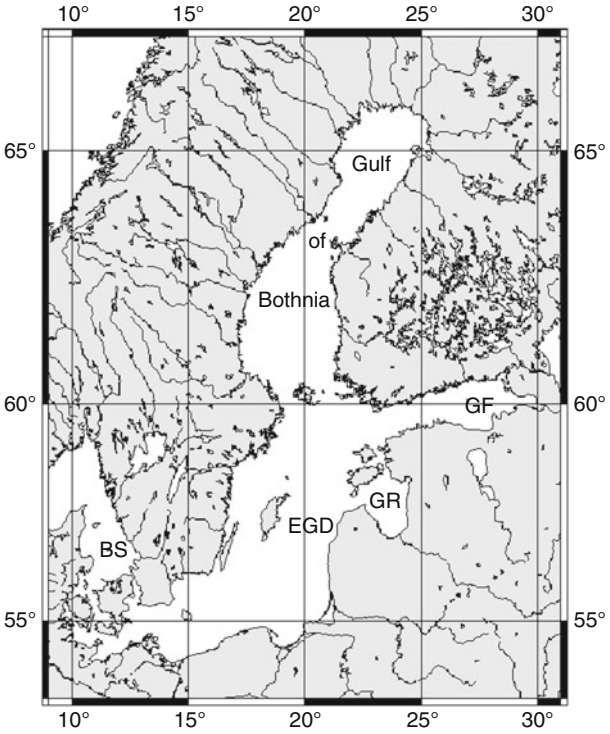

Fig. 1 The Baltic Sea and geographical objects mentioned in the text. *GF* the Gulf of Finland; *GR* the Gulf of Riga; *BS* the Baltic Straits; *EGD* the eastern Gotland Deep. Background map from (http://www.aquarius.geomar.de/omc/)

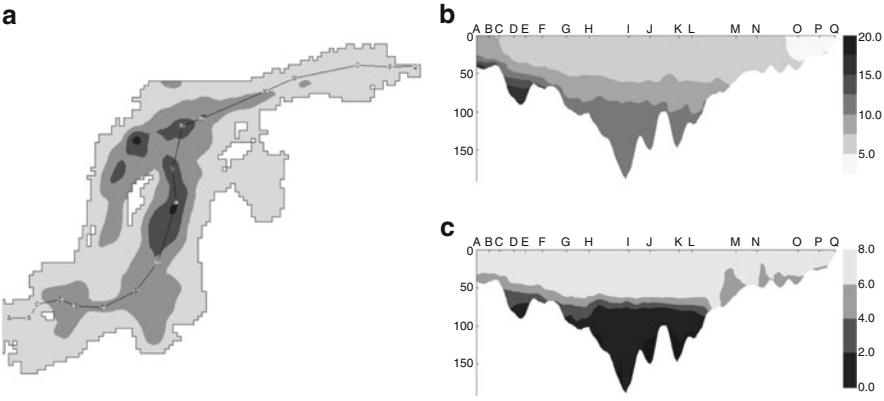

Fig. 2 Geographical prerequisites of the large-scale Baltic Sea hypoxia. (**a**) Bathymetric scheme of the Baltic Proper with horizontal resolution of five nautical miles and a depth step of 60 m, showing a transect through international monitoring stations; (**b**) Salinity (psu) and (**c**) Oxygen (mL L^{-1}) distributions averaged over September–October 1996–2005 (graphs were prepared from 3D fields reconstructed with DAS, see below)

salinity and weaker stratification. As in hundreds of other places [2], a local short-term, days to a few weeks, hypoxia sporadically or periodically occurs also in many shallow spots along the coasts, from the eastern Gulf of Finland to the Baltic Straits in the west (e.g. [10–12]). However important such events are for the local ecosystems and human communities, they are beyond the scope of this study.

Instead, this chapter focusses on the large-scale long-term oxygen dynamics and their biogeochemical consequences in the open Baltic Proper. Major aspects of these phenomena are well known for decades and have been abundantly covered in publications (e.g. [7, 13–16]). Here this knowledge is briefly reviewed and extended with estimates of such integral quantities as areas of the sediments and volumes of the water enveloped by hypoxia as well as magnitudes of the basin-wide nutrient pools, computed with special tools from big observational database. Some results obtained with this approach have already been presented in several papers (e.g. [14, 17–24]). Here these results are consistently updated and revised, including clarification of a few ambiguities and confusions that had crept into some of the above mentioned papers. One of the goals of this publication is to make computed time-series available to the readers in a numerical table form. Therefore, presentation and analysis of data is preceded by detailed description of techniques necessary for understanding the advantages and limitations of these data.

2 Data, Tools, and Methods

Data for this study are mostly taken from a marine segment of the Baltic Environment Database (BED) which contains the best part of nutrient and hydrographical measurements performed in the Baltic Sea since the end of the nineteenth century from over a hundred of research vessels belonging to all the riparian countries [25]. These data have been delivered to BED by many individuals, institutions, and agencies, whose contribution is very much appreciated (http://nest.su.se/bed/ACKNOWLE.shtml). Naturally, both the number of oceanographic stations sampled annually and the variety of chemical analyses have increased over time: from a few thousand hydrographic measurements per year in the 1900s to over 150–200 thousand measurements including finely resolved vertical profiling as well as over 20,000 nutrient samples in the 2000s. From the very beginning, the oxygen concentration has been measured by comparable modifications of the Winkler jodometric titration method, and during a century the number of measurements made annually increased by three orders of magnitude – from hundreds to amounts similar to hydrographic measurements. Following Baltic tradition [6], hydrogen sulfide concentrations, rather routinely measured in the Baltic Sea since the middle of 1960s, are stored in BED and will be presented and analyzed later as "negative oxygen" equivalents: 1 mL of H_2S L^{-1} = –2 mL O_2 L^{-1}. Comparison to studies that used different units can be made with the following conversions: 1 mL O_2 L^{-1} = 1.429 mg O_2 L^{-1} = 44.6 μM; 1 mL H_2S L^{-1} = 1.363 mg H_2S L^{-1} = 42.6 μM.

Further on, in demonstration and discussion of the long-term dynamics I will use data from one of the major long-monitored stations situated in the centre of the Gotland Deep and often considered as a representative for typical conditions in the entire Baltic Proper. This station is widely known as BY15, a number designated to it during the international Baltic Year 1969–1970 that aimed at redox alterations in the Baltic deep layers as one of the major targets. Because the exact positions of oceanographic stations sampled in this area by different research vessels have been slightly shifting both over decades and between sampling occasions, the data were extracted from BED within the range of 57° 15'–57° 25' N and 19° 50'–20° 10' E, that is within an area of about 10 × 10 nautical miles well covering all these deviations.

A prominent feature of the Baltic Sea oceanographic data is their ample temporal and spatial coverage. The importance of regular observations on a few deep-water stations was recognized already in the 1890s, and long-term measurements have been maintained in the main Baltic deeps since then by international efforts (cf. [9]). Likewise, almost from the very beginning of measurements the oceanographic surveys performed by different countries during the year would jointly cover large parts of the Baltic Sea. The spatial data coverage has particularly improved since the 1970s due to a multi-lateral coordination of research cruises and international monitoring programme under the intergovernmental Helsinki Convention (e.g. [26, 27]). In correspondence to these particular features, two specific data analysis tools accessing BED via Internet have been developed [25, 28].

SwingStations tool has been built mainly for the analysis of temporal variations of oceanographic parameters [28]. It allows users to select vertically distributed data for a specified time interval from a geographical rectangle delimited by given coordinates of its corners. The extracted data are then pooled together as if being measured in the centre of a rectangle area and in the middle of a specific depth layer, and step-wise averaged within prescribed time window, for example within a month, or 90 days, or a year, etc. These average vertical profiles are further used to plot time-depth distribution of analyzed parameter, where intervals between the profiles are filled by interpolation. When such interpolated intervals are substantially longer than the characteristic scales of studied variations, there is a risk of misinterpretation of displayed dynamics. Therefore, user is allowed to consciously limit extent of the time interval that can be filled by interpolation. If this time interval is shorter than the gap between available measurements, the plot area is left blank. Nowadays, many of these functional features are integrated into the decision support system Nest and supplemented with some statistical analysis tools [29–31].

The Data Assimilation System [25, 32] is especially useful in the analyses of spatial aspects of the Baltic Sea hydrographic and trophic conditions. The hydrographic and nutrient data extracted for specified time intervals and regions of the Baltic Sea are processed to reconstruct three-dimensional fields with a user-determined resolution. The reconstruction starts from pooling together all the measurements found within every cell of the regular three-dimensional grid formed by columns of vertical layers with a rectangular base. The average of pooled measurements is prescribed to a centre of the corresponding cell. At the next

step, the grid cells with no real measurements are filled in by linear interpolation. Since the result of 3D interpolation depends on the order of elementary one-dimensional interpolations along each of the three axes, an average of six possible permutations is used. To prevent unrealistic extrapolations, their extension should be limited by specified length interval, usually in the order of a few dozen miles, whereas concentration is kept constant further onward. After all the cells were filled in, the field is smoothed by a Tukey's cosine-filter [33].

The reconstructed original three-dimensional gridded fields can further be subjected to any of the four arithmetic operations performed either on a single field or between two fields. The resulting field can be stored and used in a further consecutively chained algorithm, for example summing up the ammonium, nitrite, and nitrate fields to reconstruct the field of dissolved inorganic nitrogen (DIN), producing the N:P ratio field, performing stoichiometric calculations of nitrate or phosphate anomalies, etc.

Both original and derivative fields can be exploited in several ways. Most conventional are graphical presentations of spatial distribution along horizontal (maps) and vertical (transects) planes (cf. Fig. 2). Besides graphical demonstration and visual analysis of distribution, these plots are also very useful in finding questionable data indicated by peculiar "spots" in the distribution. The researcher can then analyze these data, for example comparing them to measurements made nearby and closely in time by other research vessels, and decide whether to exclude such data from the reconstruction. However, such plots can be produced by many graphical program tools. The distinctive power of DAS is a possibility to compute different characteristics from the interpolated field for a specified domain within a chosen region of the sea. The domain may be bounded by space coordinates (latitude, longitude and depth interval) and by specified range of interpolated variables. Computations produce integral quantities and volume-weighted averages of the gridded variable as well as estimates of the water volumes and bottom areas occurring within these boundaries. For instance, reconstructed time series of the salinity and oxygen fields can be used to estimate temporal dynamics of the so-called "cod reproductive volume" comprising in the brackish Baltic Sea waters with salinity over 11 psu and oxygen concentration higher than 2 mL L^{-1} (e.g. [34]).

There are several peculiar consequences of the described DAS implementation, which should be borne in mind while analyzing and interpreting the original and derivative gridded fields as well as the integral and average characteristics computed from them. Each original field constructed with DAS over a specific time interval represents one unique entity, characterizing spatial distribution averaged over this interval. However, a "winter" field reconstructed for a given 3-month interval may include measurements performed only in January in one part of the region and only in March in another part. Furthermore, the actual spatial and temporal distribution of oceanographic samples used for reconstruction may irregularly differ from field to field. For instance, in generation of time-series of the winter fields, the distribution and amount of measurements may differ between each of 3-month intervals representing consecutive winters. Individual ammonium and nitrate fields summed up for the reconstruction of the DIN field may each be based

on different amount and distribution of actual samples. The annual average field would be affected by both seasonal variations in the surface layer and possible propagation of salt water inflow in the deep layers with related redox alterations.

In the following DAS computations, a threshold to hypoxic conditions is arbitrarily set at a bounding value of 2 mL O_2 L^{-1} (2.86 mg O_2 L^{-1} or 89 μM O_2). Such thresholds are often inferred from the responses and vulnerability of pelagic and benthic animals, usually in the range of 1–4 mg O_2 L^{-1} (e.g. [2, 35, 36]. Furthermore, most observational programs have routinely taken "near-bottom" samples from several meters above the bottom to both avoid contamination from the sediments and secure the equipment. As may be assumed from estimates of oxygen consumption and transfer in the Baltic deep layers [37, 38], when dissolved oxygen concentration in the near-bottom waters is below 2 mL O_2 L^{-1}, the sediment surface beneath viscous and diffusive sub-layers is actually anoxic. In other words, the sediments covered by hypoxic waters can be reasonably considered anoxic.

3 Long-Term Large-Scale Oxygen Dynamics

Actual observations of dissolved oxygen concentration are available in BED for the Gotland Deep since 1902 and are shown in Fig. 3 as time series of measurements made within certain layers. Already such, "traditional" manner of presentation can be used as a pretext for reminding on several important features of the long-term oxygen variations in the Baltic Sea.

As indicated by both direct measurements and paleoenvironmental reconstructions, the intermittent hypoxia appears to be an inherent property of the Baltic Sea.

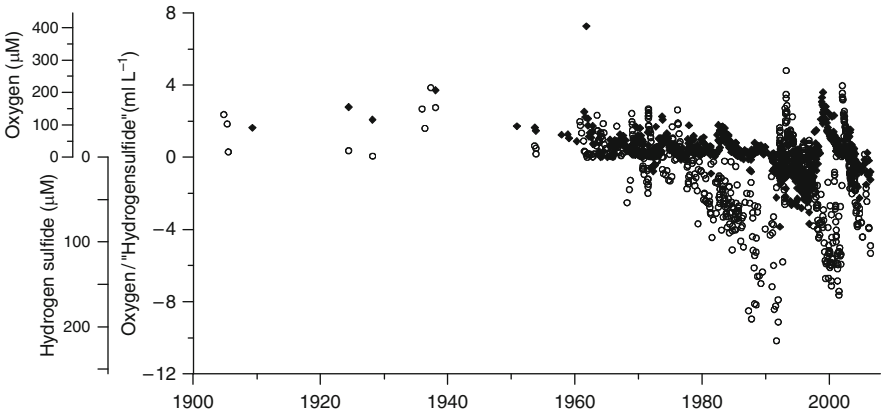

Fig. 3 Long-term variation of oxygen and hydrogen sulfide (shown as negative oxygen equivalents, mL L^{-1}) in the layers 145–155 m (*filled*) and below 230 m (*open*) at oceanographic station BY15 in the Gotland Deep (57° 15′–57° 25′ N and 19° 50′–20° 10′E). For comparisons, 10 mL O_2 L^{-1} = 446 μM of oxygen; –10 mL O_2 L^{-1} correspond to 213 μM of hydrogen sulphide

Available observations show occurrence of hypoxia already in the beginning of the previous century (cf. Fig. 3), while according to Fonselius [39], hydrogen sulfide was first found (smelled) in the samples of bottom water in 1931. Although we cannot truly quantify the intensity of anoxia in the past because of a lack of analytical measurements of hydrogen sulfide concentration, some proxies indicate sporadic occurrence of hypoxic conditions both at centennial and millennium scales. One of such proxies is the distribution of laminated sediments ([40] and references therein). Laminae are formed due to seasonal variations both in sedimentation rate and composition of sedimented material, and in anoxic conditions, in absence of benthic macrofauna, are buried undisturbed. In contrast, sediments formed and buried in oxic conditions are homogenized by different processes of bioturbation performed by active animals living in the surface sediments. Another indication of redox alterations can be found in distribution and mineral form of metals (e.g. Fe, Mn, Mo, U, V, Cu, and Zn) that would be differently affected by oxic vs. reduced conditions (e.g. [41–44]). As follows from the analysis of extensive lamination in the upper sediment layers, the deepest parts of the Baltic Proper have been anoxic for over 100–200 years [40, 45, 46]. Vertical distribution of "metallic indices" implies that alterations between oxic and anoxic marine environments have occurred in the Gotland Deep at least since the 1600s [7, 41]. Although with a lesser chronological precision and certainty, analyses of both lamination and metal's distributions show that anoxic conditions can be traced back to the Littorina Sea stage (ca. 6,000 years BC) and occurred also in the Gulf of Bothnia, which then used to be saltier and sharper stratified, compared to the later and present stages (e.g. [46, 47]).

Occasions of "inverted" vertical distribution, with oxygen concentration in the bottom layer (deeper than 230 m) being at some moments higher than that in the above layer (145–155 m; cf. Fig. 3), clearly illustrate the main mechanism of the deep water ventilation – lateral advection of the saline waters that are heavy enough to penetrate into deep layers and displace ("push up and farther") old stagnant waters. Since propagating water is continuously being diluted by ambient, less saline water, it is a combination of salinity and volume of the water arriving from the Baltic Straits, which determines how far and deep it can reach into the Baltic Sea. Investigations of this phenomenon, which is called "the major Baltic inflow", date back to the end of the nineteenth century [48] and can be summarized after Schinke and Matthäus [49] and Matthäus et al. [16] in the following way.

In the first outflow phase the high atmospheric pressure over the Baltic region, augmented by easterly winds, forces water out of the Baltic Sea, where the sea level decreases below normal. In addition, this type of atmospheric circulation reduces both atmospheric precipitation and river runoff, thus further decreasing the total water volume of the sea. During the second, main phase the well-developed zonal atmospheric circulation between the North Atlantic and Europe generates strong westerly winds and increases the sea level in Kattegat. Consequently, large volumes of water are forced into the Baltic Sea through the Baltic Straits by a combined action of sea level difference, wind stress, and "sucking" action of low atmospheric pressure over the region. To produce the necessary effect, the first

phase of elevated atmospheric pressure has to prevail over 1–2 months (usually in September–October), while the second phase of extremely strong and persistent westerly winds must last during several weeks. Neither condition is common for the Baltic region. In addition, the salinity in the Kattegat should stay high enough to provide for sufficient amount of salt [50]. Thus, the combination of consecutive events needed to create a continuous inflow of large amount of highly saline water (100–260 km^3 with salinity higher than 17 psu; [16, 51]) happens rather seldom and is difficult to predict (Figs. 4 and 5).

Further propagation of saline waters farther into the Baltic interior along the chain of depressions separated by sills depends on density of the "resident" waters, which, in turn, is defined by the recent hydrographic history. Inflowing oxygenated waters either penetrate into near-bottom layers and displace old waters (Fig. 6) or interleave into halocline and into intermediate, dynamically active layers just beneath it [50]. As estimated from the chronology of hydrographic measurements, the propagation of inflow from the Baltic Straits to the Gotland Deep, that is on a distance of about 650 km, usually takes 4–5 months (but, for instance, only 2 months in 1993 due to specific hydrographic situation; [16]. It is important also to remember that propagating waters are to a large extent composed of ambient Baltic waters, whose entrainment into the saline flow increases its volume by a factor of three [52].

In the bottom layers of the Gotland Deep, the deepest point en route of the high-salinity waters, the relation between salinity and oxygen concentration is straightforward: both are increased due to lateral advection of saltier waters and are decreased during the following stagnation. Salinity is decreased because of the slow diapycnic mixing across the density gradients, while oxygen is decreased because such mixing is too slow to override the biochemical consumption. In the

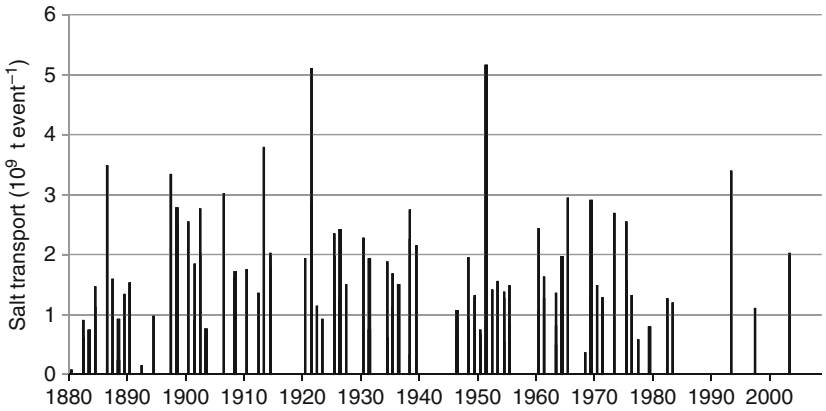

Fig. 4 Major Baltic inflows in 1880–2008 characterized by the salt transport with the inflow event (10^9 t). Thick columns indicate several events during the year, while no data are available during 1914–1920 and 1940–1946 because of two world wars. The estimates made by Fischer and Matthäus [51] and Matthäus [48] are borrowed from the Digital Supplement to Feistel et al. [8]

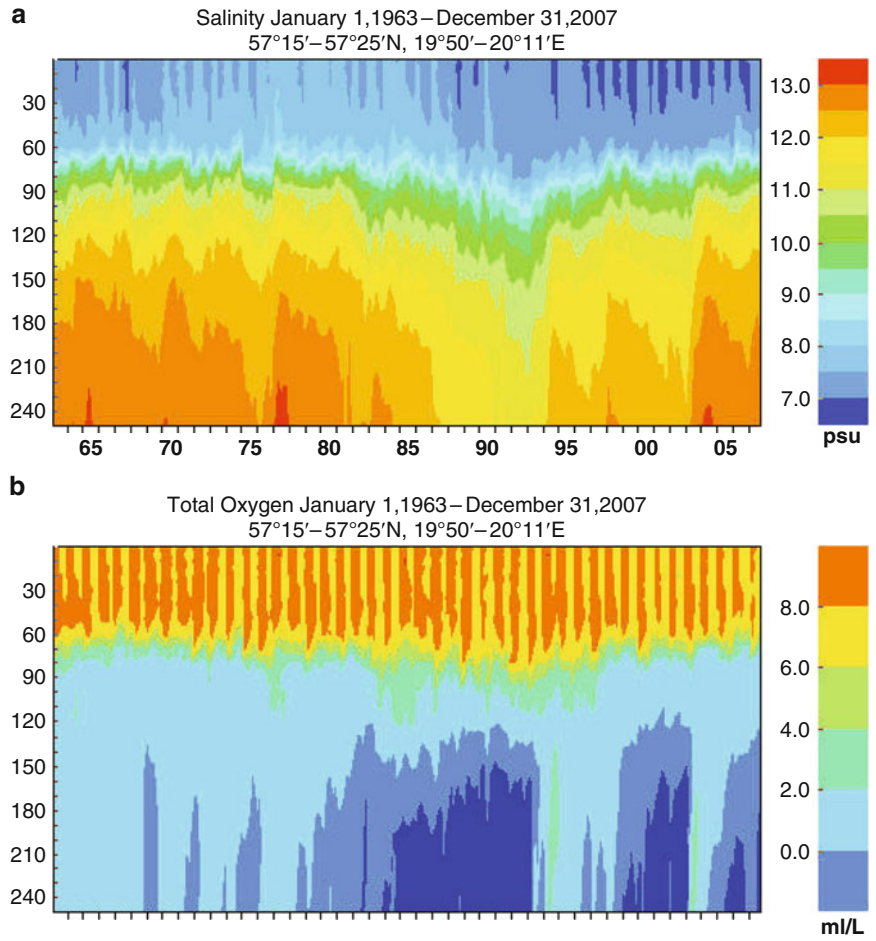

Fig. 5 Time-depth contour plots of (**a**) salinity (psu) and (**b**) oxygen (mL L^{-1}) for 1963–2007 at BY-15 (90-day aggregation)

deep active intermediate layers the relationship changes into the opposite – as illustrated by the 1980s/1990s dynamics, the decreasing salinity and weakening stratification result in improved vertical exchange and better aeration (see Fig. 5). Further to the north, at the entrances to the Gulf of Bothnia and Gulf of Finland, the advection brings in either oxygen-enriched waters propagated along the intermediate layers or oxygen-depleted waters pushed up from the "upstream" bottom layers, or often a mixture of both.

This atmospherically governed and topographically conditioned ventilation of the deep layers explains why hypoxia had occurred in the Baltic Sea already under an absent or negligible human influence. Therefore, in contrast to other regions [2, 3], a relative significance of natural vs. anthropogenic drivers of the basin

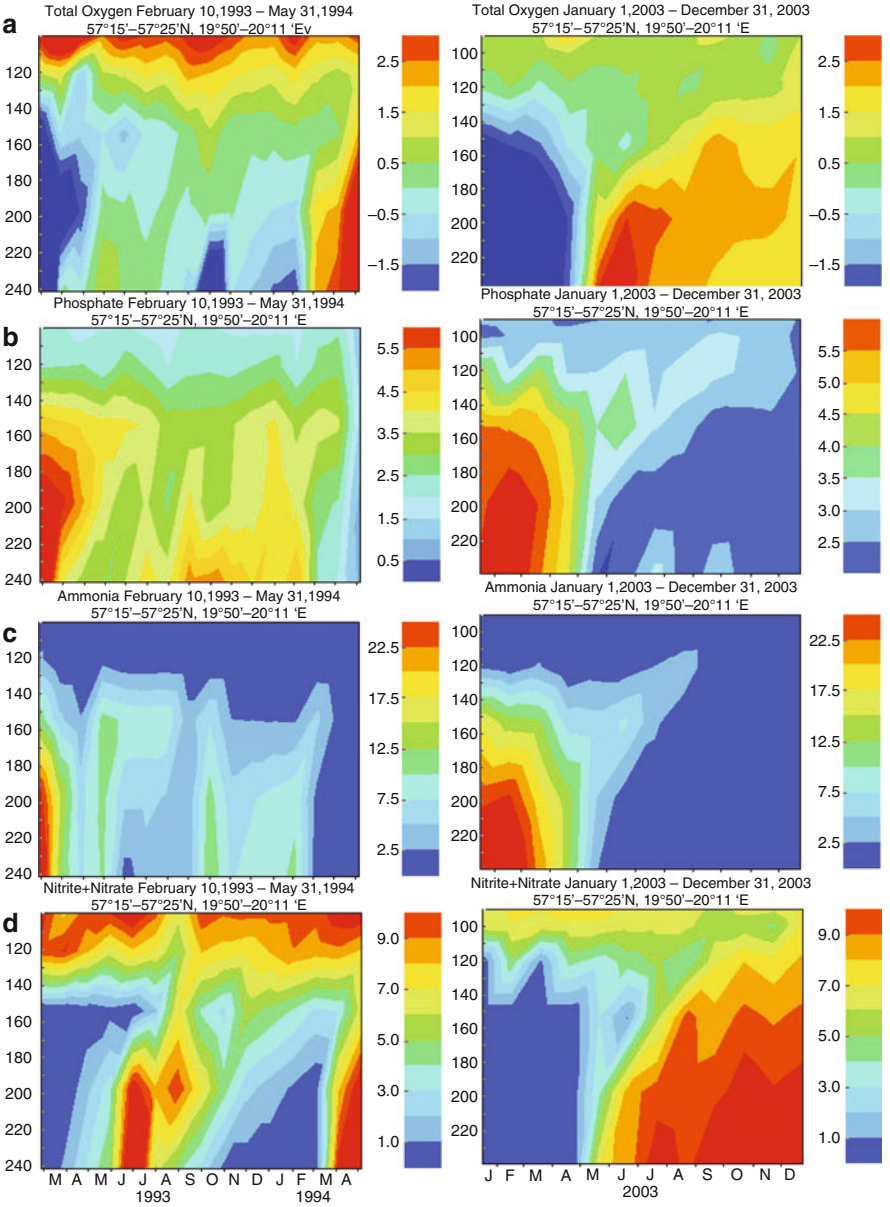

Fig. 6 Displacement of deep waters in the Gotland Deep by the major Baltic inflows of 1993/1994 (*left*) and 2003 (*right*) as indicated by isopleths of (**a**) oxygen (mL L^{-1}), (**b**) phosphate (μM $P–PO_4$), (**c**) ammonium (μM $N–NH_4$) and (**d**) nitrite + nitrate (μM $N–NO_{2+3}$) based on 30-day aggregation

scale hypoxia in the Baltic Sea has been a subject of long lasting discussion (e.g. [6, 23, 53–57]). Apparently, a measure of anthropogenic impact could be related to the oxygen consumption that should intensify along with the increasing primary production. Indeed, a long-term worsening of oxygen conditions since the 1900s, clearly seen in Fig. 3 until 1993, has been widely considered as an indicator of man-made eutrophication [6, 58]. Another indication of intensified oxygen consumption is often sought in the observation that, even though inflows of 1993/1994 and 2003 were able to aerate bottom waters in the Gotland Deep up to 3–4 mL O_2 L^{-1}, that is to the levels of the 1930s, their effects did not last long and anoxia set in faster and became "severer" than before (cf. Fig. 3).

However, as pointed out by Matthäus et al. [16], since the late nineteenth century and till the early 1980s, the episodic major inflows had occurred more or less regularly and in clusters, while only three strong inflows have happened during past quarter of the twentieth century (cf. Fig. 4). As can be estimated from the salt transport (original data by Matthäus and co-workers referred to in Fig. 4), the major inflows that occurred from 1960 to 1975 had integrally delivered through the Baltic Straits 24.1×10^9 t of salt, the weak inflows of 1976–1983 transported another 3.9×10^9 t and then, after a 10-year break, the latest three inflow brought in during 10 years (1993–2003) only 2.7×10^9 t. Considering these estimates as proxies of oxygen transport to the deep layers, the severe reduction in the natural ventilation potential is evident. On the other hand, a rate of the net decrease of oxygen concentration, which can roughly be estimated as a difference between local maximal and minimal values during several "stagnation" periods in the last 50 years, spans the range of 2–12 μL O_2 L^{-1} d^{-1} and was actually higher in the 1960s (cf. Fig. 3). More sophisticated estimates of the integral oxygen consumption, which have also taken into account the oxygen transport supply, fell within the same order of magnitude and did not reveal any trends either [58, 59]. This drastic reduction of oxygen supply in combination with the relatively unchanged rate of oxygen consumption clearly indicates that the importance of anthropogenic contribution to the intensification of large-scale hypoxia should be revaluated.

In addition to site-specific data on concentration that are useful for the demonstration and analysis of the temporal oxygen dynamics, even more important at the entire ecosystem scale are the sediment areas and water volumes enveloped by hypoxia (Table 1 and Fig. 7). As was demonstrated by Andersin et al. [60] and ourselves ([14, 17]) and can be seen in Figs. 3 and 7, the hypoxic zone extension varies both seasonally and inter-annually. Being averaged over 1961–2005, the seasonal changes caused by intensification of oxygen consumption for oxidation of freshly produced and sedimented OM result in an increase of the hypoxic area from winter (January–March) extension of 43,363 ±12,567 km^2 to autumn (August–September) extension of 49,124 ± 12,097 km^2 (mean ± standard deviation), that is by about 13%.

Time-series in Table 1 are estimated from annually averaged fields, each of which has been reconstructed from all the measurements made during the year and pooled together. At the sites with regular observations, this DAS algorithm results in averaging of several measurements, while the inclusion of sites with occasional

Table 1 Long-term dynamics of hypoxic area (HA) and volume (HV), cod reproductive volume (CRV) and nutrient pools below 60 m in the Baltic Proper

Year	HA (km^2)	HV (km^3)	CRV (km^3)	DIN (t)	DIP (t)
1969	51,050	1,926	518	159,337	171,753
1970	55,309	1,975	385	178,962	217,278
1971	67,092	2,049	126	167,748	197,619
1972	51,366	1,765	385	188,775	212,104
1973	63,357	1,990	310	182,233	225,555
1974	56,351	1,834	395	235,501	213,139
1975	62,400	1,793	98	230,828	209,001
1976	37,786	1,302	455	233,165	198,654
1977	50,787	1,531	440	281,760	225,555
1978	55,407	1,733	286	310,263	206,931
1979	51,876	1,573	230	320,543	190,377
1980	53,854	1,773	393	283,629	211,070
1981	58,877	1,745	97	289,236	212,104
1982	58,217	1,656	132	256,995	239,006
1983	39,594	1,189	278	284,564	209,001
1984	32,067	746	260	288,769	195,550
1985	37,423	885	204	330,356	206,931
1986	44,146	1,140	197	362,597	234,867
1987	39,867	1,013	143	363,999	169,684
1988	44,190	1,168	120	266,808	191,411
1989	43,820	1,122	75	275,218	218,312
1990	33,421	757	68	333,159	173,822
1991	25,884	660	200	406,520	203,827
1992	26,512	650	226	341,103	160,372
1993	25,070	469	298	328,019	159,337
1994	32,938	773	329	373,811	165,545
1995	40,567	894	153	393,904	167,614
1996	44,530	1,255	248	405,585	196,585
1997	45,657	1,240	271	392,502	212,104
1998	58,713	1,754	218	414,463	232,798
1999	58,622	1,799	181	399,043	256,595
2000	53,948	1,598	185	262,602	247,283
2001	62,335	1,989	190	260,733	277,288
2002	57,741	1,808	128	245,314	253,491
2003	52,607	1,883	520	254,192	255,025
2004	66,868	2,183	281	255,621	251,189
2005	58,688	1,742	128	252,790	246,248

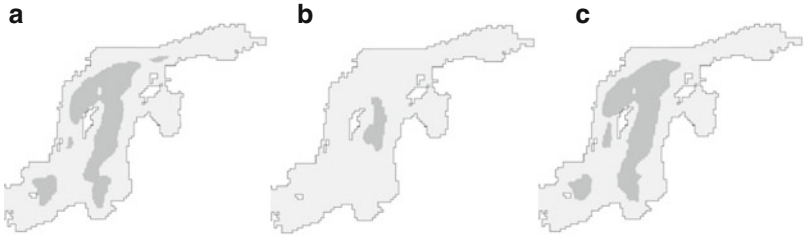

Fig. 7 Extension of the hypoxic area ($O_2 < 2$ mL L^{-1}) in (**a**) August 1971 (70,528 km^2), (**b**) March 1993 (11,659 km^2), and (**c**) November 2006 (72,354 km^2)

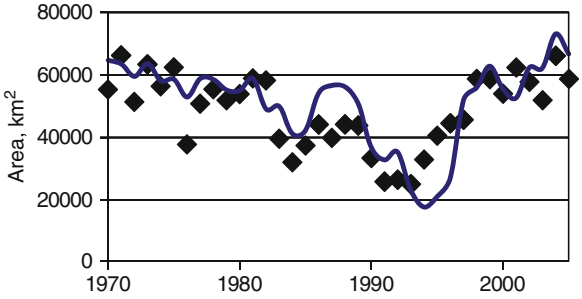

Fig. 8 Comparison between simulated (*curve*) and computed from measurements (*symbols*) hypoxic area in the Baltic Sea (hindcast made with BALTSEM model, [21, 63])

sampling during specialised cruises results in a kind of "cumulative" effect, that is concentration measured at such sites only once would represent the entire year. That is why the long-term (1961–2005) mean annual extension of the hypoxic area of 49,349 ± 11,077 km^2 is practically equal to its maximal autumn extension presented above. In a certain sense, these annual estimates are more appropriate for studies of ecosystem effects of hypoxia, especially in the deeper layers less subject to seasonal variations. For instance, spatial expansion of hypoxia determines distribution and abundance of zoobenthos [60–62] and controls the cod reproductive volume [34]. Even a short-term anoxia could result in "dead bottoms" that would not be re-colonized fast, for example during the same year. Similarly, even a short-term occurrence of hypoxia over restricted sediment area and water volume would cause nutrient transformations and fluxes with long-lasting biogeochemical consequences.

Generally, our quantitative understanding of the main governing mechanisms has been sufficient enough to realistically simulate contemporary hypoxia and its biogeochemical consequences in mathematical models of the Baltic Sea (e.g. Fig. 8, [21, 63–68]).

4 Redox Alterations of Biogeochemical Cycles

Hypoxia-induced alterations of nitrogen and phosphorus biogeochemical cycles (Fig. 9, see also Fig. 6 above) constitute another important effect of oxygen spatial and temporal variations on ecosystem dynamics, particularly, on its eutrophication aspects.

Many evidences point at a strong dependence between redox conditions and phosphorus transformations in the water column and sediments of aquatic systems, including the Baltic Sea, although exact physical–chemical mechanisms and quantitative relationships found in different water bodies are still under debates

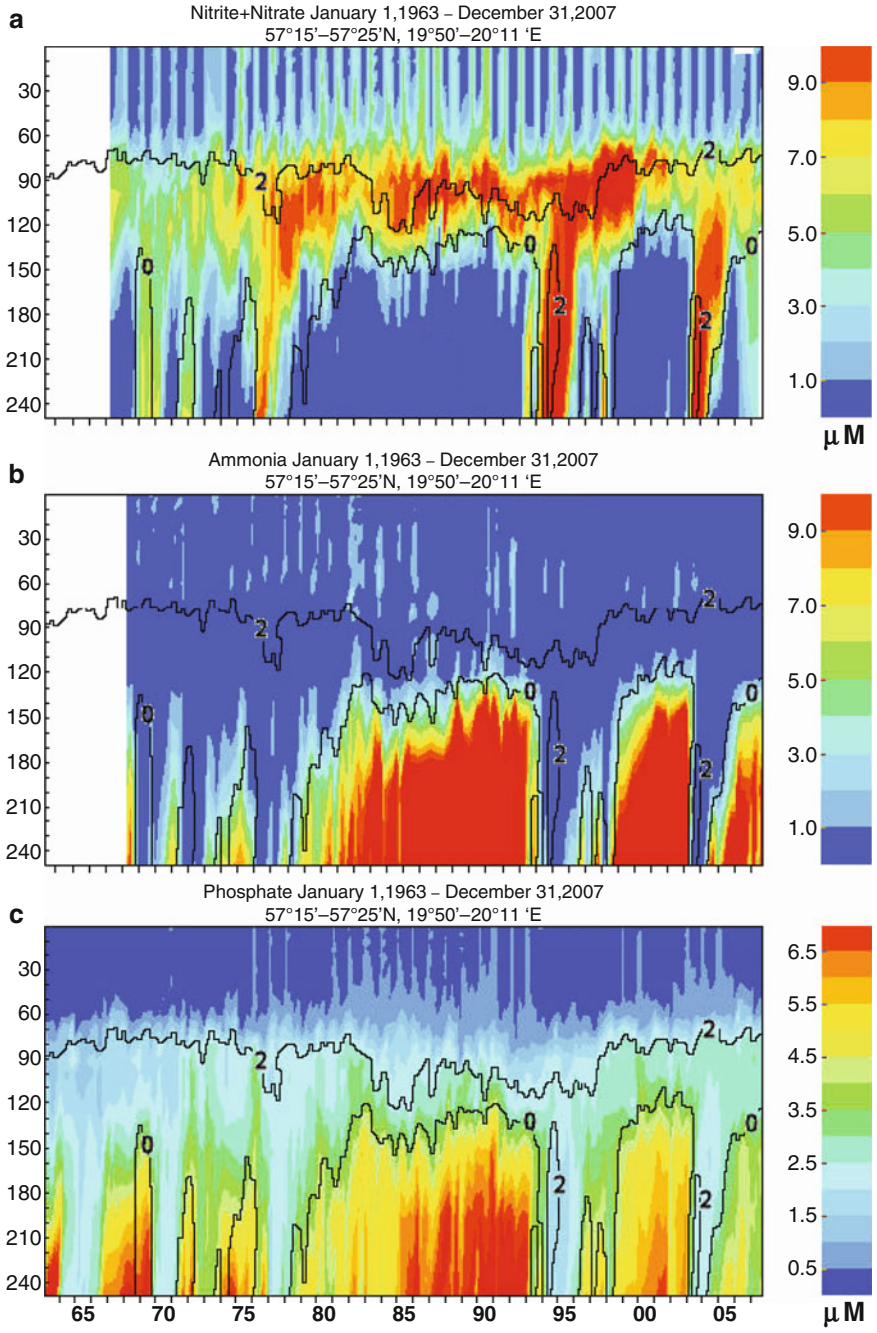

Fig. 9 Time-depth contour plots of (**a**) nitrite + nitrate (µM $N–NO_{2+3}$), (**b**) ammonium (µM $N–NH_4$) and (**c**) phosphate (µM $P–PO_4$) for 1963–2007 at BY-15 (90-day aggregation) superimposed with oxygen isopleths of 0 and 2 mL L^{-1}

(e.g. [6, 68–77]). Phenomenologically, in oxic conditions, dissolved inorganic phosphorus (DIP) is transformed into particulate state and removed from the water column and pore waters of sediments, while in anoxic conditions it is released back into the solution. Local manifestation of these processes is seen in Fig. 9c as accumulation of DIP in hypoxic and especially anoxic waters. A basin-wide relationship between hypoxia and phosphorus pool in the Baltic Sea was first demonstrated by us [17] on time-series estimated from three-dimensional oxygen and phosphate fields reconstructed with DAS for every winter (January–March) of 1970–2000. Here I update this large scale quantitative description of reversible phosphorus transformations and expand it over 1963–2005.

Within the larger Baltic Proper, including the Gulf of Finland and the Gulf of Riga, winter-to-winter changes of hypoxic area up to 20–30 thousand square kilometers induce the changes of integral DIP pool in the order of dozens and up to hundred thousand tonnes of phosphorus (Fig. 10). Being expressed on daily basis, the average exchange rate correspondent to empirical regression in Fig. 10b is about 0.2 mmol DIP-P m^{-2} day^{-1}. Both integral and area-specific rates are quite comparable to other available estimates [17–19, 72, 78, 79]. The inter-annual changes of marine DIP pool are also comparable to and often larger than the annual net exchange with neighbouring basins [18], [19], but also, what is even more important, than the annual TP input from land to the entire Baltic Sea of $29.9 \pm 4.9 \times 10^3$ t TP (mean $\pm$ SD, 1994–2006, [80]). The fact that the large scale variations of DIP pool caused by naturally occurring major Baltic inflows are up to two orders of magnitude larger than the variations of external phosphorus input has further fuelled the discussion about relative significance of climatic vs. anthropogenic drivers of the Baltic Sea eutrophication (e.g. [17, 23, 80]). However, as can be deduced from the long-term averages of winter-to-winter changes of $0.4 \pm 11.2 \times 10^3$ km^2 and $8 \pm 45 \times 10^3$ t P, these large scale internal transformations are completely reversible, that is dozens of thousand tonnes of phosphorus are just going back and forth between the particulate and dissolved fractions. On the other hand, the total external input is unidirectional and, according to the recent reconstruction by Savchuk and Wulff [21], could have brought into the Baltic Sea about $1{,}800 \times 10^3$ t P over past 40 years. Apparently, this permanent addition has not been balanced by the net export to neighbouring basins and permanent sediment burial. The resulting accumulation caused by this misbalance is the reason of a 200–300 thousand tonnes difference in DIP pool between the 1960s and the 2000s; in spite of about the same extension and variation of the hypoxic area (cf. Fig. 10a).

Effects of hypoxia on the nitrogen biochemical cycle are less straightforward and cannot be reliably quantified from the site-specific observations (cf. Fig. 9a and b). On the one hand, variations of hypoxia directly determine the rate and integral amount of denitrification, especially evident in dynamics of oxidised nitrogen. Here we consider denitrification as a removal of nitrogen from the biotic cycling by any processes that lead to transformation of combined nitrogen into gaseous end products [81]. According to this biogeochemically relevant definition, denitrification comprises both canonical heterotrophic denitrification and autotrophic anammox metabolism regardless of their localization in space and time. On the other

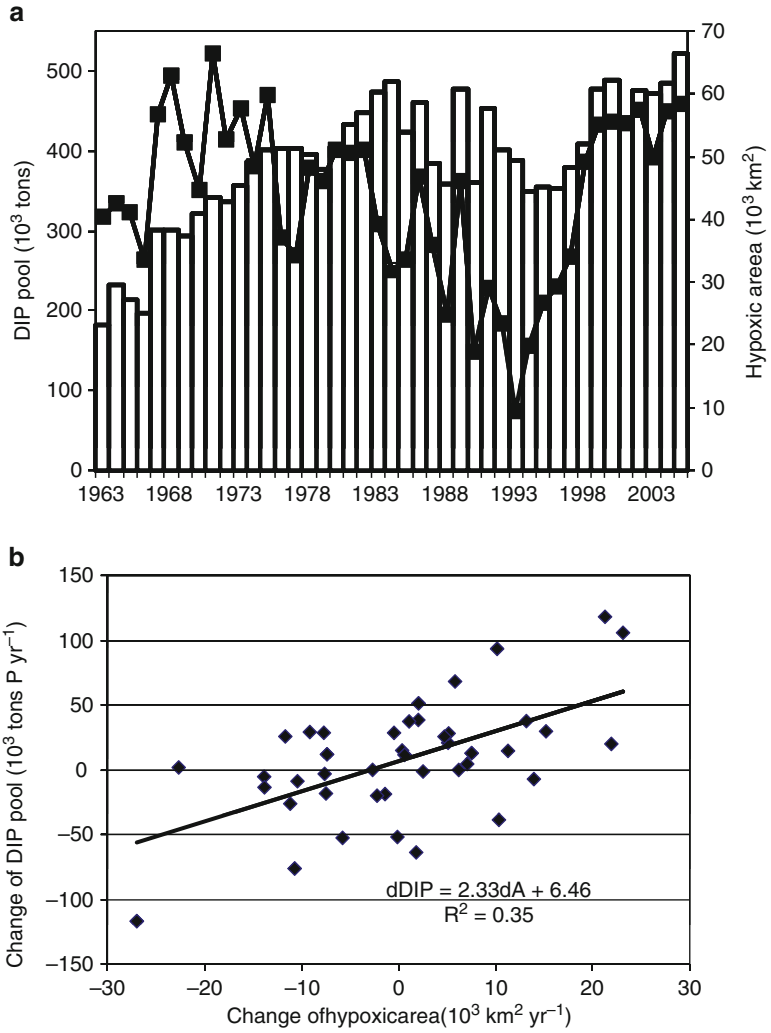

Fig. 10 Hypoxia and phosphate in the Baltic Proper, including the Gulf of Finland and the Gulf of Riga (cf. Fig 1). (**a**) Long-term dynamics of winter (January–March) extension of hypoxic area (*line*) and total DIP content (*columns*) and (**b**) Winter-to-winter changes of hypoxic area and DIP pool derived from data in (**a**)

hand, in the absence of oxidized nitrogen in developed anoxic conditions, nitrogen in the form of ammonium is preserved in the system, becoming available for the biotic cycling after the redox conditions flop over. However, as we have already demonstrated [23], the resulting integral basin-wide effect of hypoxia on the nitrogen pelagic pool is quite definitely negative, that is opposite to the consequences for DIP pool (Fig. 11).

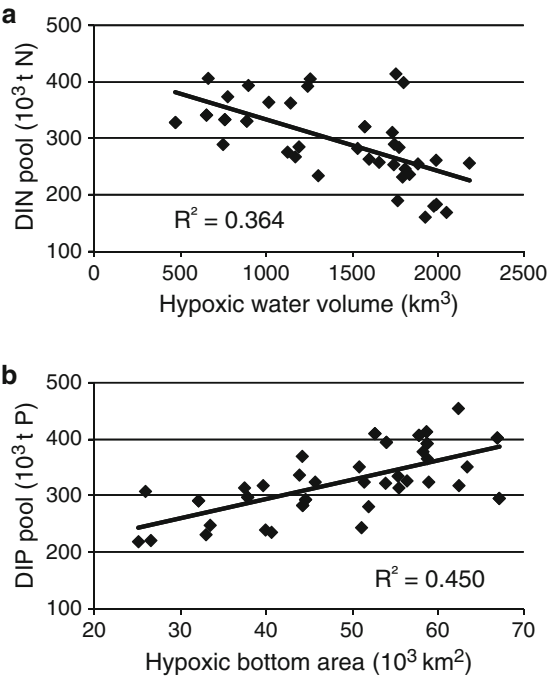

Fig. 11 Relationships between hypoxia and deep-water (>60 m) annual nutrient pools in the Baltic Proper. (**a**) DIN pool vs. hypoxic water volume containing waters with $O_2 < 2$ mL L^{-1}, (**b**) DIP pool vs. hypoxic sediment area covered by waters with $O_2 < 2$ mL L^{-1}. R^2 coefficient of determination

Note that being interested in simultaneous effect of hypoxia on both N and P cycles, here I use estimates that are slightly different from those used earlier in Vahtera et al. [23] and in Fig. 10. The annual deep-water nutrient pool computed only for the domain below 60 m (see Table 1) is used instead of the total basin-wide integral winter amount because the total DIP amount is weaker related to the extension of hypoxia, in contrast to their year-to-year changes (cf. Fig. 10). In an attempt to better account for a possible denitrification also in anoxic waters, the hypoxic volume comprising all the waters with oxygen concentration less than 2 mL L^{-1} is used instead of the denitrification volume with oxygen concentration ranging from 0 to 1 mL L^{-1}. Although these replacements have not qualitatively affected the empirically justified theoretically casual relationships, quantitatively they resulted in slightly higher coefficients of determination.

Simultaneous nitrogen depletion and phosphorus enrichment of the pelagic nutrient pools result in a shift of marine ecosystem towards nitrogen limitation. Most importantly, the high linear correlation between the hypoxic volume and the inorganic N:P molar ratio is found not only in the deep water pools below 60 m in the Baltic Proper (coefficient of determination $R^2 = 0.63$) but also within the entire Baltic Proper from surface to bottom, including the Gulf of Finland and the Gulf of Riga (Fig. 12). With a 2-year lag between annual extension of hypoxia and basin-wide inorganic N:P ratio, the relationship becomes even stronger, rising up to $R^2 = 0.80$ in deep layers and $R^2 = 0.75$ in the entire system. For the time being, I have no quantitative explanation for this delay except of some vague qualitative

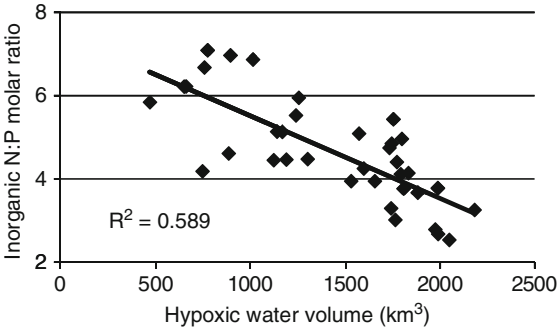

Fig. 12 Relationship between hypoxic water ($O_2 < 2\,mL\,L^{-1}$) volume and inorganic N:P molar ratio estimated from annual nutrient pools for the entire Baltic Proper from surface to bottom, including the Gulf of Finland and the Gulf of Riga. R^2 coefficient of determination

guesses about the time needed for changes generated in the central deep layers to envelope the entire water body.

In the Baltic Proper, variations in a degree of nitrogen limitation affect not only the primary production of OM by the common phytoplankton, but also the occurrence and extension of spectacular and noxious cyanobacteria blooms (e.g. [82–85]) that are believed to be occurring here for millennia [86]. Even more important in the eutrophication perspective is that these cyanobacteria fix substantial amounts of molecular dinitrogen in the range of 200–500 $\times$ 10^3 t N per year [87, 88], which are quite comparable to the contemporary external input of total nitrogen from the land and atmosphere of 850 $\times$ 10^3 t N per year [80]. The significance of this nitrogen source, which is governed by the internal biogeochemical feedbacks, for counteracting the nitrogen load reductions is crucially important in discussions and decisions within the ecosystem approach to the environmental management [23, 80, 89].

The hypoxia-related perturbations occurring mostly in the Baltic Proper are also very important for the ecosystem dynamics in neighbouring basins. A good example is a well-documented fate of saline, oxygen-depleted and phosphate-enriched waters that were displaced in the Gotland Deep by the 1993/1994 deepwater inflows (cf. Fig. 6). Being pushed up and farther, these waters reached the Eastern Gulf of Finland by autumn 1995–spring 1996, where they significantly sharpened vertical stratification and reduced deep water oxygen concentrations [90]. Extensive autumn hypoxia, determined by these settings, not only adversely affected macrozoobenthos [91] but also induced massive internal loading of phosphate equivalent to about half of annual land loads that were added to the phosphorus exported from the west [92]. According to DAS computations, comparing to the early 1990s, this expansion of hypoxia resulted in 1997 in almost a doubling of the annual DIP pool up to 20 $\times$ 10^3 t P and decrease of the DIN pool from about 90 $\times$ 10^3 t N to 60 $\times$ 10^3 t N. Corresponding phosphorus surplus indicated by reduction of the N:P ratio from almost Redfield to cyanobacteria-favouring values of 6–7 [85, 93, 94] caused an expansion of cyanobacteria over the entire Gulf of Finland, in contrast to previous years when the bloom did not extend beyond its entrance [94].

5 Conclusions

The large-scale hypoxia is an inherent property of the Baltic Sea caused by geographically and climatically determined insufficiency of oxygen supply to the deep water layers. Occurrence of hypoxia are documented by direct oxygen measurements from the beginning of the twentieth century and inferred backwards over centuries and millennia from lamination and metallic indices in the dated sediment cores. Therefore, in contrast to local coastal areas, where the recent hypoxia is often related to man-made eutrophication, the anthropogenic contribution into extension and intensity of hypoxia in the deep offshore waters is still under debate. Apparently, the convincing quantitative estimates of such contribution should be obtained with the aid of mathematical models that are already now capable to realistically simulate the long-term variations of large scale hypoxia and its biogeochemical consequences.

The extension of hypoxia varies both seasonally and from year to year. The inter-annual variations reaching dozens of thousand square kilometres generate large scale effects in basin-wide nutrient pools. In the expansion phase, DIN pool is reduced by denitrification and DIP pool increases due to phosphate release from anoxic sediments, while in the shrinkage phase the changes are opposite. The expansion of hypoxia results in decreased N:P ratio that is favourable for the blooms of dinitrogen fixing cyanobacteria, another common feature of the Baltic Sea ecosystem. Nitrogen fixed by cyanobacteria becomes available for further biotic cycling, thus to a large degree compensating for the nitrogen removal by denitrification.

A historical misbalance between external input of phosphorus vs. its insufficient removal by advection and sediment burial resulted in "extra" 200–300 $\times$ 10^3 t of phosphorus, accumulated in the Baltic Proper since the 1960s, that in two ways counteract the environmental management measures aimed at reducing eutrophication. First, a longer time is needed to deplete the larger phosphorus pool even by the drastic reductions of the phosphorus land loads. Second, this excessive phosphorus stock supports the cyanobacterial nitrogen fixation that counteracts the nitrogen land load reductions. Therefore, it is the phosphorus load reduction that should be the priority managerial target in the Baltic Proper. The possibility to speed up the reduction of excessive phosphorus pool by such engineering methods as the forced ventilation of intermediate water layers [63, 96], or the artificial co-precipitation of phosphate should be studied in a greater quantitative detail.

References

1. Conley DJ, Carstensen J, Raquer-Sunyer R, Duarte CM (2009) Ecosystem thresholds with hypoxia. Hydrobiologia 629:21–29
2. Diaz RJ, Rosenberg R (2008) Spreading dead zones and consequences for marine ecosystems. Science 321:926–929

3. Rabalais NN, Turner RE, Diaz RJ, Justić D (2009) Global change and eutrophication of coastal waters. ICES J Mar Sci 66:1528–1537
4. Stramma L, Johson GC, Sprintall J, Mohrholz V (2008) Expanding oxygen-minimum zones in the tropical oceans. Science 320:655–658
5. Richards FA (1965) Anoxic basins and fjords. In: Riley JP, Skirrow G (eds) Chemical oceanography, Vol I. Acad Press, London
6. Fonselius SH (1969) Hydrography of the Baltic deep basins. III. Fish Bd Sweden, Ser Hydrogr 23
7. Grasshoff K, Voipio A (1981) Chemical oceanography. In: Voipio A (ed) The Baltic Sea. Elsevier, Amsterdam
8. Feistel R, Nausch G, Wasmund N (eds) (2008) State and evolution of the Baltic Sea, 1952–2005. Wiley, New Jersey
9. Fonselius S, Valderrama J (2003) One hundred years of hydrographic measurements in the Baltic Sea. J Sea Res 49:229–241
10. Conley DJ, Carstensen J, Ærtebjerg G, Christensen PB, Dalsgaard T, Hansen JLS, Josefson AB (2007) Long-term changes and impacts of hypoxia in Danish coastal waters. Ecol Appl 17(Suppl):S165–S184
11. Karlson K, Rosenberg R, Bonsdorff E (2002) Temporal and spatial large-scale effects of eutrophication and oxygen deficiency on benthic fauna in Scandinavian and Baltic waters – a review. Oceanogr Mar Biol Ann Rev 40:427–489
12. Maximov AA (2006) Causes of the bottom hypoxia in the eastern part of the Gulf of Finland in the Baltic Sea. Oceanology 46:185–191
13. Fonselius SH (1981) Oxygen and hydrogen sulphide conditions in the Baltic Sea. Mar Poll Bull 12:187–194
14. Conley DJ, Björck S, Bonsdorff E, Carstensen J, Destouni G, Gustafsson BG, Hietanen S, Kortekaas M, Kuosa H, Meier HEM, Müller-Karulis B, Nordberg K, Norkko A, Nürnberg G, Pitkänen H, Rabalais NN, Rosenberg R, Savchuk OP, Slomp CP, Voss M, Wulff F, Zillén L (2009) Hypoxia-related processes in the Baltic Sea. Environ Sci Technol 43:3412–3420
15. Kalejs M (1989) Oxygen. In: Davidan IN, Savchuk OP (eds) Problems of studies and mathematical modelling of the Baltic Sea ecosystem. 4. Main tendencies of the ecosystem's evolution. Gidrometeoizdat, Leningrad (In Russian)
16. Matthäus W, Nehring D, Feistel R, Nausch G, Mohrholz LH-U (2008) The inflow of highly saline water into the Baltic. In: Feistel R, Nausch G, Wasmund N (eds) State and evolution of the Baltic Sea. Wiley, New Jersey, pp 1952–2005
17. Conley DJ, Humborg C, Rahm L, Savchuk OP, Wulff F (2002) Hypoxia in the Baltic Sea and basin-scale changes in phosphorus biogeochemistry. Environ Sci Technol 36:5315–5320
18. Savchuk OP (2005) Resolving the Baltic Sea into seven subbasins: N and P budgets for 1991–1999. J Mar Syst 56:1–15
19. Savchuk OP (2005) Studies of the Baltic Sea eutrophication. Proc Russ State Oceanogr Inst 209:272–285 (In Russian)
20. Savchuk OP, Wulff F (2007) Modeling the Baltic Sea eutrophication in a decision support system. Ambio 36:141–148
21. Savchuk OP, Wulff F (2009) Long-term modeling of large-scale nutrient cycles in the entire Baltic Sea. Hydrobiologia 629:209–224
22. Savchuk OP, Wulff F, Hille S, Humborg C, Pollehne F (2008) The Baltic Sea a century ago – a reconstruction from model simulations, verified by observations. J Mar Syst 74:485–494
23. Vahtera E, Conley DJ, Gustafsson BG, Kuosa H, Pitkänen H, Savchuk OP, Tamminen T, Viitasalo M, Voss M, Wasmund N, Wulff F (2007) Internal ecosystem feedbacks enhance nitrogen-fixing cyanobacteria blooms and complicate management in the Baltic Sea. Ambio 36:186–194
24. Witek Z, Humborg C, Savchuk O, Grelowski A, Lysiak-Pastuszak E (2003) Nitrogen and phosphorus budgets of the Gulf of Gdansk (Baltic Sea). Estuar Coast Shelf Sci 57:239–248

25. Sokolov A, Andrejev O, Wulff F, Rodriguez Medina M (1997) The data assimilation system for data analysis in the Baltic Sea. Systems Ecology Contributions 3, Stockholm University, Stockholm
26. HELCOM (1984) Guidelines for the Baltic Monitoring Programme for the second stage. Balt Sea Environ Proc 12:1–249
27. HELCOM (2008) Manual for marine monitoring in the COMBINE programme of HELCOM. http://www.helcom.fi/groups/monas/CombineManual/en_GB/main. Accessed 21 May 2009
28. Sokolov A, Wulff F (1999) SwingStations: a web-based client tool for the Baltic environmental database. Comput Geosci 25:863–871
29. Johansson S, Wulff F, Bonsdorff E (2007) The MARE Research Programme 1999–2006: reflections on program management. Ambio 36:119–122
30. Nest – an information environment for decision support system at the Baltic Nest Institute, Stockholm University. http://nest.su.se/nest. Accessed on 2 Dec 2009
31. Sokolov A (2002) Information environment and architecture of decision support system for nutrient reduction in the Baltic Sea. http://nest.su.se/nest. Accessed 22 May 2009
32. DAS – Data Assimilation System and Baltic Environment Database at the Baltic Nest Institute, Stockholm University. http://nest.su.se/das Accessed 2 Dec 2009
33. Tukey JW (1977) Exploratory data analysis. Addison-Wesley, Reading, Mass
34. MacKenzie BR, Hinrichsen H-H, Plikshs M, Wieland K, Zezera A (2000) Quantifying environmental heterogeneity: estimating the size of habitat for successful cod *Gadus morhua* egg development in the Baltic Sea. Mar Ecol Progr Ser 193:143–156
35. Diaz RJ (2001) Overview of hypoxia around the world. J Environ Qual 30:275–281
36. Vaquer-Sunyer R, Duarte CM (2008) Thresholds of hypoxia for marine biodiversity. Proc Nat Acad Sci 105:15452–15457
37. Rahm L (1987) Oxygen consumption in the Baltic proper. Limnol Oceanogr 32:973–978
38. Rahm L, Svensson U (1989) On the mass transfer properties of the benthic boundary layer with an application to oxygen fluxes. Neth J Sea Res 24:27–35
39. Fonselius S (1962) Hydrography of the Baltic Deep Basins. Fish Bd Sweden, Ser. Hydrogr 13
40. Jonsson P, Carman R, Wulff F (1990) Laminated sediments in the Baltic – a tool for evaluating nutrient mass balances. Ambio 19:152–157
41. Hallberg RO (1974) Paleoredox conditions in the Eastern Gotland Basin during the recent centuries. Merentuttkimuslait Julk 238:3–16
42. Sohlenius G, Emies KC, Andrén E, Andrén T, Kohly A (2001) Development of anoxia during the Holocene fresh – brackish water transition in the Baltic Sea. Mar Geol 177:221–242
43. Sternbeck J, Sohlenius G, Hallberg RO (2000) Sedimentary trace elements as proxies to depositional changes induced by a Holocene fresh-brackish transition. Aquat Geochem 6:325–345
44. Swarzenski PW, Campbell PL, Osterman LE, Poore RZ (2008) A 1000-year sediment record of recurring hypoxia off the Mississippi River: the potential role of terrestrially-derived organic matter inputs. Mar Chem 109:130–142
45. Hille S, Leipe T, Seifert T (2006) Spatial variability of recent sedimentation rates in the Eastern Gotland Basin (Baltic Sea). Oceanologia 48:297–317
46. Zillén L, Conley DJ, Andrén T, Andrén E, Björck S (2008) Past occurrences of hypoxia in the Baltic Sea and the role of climate variability, environmental change and human impact. Earth-Sci Rev 91:77–92
47. Ignatius H, Axberg S, Niemistö L, Winterhalter B (1981) Quaternary geology of the Baltic Sea. In: Voipio A (ed) The Baltic Sea. Elsevier, Amsterdam
48. Matthäus W (2006) The history of investigation of salt water inflows into the Baltic Sea – from the early beginning to recent results. Mar Sci Rep 65:1–73
49. Schinke H, Matthäus W (1998) On the causes of major Baltic inflows – an analysis of long time series. Cont Shelf Res 18:67–97
50. Stigebrandt A (2001) Physical Oceanography of the Baltic Sea. In: Wulff F, Rahm L, Larsson P (eds) A systems analysis of the changing Baltic Sea. Springer, Berlin, Heidelberg, New York

51. Fischer H, Matthäus W (1996) The importance of the Drogden Sill in the sound for major Baltic inflows. J Mar Res 9:137–157
52. Stigebrandt A, Gustafsson BG (2003) The response of the Baltic Sea to climate change – theory and observations. J Sea Res 49:243–256
53. Conley DJ, Bonsdorff E, Carstensen J, Destouni G, Gustafsson BG, Hansson L-A, Rabalais NA, Voss M, Zillén L (2009) Tackling hypoxia in the Baltic Sea: is engineering a solution? Environ Sci Technol 43:3407–3411
54. Elmgren R (2001) Understanding human impact on the Baltic ecosystem: changing views in recent decades. Ambio 30:222–231
55. Kuparinen J, Tuominen L (2001) Eutrophication and self-purufication: counteractions forced by large-scale cycles and hydrodynamic processes. Ambio 30:190–194
56. Nehring D, Matthäus W (1991) Current trends in hydrographic and chemical parameters and eutrophication in the Baltic Sea. Int Rev Gesamten Hydrobiol 76:297–316
57. Savchuk OP (1989) On relative significance of natural and anthropogenic factors of eutrophication. In: Davidan IN, Savchuk OP (eds) "Baltica" Project. Problems of research and modelling of the Baltic Sea ecosystem. Issue 4. Main tendencies of the ecosystem's evolution. Hydrometeoizdat, Leningrad (In Russian)
58. Gustafsson BG, Stigebrandt A (2007) Dynamics of nutrients and oxygen/hydrogensulfide in the Baltic Sea deep water. J Geophys Res 112:G02023
59. Pers C, Rahm L (2000) Changes in apparent oxygen removal rate in the Baltic Proper deep water. J Mar Syst 25:421–429
60. Andersin A-B, Lassig J, Parkkonen L, Sandler H (1978) The decline of macrofauna in the deeper parts of the Baltic proper and the Gulf of Finland. Kieler Meeresforsch Sonderhft 4:23–52
61. Laine AO, Sandler H, Andersin A-B, Stigzelius J (1997) Long-term changes of macrozoobenthos in the Eastern Gotland Basin and the Gulf of Finland (Baltic Sea) in relation to the hydrographical regime. J Sea Res 38:135–159
62. Zmudzinski L (1975) The Baltic Sea pollution. Pol Arch Hydrobiol 22:601–614
63. Gustafsson BG, Meier HEM, Savchuk OP, Eilola OP, Axell L, Almroth E (2008) Simulation of some engineering measures aiming at reducing effects from eutrophication of the Baltic Sea. Earth Sci Rep Ser, C82, Göteborg University
64. Eilola K, Meier HEM, Almroth E (2009) On the dynamics of oxygen, phosphorus and cyanobacteria in the Baltic Sea; a model study. J Mar Syst 75:163–184
65. Kuznetsov I, Neumann T, Burchard H (2008) Model study on the ecosystem impact of a variable C:N:P ratio for cyanobacteria in the Baltic Proper. Ecol Mod 219:107–114
66. Savchuk O, Wulff F (1996) Biogeochemical transformations of nitrogen and phosphorus in the marine environment, Systems Ecology Contributions 2. Stockholm University, Stockholm, Sweden
67. Stigebrandt A, Wulff F (1987) A model for the dynamics of nutrients and oxygen in the Baltic Sea. J Mar Res 45:729–759
68. Yakushev EV, Pollehne F, Jost G, Kuznetsov I, Schneider B, Umlauf L (2007) Analysis of the water column oxic/anoxic interface in the Black and Baltic seas with a numerical model. Mar Chem 107:388–410
69. Blomqvist S, Gunnars A, Elmgren R (2004) Why the limiting nutrient differs between temperate coastal seas and freshwater lakes: a matter of salt. Limnol Oceanogr 49:2236–2241
70. Caraco N, Cole J, Likens GE (1990) A comparison of phosphorus immobilization in sediments of freshwater and coastal marine systems. Biogeochemistry 9:277–290
71. Golterman HL (2001) Phosphate release from anoxic sediments or 'What did Mortimer really write?'. Hydrobiologia 450:99–106
72. Lehtoranta J, Ekholm P, Pitkänen H (2008) Eutrophication-driven sediment microbial processes can explain the regional variation in phosphorus concentrations between Baltic Sea sub-basins. J Mar Syst 74:495–504
73. Lukkari K, Leivuori VH, Kotilainen A (2009) The chemical character and burial of phosphorus in shallow coastal sediments in the northeastern Baltic Sea. Biogeochemistry 94:141–162

74. Mortimer CH (1971) Chemical exchanges between sediments and water in the Great Lakes – speculations on probable regulatory mechanisms. Limnol Oceanogr 16:387–404
75. Nehring D (1987) Temporal variations of phosphate and inorganic nitrogen compounds in central Baltic deep waters. Limnol Oceanogr 32:494–499
76. Santschi P, Hohener P, Benoit G, Buchholtz-ten Brink M (1990) Chemical processes at the sediment-water interface. Mar Chem 30:269–315
77. Sundby B, Gobeil C, Siverberg N, Mucci A (1992) The phosphorus cycle in coastal marine sediments. Limnol Oceanogr 37:1129–1145
78. Emeis K-C, Struck U, Leipe T, Pollehne F, Kunzendorf H, Christiansen C (2000) Changes in the burial rates and C:N:P ratios in the Baltic Sea sediments over the last 150 years. Mar Geol 167:43–59
79. Hille S, Nausch G, Leipe T (2005) Sedimentary deposition and reflux of phosphorus (P) in the Eastern Gotland Basin and their coupling with P concentrations in the water column. Oceanologia 17:663–679
80. HELCOM (2009) Eutrophication in the Baltic Sea – an intergrated thematic assessement of the effects of nutrient enrichment and eutrophication in the Baltic Sea region. Balt Sea Environ Proc 115B:1–152
81. Devol AH (2008) Denitrification including anammox. In: Capone DG, Bronk DA, Mulholland MR, Carpenter EJ (eds) Nitrogen in the marine environment, 2nd edn. Elsevier, Amsterdam
82. Finni T, Kononen K, Olsonen R, Wallström K (2001) The history of cyanobacterial blooms in the Baltic Sea. Ambio 30:172–178
83. Kahru M, Horstmann U, Rud O (1994) Satellite detection of increased cyanobacteria blooms in the Baltic Sea: natural fluctuation or ecosystem change? Ambio 23:469–472
84. Kahru M, Savchuk OP, Elmgren R (2007) Satellite measurements of cyanobacterial bloom frequency in the Baltic Sea: interannual and spatial variability. Mar Ecol Progr Ser 343:15–23
85. Niemi Å (1979) Blue-green algal blooms and N:P ratio in the Baltic Sea. Acta Bot Fenn 110:57–61
86. Bianchi TS, Engelhaupt E, Westman P, Andren T, Rolff C, Elmgren R (2000) Cyanobacterial blooms in the Baltic Sea: natural or human-induced? Limnol Oceanogr 45:716–726
87. Larsson U, Hajdu S, Walve J, Elmgren R (2001) Estimating Baltic nitrogen fixation from the summer increase in upper mixed layer total nitrogen. Limnol Oceanogr 46:811–820
88. Wasmund N, Nausch G, Schneider B, Nagel K, Voss M (2005) Comparison of nitrogen fixation rates determined with different methods: a study in the Baltic Proper. Mar Ecol Progr Ser 297:23–31
89. Savchuk O, Wulff F (1999) Modelling regional and large-scale response of Baltic Sea ecosystems to nutrient load reductions. Hydrobiologia 393:35–43
90. Lyakhin Ju A, Makarova SV, Maximov AA, Savchuk OP, Silina NI (1997) Ecological situation in the Eastern Gulf of Finland in July 1996. In: Davidan IN, Savchuk OP (eds) "Baltica" Project. Problems of research and modelling of the Baltic Sea ecosystem. Issue 5. Ecosystem models. Assessement of the modern state of the Gulf of Finland. Hydrometeoizdat, St Petersburg (In Russian)
91. Laine AO, Andersin A-B, Leiniö S, Zuur AF (2007) Stratification-induced hypoxia as a structuring factor of macrozoobenthos in the open Gulf of Finland (Baltic Sea). J Sea Res 57:65–77
92. Lehtoranta J (2003) Dynamics of sediment phosphorus in the brackish Gulf of Finland. Monogr Boreal Environ Res 24:1–58
93. Kononen K (1992) Dynamics of the toxic cyanobacterial blooms in the Baltic Sea. Finn Mar Res 261:3–36
94. Kononen K, Kuparinen J, Mäkelä K (1996) Initiation of cyanobacterial blooms in a frontal region at the entrance to the Gulf of Finland, Baltic Sea. Limnol Oceanogr 40:98–112
95. Kahru M, Leppänen J-M, Rud O, Savchuk OP (2000) Cyanobacteria blooms in the Gulf of Finland triggered by saltwater inflow into the Baltic Sea. Mar Ecol Progr Ser 207:13–18
96. Stigebrandt A, Gustafsson BG (2007) Improvement of Baltic Proper water quality using large-scale ecological engineering. Ambio 36:280–286

Biogeochemical Characteristics in the Elefsis Bay (Aegean Sea, Eastern Mediterranean) in Relation to Anoxia and Climate Changes

A. Pavlidou, H. Kontoyiannis, Ch. Anagnostou, I. Siokou–Frangou, K. Pagou, E. Krasakopoulou, G. Assimakopoulou, S. Zervoudaki, Ch. Zeri, J. Chatzianestis, and R. Psyllidou-Giouranovits

Abstract Historical data on physico-chemical and biological characteristics during the last 30 years were used to examine the seasonal nutrient and plankton dynamics in a semi-enclosed area of the Mediterranean Sea, Elefsis Bay, in phase with the development of intermittently hypoxic and anoxic conditions. Sediment records covering most of the Holocene showed that the area was affected by hypoxia and/or anoxia in the past. However, the occurrence of hypoxia in Elefsis Bay need not necessarily be attributed to anthropogenic activities but could be naturally driven by oceanographic – climate forcing.

The ecosystem of the Elefsis Bay seems to be very complicated and variable. Its variability over the last 30 years can be attributed to the differences in anoxia intense and the amount of the accumulated organic material. The first observations in the temporal variations of environmental parameters in the bay primarily reflect the impact of decreasing pollution during the last decade rather than climate variability. On the contrary, the observed variation in the intensity of the hypoxia/anoxia developed in the bay appears to be related to local climate variability. However, this variation, together with the decrease in pollution levels in the bay during the last years, seem to have an effect on the N:P ratio which controls planktonic production.

Keywords Aegean Sea, Anoxia, Elefsis Bay, Hypoxia

A. Pavlidou (✉), H. Kontoyiannis, Ch. Anagnostou, I. Siokou–Frangou, K. Pagou, E. Krasakopoulou, G. Assimakopoulou, S. Zervoudaki, Ch. Zeri, J. Chatzianestis and R. Psyllidou-Giouranovits
Hellenic Center for Marine Research, Institute of Oceanography, 47th Km of Athens-Sounio Avenue, Anavyssos 19013, Greece
e-mail: aleka@ath.hcmr.gr

E.V. Yakushev (ed.), *Chemical Structure of Pelagic Redox Interfaces: Observation and Modeling*, Hdb Env Chem (2013) 22: 161–202, DOI 10.1007/698_2010_55,

Contents

Abbreviations

C_{org}	Organic carbon
DO	Dissolved oxygen
DIN	Dissolved inorganic nitrogen
DIP	Dissolved inorganic phosphorus
DOC	Dissolved organic carbon
DOM	Dissolved organic matter
DON	Dissolved organic nitrogen
DOP	Dissolved organic phosphorus
MDS	Multidimensional scaling analysis
NAO	North Atlantic oscillation
PCA	Principal component analysis
PCBs	Polychlorinated biphenyls
POC	Particulate organic carbon
PON	Particulate organic nitrogen
POP	Particulate organic phosphorus
TDN	Total dissolved nitrogen
TDP	Total dissolved phosphorus
TOC	Total organic carbon
TON	Total organic nitrogen (DON + PON)

1 Introduction

The condition of low dissolved oxygen (DO) is known as hypoxia. Hypoxia, defined as <2 ml/L (<89.3 μM) DO, occurs in aquatic environments when DO becomes reduced in concentration to a point where it becomes harmful to organisms living in that environment [1, 2]. Anoxia indicates the complete absence of oxygen, but in some cases, there is a transition zone, the suboxic zone, which is characterized by oxygen concentrations less than 5 μM. The suboxic zone was discovered in Black Sea by Murray et al. [3]. The existence of the suboxic zone makes the cycling

of the oxygen and sulfide in aquatic ecosystems more complicated. Murray et al. [4] suggested that the suboxic zone is defined as the layer where oxygen varied from less than 2–10 μM and sulfide less than 5 nM [5].

The two principal factors leading to the development of hypoxia, and sometimes to anoxia, are water column stratification, which isolates the bottom water from exchange with the oxygen-rich surface water, and decomposition of organic matter in the bottom water, which reduces oxygen levels. Both conditions must occur for hypoxia/anoxia to develop and persist [6].

In general, eutrophication links anthropogenic nutrient enrichment in aquatic ecosystems to increased supply of organic matter, which subsequently causes deleterious environmental perturbations. It is well known that anoxia causes severe ecosystem disturbances and also affects the nutrient biogeochemical cycles forming hydrogen sulfide which is hazardous to numerous fauna and flora communities [1, 2, 7].

Land use changes and local climatic fluctuations play an essential role in material cycling, such as nutrient, in the long term. However, climatic variations are supposed to be a critical factor affecting the stratification of the waters and the intensity of hypoxia. The intensity and local extension of anoxic marine areas is related to the local climatic variations which may, in turn, be influenced by global phenomena. In this frame, human-induced climatic changes may amplify the natural oscillations of the climate system. The variability of biogeochemical processes and periodic formation of bottom anoxia in certain regions of the European Seas (Baltic, Black, Azov and Caspian Seas) is a well-known phenomenon with changing intensities on annual or decadal scales. For example, in the Northern Adriatic Sea, periodic anoxia events were caused by a simultaneous increase of nutrients introduced into the sea by the Po River and weather conditions favorable to stronger density stratification. It has been documented that weather conditions directly affecting the redox balance of the Azov and Black Seas, as well as of the shallow areas of the Baltic and Mediterranean Seas [8–10] showed that periodically, near-anoxic conditions can occur at the water–sediment interface in late summer or early autumn due to heavy organic matter loads and/or minimal water exchange with the central Adriatic Sea, driving change in fisheries yields. In the Eastern Mediterranean Sea, periodical anoxic events occur in a shallow semi-enclosed area of Aegean Sea, Elefsis Bay.

In Elefsis Bay, the anoxic layer is an intermittent feature that is developed every year, but its intensity varies manifold. During the warm period (May–late October), the development of a strong temperature-driven pycnocline results in the isolation of the deeper part of the water column, leading to insufficient oxygen supply from either atmospheric or photosynthetic sources. As a consequence, the near-bottom layers remain periodically hypoxic and anoxic (0.00 μM for 2–3 months) with high amounts of silicate, phosphate and ammonium [8, 11–14]. Significant low oxygen concentrations have also been recorded in the deep layers (>150 m) of the Western Basin of Saronikos Gulf, in Aegean Sea, since 1987. The deep layers remain physically and dynamically isolated from any lateral or vertical interactions with the rest of the west basin [15]. In 1990–1992, the last occurred deep homogenization resulted in the recovery of the oxygen values near the bottom layer. From 1992 till

today, the oxygen concentrations show a continuous decreasing trend. Ever since the last decade, hypoxic conditions prevail in the area, causing major changes in the ecosystem.

In this work, we analyze hypoxia and anoxia during the last 30 years in a shallow semi-enclosed area of Mediterranean Sea, Elefsis Bay. Historical data on physico-chemical and biological characteristics from 1987 to 2009 were used to examine the seasonal nutrient and plankton dynamics in the selected area of the Mediterranean Sea, to establish how the variability in the hydrological pattern determines both the nutrient composition and plankton dynamics and to link these to the DO and environmental records. In addition, we study the ecological response to the local climate changes.

Finally, we summarize the current knowledge in the selected semi-enclosed polluted bay of the Eastern Mediterranean regarding the appearance of hypoxia and mostly anoxia, in modern times (last 30 years), modern historical times (30–200 years ago), and in the geological past (last c. 10,000 years). We present sediment records covering most of the Holocene and explore possible connections with the presence of past hypoxia/anoxia and the role of climate and environmental variability and human impact. Our main objective is to answer three basic questions: where, when and why was the study area hypoxic or anoxic in the past.

2 Description of the Area

Elefsis Bay (Longitude: between 23° 25′ 48″ E 23° 36′ 36″ E; Latitude: between 27° 59′ 24″ N and 38° 03′ N) is a small and shallow (ca. 68 m^2 with a mean and maximum depth of 20 m and ~35 m, respectively), almost enclosed embayment in the Aegean Sea (Eastern Mediterranean Sea). It is connected to the Saronikos Gulf by narrow and shallow channels on both the eastern and western side (8 m minimum depth at the western and 12 m minimum depth at the eastern; Fig. 1). Estimates of the surface flow in Elefsis Bay showed a flow of around 250 $m^3 \cdot s^{-1}$ from east to west during winter and a higher (~450 $m^3 \cdot s^{-1}$) reversed flow in summer [16, 17]. The Elefsis Bay differs from the Saronikos Gulf not only in its morphology but also in the extent of pollution suffered during the last decades, mainly by industrial activities on its coastline. A significant number of industries (oil refineries, shipyards, chemical plants, food, metal cement industries etc.) are located along the northern coastline of the Bay. Extended water pollution caused by organic matter and metal enrichment from hot spots, casts a shadow over human population growth and development. In the eastern reach of Elefsis Bay lies the city of Athens with a population of over five million. The eastern Keratsini channel is enriched by the industrial and shipyard area of Piraeus harbor. Until 1994, Keratsini channel was receiving the untreated domestic and industrial sewage of the Athens Metropolitan area which was discharged into the surface water layer of the channel and enriched the bay with metals, nutrients and organic matter. After 1994, the sewage of the Athens Metropolitan area was primarily treated in the Psitallia Sewage Treatment Plant and discharged into the inner

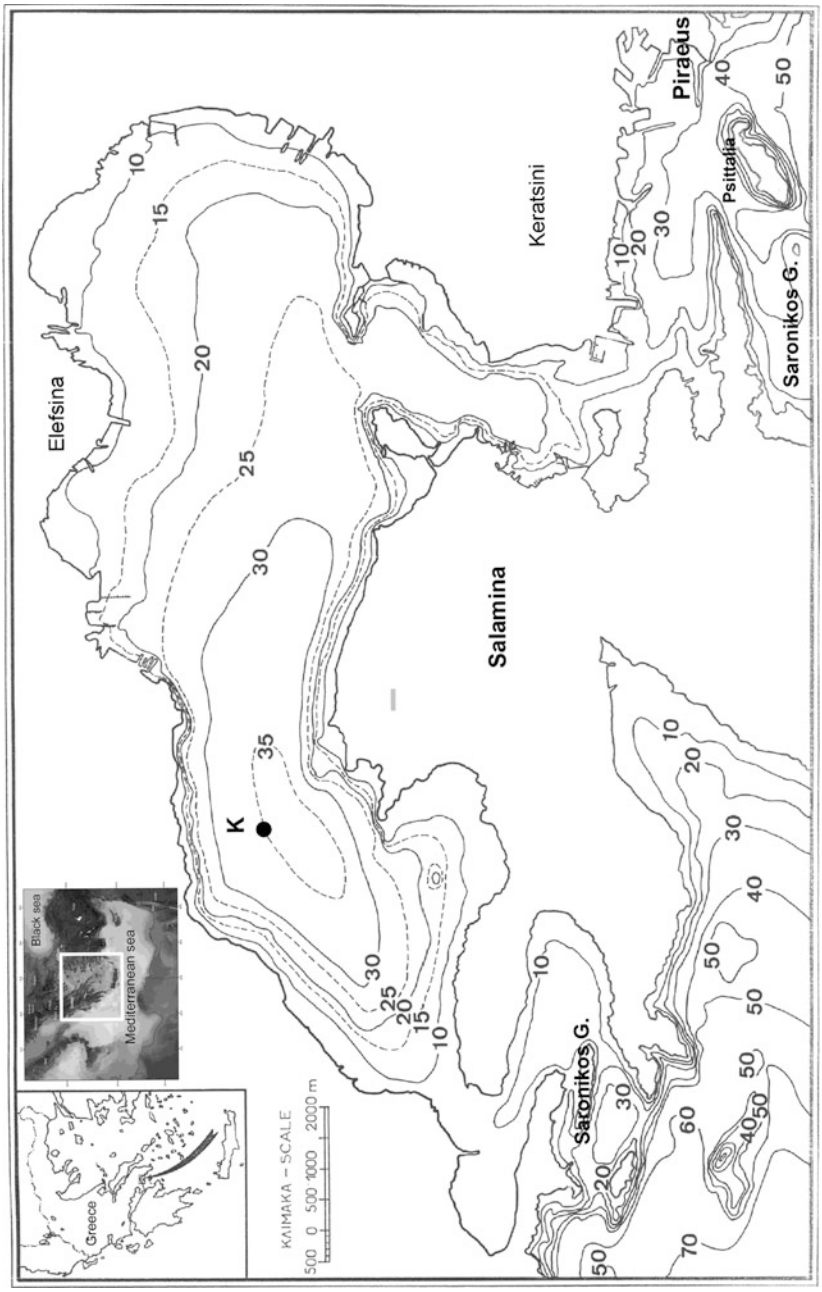

Fig. 1 Bathymetric map of the Elefsis Bay (map produced by Anagnostou, unpublished data)

Saronikos Gulf (Fig. 1). Additionally, by the end of 2004, the secondary stage of the Psittalia Sewage Plant became operational.

The extended anthropogenic pollution of the area occurred after the Second World War, when rapid population growth and development followed with increasing industrialization. At that time, population growth, a large fertilizer factory situated just outside the entrance of Pireaus Harbor and the discharge of the untreated nutrient-rich sewage enhanced the point-source nutrient loading. After 1994, the pollution in the Bay decreased significantly, either because many industries closed or decreased the amount of their pollutants according to the European and National directives. However, during the last years, there has been a turn towards cleaner technologies, and the bay does not receive the large amount of untreated sewage of Athens any longer. At the same time, the bay does not receive any significant amounts of natural fresh waters either, since no river water flows into the bay, except for some ephemeral streams in winter.

The aforementioned anthropogenic inputs lead to ecological stress in the bay. Documented anoxic conditions in the deepest western part (>25 m depth) of the Bay date back to the summer of 1973 [18], when the zooplanktonic biomass remained near zero [19]. Following the initial documentation of anoxia, several low DO conditions have been referred [8, 20–24]. Hypoxic and anoxic conditions are developed every year only in the western part of the Elefsis Bay.

In summary, the physical setting of the Elefsis Bay, the narrow and shallow connections to the Saronikos Gulf with low freshwater inflows and limited water exchange, leads to a strong seasonal density stratification of the water mass and influences the oxygen distribution in the basin, resulting in hypoxia and anoxia, existing for about 5 months. The summer stratification reduces the supply of DO to the bottom layers, whereas, oxidation of the organic matter results in the disappearance of oxygen and the formation of anaerobic conditions. This situation retains nutrients and organic matter within the basin and leads to high nutrient accumulation.

3 History of the Area

Elefsis Bay is the result of the geodynamical evolution of the Hellenic area. It is an embayment of tectonical origin. Active neotectonism is the prevalent driving mechanism which formed the Elefsis bay and continues to regulate the morphology of the broader area. Intensive faulting resulted in the fragmentation of the upper crust into individual tectonic blocks, which undergo vertical or horizontal movements. These processes led to the formation of a complicated geomorphology of the area. This morphotectonical regime has, as a consequence, the formation of a variety of basins, drainage systems and coastal forms. Figure 1 shows the complicated coastline and the bathymetry of Elefsis Bay and Fig. 2 the drainage area.

The drainage area is relatively small and extends in the northern part of Elefsis Bay. Historically, it contributed to the formation of the Elefsis plain where large-

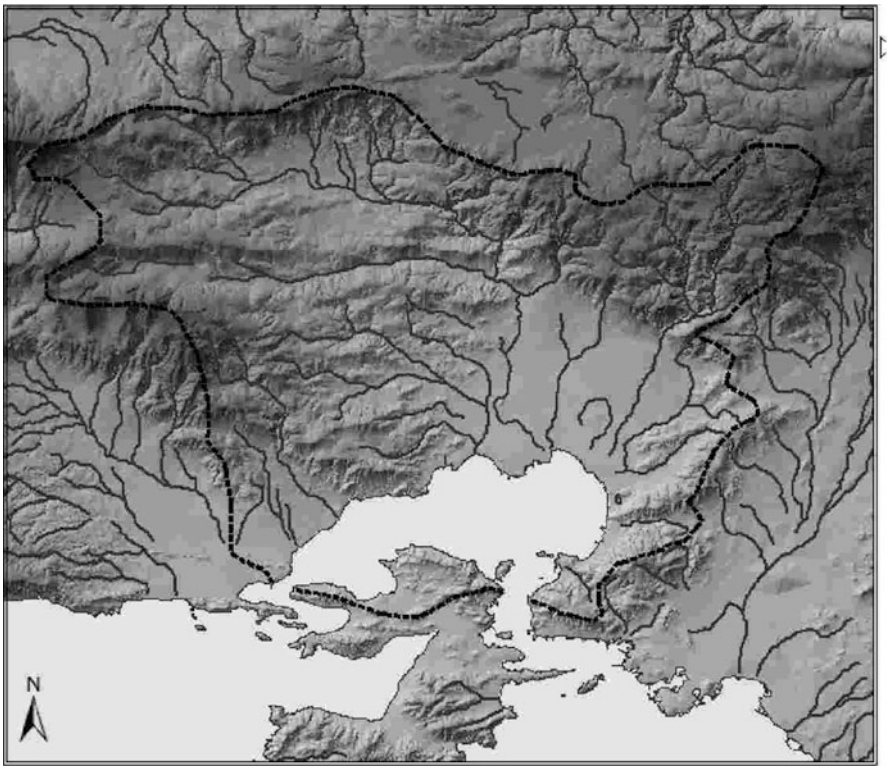

Fig. 2 The drainage area of the Elefsis Bay. It extends in the northern boundary of the bay and contribute with terrigenous sediment particles supply to the sedimentation processes of the bay

scale industrial activities take place. Small tributaries drain into the bay with low freshwater input and sediment particle supply.

The bathymetric map differentiates the marine area in two parts; the eastern part with smaller depth (10–25 m) and the western part, tectonically subsided, which shows depth of more than 30 m and which acts as a sediment trap.

Systematic bottom profiling in the Elefsis Bay (Anagnostou, unpublished data) show that in the eastern part, the thickness of the Holocene sediment cover reaches values from 3 to 5 m and in the western part from 10 to 15 m (Fig. 3).

Historically, the bay was isolated from the Saronicos Gulf and formed land, and probably, a small lake in the western part. According to the sea level stand evolution, a connection of the lake to the sea probably took place approx. 8,000 years ago [25–27].

The physiography of the Elefsis Bay, as a small and shallow basin, with the narrower and shallower connections (west and east) to Saronikos Gulf and the low freshwater input from the northern drainage basin, leads to a limited water exchange with the Saronikos system, resulting in hypoxic and anoxic conditions in the Elefsis Bay system.

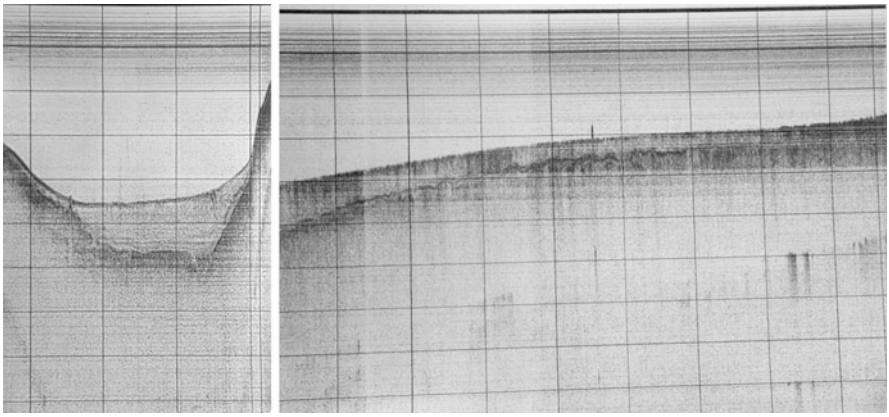

Fig. 3 Sub-bottom profiles show clear the Holocene marine sediments cover and the pre-depositional unconformity. *On the left* one profile from the western part of the Elefsis bay, where the Holocene sediments thickness reach 8–13 m. *On the right* the Holocene sediment cover with thickness from 3 to 5 m

Hypoxic and anoxic conditions in the water column above the sediment–water interface are leading to an enrichment of organic matter in the sediments. The dark to black color of the surface sediments is an index of the high content of organic matter in the sediments. Careful observations during the winter period (hypoxic conditions in the water column above the sediment–water interface) have shown a very thin layer, like a thin film (less than 1 mm) of oxidized surface sediments. During the summer period, anoxic conditions in the water column above the sediment–water interface lead to totally anoxic conditions in the bottom sediments (black color).

The present situation and the dynamic of the semi-enclosed marine system of Elefsis Bay bring forth the question: are the hypoxic/anoxic conditions in the bay a phenomenon of the last decade or a historical natural phenomenon of the studied marine system?

To approach this issue, a representative sediment core from the western part of the bay was taken and a sediment sampling for every three centimeter was carried out for an organic matter analysis. The core was taken in September 1989 in the frame of a Greek-German Bilateral Cooperation's Project. The location of the core sampling is the same location of the samplings for all the biochemical measurements in the water column presented in this work (station K in Fig. 1).

The length of the sediment core reached 357 cm and a total number of 120 samples were taken and analyzed for determining the organic carbon content. The dominant sediment type of the core is the silty clay type.

The results of the organic matter content of the sediments are given in Table 1. Figure 4 shows the fluctuation of the values of the organic matter through the core. The interpretation of the analytical results showed that an important number of anoxic events occurred in Elefsis Bay in the past. At the bottom of the core, an anoxic event left its footprint in the sediments, where organic matter content in the

Table 1 Organic matter content in the core sediment samples

Nr	Core depth (cm)	C_{org} (%)	Nr	Core depth	C_{org} (%)	Nr	Core depth (cm)	C_{org} (%)	Nr	Core depth (cm)	C_{org} (%)
1	1	3.3	31	90	0.9	61	180	1.2	91	270	1.1
2	3	3.6	32	93	1.0	62	183	1.4	92	273	1.2
3	6	4.3	33	96	1.1	63	186	1.2	93	276	1.2
4	9	4.5	34	99	0.9	64	189	1.1	94	279	1.1
5	12	4.7	35	102	1.0	65	192	1.2	95	282	1.1
6	15	2.4	36	105	1.0	66	195	1.1	96	285	1.0
7	18	1.3	37	108	1.0	67	198	1.4	97	288	1.3
8	21	1.2	38	111	1.0	68	201	1.6	98	291	1.1
9	24	1.2	39	114	1.2	69	204	1.8	99	294	1.2
10	27	1.2	40	117	1.1	70	207	1.6	100	297	1.1
11	30	1.2	41	120	1.2	71	210	1.4	101	300	1.2
12	33	1.3	42	123	1.3	72	213	1.4	102	303	3.1
13	36	1.1	43	126	1.2	73	216	1.4	103	306	2.8
14	39	1.2	44	129	1.2	74	219	1.3	104	309	3.0
15	42	1.1	45	132	1.2	75	222	1.5	105	312	2.8
16	45	1.2	46	135	1.1	76	225	1.4	106	315	2.4
17	48	1.2	47	138	1.2	77	228	1.3	107	318	2.2
18	51	1.0	48	141	1.3	78	231	1.4	108	321	1.7
19	54	1.1	49	144	1.3	79	234	1.6	109	324	1.4
20	57	1.1	50	147	1.2	80	237	1.7	110	327	1.7
21	60	1.2	51	150	1.2	81	240	1.4	111	330	1.9
22	63	1.1	52	153	1.1	82	243	1.3	112	333	1.6
23	66	1.1	53	156	1.2	83	246	1.4	113	336	1.8
24	69	0.9	54	159	1.2	84	249	1.4	114	339	1.7
25	72	1.2	55	162	1.2	85	252	1.5	115	342	1.6
26	75	1.0	56	165	1.2	86	255	1.4	116	345	1.6
27	78	1.1	57	168	1.2	87	258	1.3	117	348	1.5
28	81	0.9	58	171	1.2	88	261	1.2	118	351	1.7
29	84	1.1	59	174	1.2	89	264	1.1	119	354	1.6
30	87	1.2	60	177	1.3	90	267	1.2	120	357	1.5

sediments reached high values of more than 3.0%. This was followed by a number of four remarkable anoxic events, with organic matter fluctuating from 1.0 to 1.8%. In more recent sediments, the organic matter content fluctuates from 0.8 to 1.3%. A trend to higher values in the very recent sediments can be seen clearly. The last 20 cm (top of the core) are sediments influenced by anthropogenic activities. The recorded trend towards higher values also shows the impact of human activities on the semi-enclosed Elefsis Bay. The influence of human activities in the last 20 cm was further demonstrated by analyzing another sediment core collected from the same station in 2001 for the presence of organic pollutants. The results have shown that very high quantities of anthropogenic organic pollutants (aliphatic and polycyclic aromatic hydrocarbons, PCBs etc.) were present in the upper part (~25 cm) of this core. For this core, the sedimentation rate was also estimated using ^{210}Pb measurements and found to be approximately 0.29 cm per year [28]. It is noteworthy that the highest pollutant inputs were recorded in the 5–9 cm part of the core, which, according to the aforementioned sedimentation rate, correspond to the

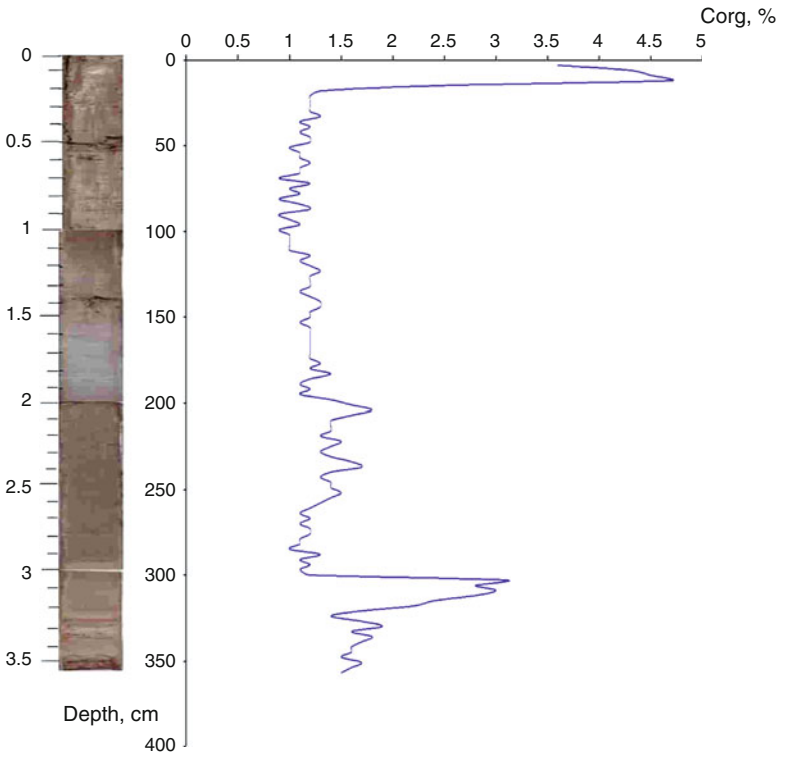

Fig. 4 The sediment core from the western part of Elefsis Bay (depth 33 m) and the distribution of the organic matter percentage along the core (120 samples are analyzed)

1970 and 1980 decades when many industrial units were developed indiscriminately in the area. In the first 5 cm, the pollutant inputs were clearly lower, reflecting both the application of cleaner technologies in the industries of the area during the last years and the discontinuance of discharging untreated effluents in Keratsini channel in 1994.

Geological records demonstrate that the area was affected by hypoxia and/or anoxia in the past. However, the occurrence of hypoxia in Elefsis Bay may not necessarily be attributed to anthropogenic activities but could be naturally driven by oceanographic–climate forcing; although in the last 50 years, both oceanographic–climate variability and anthropogenic impact have had the potential to greatly affect the marine environment in the semi-enclosed Elefsis Bay.

The present work placed emphasis on the appearance of hypoxia in the last 5,000 years based on organic matter analyses in a sediment core. It seems to be clear that both oceanographic–climate and anthropogenic pressures have played a role as drivers for hypoxia through time. The occurrence of hypoxia in Elefsis Bay on the "geological" timescale seems to be related to climate fluctuations. Warmer periods contributed to the stratification of the water column and to relative higher productivity. These factors were the primary forces for hypoxia in the Elefsis Bay.

However, it is open for future work to perform dating of the sediment core samples in order to study the chronological follow-up of these fluctuations.

4 Elefsis Bay Characteristics

4.1 Field, Laboratory Analysis and Data Assessment

Data used in this study were obtained from four to twelve cruises per year from 1987 to 2009 (total 263 cruises), at Elefsis Bay and Saronikos Gulf, using small boats and the research vessels « Aegaeo » and « Filia » of the Hellenic Center for Marine Research (HCMR). At the selected station in the deepest area of Elefsis Bay (Fig. 1), seawater samples were collected from standard depths (surface, 10 m, 20 m, near bottom) with Niskin bottles, either mounted on a rosette or individually on a hydro wire.

The temperature, salinity and density in the water column were measured with a CTD profiler (Sea Bird Electronics) which was equipped with pressure, temperature and conductivity sensors. Before the 1990s, measurements were performed with reversing thermometers attached to NIO bottles, whereas, the salinity was determined with an autolab inductive salinometer.

For the determination of oxygen, samples were first taken from a sampling bottle with the recommended precautions to prevent any biological activity and gas exchanges with the atmosphere [29] and analyzed immediately after collection, on board, with the Winkler method according to [30, 31].

Water samples for nutrient analysis were collected in 100 mL polyethylene bottles “aged” with HCl 10% and kept deep-frozen (–20°C) until their analysis for nitrate, nitrite, silicate, dissolved organic nitrogen (DON) and dissolved organic phosphorus (DOP) in the laboratory. Filtered samples, from 1987 to 1995, were analyzed with a TECHNIKON CSM-6 Autoanalyser, between 1996 and 1999, with an ALPKEM autoanalyser and after 1999 till today, with a BRAN + LUEBBE II autoanalyser according to standard methods ([32] for silicate; [29] for nitrate-nitrite and [33] for phosphate).

The determination of ammonium and phosphate was performed, first using a Hitachi and then a Perkin Elmer 20 Lambda and 25 Lambda spectrophotometer according to standard methods ([34] for ammonium and [33], for phosphate).

For the measurement of DON and DOP, a conversion of dissolved organic matter DOM to inorganic products, nitrate + nitrite and soluble reactive phosphate, was performed by a persulfate wet-oxidation in low alkaline conditions. The concentration of the inorganic products dissolved in the sample was measured automatically by colorimetry using a BRAN + LUEBBE II autoanalyser [35–37]. The values obtained were corrected for the reagent blank.

Water samples for TOC analysis were collected in precombusted (480°C, 12 h) glass ampoules, acidified with 2.5 M HCl to pH ∼2 and flame-sealed immediately

on board. TOC analysis was carried out in the laboratory following the catalytic oxidation method described by [38] using a commercially available automatic analyzer (Shimadzu TOC-5000).

Seawater samples for the POC and PON (1–2 L for each parameter) and the particulate phosphorus (POP; 0.2–0.3 L) determination were filtered through Whatman GF/F filters (nominal pore size 0.7 m, 25 mm) precombusted at 450°C. Filters were stored in Petri dishes and kept continuously under deep freeze (–20°C) in the dark until their analysis in the lab. POC and PON were measured on a EA 1108 CHN Fisons Instruments CHN analyser according to the methodology suggested by Verardo et al. [39]. Particulate phosphorus was determined using a persulfate wet-oxidation method [35–37].

Organic carbon in sediments were analyzed according to the Gaudette method [40].

For obtaining total chlorophyll measurements, water samples (1.5 L) were filtered through Whatman GF/F filters. The analysis was performed fluorometrically according to Holm-Hansen et al. [41], using a TURNER 00-AU-10 instrument.

Meso-zooplankton samples were collected by the vertical hauls of a WP-*2* net (200 μm mesh size) from near bottom to the surface. All samples were fixed by borate-buffered formalin to 4% final concentration. Two subsamples were obtained by the Folsom splitter: the first was used for the estimation of biomass and the second one for the enumeration of groups and species. The dry-weight method [42] was used for the estimation of biomass and values were expressed in mg m^{-3}. Taxonomic diversity of the copepod and cladoceran assemblages was calculated at all study seasons and years with the Shannon_Wiener Index (H'). These analyses were performed using the PRIMER program (Plymouth Marine Laboratory, UK).

In order to test similarities among seasons and years regarding the mesozooplankton community composition and structure, a nonmetric Multidimensional Scaling Analysis was performed based on the Bray-Curtis similarity index. This analysis was performed using the PRIMER program (Plymouth Marine Laboratory, UK).

Principal component analysis (PCA) was used to extract composite variables (principal components) from the original variables for assessing the underlying patterns in the distribution of the measured parameters in Elefsis Bay. The PCA solution was rotated (using VARIMAX rotation) to facilitate the interpretation of the principal components. The factor score for each variable was calculated. The PCA analysis was performed with the SPSS (version 17) statistical program.

Linear Regression Analysis was used to assess if there is any significant trend of the measured parameters with time. The SPSS (version 17) statistical program was also used.

4.2 Description of the Ecosystem Dynamics

In the last 40 years, there has been a thorough study of the Elefsis Bay mainly by the HCMR ([8, 18, 20–23, 43–58], etc.), the NRC "Demokritos" [59–67] and the University of Athens ([12, 13, 24, 68–72]; etc.).

According to [22, 23], a general pattern of cycling of temperature across the year is followed in Elefsis Bay. According to this pattern, the cooling of the upper layers reaches a minimum temperature from February to April, with temperatures of about 12–14°C. Then, the water mass begins to warm up to maximum value of about 25°C from August to September. In summer, temperature differences of 10°C between the sea surface and bottom result in the development of a strong stratification, which persists for about 5 months and causes anoxic conditions. The pycnocline is formed at depths varying between c. 15 m in early summer and 25–30 m from August to October [73]. As a consequence, the near-bottom layer remains periodically hypoxic and anoxic for 2–3 months with high amounts of silicate, phosphate and ammonium [8, 12–14, 50] (Fig. 5). Macrozoobethos studies in Elefsis Bay showed seasonal changes in both number of species and individuals and the total absence of alive zoobenthos from July to August till late autumn. It is noteworthy that in both

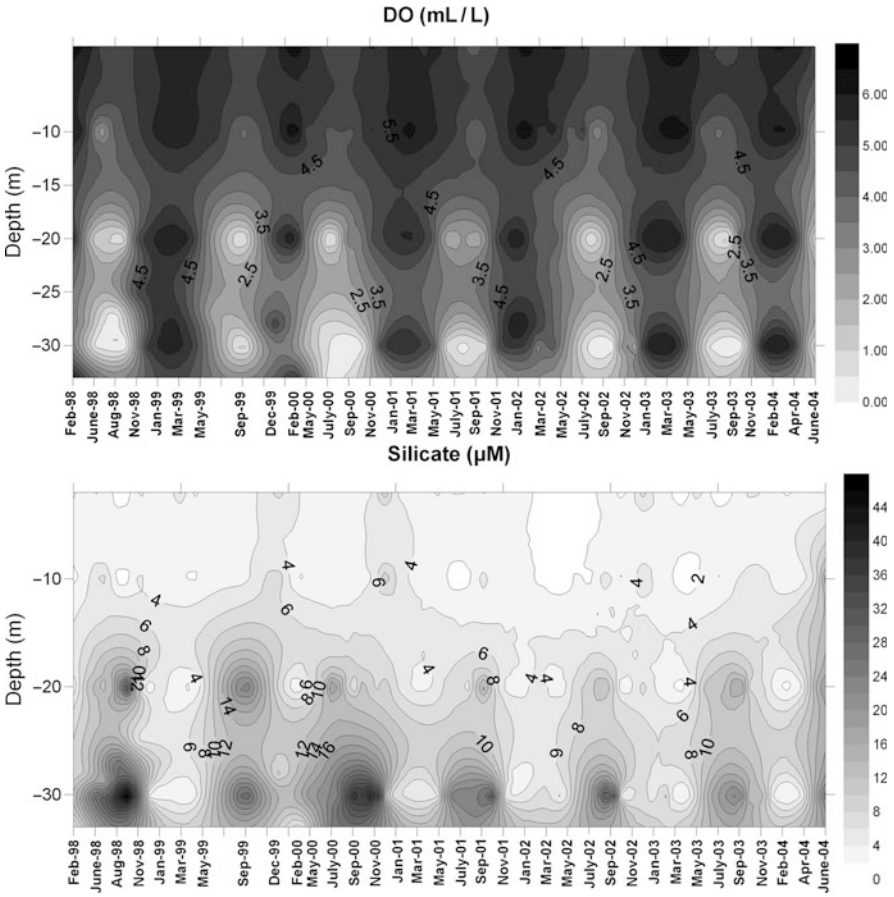

Fig. 5 Vertical distribution of DO and silicate concentrations in the water column of Elefsis Bay during 1998–2004

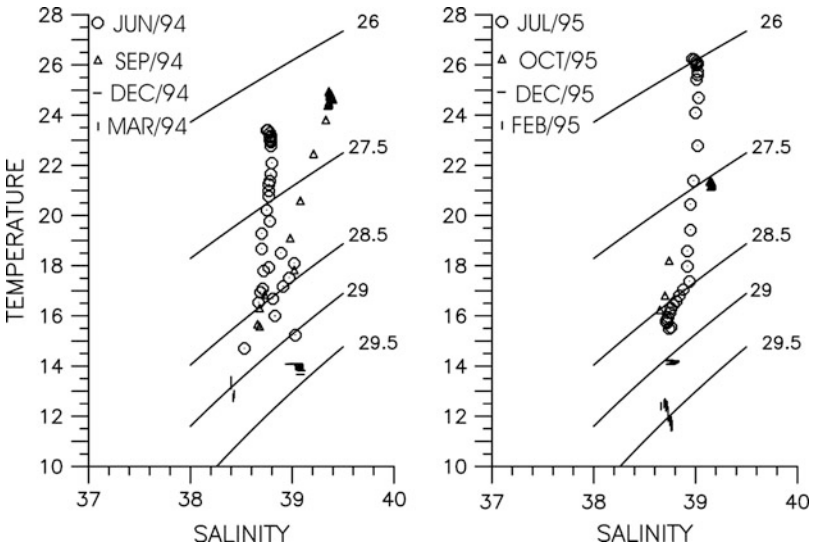

Fig. 6 T/S diagrams in Elefsis Bay during 1994–1995

winter and summer, abundance and diversity were higher in the western part of the bay than in the eastern part [54, 74–76].

4.2.1 Hydrography

The sea water of the Elefsis Bay, being an almost isolated shallow water body, is strongly coupled with the atmosphere and exhibits a broad seasonal cycle in its temperature and salinity throughout the year. Figure 6 shows the T/S characteristics on a seasonal basis for years 1994 and 1995. The water temperature variations respond fast to those of the atmosphere, and in early winter (December 1994, 1995), typical temperatures are less than 14°C. The signature of low near-bottom temperatures is preserved during summer and early fall because of the strong pycnocline developed in summer, which isolates the near-bottom layer. In this way, the winter characteristics of the near-bottom layer with lower temperatures and salinities are preserved until mid fall. After mid fall, densities increase rapidly throughout the water column because the vertical mixing carries to the sea bottom the high salinities which are developed in the surface layer during summer.

Figure 7 shows a typical seasonal evolution of the vertical structure in temperature salinity and density. The example is taken from 1995. In the upper ∼15 m, temperature and salinity increase fast in summer due to atmospheric heating and evaporation, and a strong pycnocline develops with a nearly 3-unit (26-to-29) surface-to-bottom difference in density. This pycnocline isolates the near-bottom layer (∼25–30 m) and persists until mid fall, as shown in Fig. 7 for October 1995.

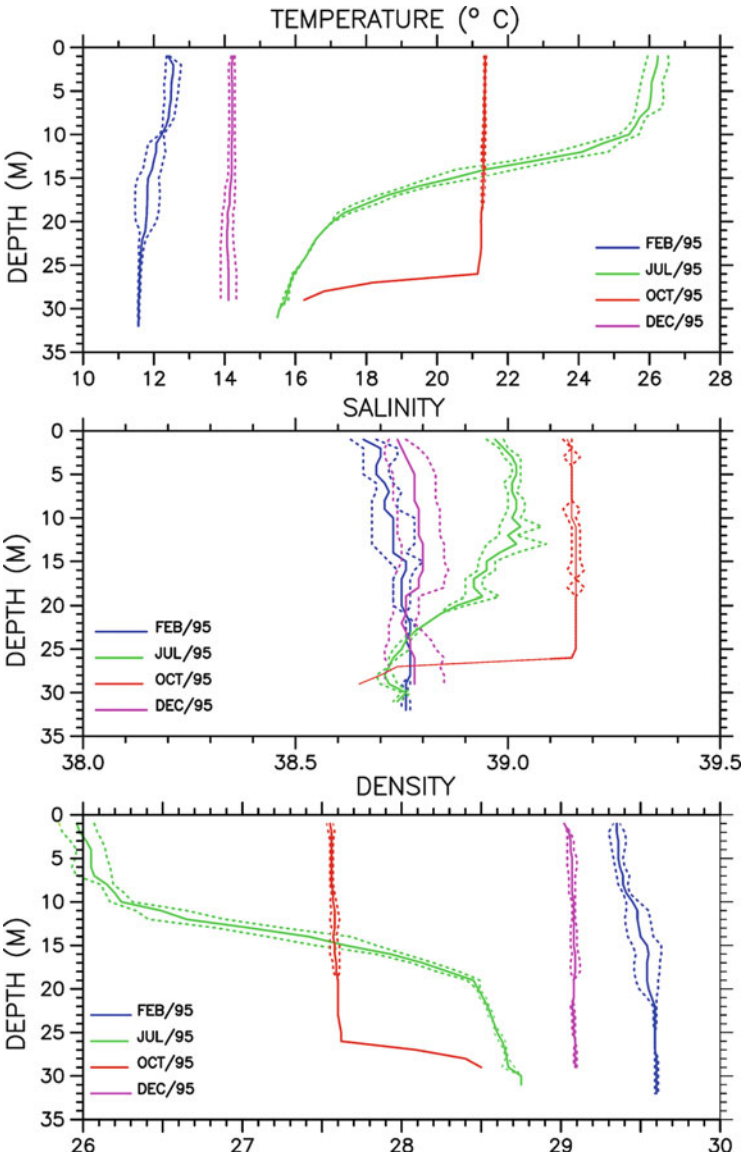

Fig. 7 Seasonal evolution of temperature, salinity and density vertical structure in Elefsis Bay during 1995. *Dashed lines* indicate plus/minus one standard deviation

4.2.2 Biochemical Characteristics of the Water Column

Biochemical data obtained from twelve monthly samplings during 2007 as well as from the 263 cruises obtained during 1987–2009 are used to describe the biochemical characteristics of Elefsis Bay in phase with the stratification of the

water masses and the seasonal development of hypoxia/anoxia in the western part of Elefsis.

DO and Inorganic Nutrients

Depth profiles at Elefsis Bay showed that during the warm/stratified period (August–October), nutrients and oxygen remain constant between 0 and 10 m, whereas, below 10 m, there is a rapid decrease of oxygen reaching near extinction at 20 m and anoxia near the bottom. Ammonium, phosphate and silicate increased markedly with a depth below 10 m. Thus, during the warm months (August–September, and in some cases, October), the bottom layer is characterized by the presence of an anoxic zone. The thickness of the hypoxic/anoxic zone varies between the sampling periods from 1 to 3 m to 8–10 m above the bottom . It is noteworthy that during the winter of 2007, NO_3^- represented approximately 78% of the dissolved inorganic N pool in the water column, NO_2^- represented only 8% and NH_4^+ 13%. However, during the warm/stratified period, their relative contribution changes and NO_3^- account for 24% of the total dissolved inorganic N, NO_2^- represent only the 9% of inorganic N and NH_4^+ 67%. In the near-bottom layer, (∼1–2 m thick) ammonium is the dominant inorganic nitrogen species, representing the 93% of inorganic N. With the reversal of coastal circulation during the cold period (December–March), the water column becomes oxygenated again and nutrient concentrations revert to their previous values. In 2007, the mean integrated DIN concentration of the water column during warm months (August–September) was measured 8.11 μM, whereas in cold months, a significant decrease (2.05 μM) was observed, followed by an increase in DON concentrations indicating oxidation of organic nitrogen to inorganic forms during the warm months. The latter is a general pattern observed in Elefsis Bay. [50, 51, 77, 78].

Detailed concentrations of DO, ammonium and silicate obtained from all the cruises between 1987 and 2008 in the cold period when the water column is fully homogenized (February is taken as an example), and in the warm/stratified period (September is taken as an example), are compiled in Fig. 8.

In winter (February), the DO, ammonium, nitrite, phosphate and silicate concentrations remain almost stable with depth. The DO concentrations ranged in the surface layer (2–10 m) between 251 and 297 μM (average value 271 ± 16.0 μM) and in the near-bed layer between 204 and 291 μM (average value 250 ± 23.0 μM). The water column was characterized by low phosphate and nitrite concentrations (average values: 0.190 ± 0.160 mol/L for phosphate and 0.143 ± 0.118 mol/L for nitrite in the surface layer; 0.180 ± 0.140 mol/L for phosphate and 0.160 ± 0.100 mol/L for nitrite in the near-bed layer). In general, ammonium concentrations were low in the surface layer (average values 0.437 ± 0.300 mol/L), with the exception of the rather high ammonium concentrations observed in February 1996 (high chlorophyll concentrations were also measured in February 1996), and tended to increase slowly in the near-bottom layer (0.730 ± 0.610 mol/L). Silicate concentrations in some cases also increased in the near-bottom layer (February

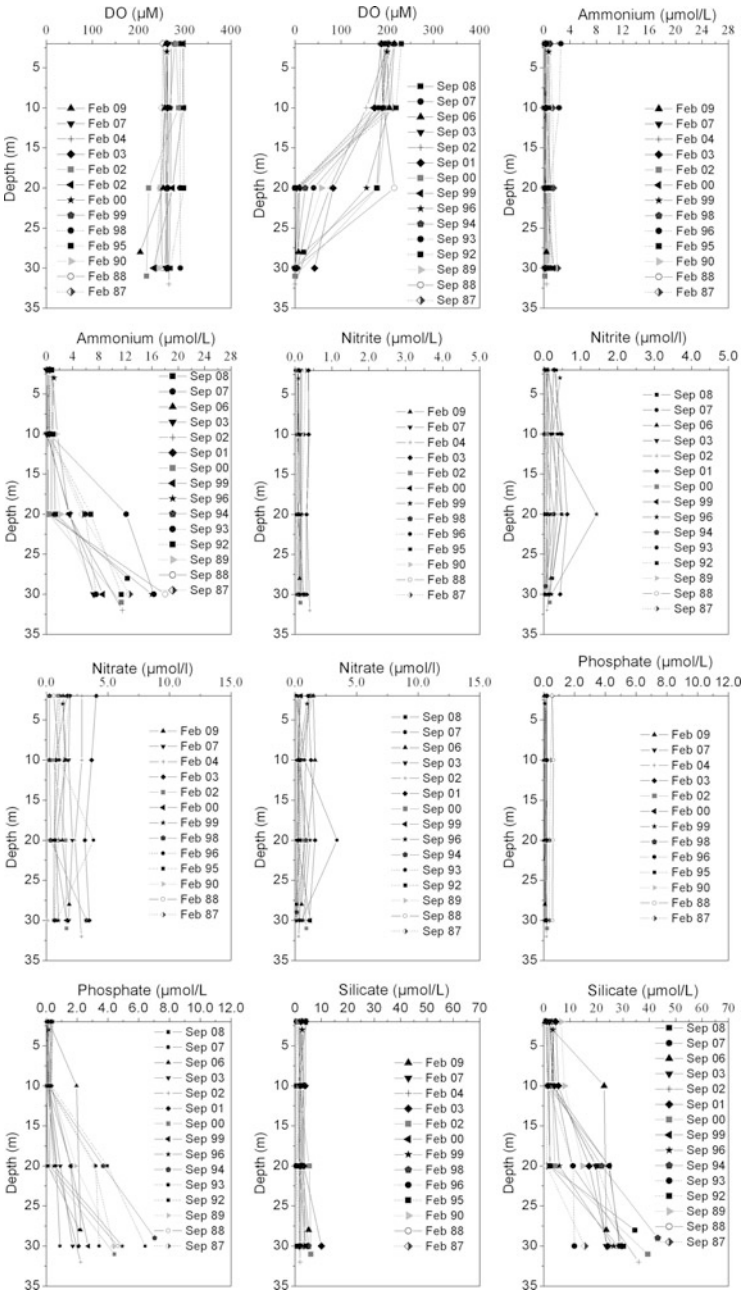

Fig. 8 Vertical distribution of DO and nutrients in Elefsis Bay in cold (February/non-stratified) and warm (September/stratified) periods during 1987–2009

2002 and 2003) but, in general, remain constant with depth, with an average value of 2.30 ± 0.86 mol/L. The water column in winter was characterized by rather elevated nitrate concentrations, without any significant variation with depth (average values: 1.41 ± 1.03 mol/L in the surface layer and 1.56 ± 1.08 mol/L in the near-bed layer). The DIN:P ratio was calculated around 20 in the water column, whereas, Si:P in the water column was calculated around 25.

During the warm/stratified period when anoxic conditions prevail, the ammonium concentrations increase significantly with depth against nitrite and nitrate but in parallel with silicate and phosphate, suggesting the occurrence of the processes of organic matter remineralization (Fig. 8). The concentration of ammonium increased from 1.242 ± 0.604 mol/L in the surface layer to 11.70 ± 3.64 mol/L in the anoxic near-bottom layer. Nitrate and nitrite reduced slightly from 0.614 ± 0.120 mol/L and 0.170 ± 0.120 mol/L, respectively, in the surface layer, to 0.470 ± 0.390 mol/L and 0.140 ± 0.110 mol/L in the near-bottom layer. It seems that nitrite concentrations remain stable all over the year, whereas, nitrate concentrations clearly decreased and were almost depleted in summer. Silicate and phosphate concentrations increased by an order of magnitude below the pycnocline from 3.03 ± 1.75 mol/L and 0.182 ± 0.122 mol/L, respectively, in the upper layer to 26.91 ± 7.39 mol/L and 3.33 ± 1.56 mol/L below the pycnocline. Si:P ratio decreased from 29.3 in the surface layer to around nine in the near-bottom layer. It seems that the fraction of sediment-released phosphorus increases rapidly when oxygen concentration falls significantly. Sorbed phosphate is released from sediments to pore waters from host Fe-oxyhydroxides [79]. Once released to pore waters, phosphate can escape from sediments via diffusional transport, resuspension, or irrigation by benthos [80].

DIN:P ratio also decreased below the pycnocline, from 13.1 in the surface layer to 4.2 in the near-bottom waters, clearly showing a N-deficit in the near-bottom waters in summer. It is likely that, besides the remineralization of organic matter and the possible phosphate release from the sediment, an additional process takes place and contributes to such low values of the ratio. Denitrification occurs within the water column and the upper few millimeters of the sediments under low oxygen conditions, converts nitrate to nitrogen gases released from the system and represents a sink of nitrate. It is evident that denitrification could be the controlling factor of the DIN:P values in the near-bottom waters of Elefsis Bay.

The chemical characteristics of the anoxic layer indicate that denitrification occurs, even though this has not been confirmed by direct measurements of denitrification in the water column nor measurements of sulfide concentrations, so the evidence for denitrification is indirect. However, under these conditions, facultative heterotrophs switch over to alternate respiratory oxidants (electron acceptors) and the most abundant in seawater is NO_3^-. Denitrification removes most of the NO_3^-, and as sulfate reduction sets in, NH_4^+ accumulates in the anoxic waters [81–84]. It is noteworthy that in September, the bottom concentration of ammonium was about five times higher than in July and the concentrations of phosphate three times higher. The ammonium, phosphate and silicate accumulation results from the oxidation of organic matter accompanying the reduction of, first,

nitrate and then, sulfate [22]. It is known that MnO_2 reduction occurs next, with Mn^{4+} being the electron acceptor, followed by SO_4^{2-} as an electron acceptor, and sulfate reduction occurs with H_2S accumulation in anoxic waters [85]. However, the measurements of dissolved and particulate manganese in the Elefsis Bay during 2004, did not show high dissolved and/or particulate concentrations of manganese in the near-bottom waters (0.82 μg/L for dissolved and 0.35 μg/L for particulate manganese) [86]. Unfortunately, there are no available data from 2004 until 2008. Although, previous data concerning the period 1992–1995, showed that in many cases (i.e. September 1994), elevated dissolved (112 μg/L) and particulate Mn (171 μg/L) concentrations were recorded in the near-bottom waters when anoxic conditions occur, the role of Mn in the area cannot be established (Dasenakis and Pavlidou, unpublished data). New measurements of dissolved and particulate manganese for 2008 and 2009 still continue and the role of manganese in the anoxic waters of Elefsis Bay will be investigated in the future.

When we examined all the data from 1987 to 2009, we observed that there were differences between the shapes of the plots of DO or nutrients between the years. No accumulation of nitrite was noted in the waters where DO concentrations were higher than 2.00 mL/L (89 μM).

The DO and nutrient concentrations measured in the intermediate layer of 20 m showed interesting differences. The layer of 20 m depth can be assumed as a transition zone between the oxygenated surface layer and the anoxic near-bottom layer. Our observations showed that about 50% of the DO measurements in the transition zone was near extinction with concentrations <22 μM, whereas, the rest of the measurements showed DO concentrations between 41 and 215 μM. On the other hand, nitrate and nitrite peaks were observed at 20 m in most of the measurements during the September period. A conspicuous nitrite-peak (1.48 mol/L) observed in September 1996 corresponded to DO values of 156 μM, nitrate values of 1.2 mol/L and low ammonium. It seems that in some cases, waters with relatively high amounts of oxygen contained relatively high amounts of nitrite. The relatively high nitrite could be explained either by the reduction of nitrate or by the oxidation of ammonium. However, nitrification is the most likely process to occur [83]. In September 2007, maximum nitrate concentration (3.41 mol/L) at the transition zone corresponded to nitrite concentration 0.48 mol/L, ammonium concentration 1.36 mol/L and relatively low DO concentrations (40.6 μM). These chemical characteristics may indicate suboxic nitrification process. Probably, manganese reduction occurred via suboxic nitrification [87], but there are no available data of manganese measurements to support this hypothesis. However, according to Scoullos [69], in Elefsis bay, at a depth where a transition occurs from oxic to anoxic conditions, Mn^{4+}, present mainly as MnO_2 in the sediments, is reduced to dissolved Mn^{2+} which emanates from the sediments and moves slowly upwards. However, because of the presence of appreciable concentrations of oxygen, the Mn liberated from the sediments quickly re-precipitates as MnO_2 at the interface of the oxic/anoxic layer which is very close to the bottom. According to this theory, it is obvious that the Mn oxide dissolution and precipitation that can play an important role in the water chemistry, takes place in that transition zone of Elefsis Bay [69].

The ecosystem of Elefsis Bay seems to be very complicated and variable. Its variability is probably related to the differences in anoxia intense and the amount of the accumulated organic material. In general, we observed low nitrite concentrations in the anoxic, ammonium-rich waters. Nitrite is the first intermediate of denitrification and provides a diagnostic tool for its occurrence. Probably, denitrification at very low rates occurs without much accumulation of nitrite. However, mineralization processes (i.e. ammonification) are favored and supported by the high concentrations of organic matter. On the other hand, benthic nutrient recycling could be another source for the supply of the water column with ammonium.

Using data from 1987 to 2009, the mean values of DO, and nutrient concentrations at the near-bottom waters were calculated for each sampling period (Fig. 9).

Low DO values (<44.6 μM) were observed during July to October near the bottom of Elefsis Bay. The annual minimum of DO in the bottom waters of the bay was observed during September (Fig. 9), the mean ± 1SE was 4.46 ± 5.36 μM (Table 2). DO rise after October and the annual maximum was observed in January (mean ± 1SE was 256 ± 17.4 μM).

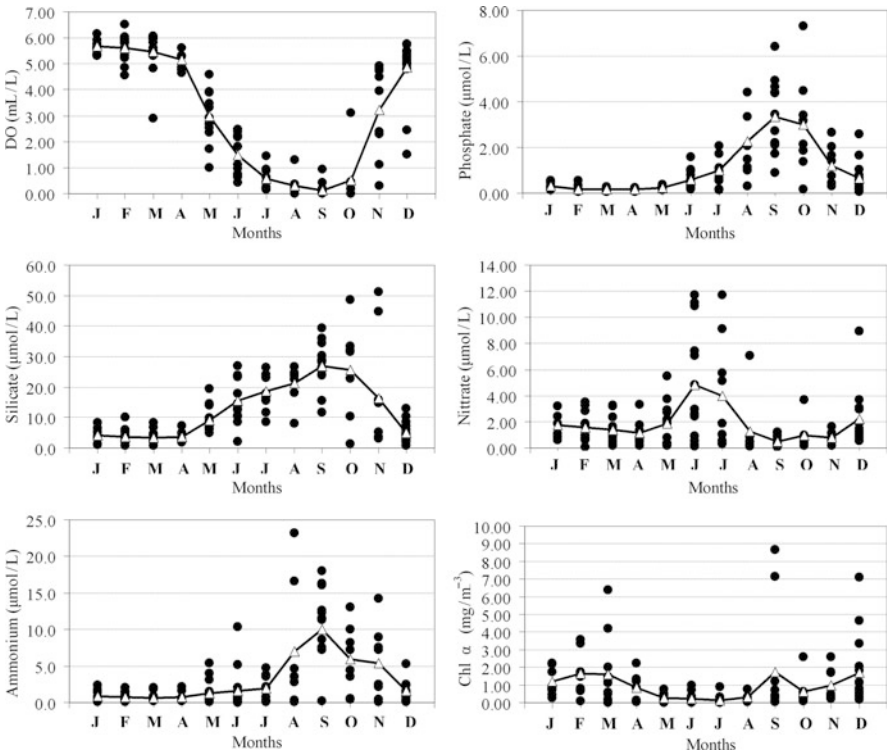

Fig. 9 Seasonal variations of DO phosphate, silicate nitrate, ammonium and chlorophyll in near bottom waters of the Elefsis Bay. *Triangles connected by lines* indicate the mean of each cruise period

Table 2 Mean annual maximum and minimum values in DO, nutrients their ratios and chlorophyll in the surface and bottom waters of Elefsis Bay during 1987–2009

		Max	Min[a]	Δyear[a]
DO (μM)	surf	276 ± 15.6	188 ± 25.0	89.3 ± 28.1
	bot	256 ± 17.4	4.46 ± 5.36	252 ± 21.9
Phosphate (mol/L)	surf	0.52 ± 0.42	0.1 ± 0.06	0.43 ± 0.45
	bot	3.16 ± 1.88	0.15 ± 0.08	3.01 ± 1.67
Silicate (mol/L)	surf	5.5 ± 2.68	1 ± 0.63	4.3 ± 2.64
	bot	27.27 ± 12.25	2.12 ± 0.99	25.15 ± 10.1
Nitrite (mol/L)	surf	0.41 ± 0.32	0.05 ± 0.03	0.37 ± 0.33
	bot	0.79 ± 0.61	0.08 ± 0.03	0.72 ± 0.64
Nitrate (mol/L)	surf	2.42 ± 1.86	0.29 ± 0.15	2.1 ± 2
	bot	4.34 ± 3.81	0.32 ± 0.25	4.02 ± 3.93
Ammonium (mol/L)	surf	1.49 ± 1.03	0.22 ± 0.22	1.32 ± 0.98
	bot	9.64 ± 6.38	0.33 ± 0.26	9.31 ± 5.73
DIN (mol/L)	surf	3.97 ± 2.18	0.73 ± 0.45	3.26 ± 2.31
	bot	10.70 ± 5.64	1.09 ± 0.45	9.62 ± 4.97
Si:DIN	surf	24.53 ± 19.07	6.26 ± 7.95	18.45 ± 19.63
	bot	9.59 ± 7.9	0.96 ± 0.5	8.83 ± 8.23
DIN:PO_4	surf	6.47 ± 5.4	0.8 ± 0.33	5.72 ± 5.82
	bot	24.89 ± 16.83	2.01 ± 1.3	23 ± 18.23
Si:NO_3	surf	24.42 ± 37.49	2.14 ± 1.65	22.72 ± 41.35
	bot	118.28 ± 126.18	2.29 ± 1.45	121.89 ± 129.76
Si:PO_4	surf	44.63 ± 41.52	6.35 ± 7.97	38.62 ± 41.65
	bot	54.42 ± 39.59	6.56 ± 4.08	46.97 ± 41.87
Chlorophyll (mg/m^3)	surf	5.27 ± 2.83	0.34 ± 0.18	4.93 ± 2.80
	bot	4.67 ± 0.34	0.08 ± 0.02	4.59 ± 3.36
Zooplankton Biomass[b]	Water column	60.7 ± 6.3	6.3 ± 1.2	50.8 ± 6.01

The magnitudes of seasonal difference (Δyear) are also shown
[a]Calculated except for 1990, 1995, 1997, 2004, 2005, 2009
[b]Calculated except for 1995, 1996, 2005

Phosphate, silicate, DIN and ammonium concentrations at the near-bottom waters were usually maximal in September, but elevated concentrations were found during July to November (Fig. 9). Mean (± 1SE) annual maxima in phosphate, silicate, DIN and ammonium were 3.16 ± 1.88, 27.27 ± 12.25, 10.70 ± 5.64 and 9.64 ± 6.38 mol/L, respectively (Table 2) and the ratio of Si:DIN was 7.2. In late November, the aforementioned nutrients start to decrease simultaneously and minimum values are observed from February to April. The minimum was observed in April. Mean ±1 SE of the annual minimum concentrations of phosphate, silicate, DIN and ammonium were 0.15 ± 0.08, 2.12 ± 0.99, 1.09 ± 0.45 and 0.33 ± 0.26 mol/L, respectively. The decreased concentrations of silicate in April reflected the development of the spring diatom bloom.

The ratio of Si:DIN in April was 4.7. Nitrate was maximal in June. Mean (± 1SE) annual maxima in nitrate concentration was 4.34 ± 3.81 mol/L. Nitrite was maximal in July (mean 0.79 ± 0.61 mol/L). Nitrate concentrations decreased after July, showing a minimum in September (Fig. 9) (mean 0.32 ± 0.25 mol/L). Relatively low concentrations were observed in April. Nitrite concentrations were

minimum during March–April and September. The annual minimum concentrations of nitrate and nitrite from February to April can be related to the biological activity and the elevated chlorophyll values observed January–March (Fig. 9) and the consumption by phytoplankton where nitrate is used for biomass formation, whereas, the minimum in September is mostly related to the denitrification process occurring in anoxic conditions and to the uptake by phytoplankton during the late summer peak. The magnitudes of seasonal variation in nutrients and chlorophyll at the near-bottom waters are shown in Table 2.

It is noteworthy that the mean ratio Si:NO_3 in September was calculated as 129 and decreased dramatically in winter – February (3.8) and spring – April (6.3), whereas, the mean Si:DIN ratio also decreased from 5.2 in September to 1.9 in February and 2.6 in April. The DIN:P mean ratio was calculated around four in September and increased to 18.8 in February and 12.7 in April. The Si:P mean ratio also showed a significant variation with high values in February and also in April (29 and 21.8, respectively) and low mean values (3.93) in September. Thus, according to the calculated nutrient ratios in September, the limiting factor for phytoplankton in the near-bottom waters of Elefsis Bay was nitrogen (in 93% of the data), whereas in spring (April), the limiting factor was either nitrogen (50% of data) or phosphorus (25% of data). Si limitation was not prominent. In February, P limitation was recorded in 46% of the measurements and N-limitation in 31%. In general, in the bottom layer of Elefsis Bay, nitrogen is the limiting factor, whereas, silicate seems to be always in excess. However, the predominant species in the phytoplankton community of Elefsis Bay, especially during spring, are diatoms (Pagou and Assimakopoulou, unpublished data).

The annual minimum and maximum of DO and nutrients in the surface layer (the first 10 m) of Elefsis Bay are shown in Table 2. The maximum nutrient concentrations were significantly lower in the surface layer compared to the concentrations in the near-bottom water layer.

The calculation of the ratios DIN:P, Si:P and Si:DIN in the entire water column of Elefsis Bay ($n = 532$) during the period 1987–2009 (both warm and cold periods included) indicated stoichiometric P-limitation by about 11%. Furthermore, the data indicated significant probable N-limitation (45%), whereas Si-limitation was calculated as 15% (Fig. 10).

In the warm, well-stratified period, in particular, data ($n = 187$) showed P-limitation 10%, N-limitation 61% and Si-limitation 9%. In the cold period, a significant shift from N-limitation to Si-limitation was observed. Data ($n = 181$) indicated P-limitation by 10%, N-limitation 30% and Si-limitation 24% (Fig. 10). The nutrient ratios are shown in Table 2. A shift in nutrient limitation from the surface layer to the near-bottom waters is clearly observed during the stratified period (Table 2). The mean ($\pm$ 1SE) annual maxima in the Si:NO_3 ratio increases dramatically from 24.42 at the surface waters to 118 at the bottom, whereas, the Si:DIN ratio decreases from 24.53 at the surface to 9.59 at the bottom, indicating the significant increase of the other forms of inorganic nitrogen and the decrease of NO_3^-.

It is obvious that nutrient ratios in the Elefsis ecosystem are highly variable.

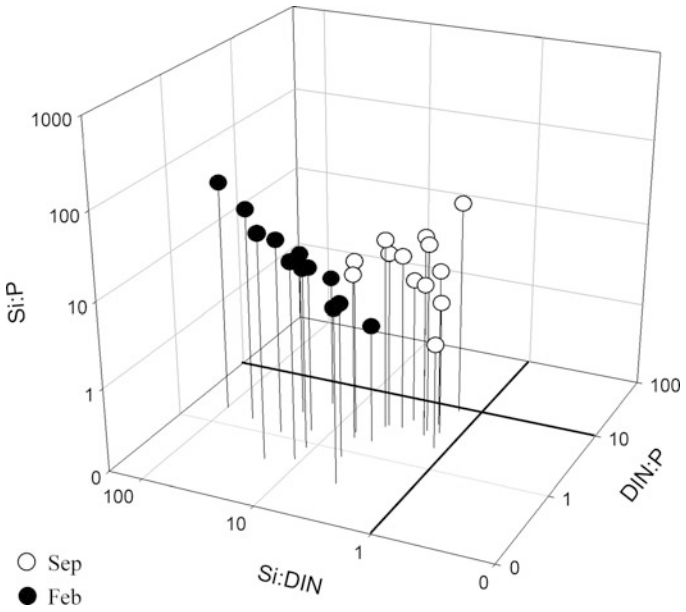

Fig. 10 Atomic ratios of dissolved inorganic nitrogen (DIN), phosphorous (P) and silica (Si) in the water column of Elefsis bay in cold (Feb) and warm (Sep) months for 1987–2009

Organic Carbon, Nitrogen and Phosphorus

Depth profiles of organic carbon, nitrogen and phosphorus in 2007 (monthly data from January to December) are presented in Fig. 11. It must be mentioned that during the first week of November 2007, the water column had all the characteristics of the warm/stratified period, so it is considered as warm/stratified period. Indeed, it has been reported [88] that the summer of 2007 was abnormally warm in many areas of southeastern Europe and the Balkan peninsula, as well as in Athens, and probably, this abnormal situation influenced the water column characteristics in early November. It is also noteworthy that during 2007, DO was not totally depleted. In September 2007, DO concentration was measured 5.36 μM, probably indicating the existence of a suboxic but not anoxic zone in the bay, which makes the system more complicated. The existence of the suboxic zone in Elefsis Bay is under investigation in the future.

DON comprises the major portion of the dissolved nitrogen pool in the water column of Elefsis Bay, especially in the cold period. In the warm period, inorganic N was significantly increased, especially in the bottom waters, since ammonification processes occur in the almost anoxic waters (DO in the near bottom layer, 5.36, 20.5 and 12.9 μM in September, October and November, respectively).

As already stated, the area receives a great amount of organic pollutants due to specific anthropogenic activities taking place there. This fact, in addition to the increased primary productivity of the area, leads to elevated amounts of organic

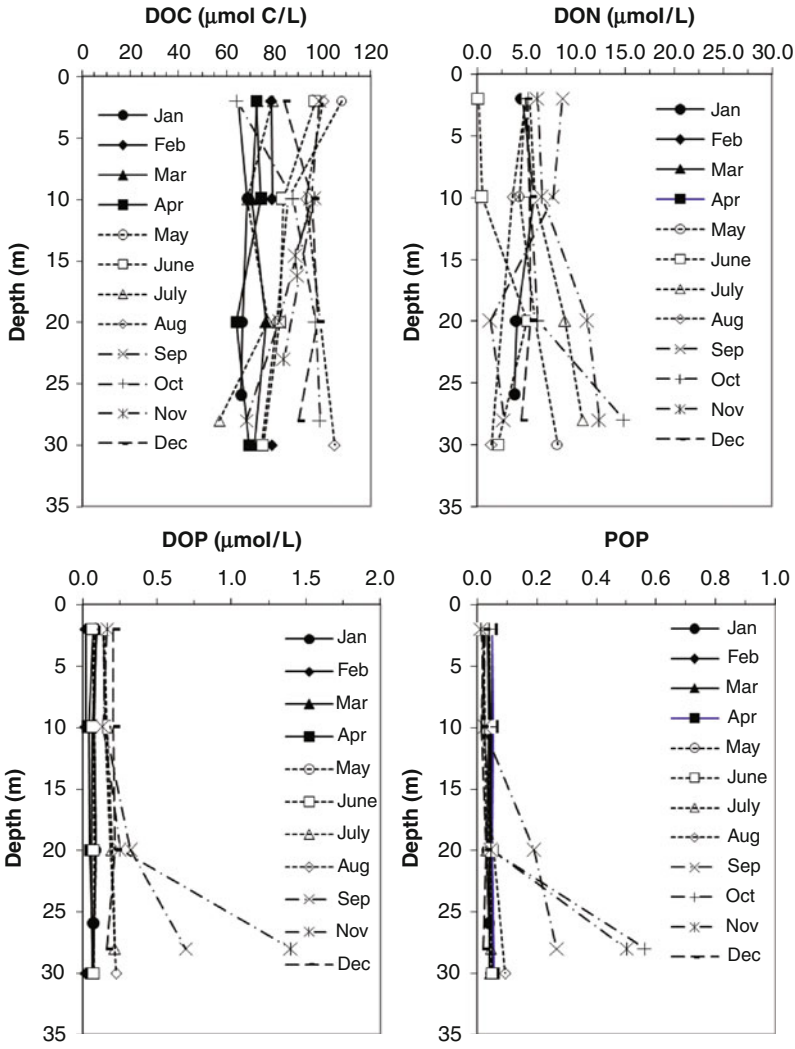

Fig. 11 Vertical distribution of organic nutrients and organic carbon in Elefsis Bay during 2007

carbon (TOC) measured in the water column (77–140 mol/L) throughout the year (Fig. 11). The intermittently anoxic conditions of the deep water layer do not seem to affect TOC distribution, either because the anoxic period is short for organic matter to decompose or the organic matter in Elefsis Bay has a strong refractory character. The latter is sustained by increased oil pollution recorded in the area. Indeed, high concentrations of aliphatic and polycyclic aromatic hydrocarbons have been detected in the surface sediments of Elefsis Bay, which are similar to those reported in other industrialized – polluted coastal areas around the world [89–91].

Thus, Elefsis Bay can be characterized as a highly contaminated area in respect to oil pollution [92, 93].

Given this fact, it should be expected that organic matter is enriched in carbon relatively to nitrogen and phosphorus. Throughout 2007, molar ratios of bulk DOC to DON concentrations (DOC:DON) ranged from 5 to 72. In the upper 10 m, DOC:DON values varied from ~12 to 26. These values are close to those reported by Ducklow et al. [94] for bulk DOM in the western Black Sea. According to these ratios, there is no apparent increased refractory character of DOM in the Elefsis Bay and the natural cycling of organic matter is indicated. In the near-bottom layer, the ratio ranges between 5 and 25 with two very high values (72 and 60) in August and September. After September, during the end of the anoxic period (October and November), the DOC:DON ratio is extremely low (~6). In contrast to what it is expected, it seems that during the anoxic period, the bottom waters are enriched in "fresh" organic matter. Since, normally under low or no oxygen conditions, organic nitrogen forms are converted to ammonia, our findings imply that in the Elefsis case, "new" organic matter enriched in nitrogen is released into the bottom waters upon oxygen removal. It is suspected that the dying zoobenthic communities during anoxic periods, which, in general, take place after August [75], are responsible for the observed distribution of organic matter. Moreover, the intermittent character of anoxia does not offer adequate time for organic matter to decompose.

DOP, not available directly to living organisms, is a significant fraction of total dissolved phosphorus (TDP) in the water column of Elefsis Bay surpassing, in some cases, the levels of DIP. During 2007, the DOC:DOP molar ratio in the water column of the bay ranged between 60 and 1,860. In general, the ratio was high, implying that organic matter in the bay during the cold period, as well as above the pycnocline during the warm period, is depleted in phosphorus relatively to carbon. Low ratios were calculated in the near-bottom waters when anoxic conditions occurred, suggesting an enrichment of phosphorus relatively to carbon in the DOM pool. The DON:DOP average was calculated ~44. In the cold period, there was no significant variation with depth and the DON:DOP ratio fluctuated between 46 and 52. During the warm/stratified period, the DON:DOP ratio decreases significantly in the near-bottom waters, from 67 in the surface layer, to 7. Unexpectedly, DOM in the anoxic-bottom waters appears enriched in phosphorus relatively to carbon and nitrogen. A possible reason for DOP accumulation in the anoxic layer of Elefsis Bay could be its release from the sediments and the suspended particulate matter. Benitez-Nelson et al. [95] have found preferential removal of phosphonate compounds in the anoxic Cariaco Basin during periods of low-particle-flux. Phosphonates are among the more recalcitrant of organophosphorus compounds (extremely resistant to chemical hydrolysis, thermal decomposition and photolysis), are prevalent in marine sediments (>25% of the total organic P), compared to their abundance in living organisms (<1%) and in sinking particulate matter (typically, less than 3%) [96]. Although they could be an important sink for P in the ocean, it is suggested that phosphonates may be an active source of DOP in the water column under anoxic conditions. The bulk POP is not preferentially

removed in the anoxic environment, since high POP concentrations in the deep anoxic layer of the Elefsis Bay are recorded (Fig. 11), and specific compounds thought to be relatively biologically unavailable (i.e., phosphonates), may be selectively regenerated [95].

Chlorophyll and Zooplankton in Elefsis Bay

Phytoplankton biomass, as indexed by chlorophyll concentrations, presented the typical annual cycle for temperate/subtropical coastal regions with two peaks: one in late winter (February) and the other in autumn, though the most important maximum was often recorded in autumn (Figs. 9, 12). However, on several occasions, an increase in chlorophyll concentrations was obvious in December. The annual

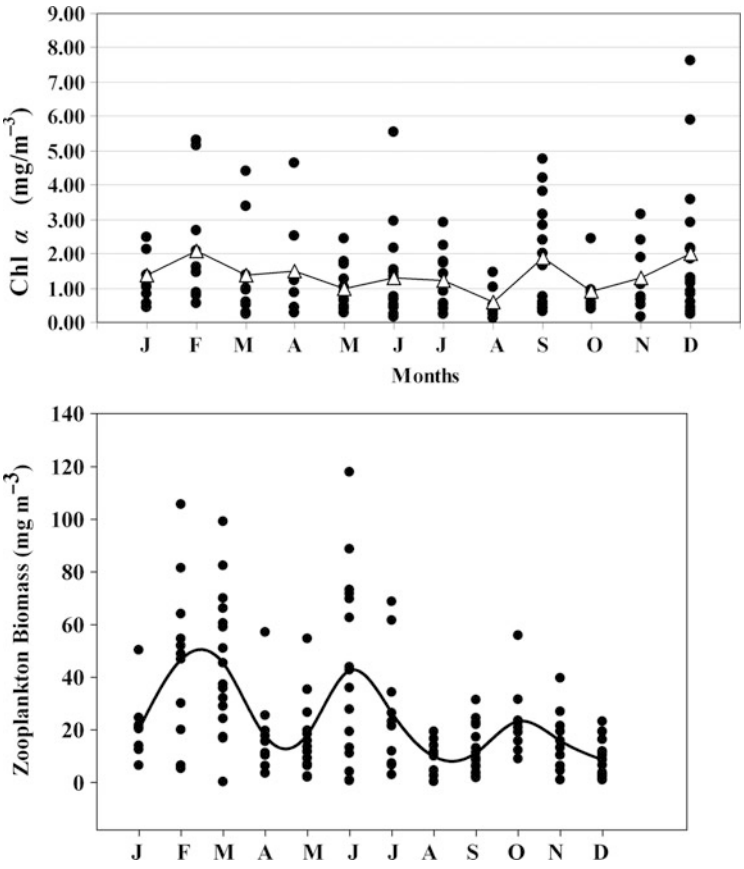

Fig. 12 Seasonal variations of chlorophyll (*upper*) and mesozooplankton (*low*) in Elefsis Bay. Chlorophyll as mean integrated values in the water column. Biomass in the water column (0–30). The *line* indicate the mean of each cruise period, i.e. January, February, ... December

maxima in chlorophyll concentration were 5.27 ± 2.83 mg/m^3 in the surface layer and 4.67 ± 0.34 mg/m^3 in the near-bottom layer. The minimum was observed in May or August (0.34 ± 0.18 mg/m^3 in the surface and 0.08 ± 0.02 in the near-bottom).

Mesozooplankton biomass varied within a very wide range of values (Fig. 12) with minimum annual mean values 6.3 ± 1.2 and max 60.7 ± 6.3 (Table 2). The abrupt outbursts of a few species result in extremely large numbers of zooplankters, followed by a strong decline. The mean annual cycle is characterized by three successively decreasing peaks, the first one during February–March, the second in June and the third in October. Interestingly, biomass values vary considerably during the former two maxima periods (Fig. 12), suggesting a great interannual variability of the annual cycle. The smaller variability of phytoplankton biomass (chlorophyll) assumes a rather strong grazing control of mesozooplankters upon autotrophs. The minimum annual mean values were observed during August–September, a period of mass development of the scyphomedusa *Aurelia aurita*, an important predator of mesozooplankton in the area [97].

The mesozooplankton community is characterized by a low number of species compared to the neighboring Saronikos Gulf. In parallel, one or two species reveal very high dominance. Species poorness and high dominance were attributed to the pollution impact and the morphological characteristics of the bay, being shallow and enclosed, [98]. Among the dominant species, we should refer to the copepod *Acartia clausi,* which attain very high numbers during February–March, contributing up to 98% to mesozooplankton in some years (e.g. 1993, 2004 etc). This species was found abundant in other seasons also, but with lower dominance. During February–March, it is accompanied by the cladocerans *Evadne nordmanii, Pleopis polyphemoides*. The latter also dominates in September and December. During late spring and summer, the community appears more diversified, characterized by the abundance of the cladocerans *Penilia avirostris, Pseudoevadne tergestina* and the copepods *Paracalanus parvus, Centropages ponticus, Oithona nana, Temora stylifera*. Meroplanktonic larvae can grow in large numbers in the area (e.g. gastropods larvae, bivalves larvae and crustaceans larvae) depending on the season. Apart from appendicularians, other zooplankton groups (e.g. chaetognaths, salps, doliolids, siphonophores and hydromedusae) are represented by a few individuals. Overall, the mesozooplankton community of Elefsis Bay is characterized by low diversity, high dominance of opportunistic species and very strong temporal variability, reflecting the disturbed environment, as already mentioned in previous studies in the area [98]. This community is significantly different from that occurring in the neighboring Saronikos Gulf [99].

Statistical Analysis

All data from twelve monthly samplings in 2007 were treated with PCA to assess the underlying patterns in the distribution of the measured parameters. According to the results (Table 3), the first two axes (principal components) explain 63% of the

Table 3 Results of principal components analysis, factor loadings for five principal components after rotation (VARIMAX rotation)

	Principal component				
Variable	1	2	3	4	5
DO	**–0.696**	–0.558	–0.341	0.178	–0.017
PO_4^{3-}	**0.936**	0.122	0.015	0.126	–0.139
SiO_4^{2-}	**0.733**	0.125	0.538	–0.295	0.208
NO_2^-	0.079	0.031	0.176	–0.072	**0.955**
NO_3^-	–0.169	0.163	–0.129	**–0.881**	0.155
NH_4^+	0.244	**0.854**	0.128	0.238	0.148
TOC	0.144	0.551	0.338	0.450	0.129
POC	0.084	0.015	**0.979**	0.031	0.099
TDP	**0.913**	0.108	0.062	0.249	0.254
DOP	0.562	0.052	0.10	0.316	**0.662**
DIN	0.176	**0.921**	0.079	–0.131	0.241
TON	0.472	–0.518	0.596	0.289	0.208
DON	0.491	**–0.636**	0.366	0.351	0.198
TDN	**0.602**	0.449	0.393	0.156	0.425
PON	0.118	0.173	**0.941**	–0.083	0.108
chlorophyll	–0.150	**–0.843**	0.048	0.251	0.255
zoo	–0.171	0.010	0.397	**–0.806**	–0.285
% Total Variation	43.4	19.3	13.5	9.1	6.9

For clarity, loadings with a magnitude >0.60 are shown in *boldface* type

total variance. Along the first axis are opposed DO with Phosphate, Silicate, TDP and Total Dissolved Nitrogen (TDN). Apparently, this axis is related to the anoxic conditions occurring in the bay. Chlorophyll and DON are opposed to DIN (ammonium) along the second axis, suggesting the consumption of DIN by phytoplakton. PCA was also performed on the time-series data for the period 1987–2004 of the parameters DO, phosphate, silicate, nitrate, nitrite, chlorophyll and zooplankton biomass. Phosphate and silicate are opposite to DO along the first axis, as it was also depicted for the 2007 data. Similarly, DIN is opposed to chlorophyll along the second axis.

The factor loadings in Table 3 are the correlation between the original variables and the principal components. The coefficients for the correlations given in Table 3, show that phosphorus gives the strongest correlations. Elefsis Bay is a complicated and fragile ecosystem in which the nutrient ratios show significant variability and hypothetically can be controlled by phosphorus inputs. This will be investigated in the future.

5 Interannual Variability

Historical data for the last 30 years are used to examine the interannual variability of DO, nutrients and plankton in the selected area of the Mediterranean Sea and to investigate if the variability in the hydrological pattern affects the occurrence of the anoxic events as well as the nutrients and plankton dynamics.

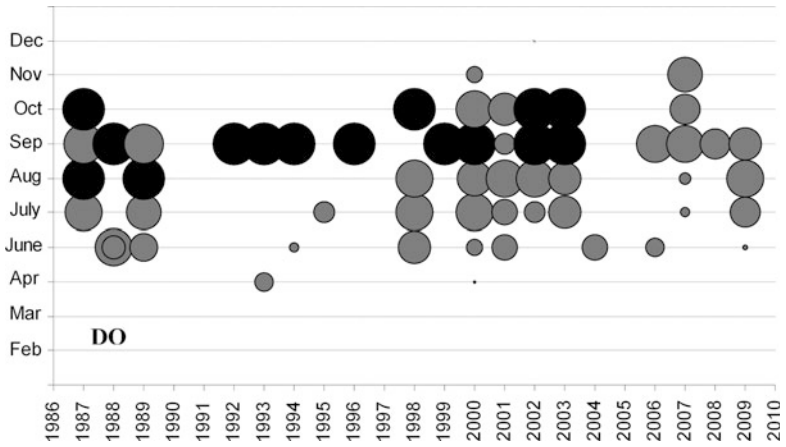

Fig. 13 DO concentrations correspond to waters with DO $<$ 89 μM. *Big circles* correspond to low concentrations and *small circles* to high concentrations (Range: 0.00–89 μM).The *blank circles* correspond to anoxic conditions (DO $=$ 0.00 μM)

Since the 1970s, numerous measurements of temperature, salinity, DO, nutrients, Chlorophyll and mesozooplankton biomass have been made, primarily to study the functioning of the ecosystem in phase with the stratification of the water masses and hypoxia/anoxia.

Temporal variations of DO and nutrient levels are analyzed for the waters with DO concentrations below 89 μM. We observed that in some cases, that is, in 1987, 2000–2004 and 2007, anoxic (black circles in Fig. 13) and hypoxic (gray circles) waters were also recorded in October and November. In 1992 and 2000, low DO concentrations were observed during May (Fig. 13).

After 2000 till today, relatively low phosphate concentrations were observed in the hypoxic and anoxic waters of Elefsis Bay. Additionally, low nitrate concentrations were recorded after 2001 till today, with the highest concentrations recorded in 2000 and 2001. It is noteworthy that higher silicate concentrations were recorded in hypoxic and anoxic waters in 1998, 2000 and 2007, whereas, in 2000 and 2007, significantly high silicate concentrations were recorded in November. Ammonium concentrations did not show any trend, whereas, the DIN:P ratio increased significantly after 2000, indicating phosphorus limitation for phytoplankton growth after 2000 (Fig. 14).

The Elefsis Bay time series for DO and nutrients were plotted as February–March (cold) and July–October (warm) medians. Also, during the warm period, time series in the surface layer and in waters with DO $<$ 89 μM (hypoxic, suboxic and anoxic waters) were plotted using single regression analysis and the significance of their trends are reported in Table 4.

In the warm period (July–October) of the years 1987–2008, the chemical parameters did not show any significant temporal trend, with the exception of phosphates that revealed a decreasing trend.

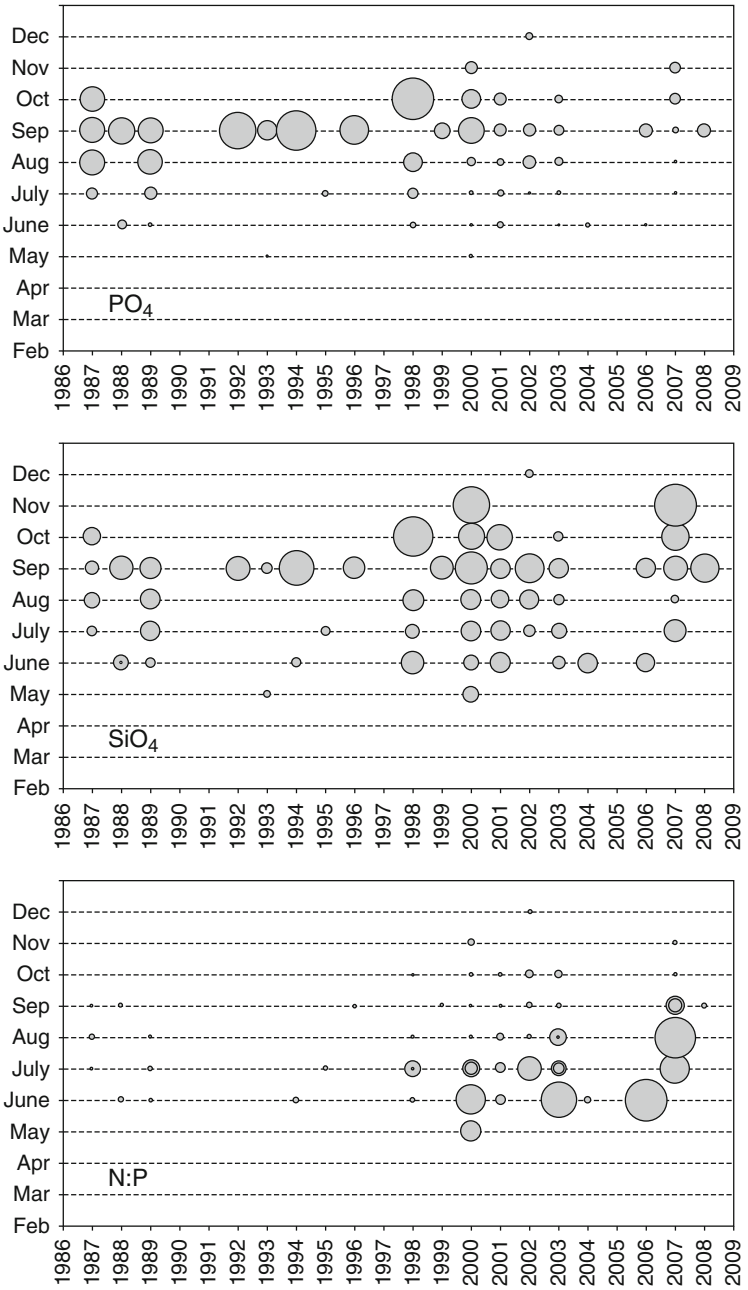

Fig. 14 Nutrient concentrations corresponding to waters with DO < 89 μM. *Small circles* correspond to low concentrations and *big circles* to high concentrations (Ranges: for phosphate 0.14–7.30 mol/L; silicate 1.12–51.3 mol/L and N:P 0.4–57)

Table 4 Trends of DO, nutrient and DIN:P ratio time-series and R^2 for Elefsis Bay water column, surface layer and below thermocline with DO $<$ 89 μM for the period 1987–2009

	Cold period (Feb–Mar) Water column	Warm period (July–Oct) Water column	Warm period Surface	Warm period Hypoxic/anoxic waters
DO	No trend	No trend	No trend	No trend
Phosphate	No trend	Decreasing $R^2 = 0.201$	Decreasing $R^2 = 0.224$	Decreasing $R^2 = 0.227$
Silicate	Increasing $R^2 = 0.249$	No trend	No trend	No trend
Nitrite	Increasing $R^2 = 0.163$	No trend	No trend	No trend
Nitrate	Increasing $R^2 = 0.491$	No trend	No trend	No trend
Ammonium	No trend	No trend	No trend	No trend
DIN	Increasing $R^2 = 0.176$	No trend	No trend	No trend
DIN:P	Increasing $R^2 = 0.272$	Increasing $R^2 = 0.223$	No trend	Increasing $R^2 = 0.183$

In the winter periods from 1987 to 2009, a significantly increased trend of silicate, nitrite, nitrate and DIN:P ratio was recorded in the water column. It is very interesting that the Elefsis ecosystem showed an increasing trend of the DIN:P ratio during both periods. This trend of shifting from N-limitation to P-limitation is due to the decrease of phosphate inputs in the system in the warm period and the increase of nitrate inputs during winter.

A decreasing trend of chlorophyll in both the surface and the near-bottom layer was recorded from 1998 and after (Fig. 15), coinciding with the decreasing variation of nutrients (mainly phosphate). It is noteworthy that the sharp decrease of the phytoplankton biomass during 2001–2002 coincides with the drastic decrease of nutrients after 2000–2001, as mentioned earlier, and the significant increase of the N:P ratio. This feature indicates a change of the system after 2000, which possibly reflects the decrease of the nutrient enrichment in the bay mainly due to the operation of the Sewage Treatment Plant in Psitallia started in late 1994.

On the contrary, regardless of the nonsignificant R^2 values in the trend for the zooplankton biomass (Fig. 16), the results from our data indicated that mesozooplankton biomass increased over the period 1996–2004. It is noteworthy that extreme values, above 90 mg m^{-3} and below 5 mg m^{-3}, were common before 1998, when the bay was influenced by the Athens sewage outfalls. Nevertheless, biomass showed an overall increase after 1998; this fact, in combination with the observed parallel decline of phytoplankton biomass, could suggest a stronger grazing control on the autotrophs after 1998 than before that year. Diversity index values are generally low (0.5–2 bits ind^{-1}), as it has been detected in 1984–1985 [98]; no clear seasonal pattern was depicted and a few high values (>3 bits ind^{-1}) were estimated in September 1989 and 2003 and in February 1999 (Fig. 17).

The community taxonomic composition and structure varied interannually as it is shown in the MDS plot (Fig.18). Samples collected during the same season of different years are not plotted closely (e.g. February 1987, 1995 and 1999 and March 1997), and are plotted far from February and March of the other years. Distances among samples are due to the low similarity level (only 38%) among

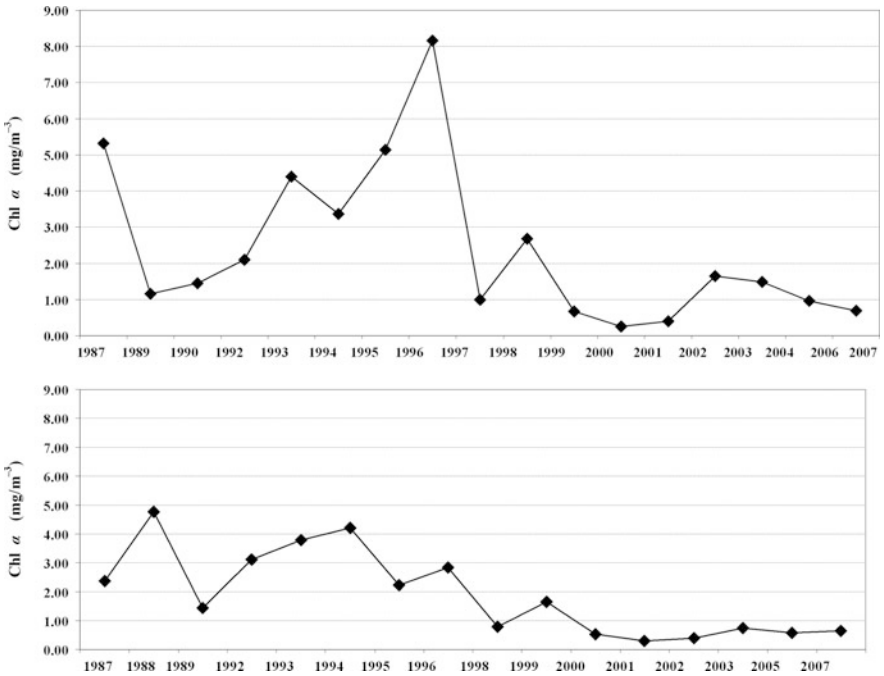

Fig. 15 Interannual variability of mean integrated over depth concentrations of chlorophyll during homogenized (*upper*) and stratified (*low*) period (1987–2007) (mg/m^3) in the Elefsis Bay. February and March are considered as homogenized period, whereas the period from July to October is considered as stratified

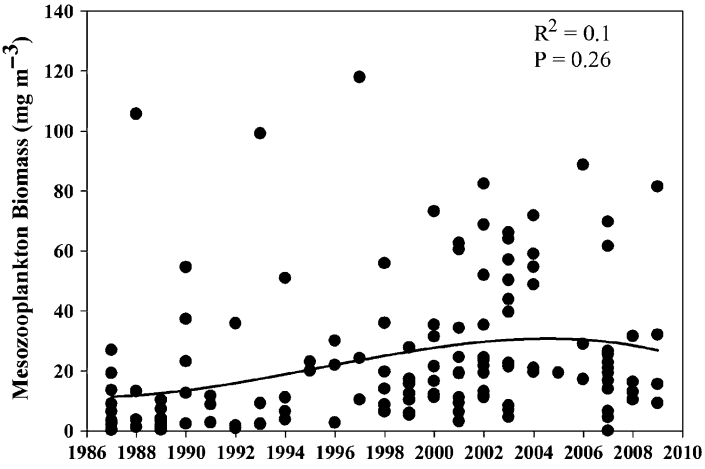

Fig. 16 Interannual variability of mesozooplankton biomass in Elefsis Bay during 1987–2009

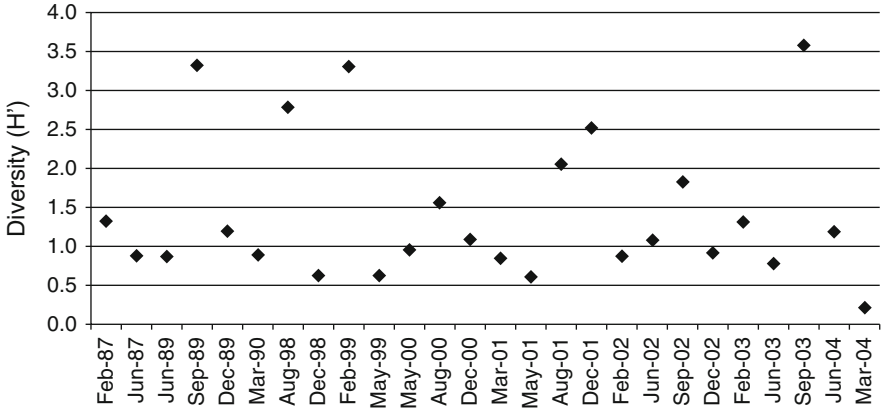

Fig. 17 Interannual variability of mesozooplankton diversity (bits ind^{-1}) in Elefsis Bay during 1987–2004

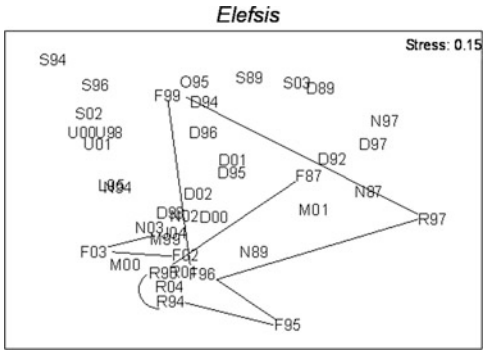

Fig. 18 MDS plot of mesozooplankton samples collected seasonally from 1987 till 2004 (*J* January; *F* February; *R* March; *M* May; *N* June; *L* July; *U* August; *S* September; *O* October; *D* December, 87-04: 1987–2004)

them in the matter of species composition and dominance. Indeed, the aforementioned samples are characterized by low abundance values of *A. clausi, P. polyphemoides* or *E. nordmanii*, whereas, in all other years, *A. clausi* was highly abundant and dominant. Similarly, differences among years existed for the samples collected during May–June, August–September and December. This interannual variability is related to the opportunistic character of the species that compose the mesozooplankton community of the bay; these species do not constitute clear seasonal assemblages as those recognized in the neighboring Saronikos Gulf [99]. In addition, the abundance of scyphomedusa *A. aurita*, major predator of mesozooplankton, revealed significant interrannual variability, probably related to the availability to the polyps of large surface substratum by the ships occasionally anchored in the bay. Overall, the mesozooplankton community in Elefsis Bay reflects the strong variability of the environment, both biotic and abiotic.

Figure 19 shows climatic time series for the period 1985–2009 of mean temperatures for air and sea-water in Elefsis Bay during winter and summer in parallel to NAO index. The winter temperatures are for the period February–March and the

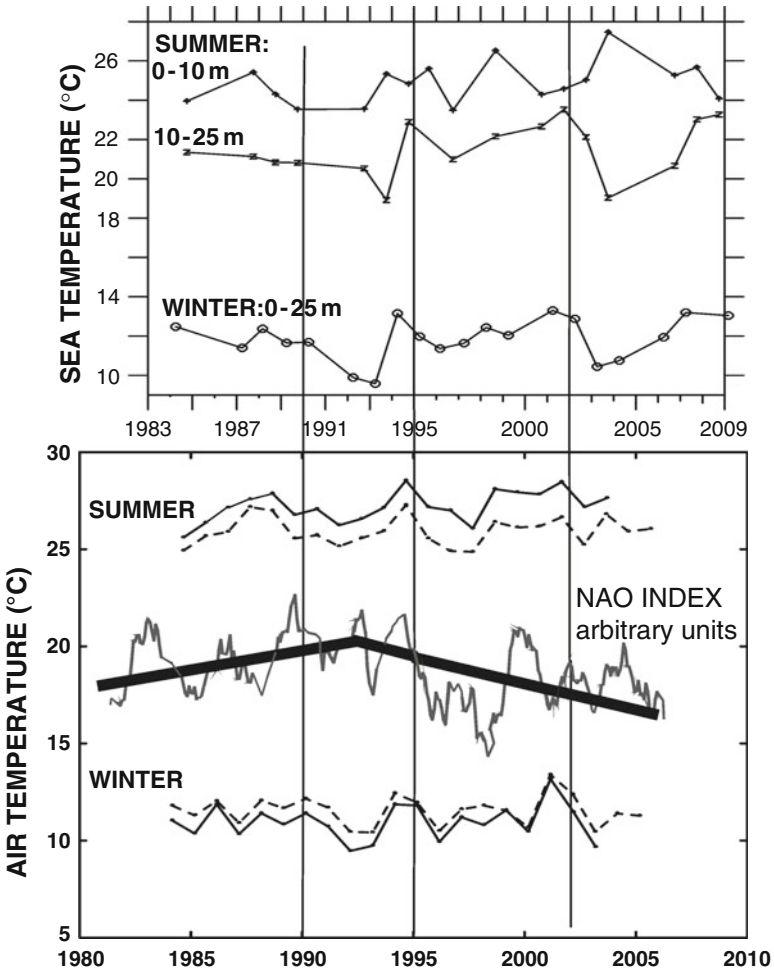

Fig. 19 *Upper panel*: Water temperatures in Elefsis Bay during winter and summer for the period 1984–2009. *Lower panel*: Air temperatures for Elefsis Bay during winter and summer for the period 1984–2006 in parallel to NAO index. *Solid* is data from a local meteorologic station and *dashed* is data from NCEP reanalysis (see text)

summer temperatures for July–September. The dashed lines in air-temperature are from reanalysis NCEP data [100], whereas, the solid are from a station of the Hellenic National Meteorologic Service ∼20 km away from Elefsis. The lowest air and water temperatures occurred in the mid 90s (1992–1993), during a period which is characterized as a regime shift between prior long-term cooling and afterwards warming trends in surface water in the Aegean examined for the period 1950–2000 [101]. The regime shift is also indicated in the trend changes that occurred in the North Atlantic Oscillation (NAO) index in the same period. Increasing/decreasing values NAO are associated with the predominance of

northerly/southerly winds, and consequently with cooling/warming trends, in atmospheric temperatures at a particular location for which the NAO index can be considered as an appropriate indicator of the general atmospheric conditions. Summer air temperatures are, in general, correlated with summer upper-layer sea temperatures, whereas, winter air temperatures are correlated with winter sea temperatures and summer deep-layer sea temperatures. Therefore, it is a remarkable fact that the summer temperatures in the deeper layer (10–25 m) are very closely correlated on climatic time-scales with the winter temperatures (0–25 m), indicating once again that the deep layer in summer is isolated and preserves the winter characteristics.

The temperature difference between the upper (0–10 m) layer and the deeper (10–25 m) layer during summer is an indirect indication of the strength of the summer pycnocline; salinity also plays a role, but in Elefsis, the pycnocline is basically due to the temperature differences as shown in Fig. 6. A remarkable signal of variability in the strength of the summer pycnocline appears in the upper panel of Fig. 19, during 2000 to 2009. A relatively weak pycnocline occurred in 2000 and 2001, whereas in 2003, there was a peak in the temperature difference between the upper and the lower layer, indicating a corresponding peak in pycnocline strength, and finally, in 2009, the pycnocline weakened again. This signal is qualitatively correlated with the evolution of interannual anoxic/suboxic conditions in Elefsis during the same period as shown in Fig. 13. In 2002 and 2003, strong anoxia appeared, whereas in 2008 and 2009, higher concentrations of DO occurred in the summer months.

It has been reported that the 1987s, 2000s, 2001s and 2007s had the warmest summers during the last two decades [88, 102]. According to the National Observatory of Athens (NOA), temperatures were abnormally high in July 2000 and August 2001. It is noteworthy that in July 2007, an abnormally high temperature of 46.2°C was recorded in Elefsis. In summer 2007, 26 days with temperatures greater than 37°C were recorded. Also, in 1987, July was exceptionally warm. This has possibly resulted in more persistent stratification in Elefsis Bay, probably affecting the N:P ratio, which controls the planktonic production.

Overall, our analysis showed that the first observations in temporal variations in nutrients in the bay primarily reflect the impact of decreasing pollution during the last decade rather than climate variability. The year-to-year variability of nutrients in Elefsis Bay, vary significantly depending on the point and diffused nutrient loading from the coastline and the anthropogenic activity. On the contrary, the variation in the intensity of the hypoxia/anoxia developed in the bay appears to be related to local climate variability.

6 Conclusion

The physiography of Elefsis Bay leads to a strong seasonal density stratification of the water mass and influences the oxygen distribution in the basin, resulting in hypoxia and anoxia, existing for about 5 months annually. This situation leads to

the retaining of nutrients and organic matter within the basin and also leads to high nutrient accumulation. Relatively low nitrite concentrations (0.03–0.122 μM) characterize the anoxic, ammonium-rich waters of the Bay. The nitrite concentrations were rather elevated in the suboxic zone (0.03–2.40 μM). However, mineralization processes (i.e. ammonification) are favored and supported by the high concentrations of organic matter. On the other hand, our data imply that "new" organic matter enriched in nitrogen is released into the bottom waters upon oxygen removal. We believe that the dying zoobenthic communities during anoxic periods contribute significantly to the observed distribution of organic matter. The mesozooplankton community of Elefsis Bay is characterized by low diversity, high dominance of opportunistic species and very strong temporal variability, reflecting the pollution of the bay.

Sediment records covering most of the Holocene gave evidence that the area was affected by hypoxia and/or anoxia in the past. The occurrence of hypoxia in Elefsis Bay on the "geological" timescale seems to be related to climate fluctuations. Warmer periods contributed to the stratification of the water column and to relatively higher productivity. These factors were the primary root of hypoxia in Elefsis Bay.

The interannual variability of the biochemical parameters showed a significantly increasing trend of the N:P ratio and decreasing trend for chlorophyll, which indicates a change in the ecosystem after 2000. This possibly reflects the decrease in the pollution levels in the bay mainly due to the operation of the Sewage Treatment Plant in Psitallia at the end of 1994.

The ecosystem of Elefsis Bay seems to be very complicated, variable and "fragile," due to its morphology (enclosed), bathymetry (shallow with two small basins) and intense anthropogenic activity (domestic, industrial and naval pollution). Its variability can be attributed to the differences in anoxia intense and the amount of the accumulated organic material. The weak water mass renewal, in combination with organic load and high biological production, result in the entrapment and recycling of a large amount of organic matter in the bay.

The first observations in temporal variations in nutrients in the bay primarily reflect the impact of decreasing pollution during the last decade rather than climate variability. On the contrary, the variation in the intense of the hypoxia/anoxia developed in the bay appears to be related to local climate variability.

References

1. Diaz RJ, Rosenberg R (1995) Marine benthic hypoxia: a review of its ecological effects and the behavioral responses of benthic macrofauna. Oceanogr Mar Biol 33:245–303, An Annual Review
2. Zillén L, Conley DJ, Andrén T, Andrén E, Björck S (2008) Past occurrences of hypoxia in the Baltic Sea and the role of climate variability, environmental change and human impact. Earth Sci Rev 91:77–92

3. Murray JW, Jannasch HW, Honjo S, Anderson RF, Reeburgh WS, To GZ, Friederich GE, Codispoti LA, Izdar E (1989) Unexpected changes in the oxic/anoxic interface in the Black Sea. Nature 338:411–413
4. Murray JW, Codispoti LA, Friederich GE (1995) Oxidation-reduction environments: the suboxic zone in the Black Sea. In: Huang CP, O'Melia CR, Morgan JJ (eds). Aquatic Chemistry: interfacial and interspecies processes. ACS Advances in Chemistry Series No. 224, pp 157–176
5. Konovalov SK, Murray JW (2001) Variations in the Chemistry of the Black Sea on a time scale of decades (1960–1995). J Mar Sys 31:217–243
6. Diaz RJ (2001) Overview of hypoxia around the world. J Environ Qual 30:275–281
7. Vahtera E, Conley DJ, Gustaffson B, Kuosa H, Pitkanen H, Savchuk O, Tamminen T, Wasmund N, Viitasalo M, Voss M, Wulff F (2007) Internal ecosystem feedbacks enhance nitrogen-fixing cyanobacteria blooms and complicate management in the Baltic Sea. Ambio 36:186–194
8. Friligos N (1989) Nutrient and oxygen conditions in the Elefsis Bay, an intermittently anoxic Mediterranean Basin. Toxicol Environ Chem 19:179–186
9. Yakushev EV, Besedin DE, Lukashe YuF, Chasovnikov VK (2001) On the rise of the upper boundary of the anoxic zone in the density field of the Black Sea in 1989–2000. Oceanology 41:654–659, English Translation
10. Degobbis D (1989) Increased eutrophication of the Northern Adriatic Sea – Second act. Mar Pollut Bull 20:452–457
11. Pavlidou A, Kontoyiannis H, Psyllidou-Giouranovits R (2004) Trophic conditions and stoichiometric nutrient balance in the Inner Saronikos Gulf (Central Aegean). Fres Environ Bull 13:1509–1514
12. Scoullos M, Pavlidou A (1997) Speciation studies of trace metals in the Gulf of Elefsis. Greece Croat Chem Acta 70:299–307
13. Scoullos MJ, Pavlidou AS (1997) Speciation of trace metals in Elefsis gulf, Greece. Croat Chem Acta 70:289–307
14. Scoullos M, Pavlidou A (2003) Determination of the lability characteristics of lead, cadmium and zinc in a polluted mediterranean brackish-marine interface system. Water Air Soil Pollut 147:203–227
15. Friligos N (1986) Nutrient cycling and stoichiometric model in Epidavros, a deep basin in the Aegean Sea. Mar Ecol 7:43–57
16. Hopkins TS, Coachmann LK, Edwards RF (1974) Seasonal changes in Elefsis Bay. XXIV Congres-Assemblee Pleniere du Monaco (CIESM), Greece
17. Pantazidou S, Kapniaris A, Katsiri A, Christidis A (2007) Pollutant trends and hazard ranking in Elefsis Bay. Desalination 210:69–82
18. Friligos N (1976) Seasonal variations of nutrients around the sewage outfall in the Saronikos Gulf (1973). Thalassia Yugosl 12:441–453
19. Yannopoulos C (1976) The annual regeneration of the Elefsis Bay zooplankton ecosystem, Saronikos Gulf. Rapp Comm Int Mer Medit 5:109–111
20. Friligos N (1979) Influence of industries and sewage on the pollution of Elefsis Bay (January 21st, 1974). Rer Int d'Ocean Med 55:3–11
21. Friligos N (1981) Enrichment by inorganic nutrients and oxygen utilization rates in Elefsis Bay. Mar Pollut Bull 12:431–436
22. Friligos N (1982) Some consequences of the decomposition of organic matter in the Eiefsis Bay, an anoxic basin. Mar Pollut Bull 13:103–106
23. Friligos N (1983) Preliminary observations on nutrient cycling and a stoichiometric model for Elefsis Bay, Greece. Mar Environ Res 8:197–213
24. Scoulos MJ (1979) Chemical studies of the gulf of Elefsis, Greece. PhD Thesis University of Liverpool
25. Lambeck K (1996) Sea-level changes and shoreline evolution in Aegean Greece since upper Paleolithic time. Antiquity 70:588–611

26. Lambeck K, Bard E (2000) Sea-level change along the Mediterranean coasts since the time of the Last Glacial Maximum. Earth Planet Sci Lett 175:202–222
27. Van Andel TH (1989) Late Quarternary sea-level changes and archaeology. Antiquity 63:733–745
28. Hatzianestis I, Rori N, Sklivagou E, Rigas F (2004) PAH profiles in dated sediment cores from Elefsis bay, Greece. Fres Environ Bull 13:1253–1257
29. Strickland JDH, Parsons TR (1968) A practical handbook of sea water analysis. Bull Fish Res Bd Canada 167:310
30. Carpenter JH (1965) The accuracy of the Winkler method for the dissolved oxygen analysis. Limnol Oceanogr 10:135–140
31. Carpenter JH (1965) The Chesapeake Bay Institute technique for dissolved oxygen method. Limnol Oceanogr 10:141–143
32. Mullin JB, Riley JP (1955) The colorimetric determination of silicate with special reference to sea and natural waters. Anal Chim Acta 12:162–176
33. Murphy J, Riley JP (1962) A modified single solution method for phosphate in natural waters. Anal Chim Acta 12:162–176
34. Koroleff F (1970) Revised version of "direct determination of ammonia in natural waters as indophenol blue" Int Con Explor Sea C M 1969/ C:9 ICES information on techniques and methods for sea water analysis. Interlab Rep 3:19–22
35. Pujo-Pay M, Raimbault P (1994) Improvement of the wet-oxidation procedure for simultaneous determination of particulate organic nitrogen and phosphorus collected on filters. Mar Ecol Prog Ser 105:203–207
36. Raimbault P, Diaz F, Pouvesle W, Boudjellal B (1999) Simultaneous determination of particulate organic carbon, nitrogen and phosphorus collected on filters, using a semi-automatic wet-oxidation method. Mar Ecol Progr 180:289–295
37. Raimbault P, Pouvesle W, Diaz F, Garcia N, Sempere R (1999) Wet oxidation and automated colorimetry for simultaneous determination of organic carbon, nitrogen and phosphorus dissolved in seawater. Mar Chem 66:161–169
38. Cauwet G (1994) HTCO method for dissolved organic carbon analysis in seawater: influence of catalyst on blank estimation. Mar Chem 47:55–64
39. Verardo DJ, Froelich PN, McIntyre A (1990) Determination of organic carbon and nitrogen in marine sediments using the Carlo Erba NA-1500 Analyzer. Deep Sea Res 37:157–165
40. Gaudette H, Flight W, Tones L, Folger D (1974) An inexpensive titration method for thedetermination of organic carbon in recent sediments. J Sediment Petrol 44:249–253
41. Holm-Hansen O, Lorenzen CJ, Hormes RN, Strickland JDH (1965) Fluorometric determination of chlorophyll. J Consperm Int Explor Mer 30:3–15
42. Omori M, Ikeda T (1984) Methods in marine zooplankton ecology. Wiley, New York
43. Catsiki VA, Panayotidis P (1993) Copper, Chromium and Nickel in tissues of the Mediterranean Seagrasses Posidonia Oceanica & CymodoceA Nodosa (Potamogetonaceae) from greek coastal areas. Chemosphere 26:963–978
44. Frilligos N, Psyllidou-Giouranovits R, Pavlidou A (1998) Semi-anoxic conditions in the Elefsis Bay, A Greek Marine Bay in the Aegean Sea: recent results, vol 11. UNESCO Headquarters, Paris, France, p 36
45. Friligos N, Psyllidou R, Pavlidou A (2004) Long term changes of nutrients enrichment in a greek anoxic marine bay. Rapport du 37^{e} Congress de la CIEMS proceedings, vol 37, p 197
46. Izzo J, Pagou K (1999) Environmental status and threats – Eutrophication. In: Papathanassiou E, Izzo J, Kunitzer A (eds). State and pressures of the marine and coastal Mediterranean environment. European Environment Agency Environmental assessment series No 5:76–82
47. Moncheva S, Gotsis-Skretas O, Pagou K, Krastev A (2001) Phytoplankton blooms in Black Sea and Mediterranean coastal ecosystems: similarities and differences. Estuar Coast Shelf Sci 53:281–295
48. Pagou K (1990) Eutrophication problems in Greece. Water Poll Res Rep 16:97–114

49. Pagou K, Siokou-Frangou I, Christianidis S, Friligos N, Psyllidou-Giouranovits R (1996) Pollution effects on plankton composition and spatial distribution near the sewage outfall of Athens. MAP Tech Rep Ser 96:1–100
50. Pavlidou A, Psillidou-Giouranovits R (2004) Chemical parameters. In: Siokou-Fragou I (ed). Monitoring of the Saronikos Gulf ecosystem affected by the Psittalia sea outfalls Final Report, NCMR, Athens
51. Pavlidou A, Psyllidou-Giouranovits R, Sylaios GK (2005) Nutrients and dissolved oxygen in Hellenic coastal waters. In: Papathanasiou E, Zenetos A (eds) State of the Hellenic Marine Environment, 1st edn. Hellenic Center for Marine Research, Athens Greece
52. Psyllidou-Giouranovits R, Satsmadjis J, Pagou K (1990) Factors affecting nutrients and chlorophyll-a in a hypertrophied Greek gulf. Revue Internationale d' Oceanographie Medicale, Tomes LXXXXVII-LXXXXVIII, pp 72–89
53. Psylidou-Giouranovits R, Pavlidou A, Georgakopoulou-Grigoriadou E (1997) Recent measurements of nutrients and dissolved oxygen in the Saronikos Gulf and the Elefsis Bay. Proceedings of the Hellenic Symposium of Oceanography and Fisheries, p 467–469
54. Simpoura N, Zenetos A, Panayiotidis P, Makra A (1995) Changes in benthic community structure along an environmental pollution gradient. Mar Pollut Bull 30:470–474
55. Siokou-Frangou I (1993) Ecology of mesozooplankton in Saronikos Gulf. PhD thesis, University of Athens, p 372
56. Siokou-Frangou I, Pagou K, Gialamas V (1990) Discrimination du plancton influence par la pollution au moyen des analyses multivariees. Rapp Comm Int Mer Medit 32:213
57. Siokou-Frangou I, Assimakopoulou G, Georgakopoulou-Grigoriadou E, Zenetos A, Zeri C, Zervoudaki S, Karageorgis A, Kontoyannis H, Krasakopoulou E, Pagou K, Panagiotidis P, Panagouli S, Pancucci-Papadopoulou MA, Papadopoulos V, Pavlidou A, Sklivagou E, Symboura N, Chatjianestis I, Psyllidou-Giouranovits R (2000) Changes of the Saronikos Gulf ecosystem after the functioning of the Psittalia Treatment Centre. Proceedings of the 6th Panhellenic Symposium in Oceanography and Fisheries, Chios, 23–26 May 2000, Tome I, pp 2–6
58. Voutsinou-Taliadouri F (1981) Metal pollution in the Saronikos Gulf. Mar Pollut Bull 12:163–168
59. Dugdale RC, Hopkins TS (1978) Predicting the structure and dynamics of a pollution-driven marine ecosystem embedded in an oligotrophic sea. Thalassia Jugosl 14:107–126
60. Dugdale RC, Kelley JC, Becacos-Kontos Th (1972) Effects of effluents discharge on concentration of nutrients in the Saronikos Gulf. In: Ruivo M (ed) Marine pollution and sea life. FAO, Rome
61. Hopkins TS, Coachman LK, Edwards RF (1976) Seasonal change in Elefsis Bay, Greece. Rapp Comm Int Mer Medit 23:77–80
62. Ignatiades L, Becacos-Kontos Th (1970) Ecology of fouling organisms in a polluted area. Nature 225:293–294
63. Ignatiades L, Mimicos N (1976) A survey of petroleum hydrocarbons in Elefsis Bay, Aegean Sea, and their effects on phytoplankton growth. III^{es} Journees Etud Pollutions, Split., CIESM p. 139–142
64. Ignatiades L, Mimicos N (1977) Ecological responces of phytoplankton on chronic oil pollution. Environ Pollut 13:109–118
65. Ignatiades L, Pagou K, Gialamas V (1992) Multivariate analysis of phytoplanktonic parameters: a sample study. J Exp Mar Biol Ecol 160:103–114
66. Pagou K (1994) Ecological parameters of phytoplankton related to eutrophication of the marine environment. PhD thesis, University of Aegean, p 356
67. Vassiliou A, Ignatiades L, Karydis M (1989) Clustering of transect phytoplankton collections with a quick randomization algorithm. J Exp Mar Biol Ecol 130:135–145
68. Pavlidou A (1998) Study of metal speciation in microenvironments of Elefsis Bay using Anodic Stripping Voltammetry. PhD Thesis University of Athens

69. Scoullos M (1983) Trace metals in a landlocked intermittently anoxic basin. In: Wong C, Boyle E, Bruland K, Burton J, Goldberg E (eds) Trace metals in seawater. Plenum, New York
70. Scoullos M (1986) Lead in the coastal sediments. The case of the Elefsis Gulf, Greece. Sci Total Environ 49:199–219
71. Scoullos M, Riley JP (1978) Water circulation in the Gulf of Elefsis Greece. Thalass Jugosl 14:357–370
72. Scoullos M, Plavšić M, Karavoltsos S (2004) Speciation studies of copper in the Gulf of Elefsis: the role of the macroalgae Ulva rigida. Mar Chem 86:51–63
73. Kontoyiannis H (2004) Water masses circulation – sewage plume dispersion. In: Siokou-Fragou I (ed) Monitoring of the Saronikos Gulf ecosystem affected by the Psittalia sea outfalls Final Report. Athens, NCMR
74. Frilligos N, Zenetos A (1988) Elefsis Bay anoxia: nutrient conditions and benthic community structure. PSZNI Mar Ecol 9:273–290
75. Zarkanellas AJ (1979) The effects of pollution induced oxygen deficiency on the benthos in Elefsis Bay, Greece. Mar Environ Res 2:191–207
76. Zenetos A, Bogdanos C (1987) Benthic community structure as a tool in evaluating effects of pollution in Elefsis Bay. Thalassografica 10:7–21
77. Pavlidou A, Psillidou-Giouranovits R (2001) Nutrients. In: Siokou-Frangou I (ed). Monitoring of the Saronikos Gulf ecosystem affected by the Psittalia sea outfalls, Final Report NCMR, Athens
78. Pavlidou A, Psillidou-Giouranovits R (2002) Nutrients. In: Siokou-Frangou I (ed). Monitoring of the Saronikos Gulf ecosystem affected by the Psittalia sea outfalls, Final Report, NCMR, Athens
79. Bolan NS, Barrow NJ, Posner AM (1985) Describing the effect of time on sorption of phosphate by iron and aluminum hydroxyoxides. J Soil Sci 36:187–197
80. Ruttenberg KC (2002) The global phosphorus cycle. In: Change Goudie AS, Cuff DJ (eds) The encyclopedia of global. Oxford University Press, London
81. Bange HW, Naqvi SWA, Codispoti LA (2005) The Nitrogen cycle in the Arabia Sea. Progr Oceanogr 65:145–158
82. McCarthy JJ, Yilmaz A, Yildiz YC, Nevins J (2007) Nitrogen cycling in the offshore waters of the Black Sea. Estuar Coast Shelf Sci 74:493–514
83. Spencer CP (1975) The mictronutrient elements. In: Riley JP, Skirrow G (eds) Chemical oceanography, 2nd edn, Vol 2. Academic Press, London
84. Yakushev E, Neretin LN (1997) One dimensional modeling of nitrogen and sulfur cycles in the aphotic zones of the Black and Arabian Seas. Global Biogeochem Cy 11:401–414
85. Millero FJ, Sohn ML (1992) Processes in the Ocean. In: Millero FJ, Sohn ML (eds) Chemical oceanography. CRC Press, Boca Raton
86. Giannopoulos K (2005) Metals in the water column and sediments in Saronikos Gulf during 2004 Msc Thesis, Department of Chemistry, University of Athens
87. Bartlett R, Mortimer RJG, Morris K (2008) Anoxic nitrification: evidence from Humber Estuary sediments (UK). Chem Geol 250:29–39
88. Founda D, Giannakopoulos C (2009) The exceptionally hot summer of 2007 in Athens, Greece – A typical summer in the future climate? Glob Planet Change 67:227–236
89. Bouloubassi I, Saliot A (1993) Investigation of anthropogenic and natural organic inputs in estuarine sediments using hydrocarbon markers (NAH, LAB, PAH). Ocean Acta 16:145–161
90. Grimalt JO, Bayona JM, Albaiges J (1984) Chemical markers for the characterization of pollutant inputs in the coastal zones. VIIes Journées Etudes sur la Pollution. C.I.E.S.M, Monaco
91. Tolosa I, Bayona JM, Albaiges J (1996) Aliphatic and polycyclic aromatic hydrocarbons and sulfur/oxygen derivatives in Northwestern Mediterranean sediments: spatial and temporal variability, fluxes and budgets. Environ Sci Technol 30:2495–2503

92. Sklivagou E, Varnavas SP, Hatzianestis J (2001) Aliphatic and polycyclic aromatic hydrocarbons in surface sediments from the Elefsis Bay, Greece (Eastern Mediterranean). Toxicol Environ Chem 79:195–210
93. Sklivagou E, Varnavas SP, Hatzianestis I, Kanias G (2008) Assessment of Aliphatic and Polycyclic Aromatic Hydrocarbons and Trace Elements in Coastal sediments of the Saronikos Gulf, Greece (Eastern Mediterranean). Mar Georesour Geotechnol 26: 372–393
94. Ducklow HW, Hansell DA, Morgan JA (2007) Dissolved organic carbon and nitrogen in the Western Black Sea. Mar Chem 105:140–150
95. Benitez-Nelson CR, O'Neill L, Kolowith LC, Pelechia P, Thunell R (2004) Phosphonates and particulate organic phosphorus cycling in an anoxic marine basin. Limnol Oceanogr 49:1593–1604
96. Paytan A, McLaughlin K (2007) The oceanic phosphorus cycle. Chem Rev 107:563–576
97. Panayotidis P, Papathanassiou E, Siokou-Frangou I, Anagnostaki K, Gotsis-Skretas O (1988) Relationship between the medusae *Aurelia aurita* Lam and zooplankton in Elefsis bay (Saronikos gulf, Greece). Thalassographica 11:7–17
98. Siokou-Frangou I, Verriopoulos G, Yannopoulos C, Moraitou-Apostolopoulou M (1995) Differentiation of zooplankton communities in two neighbouring shallow areas. Eleftheriou A et al. (eds). Proc28th EMB Symposium, p 87–97
99. Siokou-Frangou I, Papathanassiou E, Lepretre A, Frontier S (1998) Zooplankton assemblages and influence of environmental parameters upon them in a Mediterranean coastal area. J Plankton Res 20:847–870
100. Kalnay E, Kanamitsu M, Kistler R, Collins W, Deaven D, Gandin L, Iredell M, Saha S, White G, Woollen J, Zhu Y, Chelliah M, Ebisuzaki HW, Janowiak J, Mo KC, Ropelewski C, Wang J, Leetmaa A, Reynolds R, Jenne R, Joseph D (1996) The NCEP/NCAR 40-year reanalysis project. B Am Meteorol Soc 77:437–471
101. Kontoyiannis H, Tragou E, Zervakis V, Georgopoulos D, Theocharis A (2007) Climatic variability in the Aegean Black-Sea system and relation to meteorologic forcing (preliminary results). XXIV Assembly of International Union of Geology and Geophysics, International Association for the Physical Sciences of the Oceans, Perugia, Italy, July 2007
102. Founda D, Papadopoulos KH, Petrakis M, Giannakopoulos C, Good P (2004) Analysis of mean, maximum, and minimum temperature in Athens from 1897 to 2001 with emphasis on the last decade: trends, warm events, and cold events. Glob Planet Change 44:27–38

RedOx Layer Model: A Tool for Analysis of the Water Column Oxic/Anoxic Interface Processes

E.V. Yakushev

Abstract The goal of the elaboration of the RedOx Layer Model (ROLM) was to create an instrument for a complex analysis of the structures of the pelagic redox-interfaces in the seas with anoxic conditions. The processes of formation and decay of organic matter (OM), reduction and oxidation of species of nitrogen, sulfur, manganese and iron, and transformation of phosphorus forms were parameterized. This chapter is devoted to the detailed description of the assumptions and parameterizations of the processes considered. Examples of the ROLM application are given in other chapters of this volume.

Keywords Anoxic conditions, Biogeochemical modeling, Oxic/anoxic interface, Water column redox layer

Contents

Abbreviations

GOTM	General ocean turbulent model
OM	Organic matter
ROLM	RedOx Layer Model

E.V. Yakushev (✉)
Norwegian Institute for Water Research, Gaustadalleen 21, NO-0349 Oslo, Norway
e-mail: eya@niva.no

E.V. Yakushev (ed.), *Chemical Structure of Pelagic Redox Interfaces: Observation and Modeling*, Hdb Env Chem (2013) 22: 203–234, DOI 10.1007/698_2012_145,

1 Introduction

The goal of this chapter is to describe a model of the biogeochemical transformations of the chemical elements in the changeable redox conditions. On the one hand, this is a conceptual model that presents the theoretical mechanism controlling the redox transformations, and on the other hand it is a biogeochemical model construction block that can be coupled with the hydrodynamical models of the certain geographical objects.

In contrasted to modeling in the typical oceanic and marine waters oxic conditions, the modeling of the oxic/anoxic transformation can not only gives numerical estimates, but can also reveals the mechanisms of the main processes occurring there, because there is still not much known about it. From this point of view, the main goal of oxic/anoxic modeling is to compare the knowledge of events, processes, and systems with the observed situation. A model seems to be the single tool that will permit one to check the hypothesis of what processes are responsible for the origin and maintenance of the observed phenomena.

Redox interfaces of the different marine basins are characterized by a range of common features of the water column redox interfaces [1], i.e.:

- Nitrate maximum is observed at the depth where the vertical gradient of oxygen decreases (lower part of oxycline).
- The onset depths of increasing concentrations of ammonia and dissolved manganese correspond to the depth of the oxygen depletion and the position of the shallower phosphate minimum.
- Hydrogen sulfide appears deeper (about 10 m in the Black Sea), leaving this space for the suboxic zone.

This similarity of the chemical parameter distributions testifies to a similarity of the processes occurring. The parameterization of these processes becomes the aim of the model development.

When modeling nutrient cycling in oxic conditions, it is possible to use the stoichiometric law (Redfield ratios) and to describe the cycle of only one element. However, when modeling of oxic/anoxic transformation, it is necessary to parameterize the cycles of several elements simultaneously. The model should parameterize the mineralization of organic matter (OM) with oxygen, nitrate, redox metals, sulfate, and it should describe that dissolved oxygen can be consumed for the oxidation of the reduced compounds, etc. Another feature of the oxic/anoxic transformation modeling is a necessity of parameterizing the redox-dependent switches that should reflect an inhibition of the certain processes in accordance with the redox potential.

The goal of the elaboration of this model was to create an instrument for a complex analysis of the structures of the pelagic redox-interfaces in the seas with anoxic conditions. This model aims to simulate the vertical distributions of parameters, rates of processes controlling the formation of the observed distributions,

and analyze reaction of the studied system on the variability in external forcing factors.

The work on this model started with a coupled nitrogen and oxygen cycles model [2] that allowed to demonstrate that the anoxic conditions form as a result of OM oxidation in conditions of restricted aeration. The further modifications of this model included addition of the sulfur cycle [3], Mn cycle [4], the cycles of Fe, P, and biological components [5]. The goal of all these modification was to improve the possibility of the model to reproduce the observed distributions. During this work, an important role played a possibility of using the data received in different region (the Black Sea, the Sea of Azov, the Baltic Sea, Norwegian Fjords) in the expeditions, where we had possibility to perform measurements necessary to the model validation.

The presented here biogeochemical O–N–S–P–Mn–Fe model ROLM (RedOx Layer Model) allowed to simulate the main features of biogeochemical structure of the redox interfaces [5, 6] and to analyze a potential reaction on the oxygenated intrusions [7].

This chapter is devoted to the detailed description of the model assumptions and parameterizations of the processes considered. Examples of an application of ROLM for some goals are given in the other chapters of this volume [8–10].

2 Formulation of Model

ROLM describes the biogeochemical transformations of the following compartments listed in Table 1.

In the following description of the model, we will use the names of variables assumed in the formulas of the model (i.e., "NO3" for NO_3^-, "Mn2" for Mn(II), "Phy" for phytoplankton, etc.).

For the formal description of the chemical and biological pathways (shown in Fig. 1), we used our own parameterizations [2–4, 11] as well as that of others [12–19]. The values of the coefficients necessary for the rates descriptions were obtained from literature or from fitting model to measure the concentrations profiles.

In general, the parameterization of rates of the biogeochemical interactions, $\mathrm{Rate}_{\mathrm{BG},}$ is as follows:

$$\mathrm{Rate}_{\mathrm{BG}} = K_{\mathrm{BG}}\mathrm{Dep}_{\mathrm{re1}}\mathrm{Dep}_{\mathrm{re2}}[\mathrm{Dep}_{\mathrm{inh}}],$$

where K_{BG} is a constant; $\mathrm{Dep}_{\mathrm{re1}}$ is a dependence on concentration of the first reacting variable; $\mathrm{Dep}_{\mathrm{re2}}$ is a dependence on concentration of the second reacting variable; $\mathrm{Dep}_{\mathrm{inh}}$ is a dependence on concentration of a variable that inhibits the reaction.

A simplest linear dependence (such as the first-order kinetics) is appropriate for the reactions of substances that coexist in small concentrations as O2 and H2S or

Table 1 State variables of model. Concentrations are presented in micromoles for chemical variables and in wet weight (WW) for biological parameters

Variable	Meaning	Dimension
O2	Dissolved oxygen	μM O
S		
H2S	Hydrogen sulfide	μM S
S0	Elemental sulfur	μM S
S2O3	Thiosulfate	μM S
SO4	Sulfate	μM S
N		
NH4	Ammonia	μM N
NO2	Nitrite	μM N
NO3	Nitrate	μM N
PON	Particulate organic nitrogen	μM N
DON	Dissolved organic nitrogen	μM N
P		
PO4	Phosphate	μM P
POP	Particulate organic phosphorus	μM P
DOP	Dissolved organic phosphorus	μM P
Mn		
Mn2	Bivalent manganese	μM Mn
Mn3	Trivalent manganese	μM Mn
Mn4	Quadrivalent manganese	μM Mn
Fe		
Fe2	Bivalent iron	μM Fe
Fe3	Trivalent iron	μM Fe
Biological parameters		
Phy	Phytoplankton	mg WW m^{-3}
Zoo	Zooplankton	mg WW m^{-3}
Bhe	Aerobic heterotrophic bacteria	mg WW m^{-3}
Baa	Aerobic autotrophic bacteria	mg WW m^{-3}
Bha	Anaerobic heterotrophic bacteria	mg WW m^{-3}
Baa	Anaerobic autotrophic bacteria	mg WW m^{-3}

NO3 and Fe2. A nonlinear dependence with "switches" (quasi-linear, Michaelis–Menten in different modifications, hyperbolic tangents) in situations when the concentrations of the considered substances differed significantly or were mediated by biological organisms (e.g., a description of a switch between oxic OM decay and denitrification).

There can be also added a function of inhibition as an additional switch to describe, for instance, a switch between the reactions in suboxic and anoxic conditions.

The notation, typical values, and units of the model coefficients are summarized in Tables 1–3. The values of the constant used differed during the model application to different objects as it is described in the other chapters of this volume [8–10].

These $Rate_{BG}$ were parameterized for specific processes as follows.

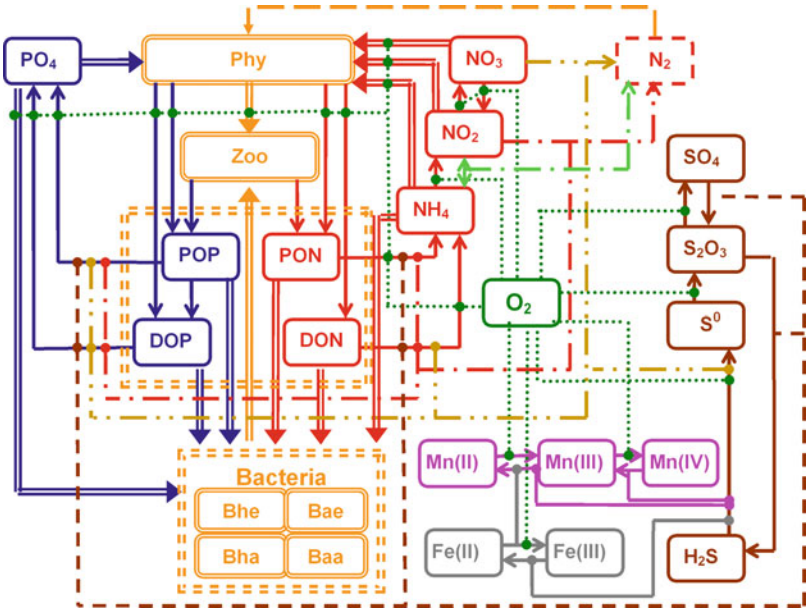

Fig. 1 Flow-chart of biogeochemical processes in the model. Explanations are in text

2.1 Biogeochemical Processes Parameterization

2.1.1 Autolysis

The process of decomposition of particulate to dissolved OM is usually described with a first-order equation with a constant rate coefficient K_{PD}:

$$\text{Autolis } P = K_{PD}\text{POP}.$$

Typical values for this coefficient are 0.004–0.18 day^{-1} [18].

2.1.2 Mineralization of OM

Mineralization of OM is a key process for modeling of formation of the oxygen-deficient and anoxic conditions in the marine environment, because the electron acceptor of this reaction changes subsequently from oxygen to nitrate, to oxides of iron and manganese and to sulfate. Mineralization of OM with CO_2 (methanogenesis) or fermentation of OM to methane and CO_2 should not be significant in sea water, because of the large amount of sulfate. The rates of mineralization with different electron acceptors are different [20]. The microbial degradation of different groups of OM with different labilities differs over time scales ranging from hours to millions of years [20, 21]. The detailed kinetics of

Table 2 Parameters names, notations, values and units of the coefficients used in the model

Parameter	Notation	Value
Specific rate of decomposition of POM to DOM	K_{PD}	0.10 day^{-1}
Mineralization in oxic conditions		
Specific rate of decomposition of DON	K_{ND4}	0.1 day^{-1}
Specific rate of decomposition of PON	K_{NP4}	0.04 day^{-1}
Temperature parameter for oxic mineralization	K_{tox}	0.15°C^{-1}
Oxygen parameter for oxic mineralization	$O2_{ox}$	0 μM
Oxygen parameter for oxic mineralization	K_{ox}	15 μM
Denitrification		
Specific rate of 1st stage of denitrification	K_{N32}	0.12 day^{-1}
Specific rate of 2nd stage of denitrification	K_{N24}	0.20 day^{-1}
Oxygen parameter for denitrification	$O2_{dn}$	25 μM
NO3 parameter for denitrification	$NO3_{mi}$	1×10^{-3} μM
NO2 parameter for denitrification	$NO2_{mi}$	1×10^{-4} μM
Sulfate reduction		
Specific rate of sulfate reduction with sulfate	K_s4_rd	2.5×10^{-7} day^{-1}
Specific rate of sulfate reduction with thiosulfate	K_s23_rd	1.2 day^{-1}
Oxygen parameter for sulfate reduction	$O2_{sr}$	25 μM
NO3 and NO2 parameter for sulfate reduction	NO_{sr}	0.5 μM
Nitrification		
Specific rate of the 1st stage of nitrification	K_{N42}	0.9 day^{-1}
Specific rate of the 2nd stage of nitrification	K_{N23}	2.5 day^{-1}
Oxygen parameter for nitrification	$O2_{nf}$	1 μM
Nitrogen fixation		
Specific rate of nitrogen fixation	K_{Nfix}^{max}	20 day^{-1}
Anammox		
Anammox constant	$K_{annamox}$	0.03 day^{-1}
Oxidation of the hydrogen sulfide		
Specific rate of oxidation of H2S with O2	$K_{\_hs\_ox}$	0.2 day^{-1}
Specific rate of oxidation of S0 with O2	$K_{\_s0\_ox}$	4.0 day^{-1}
Specific rate of oxidation of S2O3 with O2	$K_{\_s23\_ox}$	1.5 day^{-1}
S0 disproportionation		
Specific rate of S0 disproportionation	K_{disp}	0.01 day^{-1}
Thiodenitrification		
Thiodenitrification constant	K_T	0.8 μM^{-1} day^{-1}
Oxidation and reduction of Mn and Fe		
Mn(II) oxidation with O2 constant	$K_{\_mn\_ox}$	2 day^{-1}
Mn(IV) reduction with sulfide constant	$K_{\_mn\_rd}$	22 day^{-1}
Mn(III) oxidation with O2 constant	$K_{\_mn\_ox2}$	18 day^{-1}
Mn(IV) reduction with sulfide constant	$K_{\_mn\_rd2}$	2 day^{-1}
Fe oxidation with O2 constant	$K_{\_fe\_ox}$	4 day^{-1}
Fe oxidation with Mn(IV) constant	K_fe_mnox	1 day^{-1}
Fe oxidation with NO3 constant	K_fe_nox	5 day^{-1}
Fe(III) reduction by sulfide	K_fe_rd	0.05 day^{-1}
Phytoplankton		
Maximum specific growth rate	K_{NF}	1.86 day^{-1}
Specific respiration rate	K_{FN}	0.05 day^{-1}

(continued)

Table 2 (continued)

Parameter	Notation	Value
Incident light	I_0	80
Optimal light	I_{opt}	25
Extinction coefficient	K	0.07
Half-saturation constant for uptake of PO_4	K_{PO4}	0.01 μM
Strength of ammonium inhibition of nitrate uptake constant	K_{psi}	1.46
Half saturation constant for uptake of NH4	K_{NH4}	0.02 μM
Half saturation constant for uptake of NO3 + NO2	K_{NO3}	0.03 μM
Specific rate of mortality	K_{FP}	0.05 day^{-1}
Specific rate of excretion	K_{FD}	0.05 day^{-1}
Zooplankton		
Specific respiration rate	K_{ZN}	0.1 day^{-1}
Maximum specific rate of grazing of Zoo on Phy	K_{FZ}	0.5 day^{-1}
Half-saturation constant for the grazing of Zoo on Phy for Phy/Zoo ratio	K_F	1
Maximum specific rate of grazing of Zoo on POP	K_{PZ}	0.6 day^{-1}
Half-saturation constant for the grazing of Zoo on POP in dependence to ratio POP/Zoo	K_{PP}	200
Maximum specific rate of grazing of Zoo on Baut	K_{BoaZ}	0.6 day^{-1}
Half-saturation constant for the grazing of Zoo on Baut for Baut/Zoo ratio	K_{Boa}	1.5
Maximum specific rate of grazing of Zoo on Bhet	K_{BohZ}	1.02 day^{-1}
Half-saturation constant for the grazing of Zoo on Bhet for Bhet/Zoo ratio	K_{Boh}	1.1
Maximum specific rate of grazing of Zoo on BautA	K_{BaaZ}	0.78 day^{-1}
Half-saturation constant for the grazing of Zoo on BautA for BautA/Zoo ratio	K_{Baa}	1.5
Maximum specific rate of grazing of Zoo on BhetA	K_{BahZ}	0.6 day^{-1}
Half-saturation constant for the grazing of Zoo on BhetA for BhetA/Zoo ratio	K_{Bah}	1
Maximum specific rate of mortality of Zoo	K_{ZP}	0.001 day^{-1} if: $H_2S < 20$ μM 0.9 day^{-1} if: $H_2S > 20$ μM
Food absorbency for zooplankton	U_z	0.7
Ratio between dissolved and particulate excretes of zooplankton	H_z	0.6
Aerobic heterotrophic bacteria		
Maximum specific growth rate of *B*_ae_het	$K^{max}_{B\_ae\_het}$	2 μM^{-1}
Half-saturation constant for the dependence of maximum specific growth rate of *B*_ae_het on POM and DOM content	$K^{N}_{B\_ae\_het}$	0.5 μM
Maximum specific rate of mortality of *B*_ae_het	$K^{Mort}_{B\_ae\_het}$	0.03 day^{-1} if: $O_2 > 1$ μM 0.99 day^{-1} if: $O_2 < 1$ μM

(continued)

Table 2 (continued)

Parameter	Notation	Value
Aerobic autotrophic bacteria		
Maximum specific growth rate of *B*_ae_aut	$K^{max}_{B\_ae\_aut}$	1 μM^{-1}
Half-saturation constant for the dependence of maximum specific growth rate of *B*_ae_aut on NH4	$K^{N}_{B\_ae\_aut}$	0.05 μM
Half-saturation constants for the dependence of maximum specific growth rate of *B*_ae_aut on PO4	$K^{P}_{B\_ae\_aut}$	0.3 μM
Maximum specific rate of mortality of *B*_ae_aut	$K^{Mort}_{B\_ae\_aut}$	0.01 day^{-1} if: $O_2 > 1$ μM 0.99 day^{-1} if: $O_2 < 1$ μM
Anaerobic heterotrophic bacteria		
Maximum specific growth rate of *B*_anae_het	$K^{max}_{B\_anae\_het}$	2 μM^{-1}
Half-saturation constant for the dependence of maximum specific growth rate of *B*_anae_het on POM and DOM	$K^{N}_{B\_anae\_het}$	6 μM
Maximum specific rate of mortality of *B*_anae_het	$K^{Mort}_{B\_anae\_het}$	0.01 day^{-1}
Anaerobic autotrophic bacteria		
Maximum specific growth rate of *B*_anae_aut	$K^{max}_{B\_anae\_aut}$	6.5 μM^{-1}
Half-saturation constants for the dependence of maximum specific growth rate of *B*_ae_aut on NH4	$K^{N}_{B\_anae\_aut}$	3 μM
Half-saturation constants for the dependence of maximum specific growth rate of *B*_ae_aut on PO4	$K^{P}_{B\_anae\_aut}$	3 μM
Maximum specific rate of mortality of *B*_anae_aut	$K^{Mort}_{B\_anae\_aut}$	0.001 day^{-1} if: $H_2S < 16$ μM 0.99 day^{-1} if: $H_2S < 16$ μM

the decomposition (needed for modeling long-term processes, for instance, in the sediments) can be described with "multi-G" models with OM divided into several compartments with different particular degradability [16].

For the water column, we used a simpler approach. The OM was divided into DOM and POM with different rates of mineralization with different electron acceptors. We considered POM as a detrital labile OM that can be "mineralized directly" in the model with instantaneous autolysis. Such an approach is widely used in the models when it is necessary to describe the processes of mineralization and sedimentation of the same matter. We used the stoichiometry of the mineralization reactions presented by Redfield [22] and Richards [23], and assumed the stoichiometric ratios to be the same in OM in oxic and anoxic conditions.

Mineralization in Oxic Conditions

The OM mineralization in the oxic conditions is usually described with the following equation, initially proposed by Redfield [22]:

$$(CH_2O)_{106}(NH_3)_{16}H_3PO_4 + 106O_2 = 106CO_2 + 16NH_3 + H_3PO_4 + 106H_2O.$$

Table 3 Rates of biogeochemical production/consumption of the model compartments

Phosphate (PO_4)	$R_{PO4} = Sp(GrowthPhy(K_{FN} - 1.) - Chemos - ChemosA + K_{ZN}Zoo) + PhosPOP + PhosDOP + Coprecip$
Dissolved organic phosphorus (DOP)	$R_{DOP} = Sp(ExcrPhy + Grazing(1. - U_z)H_z + 0.7MortBact - (Hetero + HeteroA) - DON/(DON + PON)$ (Hetero + HeteroA)) + AutolisP − PhosDOP
Particulate organic phosphorus (POP)	$R_{POP} = Sp(MortPhy + MortZoo + 0.3MortBact + Grazing(1. - U_z)(1. - H_z) - GrazPOP - PON/$ (DON + PON) * (Hetero + HeteroA)) − AutolisP − PhosPOP
Particulate organic nitrogen (PON)	$R_{PON} = Sn(MortPhy + MortZoo + 0.3MortBact + Grazing(1. - U_z)(1. - H_z) - GrazPOP - PON/(DON + PON)$ (Hetero + HeteroA)) − AutolisN − AmmonPON
Dissolved Organic Phosphorus (DON)	$R_{DON} = Sn(ExcrPhy + Grazing(1. - U_z)H_z + 0.7MortBact - (Hetero + HeteroA)) + AutolisN - AmmonDON$
Ammonia (NH_4)	$R_{NH4} = Sn * (GrowthPhy(K_{FN} - 1.)(LimNH4/LimN) - Chemos - ChemosA + K_{ZN} * Zoo)$ AmmonPON + AmmonDON − Nitrif1 + Nfixation
Nitrite (NO_2)	$R_{NO2} = Sn * (GrowthPhy * (K_{FN} - 1.) * (LimNO3/LimN) * (NO_2/(NO_2 + NO_3))) +$ Nitrif1 − Nitrif2 + Denitr1–Denitr2 − hs_NO2
Nitrate (NO_3)	$R_{NO3} = Sn * (GrowthPhy * (K_{FN}–1.) * (LimNO3/LimN) * (NO_3/(NO_2 + NO_3))) +$ Nitrif2–Denitr1 − 1.25hs_NO_3 − ox-fe_nox
Oxygen (O_2)	$R_{O2} = OkP\ Sp\ GrowthPhy + 2.Sn\ GrowthPhy(NO_3/(NO_2 + NO_3))(LimNO3/LimN) + 0.5Sn\ GrowthPhy$ $(NO_2/(NO_2 + NO_3))(LimNO3/LimN) - DcDM\_O2 - DcPM\_O2 - OkP\ Sp(GrowthPhy\ KFN + KZN$ Zoo) − 1.5Nitrif1–0.5Nitrif2–0.5hs_ox − 1.s0_ox − 2.s23_ox − 1.mn_ox − fe_ox
Hydrogen sulfide (H_2S)	$R_{H2S} = -hs\_ox + s23\_rd - 0.5fe\_rd - mn\_rd - hs\_NO3 - hs\_NO2 + 0.5Disprop$
Elemental sulfur (S^0)	$R_{S0} = hs\_ox - s0\_ox + 1.mn\_rd - Disprop$
Thiosulfate (S_2O_3)	$R_{S2O3} = s0\_ox - s23\_ox + s4\_rd - s23\_rd + 0.5Disprop$
Sulfate (SO_4)	$R_{SO4} = s23\_ox - s4\_rd + hs\_NO3 + hs\_NO2$
Bivalent manganese (Mn(II))	$R_{Mn2} = mn\_rd2 - mn\_ox + 0.5 * fe\_mnox$
Quadrivalent manganese (Mn(IV))	$R_{Mn4} = mn\_ox2 - mn\_rd - 0.5 * fe\_mnox$
Trivalent manganese (Mn(III))	$R_{Mn3} = mn\_ox - mn\_ox2 + mn\_rd - mn\_rd2$
Bivalent iron (Fe(II))	$R_{Fe2} = fe\_rd - fe\_ox - fe\_mnox - 5. * fe\_nox$
Trivalent iron (Fe(III))	$R_{Fe3} = fe\_ox + fe\_mnox + 5. * fe\_nox - fe\_rd$
Phytoplankton (Phy)	$R_{Phy} = GrowthPhy(1 - K_{FN}) - MortPhy - ExcrPhy - GrasPhy$
Zooplankton (Zoo)	$R_{Zoo} = Grazing * U_z - MortZoo - K_{ZN} * Zoo$
Aerobic heterotrophic bacteria (Bhe)	$R_{Bhe} = C_{Bhe} - Mort_{Bhe} - Graz_{Bhe}$
Aerobic autotrophic bacteria (Bae)	$R_{Bae} = C_{Bae} - Mort_{Bae} - Graz_{Bae}$
Anaerobic heterotrophic bacteria (Bha)	$R_{Bha} = C_{Bha} - Mort_{Bha} - Graz_{Bha}$
Anaerobic autotrophic bacteria (Baa)	$R_{Baa} = C_{Baa} - Mort_{Baa} - Graz_{Baa}$

Where Sn = 0.016 and Sp = 0.001 are ratios between N and P content and the wet weight, OkP = 106 is the O:P ratio

It is assumed that the release of phosphate (phosphatification) and release of ammonia (ammonification) are parallel and occur with the same rate. Ammonification is carried out by heterotrophic bacteria that use amino acids and proteins as a source of nitrogen, leading to appearance of ammonia as the final product of mineralization. Phosphatification is also carried out by heterotrophs [20].

The rate of this process is described as a first-order equation, with the rate dependent on the amount of OM.

$$\mathrm{DcOM\_O2} = \mathrm{K_{ND4}OM},$$

where OM is the concentration of OM, K_{ND4} is the rate of mineralization with typical values 0.1–1 day^{-1} [24].

The dependence of ammonification on temperature, t, can be described by addition of a multiplier: $\exp(0.15t)$ [13, 15] with corresponding change of the K_{ND4} values (i.e., 0.002 day^{-1} in [15]). Concentrations of O2 significantly affect the rates of oxygen consumption [20], and it can be added an additional multiplier, i.e., $O_2^{0.5}$ in [19].

In this version of the model, we parameterized the dependence of decomposition of OM (for DON and PON) in oxic conditions as follows:

$$\mathrm{DcDM\_O2} = \exp(K_{\mathrm{tox}}t)K_{\mathrm{ND4}}\mathrm{DON}\,F_{\mathrm{ox}},$$

$$\mathrm{DcPM\_O2} = \exp(K_{\mathrm{tox}}t)K_{\mathrm{NP4}}\mathrm{PON}\,F_{\mathrm{ox}},$$

where K_{tox} is temperature coefficient and F_{ox} is the dependence on O2.

$$F_{\mathrm{ox}}(\mathrm{O2}) = 0.5(1 - \tanh(K_{\mathrm{ox}} - \mathrm{O2})),$$

where K_{ox} is a constant.

The rates of mineralization of dissolved (K_{ND4}) and particulate (K_{NP4}) OM were aussumed to differ (Table 2).

Mineralization in Suboxic Conditions

In suboxic conditions, OM mineralization can occur with oxidized compounds of nitrogen, manganese, and iron. The concentrations of iron in the sea water are very low and even in the sediments the contribution of total Mn reduction to carbon oxidation is small, $<10\%$ of the total benthic mineralizaion [25]. Thus in this model devoted to the water column, where the concentrations of the metal oxides are much lower than in the sediments, we do not consider these processes. The most significant process is denitrification. Denitrification is carried out by heterotrophic

bacteria under low concentrations of oxygen if there is availability of oxidized nitrogen compounds (mainly NO3 and NO2) [23]:

$$(CH_2O)_{106}(NH_3)_{16}H_3PO_4 + 84.8HNO_3 = 106CO_2 + 42.4N_2 + 148.4H_2O + 16NH_3 + H_3PO_4.$$

The relative consumption of NO3 and NO2 can be calculated in accordance with Anderson et al. [26]:

$$(1/2)CH_2O + NO_3^- \rightarrow NO_3^- + (1/2)H_2O + (1/2)CO_2,$$
$$(3/4)CH_2O + H^+ + NO_2^- \rightarrow (1/2)N_2 + (5/4)H_2O + (3/4)CO_2.$$

According to the observations, denitrification and nitrification have both been observed at O2 $<$ 60 μM in a fjord [27], but the transition from nitrification to nitrate reduction occurs when oxygen content decreases in various oxygen-deficient ecosystems below 0.9–6.3 μM O_2 [28]. Jost and Pollehne [29] advocate for the value of 10 μM O_2, above which the denitrification is not detectable and nitrification is the dominant chemolithotrophic process. In the suboxic water of the Gotland Basin, denitrification was detectable at oxygen concentrations below 9 μM [30]. For oceanic denitrification, oxygen concentrations above around 2 μM seem to be inhibiting [31, 32].

The influence of oxygen on the rate of denitrification is usually described with a hyperbolic function [13, 15]. Rates of denitrification in cultures follow Michaelis–Menten kinetic with average half saturation constant of 50 μM NO3 [20].

In this model, we considered denitrification of particulate (Denitr1_PM, Denitr2_PM) and dissolved (Denitr1_DM, Denitr2_DM) OM carrying out in two stages with consumption of NO_3 and NO_2, correspondingly:

$$\begin{aligned}
\text{Denitr1_PM} &= K_{N32}F_{dnox}F_{dnNO3}\text{PON},\\
\text{Denitr2_PM} &= K_{N24}F_{dnox}F_{dnNO2}\text{PON},\\
\text{Denitr1_DM} &= K_{N32}F_{dnox}F_{dnNO3}\text{DON},\\
\text{Denitr2_DM} &= K_{N24}F_{dnox}F_{dnNO2}\text{DON},
\end{aligned}$$

where K_{N32} is the rate constant for the 1st stage of denitrification, K_{N24} is the rate constant for the 2nd stage of denitrification, and F_{dnox} is the dependence on O2.

$$F_{dnox}(O2) = 0.5(1 + \tanh(O2_{dn} - O2)),$$

where $O2_{dn}$ is a constant.

F_{dnNO3} and F_{dnNO2} are the dependences of rates on concentrations of NO3 and NO2, respectively

$$F_{dnNO3}(NO3) = 0.5(1 - \tanh(NO3_{mi} - NO3)),$$

$$F_{dnNO2}(NO2) = 0.5(1 - \tanh(NO2_{mi} - NO2)),$$

where $NO3_{mi}$ and $NO2_{mi}$ are the constants.

We have ignored the influence of temperature because denitrification takes place in layers with little seasonal changes of temperature.

Sulfate Reduction

The process of sulfate reduction starts when oxygen and nitrate are exhausted.

$$(CH_2O)_{106}(NH_3)_{16}H_3PO_4 + 53SO_4^{2-} = 106CO_2 + 106H_2O + 16NH_3 + H_3PO_4 + 53S^{2-}.$$

There are few estimates on the rate of this process. In the Black Sea, Jørgensen et al. [33] measured production rates between 3 and 36 nmol $H_2S\ L^{-1}\ day^{-1}$. Albert et al. [34] measured values of up to 3.5 nmol $H_2S\ L^{-1}\ day^{-1}$ below the redox-interface, but deeper than the zone of elevated carbon dioxide fixation.

The oxygen threshold level for the sulfate reduction in the model [3] was taken as 5 μM according to the Cariaco Basin data, where the active sulfate-reducing bacteria occurred at <5 μM [35].

In this model, we considered two stages of this processes that involve reaction with sulfate and thiosulfate.

$$\begin{aligned}
&\mathrm{s4_rd_PM} = K_\mathrm{s4_rd} F_{\mathrm{sox}} F_{\mathrm{snx}} \mathrm{SO4\,PON},\\
&\mathrm{s4_rd_DM} = K_\mathrm{s4_rd} F_{\mathrm{sox}} F_{\mathrm{snx}} \mathrm{SO4\,DON},\\
&\mathrm{s23_rd_PM} = K_\mathrm{s23_rd} F_{\mathrm{sox}} F_{\mathrm{snx}} \mathrm{PON\,S2O3},\\
&\mathrm{s23_rd_DM} = K_\mathrm{s23_rd} F_{\mathrm{sox}} F_{\mathrm{snx}} \mathrm{DON\,S2O3},
\end{aligned}$$

where K_s4_rd and K_s23_rd are the rate constants.

F_{sox} and F_{snx} are dependences on oxygen and nitrate:

$$\begin{aligned}
&F_{\mathrm{sox}}(\mathrm{O2}) = 0.5(1 + \tanh(\mathrm{O2_{sr}} - \mathrm{O2})),\\
&F_{\mathrm{snx}}(\mathrm{NO3} + \mathrm{NO2}) = 0.5(1 + \tanh(\mathrm{NO_{sr}} - \mathrm{O2})),
\end{aligned}$$

where $O2_{sr}$ and NO_{sr} are constants.

According to the stoichiometry of reaction with sulfate reduction, the decay of OM (in N units) was estimated as:

$$\begin{aligned}
&\mathrm{DcPM_SO4} = 16/53(\mathrm{s4_rd_PM} + \mathrm{s23_rd_PM}),\\
&\mathrm{DcDM_SO4} = 16/53(\mathrm{s4_rd_DM} + \mathrm{s23_rd_DM}).
\end{aligned}$$

2.1.3 Ammonification and Phosphatification

The total ammonification of PON and DON was calculated as:

$$\begin{aligned}\text{AmmonPON} &= \text{DcPM\_O2} + \text{DcPM\_NO3} + \text{DcPM\_SO4},\\ \text{AmmonDON} &= \text{DcDM\_O2} + \text{DcDM\_NO3} + \text{DcDM\_SO4}.\end{aligned}$$

Phosphatification was estimated on the base of the Redfield ratio:

$$\begin{aligned}\text{PhosPOP} &= \frac{\text{AmmonPON}}{16},\\ \text{PhosDOP} &= \frac{\text{AmmonDON}}{16}.\end{aligned}$$

2.1.4 Nitrification

Nitrification, the oxidation of NH4 to NO3, occurs in several stages and is accomplished mainly by chemolithotrophic bacteria [20]:

$$\begin{aligned}&{NH_4}^+ + 1.5O_2 \rightarrow {NO_2}^- + 2H^+ + H_2O;\\ &{NO_2}^- + 0.5O_2 \rightarrow {NO_3}^-.\end{aligned}$$

Ammonia oxidation is restricted to at least suboxic environments ([29], this volume). In the Baltic Sea this process can be indicated by a nitrate peak below the halocline [36, 37], which should be related to highest ammonia-oxidation activities.

Estimates of the lowest oxygen threshold of nitrification vary from 0.4–0.9 to 3.1–4.9 μM [28].

The kinetic function for nitrification can be described as a first-order reaction for the oxic waters, but in the models for low oxygen content, an approach is used where the rate of this process depends on the content of both oxygen and ammonia [15]. It can be described using multiplication of concentrations of oxygen and ammonia or multiplication of the results from the Michaelis–Menten hyperbolic formulas [15].

We used the following functions for parameterization of nitrification in two stages:

$$\begin{aligned}\text{Nitrif1} &= \frac{K_{\text{N42}}\text{NH}_4\text{O2}}{(\text{O}_2+\text{O2}_{\text{nf}})},\\ \text{Nitrif2} &= \frac{K_{\text{N23}}\text{NO}_2\text{O2}}{(\text{O}_2+\text{O2}_{\text{nf}})},\end{aligned}$$

where K_{N42} and K_{N23} are the rate constants, and O2_{nf} is a constant.

2.1.5 Nitrogen Fixation

The nitrogen fixation process is accomplished by several species of cyanobacteria that develop in the conditions of presence of phosphate and absence of available fixed nitrogen. In this model, we used the formulation introduced by Savchuk and Wulff [15] applying a limiting nutrient criterion based on the N/P ratio:

$$\mathrm{Nfixation} = K_{\mathrm{Nfix}}^{\max} \frac{1}{1 + \left(\frac{\mathrm{NO3+NO2+NH4}}{16\mathrm{PO4}}\right)^4} \frac{\mathrm{PO4}}{\mathrm{PO4} + 0.3} \mathrm{Phy} \cdot K_{\mathrm{NF}} \cdot \mathrm{LimLight} \cdot \mathrm{LimT} \cdot \mathrm{Sn}$$

where $K_{\mathrm{Nfix}}^{\max}$ is the maximum rate of nitrogen fixation. The latter symbols are explained in the Tables. In the frame of this model, the nitrogen fixation results in increase of ammonia.

2.1.6 Anammox

Anammox, the process of anaerobic ammonia oxidation:

$$NO_2 + NH_4 \rightarrow N_2 + 2H_2O$$

was found in the marine environment only recently, in the Black Sea [38] and in the tropical coastal anoxic bay [39]. In the Baltic Sea, anammox could only be detected occasionally, rates were in the range of 0.05–0.005 μmol N L^{-1} day^{-1} [40].

It is supposed that this reaction is mediated by chemolithotrophic bacteria [20]. This reaction requires a constant source of nitrite that can be provided either from reduction of nitrate or oxidation of ammonia [41].

It was assumed that anammox would be restricted to anoxic and nonsulfidic environments, since it was completely inhibited already at oxygen concentrations as low as 2 μM [42]. But then it was found that anammox still proceeds under low oxygen concentrations [78], though under suboxic conditions anammox rates are lower than under anoxic [43].

We parameterized this process with a second-order equation:

$$\mathrm{Anammox} = \mathrm{NO2}\,\mathrm{NH4}\,K_{\mathrm{annamox}},$$

where K_{annamox} is the rate constant.

2.1.7 Oxidation of Reduced Sulfur Forms with Oxygen

We assumed that the oxidation of H_2S with O_2 occurred in three stages with S_2O_3 are S0 are intermediate forms [44]:

$$2H_2S + O_2 \rightarrow 2S^0 + 2H_2O;$$
$$2S^0 + O_2 + H_2O \rightarrow {S_2O_3}^{2-} + 2H^+;$$
$${S_2O_3}^{2-} + 2O_2 + 2OH^- \rightarrow 2{SO_4}^{2-} + H_2O;$$

and parameterized these processes as follows:

$$\text{hs\_ox} = K_{\text{\_hs\_ox}}\,\text{H2}\,\text{SO2},$$
$$\text{s0\_ox} = K_{\text{\_s0\_ox}}\,\text{S0}\,\text{O2},$$
$$\text{s23\_ox} = K_{\text{\_s23\_ox}}\,\text{S2O3}\,\text{O2},$$

where $K_{\text{\_hs\_ox}}$, $K_{\text{\_s0\_ox}}$, and $K_{\text{\_s23\_ox}}$ are the rate constants.

2.1.8 S^0 Disproportionation

We considered the S0 disproportionation in accordance with Canfield et al. [20]:

$$4S^0 + 3H_2O \rightarrow 2H_2S + S_2O_3^{2-} + 2H^+.$$

This process is assumed to be connected with autotrophic bacteria. It was parameterized as follows:

$$\text{Disprop} = K_{\text{disp}}\,\text{S0},$$

where K_{disp} is the rate constant.

2.1.9 Thiodenitrification (Chemolithotrophic Denitrification)

Thiodenitrification, a process of oxidation of sulfide with nitrate and nitrite, is carried out by autotrophic bacteria [20]. The importance of chemolithotrophic denitrification as the main loss factor for nitrogen at pelagic redox zones of the Baltic Sea was marked out by Hannig et al. [40].

$$3H_2S + 4{NO_3}^- + 6OH^- \rightarrow 3{SO_4}^{2-} + 2N_2 + 6H_2O.$$

We considered it to be independent of the oxygen content:

$$\text{sulfido} = K_{\text{T}}\text{H2S}\,\text{NO3},$$
$$\text{sulfido2} = K_{\text{T}}\text{H2S}\,\text{NO3},$$

where K_{T} is the maximum specific rate of the reactions.

2.1.10 Processes of Oxidation and Reduction of Manganese

The cycles of iron and manganese at the redox interface are similar. Both metals are present under anoxic conditions in dissolved reduced forms (Mn(II) and Fe(II)). Under oxic conditions they are oxidized by oxygen (Fe(II) also can be oxidized by nitrate or Mn(IV)) with formation of particulate hydroxides (MnO_2 and FeOOH).

These hydroxides sink and are reduced under anoxic conditions with sulfides, OM and ammonia (iron only). Recent studies revealed that both reduction and oxidation of Mn occur with Mn(III) as an intermediate form [45, 46].

Many organisms are known to oxidize manganese and in theory it should be sufficient to support chemolithoautotrophic growth ([29], this volume). Real proof is lacking, but as genes for CO_2 fixation were found in a manganese oxidizing bacterium [47] this pathway seems very likely.

Manganese(II) Oxidation with Oxygen

It is usually assumed that bacterially mediated Mn oxidation is the only process of Mn oxidation in natural waters [48, 49].

$$Mn^{2+} + 0.5O_2 + 2OH_{-} \rightarrow MnO_2 + H_2O.$$

This rate of this process depends on the concentrations of both Mn(II) and O2 [50].

Manganese(IV) Reduction with Sulfide

The kinetic of Mn reduction with sulfide is very fast with half time on the order of seconds or minutes [49, 51].

$$MnO_2 + HS^{-} + 3H^{+} \rightarrow S^0 + Mn^{2+} + 2H_2O.$$

This process can occur chemically [20, 52] and can be accomplished by autotrophs. The experimental study of Mn(IV) reduction by bacteria *Shewanella putrefaciens* [53] revealed that this processes maximum rate can reach 0.04 min^{-1} (about 60 day^{-1}). This processes rate is inhibited by nitrate.

Manganese(III) Oxidation and Reduction

Recently, production of dissolved, oxidized Mn in the form of Mn(III) by Mn(II)-oxidizing bacteria and in incubations with Black Sea suboxic zone water has been observed [46]. Dissolved Mn(III) has also been directly observed in the suboxic zone [54]. Mn(III) is an important intermediate product of the Mn cycle and can exist in both dissolved and solid forms [45].

The stoichiometry of the reactions of Mn(III) oxidation process can be the following [20]:

$$4Mn^{2+} + O_2 + 4H^+ \rightarrow 4Mn^{3+} + 2H_2O,$$
$$4Mn^{3+} + O_2 + 6OH^- \rightarrow 4MnO_2 + 6H_2O.$$

Mn(III) can be also produced as an intermediate during the Mn(IV) reduction [45, 55]:

$$2MnO_2 + 7H^+ + HS^- \rightarrow 2Mn^{3+} + 4H_2O,$$
$$2Mn^{3+} + HS^- \rightarrow 2Mn^{2+} + S^0 + H^+.$$

Mn(III) can be complexed with organic and inorganic ligands [46] and also can form insoluble hydroxides [20]:

$$Mn^{3+} + 2H_2O \rightarrow MnOOH + 3H^+.$$

In the latest variants of the model, we added these processes connected with Mn (III) formation and removal due to both reduction and oxidation of Mn. We parameterized them as follows:

$$\text{mn\_ox} = K_{\text{\_mn\_ox}}\text{O2Mn2},$$
$$\text{mn\_ox2} = K_{\text{\_mn\_ox2}}\text{O2Mn3},$$
$$\text{mn\_rd} = K_{\text{\_mn\_rd}}\text{Mn4H2S},$$
$$\text{mn\_rd2} = K_{\text{\_mn\_rd2}}\text{Mn3H2S},$$

where $K_{\text{\_mn\_ox}}$, $K_{\text{\_mn\_ox2}}$, $K_{\text{\_mn\_rd}}$, and $K_{\text{\_mn\_rd2}}$ are the rate constants.

2.1.11 Processes of Oxidation and Reduction of Iron

Iron(II) Oxidation with Oxygen

$$4Fe^{2+} + O_2 + 2H_2O \rightarrow 4Fe^{3+} + 4OH^-.$$

The process of oxidation or iron with oxygen is much faster than that of manganese [27]. Fe reacts with oxygen with a half-life of 1.8 min, and biological catalysis if this reaction is assumed to be unnecessary [56]. We assumed:

$$\text{fe\_ox} = K_{\text{\_fe\_ox}}\text{Fe2O2},$$

where $K_{\text{\_fe\_ox}}$ is the rate constant.

Iron(II) Oxidation by Manganese(IV)

$$2\text{Fe}_2{}^{+} + \text{MnO}_2 + 2\text{H}_2\text{O} \rightarrow \text{FeOOH} + \text{Mn}^{2+} + 2\text{H}^{+}.$$

Under anaerobic conditions, Fe(II) readily reduces Mn(IV) oxides (Thamdrup et al. 1997). We assumed:

$$\text{fe\_mnox} = K\text{\_fe\_mnox}\,\text{Fe2}\,\text{Mn4},$$

where K_fe_mnox is the rate constant.

Iron(II) Oxidation by Nitrate

For iron oxidation by nitrate [20]:

$$10\text{Fe}^{2+} + 2\text{NO}_3{}^{-} + 12\text{H}^{+} = 10\text{Fe}^{3+} + \text{N}_2 + 6\text{H}_2\text{O}$$

we assumed:

$$\text{fe\_nox} = K\text{\_fe\_nox}\,\text{Fe2}\,\text{NO3},$$

where K_fe_nox is the rate constant.

The oxidation of Mn2 with nitrate was not detected [49].

Iron(III) Reduction by Sulfide

$$2\text{FeOOH} + \text{H}_2\text{S} \rightarrow 2\text{Fe}^{2+} + \text{S}^{0} + 4\text{OH}^{-}.$$

The rates of Fe(III) reduction by *S. putrefaciens* were found to be 0.02–0.20 h^{-1} (0.48–4.8 day^{-1}) depending on the surface limitation effect for different forms of Fe(III) [53]. This process was inhibited by nitrate [53]. We parameterized it as:

$$\text{fe\_rd} = K\text{\_fe\_rd}\,\text{Fe3H2S},$$

where K_fe_rd is the rate constant.

2.1.12 Processes of Phosphorus Transformation

The transformations of phosphorus species during the synthesis and decay of OM were assumed to follow the Redfield ratios and have been described above. We also included in the model the processes of co-precipitation and complexation of phosphate connected with the formation and dissolution of oxidized forms of Mn and Fe.

The Fe:P ratio during co-precipitation with iron hydroxides has been reported to be 4 [57] or 2.7 (T. Leipe, 2006, personal communication). Laboratory experiments show very high ratios of Mn:P = 1000 during co-precipitation of Mn hydroxides [58]. Therefore, phosphorus removal by precipitation of Mn hydroxides may be ignored.

It is possible, however, that Mn(III), an intermediate product between Mn(IV) and Mn(II), can play a key role in precipitation of phosphate. Known Mn(III) ligands that bind with enough strength to stabilize Mn(III) in solution include inorganic ligands such as pyrophosphate [46], Mn(III)–pyrophosphate complexes are characterized by ratio Mn:P = 0.25 for $Mn(HP_2O_7)_2^{3-}$ or Mn:P =0.17 for $Mn(H_2P_2O_7)_3^{3-}$ [46].

In this model we assumed:

$$\text{Coprecip} = \frac{(\text{fe\_rd} - \text{fe\_ox} - \text{fe\_mnox})}{2.7} - \frac{(\text{mn\_ox} - \text{mn\_ox2} + \text{mn\_rd} - \text{mn\_rd2})}{0.66},$$

where coefficient 0.66 is about 4 times greater than the mentioned maximum possible Mn:P ratio, that means that about 25% of Mn(III) should have complexes with polyphosphate. The latter part of Mn(III) can probably form complexes with other ligands (i.e., OM).

2.2 *Ecosystem Processes Parameterization*

The main goal of this model was to explain processes in the redox layer processes, so we have used a simplified model of the living organisms compared with the existing models for the Black Sea [17, 18] and the Baltic Sea [13, 15]. The main role of the Phy and Zoo modeling compartments was to describe the seasonality of the production of OM. Therefore, we did not subdivide these model compartments into groups. We also assumed that the uptake rate of inorganic nutrients by phytoplankton equals the growth rate of the phytoplankton.

2.2.1 Phytoplankton (Phy)

The modeled phytoplankton evolved according to:

$$R_{\text{Phy}} = \text{GrowthPhy}(1 - K_{\text{FN}}) - \text{MortPhy} - \text{ExcrPhy} - \text{GrazPhy},$$

where GrowthPhy is the Phy specific growth rate; K_{FN} is the specific respiration rate of Phy; MortPhy is the specific natural mortality rate of Phy; ExcrPhy is the specific excretion rate of Phy; GrazPhy is the loss of Phy due to zooplankton grazing.

The phytoplankton specific growth rate,

GrowthPhy $= K_{NF} f_t(t) f_i(i) \min\{f_P(PO_4), f_N(NO_3NO_2, NH_4)\}$ is a function of temperature, light, and availability of nutrients with the maximum specific growth rate K_{NF};

The following formula [59] was chosen for dependence on temperature:

$$f_t(t) = \frac{0.2 + 0.22(\exp(0.21t) - 1)}{(1 + 0.28\exp(0.21t))}.$$

To describe the dependence on light in accordance with [60]:

$$f_i(i) = f_\varphi(\varphi)\frac{I_0}{I_{opt}}\exp(-kh)\exp\left(1 - \frac{I_0}{I_{opt}}\exp(-kh)\right)$$

we used the following parameters: incident light ($I_0 = 80$), optimal light ($I_{opt} = 25$), extinction coefficient ($k = 0.07$), depth: (h) and variation of light with latitude and time:

$$f_\varphi(\varphi) = \cos(\varphi - 23.5\sin\left(\frac{2T}{365.2}\right),$$

where T is time (days) and φ is latitude (degrees).

For nutrient limitation parameterization, we used a *minimum* function that allowed to switch between limitation on P or N:

$$\min\{f(PO_4), f(NO_3, NO_2, NO_3)\}.$$

The hyperbolic dependences were used for phosphate limitation description:

$$f(PO_4) = 0.5(1 - \tanh(K_{PO4} - PO4))$$

with K_{PO4}, a half-saturation constant for the uptake of PO4 by phytoplankton.

The dependence on nitrogen species was described following [12]:

$$\begin{aligned} f_N(NO_3, NO_2, NH_4) &= f'_N(NO_3, NO_2) + f''_N(NH_4) \\ &= \frac{(NO_3 + NO_2)\exp(-K_{psi}NH_4)}{K_{NO_3} + (NO_3 + NO_2)} + \frac{NH_4}{K_{NH_4} + NH_4}, \end{aligned}$$

where K_{NH4} and K_{NO3} are half-saturation constants for the uptake of NH4 and (NO_3 + NO_2) by phytoplankton. The constant, K_{psi}, determines the strength of ammonium inhibition of nitrate uptake.

The excretion rate of Phy was described as:

$$\text{ExcrPhy} = K_{\text{FD}}\text{Phy}$$

with specific rate of excretion K_{FD}.

The natural mortality rate of Phy was described as:

$$\text{MortPhy} = K_{\text{FP}}\text{Phy}$$

with specific rate of mortality K_{FP}.

2.2.2 Zooplankton (Zoo)

Since only a few metazoans are adapted to very low oxygen concentrations or even anoxic waters, protozoa seem to be the only organism left to fulfill the function of grazers, preying on either other protozoa, flagellates or prokaryotes ([29], this volume, [61]). Their abundance decreases with increasing concentrations of H_2S. In the central Baltic redox zone, ciliates seem to be the major grazers of bacteria within the suboxic part of the redox zone showing a peak at the oxic–anoxic interface [62]. Detmer et al. [63] reported a peak of ciliates at the chemocline followed by a drastic decrease further downwards in the sulfidic water. The similar observations exist for the Black Sea [64], the Cariaco Trench [65], and anoxic fjords [66]. This results in a decrease of grazing pressure on the prokaryotic populations over the pelagic redox zone which might at least compensate the effect of reduced bacterial productivity on the standing stock of prokaryotes ([29], this volume). A more pronounced increase in prokaryote abundance below the redox zone might be limited by increased mortality due to bacteriophages [67].

The modeled zooplankton evolved according to:

$$R_{\text{Zoo}} = \text{Grazing}\, U_z - \text{MortZoo} - K_{\text{ZN}}\text{Zoo},$$

where Grazing = GrazPhy + GrazPOP + GrazBact is the grazing of zooplankton on phytoplankton (GrazPhy), detritus (GrazPOP) and bacteria (GrazBact), $U_z = 0.7$ is the food absorbency for zooplankton, MortZoo is the specific natural mortality rate of Zoo; K_{ZN} is the specific respiration rate of Zoo.

The grazing of zooplankton on phytoplankton was described with a modified Michaelis–Menten dependence:

$$\text{GrazPhy} = K_{\text{FZ}}\text{Zoo}(\text{Phy}/\text{Zoo})/(\text{Phy}/\text{Zoo} + K_{\text{F}}),$$

where K_{FZ} is the maximum specific rate of grazing of Zoo on Phy and K_{F} is a half-saturation constant for the grazing of Zoo on Phy for Phy/Zoo ratio.

The grazing of zooplankton on phytoplankton was described with a modified Michaelis–Menten dependence:

$$\mathrm{GrazPOP} = K_{\mathrm{PZ}}\mathrm{Zoo}(\mathrm{POP}/\mathrm{Zoo})/(\mathrm{POP}/\mathrm{Zoo} + K_{\mathrm{PP}}/0.001),$$

where K_{PZ} is the maximum specific rate of grazing of Zoo on POP and K_{PP} half-saturation constant for the grazing of Zoo on POP in dependence to ratio POP/Zoo.

The grazing of Zoo on bacteria

$$\mathrm{GrazBact} = \mathrm{Graz}_{B\_\mathrm{ae}\_\mathrm{aut}} + \mathrm{Graz}_{B\_\mathrm{ae}\_\mathrm{het}} + \mathrm{Graz}_{B\_\mathrm{anae}\_\mathrm{het}} + \mathrm{Graz}_{B\_\mathrm{anae}\_\mathrm{aut}}$$

was described as a sum of grazing of the certain groups of bacteria.

Aerobic autotrophic bacteria:

$$\mathrm{Graz}_{B\_\mathrm{ae}\_\mathrm{aut}} = \frac{K_{\mathrm{BoaZ}}\mathrm{Zoo}(B\_\mathrm{ae}\_\mathrm{aut}/\mathrm{Zoo})}{(B\_\mathrm{ae}\_\mathrm{aut}/\mathrm{Zoo} + K_{\mathrm{Boa}})},$$

where K_{BoaZ} is the maximum specific rate of grazing of Zoo on Baut and K_{Boa} is a half-saturation constant for the grazing of Zoo on Baut for Baut/Zoo ratio.

Aerobic heterotrophic bacteria:

$$\mathrm{Graz}_{B\_\mathrm{ae}\_\mathrm{het}} = \frac{K_{\mathrm{BohZ}}\mathrm{Zoo}(B\_\mathrm{ae}\_\mathrm{het}/\mathrm{Zoo})}{(B\_\mathrm{ae}\_\mathrm{het}/\mathrm{Zoo} + K_{\mathrm{Boh}})},$$

where K_{BohZ} is the maximum specific rate of grazing of Zoo on Bhet and K_{Boh} is a half-saturation constant for the grazing of Zoo on Bhet for Bhet/Zoo ratio.

Anaerobic autotrophic bacteria:

$$\mathrm{Graz}_{B\_\mathrm{anae}\_\mathrm{aut}} = \frac{K_{\mathrm{BaaZ}}\mathrm{Zoo}(B\_\mathrm{an}\_\mathrm{aut}/\mathrm{Zoo})}{(B\_\mathrm{an}\_\mathrm{aut}/\mathrm{Zoo} + K_{\mathrm{Baa}})},$$

where K_{BaaZ} is the maximum specific rate of grazing of Zoo on BautA and K_{Baa} is a half-saturation constant for the grazing of Zoo on BautA for BautA/Zoo ratio.

Anaerobic heterotrophic bacteria:

$$\mathrm{Graz}_{B\_\mathrm{anae}\_\mathrm{het}} = \frac{K_{\mathrm{BahZ}}\mathrm{Zoo}(B\_\mathrm{an}\_\mathrm{het}/\mathrm{Zoo})}{(B\_\mathrm{an}\_\mathrm{het}/\mathrm{Zoo} + K_{\mathrm{Bah}})},$$

where K_{BahZ} is the maximum specific rate of grazing of Zoo on BhetA and K_{Bah} is a half-saturation constant for the grazing of Zoo on BhetA for BhetA/Zoo ratio.

$\mathrm{MortZoo} = K_{\mathrm{ZP}}\mathrm{ZooZoo}$ is the zooplankton mortality rate, with maximum specific rate of mortality of zooplankton K_{ZP} depending on the H2S:

$$K_{\mathrm{ZP}} = 0.001\,\mathrm{day}^{-1} \quad \text{for } \mathrm{H_2S} < 20\,\mu\mathrm{M} \quad \text{and}$$
$$K_{\mathrm{ZP}} = 0.9\,\mathrm{day}^{-1} \quad \text{for } \mathrm{H_2S} > 20\,\mu\mathrm{M}$$

K_{ZN} is the specific rate of respiration of zooplankton.

2.2.3 Aerobic Heterotrophic Bacteria (*B*_ae_het)

The modeled aerobic heterotrophic bacteria evolved according to:

$$R_{B\_\mathrm{ae}\_\mathrm{het}} = C_{B\_\mathrm{ae}\_\mathrm{het}} - \mathrm{Mort}_{B\_\mathrm{ae}\_\mathrm{het}} - \mathrm{Graz}_{B\_\mathrm{ae}\_\mathrm{het}},$$

where

$C_{B\_\mathrm{ae}\_\mathrm{het}} = K^{\max}_{B\_\mathrm{ae}\_\mathrm{het}} \cdot (\mathrm{DcPM\_O_2} + \mathrm{DcDM\_O_2}) \cdot f_{B\_\mathrm{ae}\_\mathrm{het}}(\mathrm{DON} + \mathrm{PON}) \cdot B\_\mathrm{ae}\_\mathrm{het}$ is the growth rate of ***B***_ae_het that we parameterized to be propositionally connected with the rates of aerobic mineralization of particulate ($\mathrm{DcPM\_O_2}$) and dissolved ($\mathrm{DcDM\_O_2}$) OM.

$K^{\max}_{B\_\mathrm{ae}\_\mathrm{het}}$ is the maximum specific growth rate of *B*_ae_het.

$f_{B\_\mathrm{ae}\_\mathrm{het}}(\mathrm{DON} + \mathrm{PON}) = \frac{\mathrm{PON}+\mathrm{DON}}{\mathrm{PON}+\mathrm{DON}+K^{\mathrm{N}}_{B\_\mathrm{ae}\_\mathrm{het}}}$ is the dependence of maximum specific growth rate of *B*_ae_het on POM and DOM content,

$K^{\mathrm{N}}_{B\_\mathrm{ae}\_\mathrm{het}}$ is a half-saturation constant for the dependence of maximum specific growth rate of *B*_ae_het on POM and DOM content.

$\mathrm{Mort}_{B\_\mathrm{ae}\_\mathrm{het}} = K^{\mathrm{Mort}}_{B\_\mathrm{ae}\_\mathrm{het}} B\_\mathrm{ae}\_\mathrm{het}^2$ is the rate of mortality of *B*_ae_het, with maximum specific rate of mortality $K^{\mathrm{Mort}}_{B\_\mathrm{ae}\_\mathrm{het}} = 0.03\,\mathrm{day}^{-1}$ if $\mathrm{O_2} > 1$ μM and $K^{\mathrm{Mort}}_{B\_\mathrm{ox}\_\mathrm{het}} = 0.99\,\mathrm{day}^{-1}$ if $\mathrm{O_2} < 1$ μM.

$\mathrm{Graz}_{B\_\mathrm{ae}\_\mathrm{het}}$ is the grazing of Zoo on *B*_ae_het.

2.2.4 Aerobic Autotrophic Bacteria (*B*_ae_aut)

In the suboxic part of the redox zone, alternative reactions allow chemolithoautotrophy ([29], this volume). The processes of Mn reduction, Fe reduction, $\mathrm{H_2S}$ oxidation by $\mathrm{O_2}$, $\mathrm{NO_3}$ and $\mathrm{NO_2}$, anammox and disproportionation of S0 are usually considered as autotrophic.

The importance of nitrifying bacteria within suboxic environments is well known [68]. However, in this layer $\mathrm{CO_2}$ fixation rates are near the detection limit ([29], this volume) and can be assigned only to the activity of chemolithoautotrophic ammonia-oxidizers [69]. This view will probably be modified by new findings that *Crenarchaeota* are also involved in the marine nitrogen cycle. It is assumed that the marine *Crenarchaeota* are also autotrophs [70, 77] and for the Black Sea it was suggested that both *Gammaproteobacteria* and *Crenarchaeota* contribute to nitrification [71].

The contribution of anammox bacteria (oxidation of NH_4 with NO_2 to N_2 and H_2O) to CO_2 fixation seems as well to be of minor importance, as their energy gain is in the same range as that of aerobic ammonia oxidizers [72]. Since these bacteria use nitrate or nitrite under anoxic conditions with an energy yield as low as nitrifying bacteria, they cannot contribute more to CO_2 fixation than the nitrifiers.

The modeled aerobic autotrophic bacteria evolved according to:

$$R_{B\_ae\_aut} = C_{B\_ae\_aut} - \mathrm{Mort}_{B\_ae\_aut} - \mathrm{Graz}_{B\_ae\_aut},$$

where

$$C_{B\_ae\_aut} = K^{\max}_{B\_ae\_aut} \cdot (\mathrm{Nitrif1} + \mathrm{Nitrif2} + \mathrm{S^0\_ox} + \mathrm{S_2O_3\_ox} + \mathrm{mn\_ox} + \mathrm{fe\_ox} + \mathrm{anammox}) \cdot f^{\mathrm{NP}}_{B\_ae\_aut}(\mathrm{NH_4}, \mathrm{PO_4}) \cdot B\_ae\_aut$$

is the growth rate of B_ae_aut, connected with nitrification, and oxidation by O_2 of reduced species of S, Mn, and Fe and anammox. These processes are usually considered as autotrophic [20].

$K^{\max}_{B\_ae\_aut}$ is the maximum specific growth rate of B_ae_aut.

$f^{\mathrm{NP}}_{B\_ae\_aut}(\mathrm{NH_4}, \mathrm{PO_4}) = \min\left\{\frac{\mathrm{NH_4}}{\mathrm{NH_4}+K^{\mathrm{N}}_{B\_ae\_aut}} \frac{\mathrm{PO_4}}{\mathrm{PO_4}+K^{\mathrm{P}}_{B\_ae\_aut}}\right\}$ is the dependence of maximum specific growth rate of B_ae_het on NH_4 and PO_4,

where: $K^{\mathrm{N}}_{B\_ae\_aut}$ and $K^{\mathrm{P}}_{B\_ae\_aut}$ are half-saturation constants for the dependence of maximum specific growth rate of B_ae_aut on NH_4 and PO_4 content.

$\mathrm{Mort}_{B\_ae\_aut} = K^{\mathrm{Mort}}_{B\_ae\_aut} B\_ae\_aut^2$ is the rate of mortality of B_ae_aut with maximum specific rate of mortality:

$K^{\mathrm{Mort}}_{B\_ae\_aut} = 0.1\,\mathrm{day}^{-1}$ if $O_2 > 1$ μM and $K^{\mathrm{Mort}}_{B\_ae\_aut} = 0.99\,\mathrm{day}^{-1}$ if $O_2 < 1$ μM.

$\mathrm{Graz}_{B\_ae\_aut}$ is the grazing of Zoo on B_ae_aut.

2.2.5 Anaerobic Heterotrophic Bacteria (*B*_anae _het)

Bacterial growth estimations around redox zones lie in the limits from 0.02 to 0.6 day^{-1} [29]. In certain conditions, the rate of growth of sulfate reduction bacteria can be very fast (with doubling times 4 h) [20]. but the averaged growth rates of about 0.1 day^{-1}.[29]

The modeled anaerobic heterotrophic bacteria evolved according to:

$$R_{B\_anae\_het} = C_{B\_anae\_het} - \mathrm{Mort}_{B\_anae\_het} - \mathrm{Graz}_{B\_anae\_het},$$

where

$$C_{B\_anae\_het} = K^{max}_{B\_anae\_het}(\text{DcPM\_NO}_3 + \text{DcDM\_NO}_3 + \text{DcPM\_SO}_4 + \text{DcDM\_SO}_4) f_{B\_anae\_het}(\text{DON} + \text{PON}) B\_anae\_het$$

is the growth rate of B_anae_het connected with denitrification and sulfate reduction of POM and DOM.

$K^{max}_{B\_anae\_het}$ is the maximum specific growth rate of B_anae_het.

$f_{B\_anae\_het}(\text{DON} + \text{PON}) = \frac{\text{PON}+\text{DON}}{\text{PON}+\text{DON}+K^{N}_{B\_anae\_het}}$ is the dependence of maximum specific growth rate of B_anae_het on OM content.

$K^{N}_{B\_anae\_het}$ is a half-saturation constant for the dependence of maximum specific growth rate of B_anae_het on POM and DOM content.

$\text{Mort}_{B\_anae\_het} = K^{Mort}_{B\_anae\_het} B\_anae\_het^2$ is the rate of mortality of B_ae_het with maximum specific rate of mortality $K^{Mort}_{B\_anae\_het}$.

$\text{Graz}_{B\_anae\_het}$ is the grazing of Zoo on B_anae_het.

2.2.6 Anaerobic Autotrophic Bacteria (*B*_anae_aut)

For anoxic layer, a clear dominance of the oxidation of reduced sulfur compounds to fuel chemolithoautotrophy could be demonstrated [29].

The modeled anaerobic heterotrophic bacteria evolved according to:

$$R_{B\_anae\_aut} = C_{B\_anae\_aut} - \text{Mort}_{B\_anae\_aut} - \text{Graz}_{B\_anae\_aut},$$

where

$C_{B\_anae\_aut} = K^{max}_{B\_anae\_aut}(\text{mn\_rd} + \text{fe\_rd} + \text{hs\_ox} + \text{hs\_no3} + \text{hs\_no2} + \text{Disprop})$ $f^{NP}_{B\_anae\_aut}(\text{NH}_4, \text{PO}_4) B\_anae\_aut$ is the growth rate of B_anae_aut connected with sulfide oxidation with Mn, Fe, O_2, NO_3, and NO_2, and disproportionation of S^0.

$K^{max}_{B_anae_aut}$is the maximum specific growth rate of B_anae_aut.

$f^{NP}_{B\_anae\_aut}(\text{NH}_4, \text{PO}_4) = \min\left\{\frac{\text{NH}_4}{\text{NH}_4+K^{N}_{B\_anae\_aut}} \frac{\text{PO}_4}{\text{PO}_4+K^{P}_{B\_anae\_aut}}\right\}$ is the dependence of maximum specific growth rate of B_anae_aut on NH_4 and PO_4, where:

$K^{N}_{B\_anae\_aut}$ and $K^{P}_{B\_anae\_aut}$ are half-saturation constants for the dependence of maximum specific growth rate of B_ae_aut on NH4 and PO4 content.

$\text{Mort}_{B\_anox\_aut} = K^{Mort}_{B\_anox\_aut} B\_anox\_aut^2$ is the rate of mortality of B_anox_aut with maximum specific rate of mortality

$K^{Mort}_{B\_anae\_aut} = 0.001\,\text{day}^{-1}$ if $H_2S < 16$ μM and $K^{Mort}_{B\_anae\_aut} = 0.99\,\text{day}^{-1}$ if $H_2S > 16$ μM.

$\text{Graz}_{B\_anae\_aut}$ is the grazing of Zoo on B_anae_het.

The mortality of anaerobic autotrophic bacteria was assumed to be dependent on H_2S because from observations in the Black Sea (N. Pimenov, 2005, personal communication) an abrupt decrease of dark CO_2 fixation is marked at about $H_2S > 20$ μM. Jost and Pollehne ([29], this volume) described that the lower boundary of the carbon fixation peak in the Baltic Sea is within the sulfidic layer, at a concentration of about 10–15 μM hydrogen sulfide. This sulfide concentration seems to be the upper limit for a peak of enhanced carbon dioxide fixation [33, 69, 73].

2.3 Equations for the Biogeochemical Sources R_C

The list of the formulation for the sources R_C for chemical and biological compartments of the model as an algebraic sum of reactions described above is given in Table 3.

ROLM was coupled as a biogeochemical model with the general ocean turbulent model, GOTM [74], and we used GOTM software to perform numerical calculations and to estimate the vertical diffusion coefficient. The code of ROLM is available along with the GOTM code at http://www.gotm.net.

3 Discussion

The earlier performed applications of ROLM for analyzing the water column redox layer structure enabled common features to be revealed that demonstrate the similarity of the redox-layer formation mechanism in the different geographical regions [5–7].

Modeling results showed that the manganese cycle (formation of sinking Mn (IV) and presence of dissolved Mn(III)) is the main reason of oxygen and hydrogen sulfide absence of direct contact. The particulate manganese may be a primary oxidant of hydrogen sulfide into elementary sulfur. The intense vertical transfer of detritus particles with the heavy particles of Mn(IV) oxide is a cause of the existence of the suboxic zone with no detectable oxygen concentrations. This makes possible the presence processes of anoxic oxidation of reduced compounds, such as methane, reduced iron, and ammonium [5].

The formation of Mn(IV) might considerably affect the distribution of the suspended matter and the formation, the layer of turbidity [75]. The theoretical requirement of the occurrence of seasonal variations of the particulate manganese concentrations was also confirmed by means of the model [5] that treated this phenomenon according to the competition for dissolved oxygen between the OM supplied from the upper layers and the reduced compounds supplied from the hydrosulfide zone. The competition results in the fact that the processes of OM mineralization become more intense in the summer; hence, less oxygen is available

for the oxidation of the reduced forms of manganese, iron, and sulfur. At the same time, more oxygen is available for the formation of particulate manganese and iron. Because of the small concentrations, the role of the iron cycle is insignificant in the processes of the redox interfaces in the water column compared with those in the sediments.

Application of ROLM allowed to explain the formation of so-called "phosphate dipole" [76]. The shallow minimum of phosphate above the sulfidic boundary can be formed due to formation of complexes between Mn(III) and P-containing ligands [6, 10].

The results of applications of this latest version of ROLM are described in the other chapters of this volume [8–10].

Acknowledgements The chapter was supported by project HYPOX 557 (No. EC Grant 226213).

References

1. Yakushev EV, Chasovnikov VK, Murray JW, Pakhomova SV, Podymov OI, Stunzhas PA (2008) Vertical hydrochemical structure of the Black Sea. In: Kostyanoy AG, Kosarev AN (eds) The Black Sea environment. Springer, Berlin, pp 277–307
2. Yakushev EV (1992) Numerical modeling of transformation of nitrogen compounds in the redox zone of the Black Sea. Oceanology 32(2):173–177
3. Yakushev EV, Neretin LN (1997) One-dimensional modeling of nitrogen and sulfur cycles in the aphotic zones of the Black and Arabian Seas. Global Biogeochem Cycles 11(3):401–414
4. Yakushev EV (1998) Mathematical modelling of oxygen, nitrogen, sulfur and manganese cycling in the Black Sea. In: Ivanov L, Oguz T (eds) NATO TU-Black Sea Project. Ecosystem modeling as a tool for the Black Sea. Symposium on scientific results, vol 1. Kluwer Academic, New York, pp 373–384
5. Yakushev EV, Pollehne F, Jost G, Umlauf L, Kuznetsov I, Schneider B (2007) Analysis of the water column oxic/anoxic interface in the Black and Baltic seas with a redox-layer model. Mar Chem 107:388–410
6. Yakushev E, Pakhomova S, Sørenson K, Skei J (2009) Importance of the different manganese species in the formation of water column redox zones: observations and modeling. Mar Chem 117:59–70
7. Yakushev EV, Kuznetsov IS, Podymov OI, Burchard H, Neumann T, Pollehne F (2011) Modeling of influence of oxygenated inflows on biogeochemical structure of the Gotland Sea, central Baltic Sea: changes in distribution of manganese. Comput Geosci 37:398–409
8. He Y, Stanev E, Yakushev E, Staneva J (2011) Numerical modeling of biogeochemical regime response to decadal atmospheric variability during 1960–2000 in the Black Sea. In: Yakushev EV (ed) Chemical structure of pelagic redox interfaces: observation and modeling, Hdb Environ Chem. Springer, Berlin. doi:10.1007/698_2011_103
9. Kamyshny Jr A, Yakushev EV, Jost G, Podymov OI (2010). Role of sulfide oxidation intermediates in the redox balance of the oxic–anoxic interface of the Gotland Deep, Baltic Sea. In: Yakushev EV (ed) Chemical structure of pelagic redox interfaces: observation and modeling, Hdb Environ Chem. Springer, Berlin. doi:10.1007/698_2010_83
10. Pakhomova SV, Yakushev EV (2011) On the role of iron and manganese species in the formation of the redox-interface structure in the Black Sea, Baltic Sea and Oslo Fjord. In: Yakushev EV (ed) Chemical structure of pelagic redox interfaces: observation and modeling, Hdb Environ Chem. Springer, Berlin. doi:10.1007/698_2011_98

11. Yakushev EV, Mikhailovsky GE (1995) Mathematical modelling of the influence of marine biota on the carbon dioxide ocean-atmosphere exchange in high latitudes. In: Jaehne B, Monahan EC (eds) Air-water gas transfer, selected papers from the third international symposium on air-water gas transfer, July 24–27, Heidelberg University. AEON Verlag & Studio, Hanau, pp 37–48
12. Fasham MJ, Ducklow HW, McKelvie SM (1990) A nitrogen-based model of plankton dynamics in the oceanic mixed layer. J Mar Res 48:591–639
13. Fennel W, Neumann T (2004) Introduction to the modeling of marine ecosystems. In: Halpne D (ed) Oceanography, vol 72. Elsevier, Devon, p 298
14. Ayzatulllin TA, Leonov AV (1975) Kinetics and mechanism of the oxidizing transformation of anoxic sulfur compounds in the sea water. Okeanologiya 15(6):1026–1033 (in Russian)
15. Savchuk O, Wulff F (1996) Biogeochemical transformation of nitrogen and phosphorus in the marine environment. Coupling hydrodynamic and biogeochemical processes in models for the Baltic proper. Systems ecology contributions, vol 2. Stockholm University, Stockholm
16. Boudreau BP (1996) A method-of lines code for carbon and nutrient digenesis in aquatic sediments. Comput Geosci 22(5):479–496
17. Oguz T, Ducklow H, Shushkina EA, Malonotte-Rizzoli P, Tugrul S, Lebedeva LP (1998) Simulation of upper layer biochemical structure in the Black Sea. In: Ivanov L, Oguz T (eds) NATO TU-Black Sea Project. Ecosystem modeling as a tool for the Black Sea. Symp. on Sci. Res., vol 2. Kluwer Academic, Norwell, pp 257–299
18. Gregoire M, Beckers J-M, Nihoul JCJ, Stanev E (1997) Coupled hydrodynamic ecosystem model of the Black Sea at basin scale. In: Ozsoy E, Mikaelyan A (eds) Sensitivity to change: Black Sea, Baltic Sea and North Sea. NATO Science Partnership Subseries: 2, vol 7, Kluwer Academic Publishers, The Netherlands, pp 487–499
19. Konovalov SK, Murray JW, Luther GW, Tebo BM (2006) Processes controlling the redox budget for oxic/anoxic water column of the Black Sea. Deep Sea Res (II) 53:1817–1841
20. Canfield DE, Thamdrup B, Kristensen E (2005) Aquatic geomicrobiology. In: Southward AJ, Tyler PA, Young CM, Fuiman LA (eds) Advances in marine biology, vol 48. Elsevier Academic, Amsterdam, p 640
21. Skopintsev BA (1975) Forming of the modern chemical composition of water in the Black Sea. Hydrometizdat, Leningrad (in Russian)
22. Redfield AC (1934) On the proportion of organic derivatives in sea water and their relation to the composition of plankton. James Johnstone Memorial Volume University Press, Liverpool, pp 176–192
23. Richards FA (1965) Anoxic basins and fjords. In: Riley JP, Skirrow G (eds) Chemical oceanography, vol 1. Academic, New York, pp 611–645
24. Ward BB, Kilpatrick KA (1991) Nitrogen transformations in the oxic layer of permanent anoxic basins: the Black Sea and the Cariaco Trench. In: Izdar E, Murray JW (eds) Black Sea oceanography. Kluwer Academic, Norwell, pp 111–124
25. Thamdrup B (2000) Bacterial manganese and iron reduction in aquatic sediments. In: Schrink B (ed) Advances in microbial ecology, vol 16. Plenum, New York, pp 41–84
26. Anderson JJ, Okubo A, Robbins AS, Richards FA (1982) A model for nitrite and nitrate distributions in oceanic oxygen minimum zones. Deep-Sea Res 29:1113–1140
27. Zopfi J, Ferdelman TG, Jorgensen BB, Teske A, Thamdrup B (2001) Influence of water column dynamics on sulfide oxidation and other major biogeochemical processes in the chemocline of Mariager Fjord (Denmark). Mar Chem 74:29–51
28. Lipschultz F, Wofsy SC, Ward BB, Codispoti LA, Friederich G, Elkins JW (1990) Bacterial transformations of inorganic nitrogen in the oxygen-deficient waters of the eastern tropical South Pacific Ocean. Deep Sea Res 37:1513–1541
29. Jost G, Pollehne F (2011) The energetic balance of microbial exploitation of pelagic redox gradients. In: Yakushev EV (ed) Chemical structure of pelagic redox interfaces: observation and modeling, Hdb Environ Chem. Springer, Berlin. doi:10.1007/698_2011_104

30. Rönner U, Sörensson F (1985) Denitrification rates in the low-oxygen waters of the stratified Baltic proper. Appl Environ Microbiol 50:801–806
31. Cline JD, Richards FA (1972) Oxygen deficient conditions and nitrate reduction in the eastern tropical North Pacific Ocean. Limnol Oceanogr 17:885–900
32. Devol AH (1978) Bacterial oxygen uptake kinetics as related to biological processes in oxygen deficient zones of the oceans. Deep-Sea Res 25:137–146
33. Jørgensen BB, Fossing H, Wirsen CO et al (1991) Sulfide oxidation in the anoxic Black Sea chemocline. Deep-Sea Res 38:S1083–S1103
34. Albert DB, Taylor C, Martens CS (1995) Sulfate reduction rates and low molecular weight fatty acid concentrations in the water column and surficial sediments of the Black Sea. Deep-Sea Res I 42:1239–1260
35. Hastings D, Emerson S (1988) Sulfate reduction in the presence of low oxygen levels in the water column of the Cariaco Trench. Limnol Oceanogr 33:391–396
36. Brettar I, Moore ERB, Höfle MG (2001) Phylogeny and abundance of novel denitrifying bacteria isolated from the water column of the central Baltic Sea. Microb Ecol 42:295–305
37. Labrenz M, Jost G, Jürgens K (2007) Distribution of abundant prokaryotic organisms in the water column of the central Baltic Sea with an oxic-anoxic interface. Aquat Microb Ecol 46:177–190
38. Kuypers MMM, Sliekers AO, Lavik G, Schmid M, Jorgensen BB, Kuenen JG, Sinnenghe Damste JS, Strous M, Jetten MSM (2003) Anaerobic ammonium oxidation by anammox bacteria in the Black Sea. Nature 422:608–611
39. Dalsgaard T, Canfield DE, Petersen J, Thamdrup B, Acuna-Gonzalez J (2003) N2 production by the anammox reaction in the anoxic water column of Golfo Dulce, Costa Rica. Nature 422:606–608
40. Hannig M, Lavik G, Kuypers MMM et al (2007) Shift from denitrification to anammox after inflow events in the central Baltic Sea. Limnol Oceanogr 52:1336–1345
41. Murray JW, Yakushev EV (2006) The suboxic transition zone in the Black Sea. In: Neretin LN (ed) Past and present water column anoxia. NATO Sciences Series. Springer, Dordrecht, p 105
42. Jetten MSM, Strous M, van de Pas-Schoonen KT et al (1999) The anaerobic oxidation of ammonium. FEMS Microbiol Rev 22:421–437
43. Jensen MM, Kuypers MMM, Lavik G et al (2008) Rates and regulation of anaerobic ammonium oxidation and denitrification in the Black Sea. Limnol Oceanogr 53:23–36
44. Volkov II (1974) Geokhimiya sery v osadkah okeana (Geochemistry of sulfur in the ocean sediments). Nauka, Moscow, p 272 (in Russian)
45. Kostka JE, Luther GW III, Nealson KH (1995) Chemical and biological reduction of Mn(III)-pyrophosphate complexes: potential importance of dissolved Mn(III) as an environmental oxidant. Geochim Cosmochim Acta 59:885–894
46. Webb SM, Dick GJ, Bargar JR, Tebo BM (2005) Evidence for the presence of Mn(III) intermediates in the bacterial oxidation of Mn(II). Proc Natl Acad Sci USA 102:5558–5563
47. Caspi R, Haygood MG, Tebo BM (1996) Unusual ribulose-1,5-bisphosphate carboxylase/oxygenase genes from a marine manganese-oxidizing bacterium. Microbiology 142:2549–2559
48. Tebo BM (1991) Manganese(II) oxidation in the suboxic zone of the Black Sea. Deep-Sea Res II 38:S883–S905
49. Neretin LN, Pohl C, Jost G et al (2003) Manganese cycling in the Gotland Deep, Baltic Sea. Mar Chem 82:125–143
50. Richardson LL, Aguilar C, Nealson KH (1988) Manganeses oxidation in pH and O_2 microenvironments produced by phytoplankton. Limnol Oceanogr 33(3):352–363
51. Yao W, Millero F (1996) Adsorption of Phosphate on Manganese Dioxide in Seawater. Environ Sci Technol 30:536–541
52. Nealson KH, Myers CR, Wimpee BB (1991) Isolation and identification of manganese reducing bacteria and estimates of microbial Mn(IV)-reducing potential in the Black Sea. Deep-Sea Res (II) 38:907–920

53. Dollhopf ME, Nealson KH, Simon DM, Luther GW III (2000) Kinetics of Fe(III) and Mn(IV) reduction by the Black Sea strain of Shewanella Putrefaciens using in situ solid state voltammetric AU/Hg electrodes. Mar Chem 70:171–180
54. Trouwborst RE, Brian GC, Tebo BM, Glazer BT, Luther GW III (2006) Soluble Mn(III) in suboxic zones. Science 313:1955–1957
55. Ali K, Ashiq U (2004) Study of the kinetics and activation parameters of reduction of Mn(III) to Mn(II) by SO_3^{2-} ion in $(MnSiW_{11}O_{40}H_2)_5$-heteropoly ion. J Iran Chem Soc 1:122–127
56. Nealson KN, Stahl DA (1997) Microorganisms and biogeochemical cycles: what can be learn from layered microbial communities? In: Banfield JF, Nealson KN (eds) Geomicrobiology: interactions between microbes and minerals, reviews in mineralogy, vol 35. Mineralogical Society of America, Washington, pp 5–34
57. Savenko AV (1995) Precipitation of phosphate with iron hydroxide forming by mixing of submarine hydrothermal solutions and the sea water (on the base of experimental data). Geochem Int 9:1383–1389
58. Savenko AV, Baturin GN (1996) Experimental study of the sorption of phosphorus on manganese dioxide. Geochem Int 5:472–474
59. Sergeev YN (ed) (1979) Modelirovaniye Perenosa i Transformatsii Veshchestv v More (Modeling of transport and transformation of substances in the sea). Leningrad State Univ., St. Petersburg, Russia, p 296 (in Russian)
60. Steele JH, Frost BW (1977) The structure of plankton communities. Phil Trans R Soc A 280:485–534
61. Zubkov MV, Sazhin AF, Flint MV (1992) The microplankton organisms at the oxic-anoxic interface in the pelagial of the Black Sea. FEMS Microbiol Ecol 101:245–250
62. Anderson R, Weber F, Wylezich C et al (2011) Protist diversity, distribution and bacterivory in Baltic Sea pelagic redoxclines. In: ASLO 2011 aquatic sciences meeting, San Juan, Puerto Rico
63. Detmer AE, Giesenhagen HC, Trenkel VM et al (1993) Phototrophic and heterotrophic pico- and nanoplankton in anoxic depths of the central Baltic Sea. Mar Ecol Prog Ser 99:197–203
64. Moiseev EV, Mamaeva NV (1979) Protozoa of the upper layer of the hydrogen sulphide zone in the Black Sea. Rep Acad Sci USSR 248(2):506–508
65. Stoek T, Taylor GT, Epstein SS (2003) Novel eukaryotes from the permanently anoxic Cariaco basin (Caribbean Sea). Appl Environ Microbiol:5656–5663
66. Fenchel T, Kristensen LD, Rasmussen L (1990) Water column anoxia: vertical zonation of planktonic protozoa. Mar Ecol Prog Ser 62:1–10
67. Weinbauer MG, Brettar I, Höfle MG (2003) Lysogeny and virus-induced mortality of bacterioplankton in surface, deep, and anoxic marine waters. Limnol Oceanogr 48:1457–1465
68. Ward BB (2008) Nitrification in marine systems. In: Capone DG, Bronk DA, Mulholland MR, Carpenter EJ (eds) Nitrogen in the marine environment. Academic, Amsterdam, pp 199–261
69. Jost G, Martens-Habbena W, Pollehne F et al (2010) Anaerobic sulfur oxidation in the absence of nitrate dominates microbial chemoautotrophy beneath the pelagic chemocline of the eastern Gotland Basin, Baltic Sea. FEMS Microbiol Ecol 71:226–236
70. Wuchter C, Schouten S, Boschker HTS et al (2003) Bicarbonate uptake by marine Crenarchaeota. FEMS Microbiol Lett 219:203–207
71. Lam P, Jensen MM, Lavik G et al (2007) Linking crenarchaeal and bacterial nitrification to anammox in the Black Sea. Proc Natl Acad Sci USA 104:7104–7109
72. Enrich-Prast A, Bastviken D, Crill P (2009) Chemosynthesis. In: Likens GE (ed) Encyclopedia of inland waters. Academic, Oxford
73. Taylor GT, Iabichella M, Ho T-Y et al (2001) Chemoautotrophy in the redox transition zone of the Cariaco Basin: a significant midwater source of organic carbon production. Limnol Oceanogr 46:148–163
74. Burchard H, Bolding K, Kuhn W, Meister A, Neumann T, Umlauf L (2006) Description of flexible and extendable physical-biogeochemical model system for the water column. J Mar Syst 61:180–211

75. Yakushev EV, Debolskaya EI (2000) Particulate manganese as a main factor of oxidation of hydrogen sulfide in redox zone of the Black Sea. In: Oceanic fronts and related phenomena. Konstantin Fedorov Memorial symposium, Pushkin, Saint-Petersburg, Russia, 18–22 May 1998. Proceedings. IOC Workshop Report No. 159. Kluwer Academic, New York, pp 592–597
76. Shaffer G (1986) Phosphate pumps and shuttles in the Black Sea. Nature 321:515–517
77. Kuypers MM, Blokker P, Erbacher J et al. (2001) Massive expansion of marine archaea during a mid-Cretaceous oceanic anoxic event. Science 293:92–95
78. Kuypers MMM, Lavik G, Woebken D et al. (2005) Massive nitrogen loss from the Benguela upwelling system through anaerobic ammonium oxidation. Proc Natl Acad Sci USA 102:6478–6483

Modelling of the Meromictic Fjord Hunnbunn (Norway) with an Oxygen Depletion Model (OxyDep)

E.V. Yakushev, E.I. Debolskaya, I.S. Kuznetsov, and A. Staalstrøm

Abstract A biogeochemical model OxyDep coupled with three-dimensional hydrodynamic model GETM was used to simulate the hydrophysical and biogeochemical regimes of the meromictic Fjord Hunnbunn over the summer period. The main goal was to parameterize the oxygen depletion processes resulting in formation of suboxic and anoxic conditions in the water column. OxyDep considered five state variables: dissolved oxygen, inorganic nutrient, dissolved organic matter, particulate organic matter, and biota. This model parameterized the main processes responsible for the changing of the water column oxygen conditions – i.e. organic matter (OM) synthesis; OM decay due to oxic mineralization and denitrification; consumption of oxygen from sulphur and metals oxidation; and the processes at the boundaries (air–water exchange and the sediment–water exchange). Results of numerical experiments have reproduced the main features of the observed structure and have allowed to reveal the main components responsible for the formation of biogeochemical structure of the meromictic water objects. With the hydrodynamical model block used it was impossible to reproduce the presence of a permanent pycnocline. We suppose that special attention must be paid when using terrain following vertical coordinates (i.e. GETM) to avoid spurious vertical mixing. The results also showed that an application of simplified biogeochemical model blocks can be used as a useful tool for analysing and forecasting oxygen and nutrient regime changes.

E.V. Yakushev (✉) and A. Staalstrøm
Norwegian Institute for Water Research, Gaustadalleen 21, 0349 Oslo, Norway
e-mail: eya@niva.no

E.I. Debolskaya
Water Problems Institute of The Russian Academy of Science, Gubkina 3, 119991 Moscow, Russia

I.S. Kuznetsov
Leibniz Institute for Baltic Sea Research, Warnemünde, Seestrasse 15, 18119 Rostock, Germany

E.V. Yakushev (ed.), *Chemical Structure of Pelagic Redox Interfaces: Observation and Modeling*, Hdb Env Chem (2013) 22: 235–252, DOI 10.1007/698_2011_110,

Keywords Anoxia, Hydrogen sulphide, Hypoxia, Modelling, Oxygen depletion, Stratified basin

Contents

Abbreviations

BIO	Biota
DIN	Dissolved inorganic nitrogen (i.e. a sum of nitrate, nitrite, and ammonia)
DOM	Dissolved organic matter
GETM	General Estuarine Transport Model
NUT	Inorganic nutrient
OM	Organic matter
OXY	Dissolved oxygen
OxyDep	Oxygen Depletion biogeochemical model
POM	Particulate organic matter
PSU	Practical salinity units

1 Introduction

Oxygen depletion and anoxia formation are common features observed in many inland waters and coastal areas. These conditions arise, when transport rates of organic matter (OM) and oxygen into deeper layers do not balance and oxygen is used up during OM decomposition. The OM decomposition then continues via denitrification (consumption of oxidized forms of nitrogen: nitrate, NO_3 and nitrite, NO_2), and finally with reduction of sulphate (a major constituent in seawater). According to recent estimates [1], dead zones connected with low oxygen content have spread exponentially since the 1960s. Formation of oxygen-deficient, hypoxic, and anoxic conditions depend on the combined influence of eutrophication (amounts of nutrient loading) and intensity of mixing and water renewal.

The natural state of such complex systems with changeable redox conditions can be efficiently analyzed with mathematical models. The problem of an elaboration of a biogeochemical block for different redox conditions is connected with a necessity

of parameterizing switches between the processes dominating in oxic conditions (i.e. nitrification), hypoxic conditions (denitrification), and suboxic conditions (loss of oxygen for mineralization of reduced forms of sulphur and redox metals).

As mentioned in another chapter of this book [2], a threshold from oxic to hypoxic conditions is arbitrarily set at a bounding value of 2 mg O_2 L^{-1} (~63 μM O_2). Such thresholds can be connected with responses and vulnerability of pelagic and benthic animals, usually in the range of 1–4 mg O_2 L^{-1} [3]. The threshold between hypoxic and suboxic conditions (about 10–30 μM O_2 [4]) should reflect the oxygen level where oxygen becomes an auxiliary oxidant compared with nitrates and oxidized forms of metals.

The goal of this study was to elaborate a simplified biogeochemical model for the oxygen regime simulation and to apply it for a concrete object. This model should parameterize the changes in the biogeochemical processes in case of change of the oxygen concentrations from oxic to suboxic levels. We used a coupled Oxydep/GETM model to calculate the seasonal variability of the meromictic Fjord Hunnbunn.

2 Materials and Methods

2.1 Hunnbunn Hydrophysical and Hydrochemical Structure

At present, the Fjord Hunnbunn (Fig. 1) is a natural meromictic pool with the high concentrations of hydrogen sulphide in deep layers. Stratification of the lake is caused by a strong halocline. Wind and tidal waves arriving from the sea through the narrow channel Talbergsundet (length of 1.8 km) are mixed in the upper 2 m less saline layer, while the saline bottom layer remains unmixed. The maximum depth of the Fjord is about 11 m [5, 6].

Meanwhile, a history of the observations in the Hunnbunn reveal that the oxygen conditions there were much better in the past. Information from the past indicates that there were oysters in the nineteenth century [6]. An intensive eutrophication period and an absence of periodic dredging after the 1950s resulted in changes of the surface layer ecosystem: disappearance of the oysters, decline of seagrass beds, appearance of large amounts of green algae.

The present vertical hydrochemical structure of the Fjord Hunnbunn (Fig. 2) is typical for the coastal objects with anoxic conditions in the water column.

In 2009, the chemical structure of Hunnbunn was studied twice: in spring, 07.05.2009 and in late summer, 19.08.2009. We used a specially designed pump system for the redox-layers studies that allowed us to sample water with fine-scale resolution and prevented atmospheric oxygen from interfering with our results. The analytical determinations were made at the NIVA chemical laboratory according to the accredited national and international techniques [7]. During sampling, we used an AADI Oxygen Optode to measure the in situ oxygen concentrations.

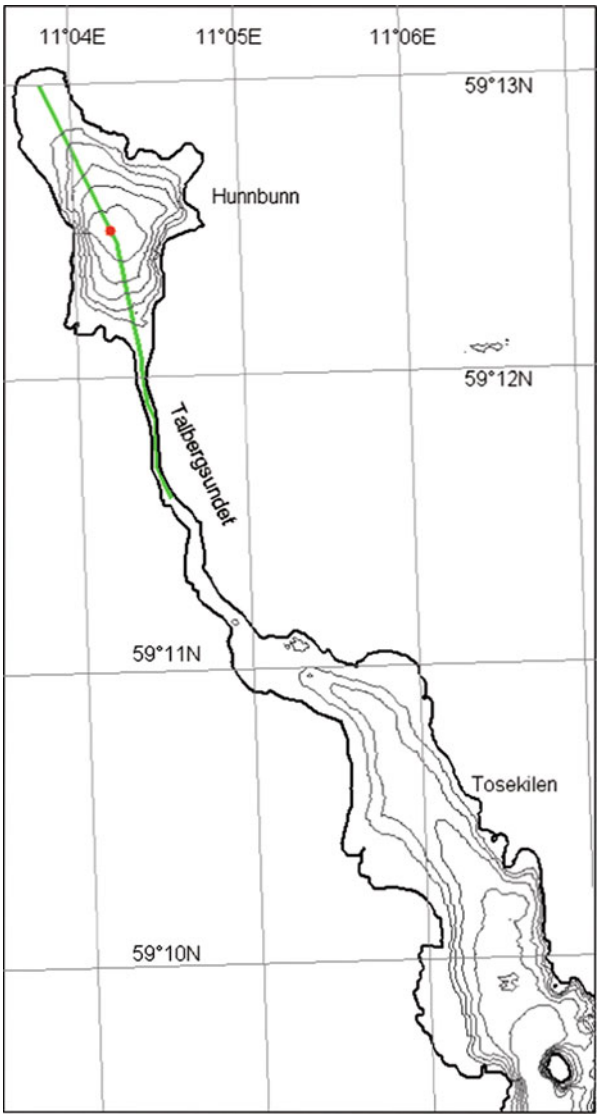

Fig. 1 A map of the Fjord Hunnbunn. Depth isolines are shown with 2-m interval. The position of hydro chemical data is marked with a red dot

The results of the studies performed in August 2009 are shown in Fig. 2. The vertical hydrochemical structure is typical for coastal objects with anoxic conditions in the water column. The concentration of dissolved inorganic nitrogen DIN (a sum of nitrate, nitrite, and ammonia) in the surface layer in May were high (5 μM), and concentrations of phosphate (0.06 μM) were low. Just below the oxygen maximum, at 4 m, the concentrations of phosphate increased to 6.5 μM, while concentrations of DIN decreased to 0.4 μM. There were no measurements in

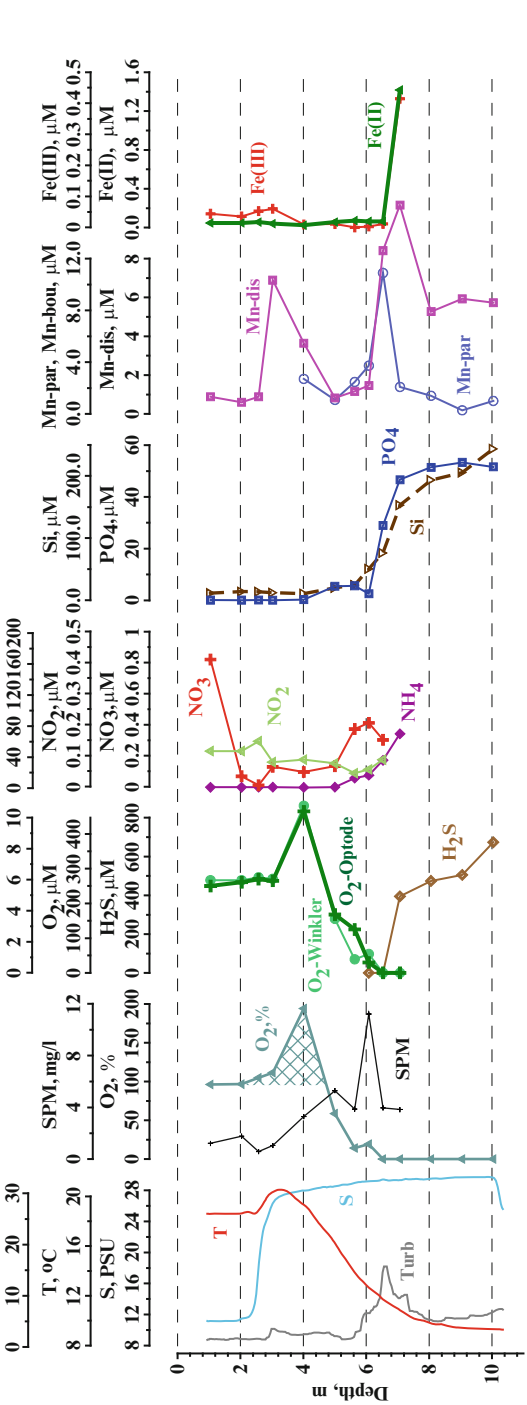

Fig. 2 Vertical hydrochemical structure of Hunnbunn 19.08.2009. *T* temperature, *S* salinity, *Turb* Turbidity, O_2% oxygen in percentages, *SPM* suspended particulate matter, *O2-Winkler* oxygen determined with Winkler technique, *O2-Optode* oxygen determined with AANDERAA Optode, H_2S hydrogen sulphide, NO_3 nitrate, NO_2 nitrite, NH_4 ammonium, PO_4 phosphate, *Si* silicate, *Mn-dis* dissolved manganese, *Mn-part* particulate manganese, *Fe(III)* dissolved trivalent iron, *Fe(II)* dissolved bivalent iron (from [5])

the vicinity of the oxygen maximum peak, but it is possible to assume that in May there were enough nutrients to support the high primary production.

In August, we made a fine resolution sampling for both oxygen and for nutrients. The oxygen concentration was slightly less than in May (10.7 ml/l in August), but the saturation value exceeded 194%, indicating very high primary production. In the vicinity of the oxygen maximum, we found 0.33 μM of phosphate, 1.2 μM DIN, and 10 μM of silicate. The vertical gradient of phosphate was more than 5 μM m^{-1} and DIN was 12 μM m^{-1}. Such large gradients ensure a permanent flux of nutrients from anoxic zone, sufficient to support the constant extremely high primary production throughout the year. The data received in August, 2009, revealed that below the depth of oxygen and nitrate depletion, reduced forms of sulphur (hydrogen sulphide), nitrogen (ammonia), manganese (Mn(II)), and iron (Fe(II)) were present. The concentrations of hydrogen sulphide increased in the bottom layer (10 m) to more than 600 μM (for a comparison, in the Black Sea the concentrations of hydrogen sulphide are 380 μM at the depth of 2,000 m). The concentrations of ammonia and phosphate in the Hunnbunn bottom layer are extraordinarily high and correspond to their concentrations in the pore water of the sediments from productive regions. All this indicates a very high level of OM concentrations in the Hunnbunn sediments and the bottom layer.

The concentrations of reduced forms of Mn and Fe are typical for the anoxic waters [8]. Mn does not accumulate in OM, and its distribution is determined by the flux from the sediments, if the water above is anoxic. That is why the observed maximum concentration of Mn(II) in Hunnbunn (12 μM) is comparable with that in the Black Sea (10–12 μM) and the Gotland Deep of the Baltic Sea (5–30 μM). Usually, Mn species are not observed in the oxic layer, because the oxidized heavy particles of Mn(IV) sink down just after their formation. The presence of significant concentrations of Mn and Fe species in the oxic zone points to an existence of their flux from the shore, that can also be observed in some other coastal regions.

The permanently observed redox-layer turbidity maximum in the Fjord Hunnbunn is a typical feature of anoxic systems. The nature of this turbid layer is not clear yet, but it is known that particulate forms of sulphur (element sulphur), manganese, iron, and bacteria can be found there. In case of the Fjord Hunnbunn, an additional large contribution to the turbidity can be made by photosynthetic purple bacteria, that can oxidize hydrogen sulphide using light. Usually, they are found in the upper part of the turbidity maximum and sometimes the turbidity maximum has two peaks as was observed in May 2009. The turbidity maximum in the Fjord Hunnbunn, might also be a "joint" maximum, where the redox-layer turbidity maximum combines with the phytoplankton maximum, typical for all the surface waters.

At present the OM produced in the Fjord Hunnbunn accelerates the depletion of oxygen and production of hydrogen sulphide, that lead to a positive feedback in a further increase in the flux of nutrients to the euphotic zone.

The anoxic layers of Fjords as Hunnbunn can be flushed with the a pulse of oxygen-rich cold water during the winter mixing either every year (Elefsis Bay in the Mediterranian Sea [9]) or every several years (Baerumsbassenget in the Oslo Fjord [10]) or every several decades (Fjord Framvaren). The probability of the

winter mixing depends on the topography, hydrophysical regime, and climate (weather conditions during the winter). The permanent pycnocline that exists in the Fjord Hunnbunn at the depth 2.5–3 m greatly hampers the flushing of the bottom layer.

2.2 GETM Application and Set Up

The model GETM (http://www.getm.eu) was used to simulate hydrodynamic and thermal regime of the Fjord, connected with the time-dependent changes in stratification and an influence of the tidal wave coming through the narrow channel. The density stratification changed in the Fjord not only due to meteorological factors, but with the seasonal fluctuations in salinity of water flowing through the channel [6]. The period of the tidal wave equaled to 12 h, the amplitude at the entrance to the lake was 0.5 m. The salinity at the entrance to the Fjord varied between 27 PSU in winter to 7 PSU during the spring flood.

These model simulations covered one year with a horizontal resolution of 50×50 m and 10 vertical layers. GETM is a terrain following model (sigma-coordinates model) and the vertical grid step changed from 20 cm to 1 m. The simulation is carried out on a grid with $90 \times 47 \times 10$ points. The time-step of calculations was 2 s.

The model was forced by the atmospheric forcing (seasonal changes in temperature and wind), and by providing information on temperature, salinity, and sea surface elevations at the lateral boundaries.

Freshwater discharge was not included in this simulation, because there are no significant fresh water flowing into Hunnbunn.

The general equation that is used for the coupled hydrodynamical–biogeochemical models is the following:

$$\frac{\partial C}{\partial t} + \nabla C\vec{V} - \nabla(K\nabla C) = R_C - \frac{\partial}{\partial z}(w_C C) \tag{1}$$

Where the first term reflects the changes with time, the second term reflects advective transport, and the third term reflects turbulent exchange. R_C is the biogeochemical sink/source terms for the considered variables, C is the concentration of a variable and w_C is the sinking rate of the particulate matter. We used GETM to calculate the velocities ($\vec{V}$) and the turbulent coefficient (K).

2.3 OxyDep Description

The idea behind OxyDep is to parameterize the changes of the biogeochemical processes in the water column and at the sediment/water boundary in case of

Table 1 State variables of the OxyDep

Variable	Meaning	Units
BIO	That is all the biota from bacteria to fish. BIO grows due to photosynthesis, loses inorganic matter due to respiration, and loses total (particulate and dissolved) organic matter due to metabolism, mortality, cannibalism, etc.	μM N
NUT	That is the oxidized forms of nutrients (i.e. NO_3 and NO_2 for N), that don't need additional oxygen for nitrification.	μM N
POM	That is all kinds of labile particulate organic matter (detritus).	μM N
DOM	That is all kinds of labile dissolved organic matter and reduced forms of inorganic nutrients (i.e. NH_4 and Urea for N).	μM N
OXY	Concentrations of dissolved oxygen.	μM O

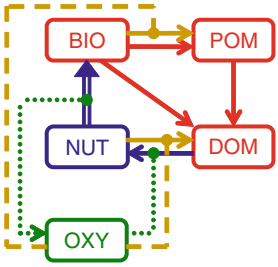

Fig. 3 Flow-chart of biogeochemical processes in the OxyDep

transition from oxic to suboxic conditions, and from suboxic to anoxic conditions in the simplest possible way. We aimed to receive a simple tool capable of being coupled to detailed 3D models (i.e. GETM [11], ROMS [12], HAMSOM/ECOSMO [19]) first of all for applications in shallow water, i.e. estuaries, inlets, and Fjords.

The amount of variables (Ci) and processes included in the parameterizations should depend on the different processes' time scales and the scales of concentrations [13]. In case of studying the behaviour of large concentration scale parameters (i.e. oxygen and nutrient, with characteristic concentrations of 10^1–10^2 μM) at relatively large time scale (seasonal) it is possible to merge the biological variables in one compartment (with characteristic concentrations less than 10^{-2}–10^{-1} μM) that was made here. List of the state variables (C_i) of the model is presented in the Table 1.

The flow-chart of biogeochemical processes considered in the OxyDep is shown in Fig. 3. Notations, values, units, and names of the model's parameters are given in Table 2. The biogeochemical changes of the considered variables, $R_{Ci,}$ were described with the following system of equations:

$$R_{BIO} = GrowthBIO - RespBIO - ExcrBIO - MortBIO$$
$$R_{POM} = -DissPOM + MortBIO - DecayPOM$$
$$R_{DOM} = DissPOM + ExcrBIO - DecayDOM$$
$$R_{NUT} = -GrowthBIO + RespBIO + DecayPOM + DecayDOM - DenitrOM$$
$$R_{OXY} = C_{OtoN}R_{NUT} + SMnOXY$$

Table 2 Notations, values, units, and names of parameters used in the model

Notation	Value	Units	Parameter
$GrowthBIO$		d^{-1}	Specific growth rate
$f_i(i)$		–	Photosynthesis dependence on irradiance
$f_\varphi(\varphi)$		–	Irradiance dependence on latitude
$f_t(t)$		–	Photosynthesis dependence on temperature
$f_n(NUT)$		–	Photosynthesis dependence on nutrient
K_{NB}	4.0	d^{-1}	Maximum specific growth rate
I_0	80.	W m^{-2}	Optimal Irradiance at the surface
k	0.10	m^{-1}	Extinction coefficient
I_{opt}	25.	W m^{-2}	Optimal irradiance
b_m	0.12	$°C^{-1}$	Coefficient for uptake rate dependence on t
c_m	1.4	–	Coefficient for uptake rate dependence on t
K_{NUT}	0.02	–	Half-saturation constant for uptake of NUT by BIO
K_{BN}	0.05	d^{-1}	Specific respiration rate
K_{BP}	0.01	d^{-1}	Specific rate of mortality in oxic conditions
K_{BD}	0.10	d^{-1}	Specific rate of excretion
K_{BP}^A	0.5	d^{-1}	Specific rate of mortality in anoxic conditions
K_{BP}^C	0.6	d^{-1}	Specific rate of additional mortality (cannibalism)
BIO_{Can}	1.	μM N	Threshold BIO value for cannibalism
K_{Can}	0.8	–	Coefficient for the cannibalism description
K_{PD}	0.10	d^{-1}	Specific rate of POM decomposition (autolis)
DecayDOM		d^{-1}	Mineralization of POM
K_{POM}	0.003	d^{-1}	Specific rate of POM oxic decay
K_{POM}^S	0.001	d^{-1}	Specific rate of POM denitrification
DecayDOM		d^{-1}	Mineralization of DOM
K_{DOM}	0.05	d^{-1}	Specific rate of DOM oxic decay
K_{DOM}^S	0.0005	d^{-1}	Specific rate of DOM denitrification
t_{da}	13.	–	Coefficient for dependence of decay on t
Bda	20.	–	Coefficient for dependence of decay on t
B_u	0.22	d^{-1} m^{-1}	Burial coefficient for lower boundary
NUT_{Den}	1.	μM N	Threshold NUT value for denitrification
C_{OtoN}	−8,625	–	O to N Redfield ratio (138/16)
$f_s(OXY)$		–	Function parameterizing a switches between oxic and suboxic processes
O_2^{bf}	20	μM O	Oxygen threshold concentration, in which the changes between suboxic and oxic processes occur
τ_L	100,000	s	Relaxation time
C_{L0}^O	0	μM O	Concentrations of OXY in the sediments in oxic conditions
C_{Li}^O	0	μM O	Concentrations of OXY in the sediments in suboxic conditions
C_{L0}^D	2	μM N	Concentrations of DOM in the sediments in oxic conditions
C_{Li}^D	5	μM N	Concentrations of DOM in the sediments in suboxic conditions
a_0	31.25	μM O,	Coefficient for the oxygen saturation calculations
a_1	14.603		Coefficient for the oxygen saturation calculations
a_2	0.4025	$°C^{-1}$	Coefficient for the oxygen saturation calculations
w_C	0.5	m d^{-1}	Sinking velocity

These biogeochemical sources where added to the general equation. These processes were parameterized as follows:

The specific growth rate of BIO,

$$GrowthBIO = K_{NB}\, f_t(t)\, f_i(i)\, f_n(NUT)BIO$$

is a function of temperature, light, and availability of nutrients with the maximum specific growth rate K_{NB}.

To describe the dependence of light in accordance to:

$$f_i(i) = f_\varphi(\varphi)\frac{i}{I_{opt}}\exp\left(1-\frac{i}{I_{opt}}\right).$$

we used the following parameters: light (i = $I_0 exp(-kh)$), incident light (I_0), optimal light (I_{opt}), extinction coefficient (k), depth (h), and variation of light with latitude and time:

$$f_\varphi(\varphi) = \cos\left(\varphi - \varphi_e \sin\left(2T/365.2\right)\right),$$

where T is time (days) and φ is latitude (degrees), $\varphi_e = 23.5$ is the ecliptic degree.

The following formula was chosen for dependence on temperature (t) with the coefficients b_m and c_m:

$$f_t(t) = \exp(b_m t - c_m).$$

A dependence with fast saturation of nutrient availability was used for NUT limitation description instead of traditional Michaelis–Menten formula:

$$f_n(NUT) = \frac{(NUT/BIO)^2}{(NUT/BIO)^2 + K_{NUT}^2},$$

where K_{NUT} is a "half saturation constant" for this dependence.

BIO respiration is described by specific rate of respiration K_{BN} as

$$RespBIO = K_{BN}BIO.$$

The excretion rate of *BIO* with specific rate of excretion K_{BD} was described as

$$ExcrBIO = K_{BD}BIO.$$

The natural mortality rate of BIO with specific rates of mortality K_{BP} in oxic and K_{BP}^A in anoxic conditions was described as:

$$\begin{aligned} MortBIO = {} & K_{BP}\mathrm{BIO} + f_S(\mathrm{OXY})K_{BP}^A\mathrm{BIO} \\ & + K_{BP}^C(0.5(1 - \tanh(BIO_{Can} - K_{Can}\mathrm{BIO})\mathrm{BIO}. \end{aligned}$$

The last term was added to parameterize an additional mortality due to "cannibalism", that starts when the BIO concentrations exceeds the threshold value BIO_{Can}.

We considered the formation of DOM from POM (autolysis) with a constant specific rate as:

$$DissPOM = K_{PD}POM.$$

The DOM decay took place due to oxic decay in oxic conditions (first term in the following equation) and denitrification in suboxic conditions (second term):

$$DecayDOM = K_{DOM}f_t^D(t)\mathrm{DOM} + K_{DOM}^S f_t^D(t) f_S(\mathrm{OXY}) f_N^D(\mathrm{NUT})\mathrm{DOM},$$

where $f_t^D(t)$ and $f_t^D(\mathrm{NUT})$ are dependences of decay on temperature and NUT.

The POM decay was parameterized as:

$$DecayPOM = K_{POM}f_t^D(t)\mathrm{POM} + K_{POM}^S f_t^D(t) f_S(\mathrm{OXY}) f_N^D(\mathrm{NUT})\mathrm{POM}.$$

The dependences of decay on temperature, $f_t^D(t)$, was parameterized as:

$$f_t^D(t) = B_{da}\frac{t^2}{t^2 + t_{da}^2},$$

where B_{da} and t_{da} are temperature control coefficients, and $f_t^D(\mathrm{NUT})$ is the dependences of decay on NUT (checking for availability of NO_3 and NO_2 necessary for denitrification).

$$f_N^D(\mathrm{NUT}) = 0.5(1 + \tanh(NUT - NUT_{Den})),$$

where NUT_{Den} is a threshold value.

The changes between the processes occurring in oxic and suboxic conditions were parameterized with soft switches based on hyperbolic tangents functions shown in Fig. 4:

$$f_O(\mathrm{OXY}) = 1 - 0.5\left(1 + \tanh\left(\mathrm{OXY} - {O_2}^{\mathrm{bf}}\right)\right)$$

and

$$f_S(\mathrm{OXY}) = 0.5\left(1 + \tanh\left(\mathrm{OXY} - {O_2}^{\mathrm{bf}}\right)\right),$$

where ${O_2}^{\mathrm{bf}}$ is a constant that defines the oxygen concentration, in which the changes occur.

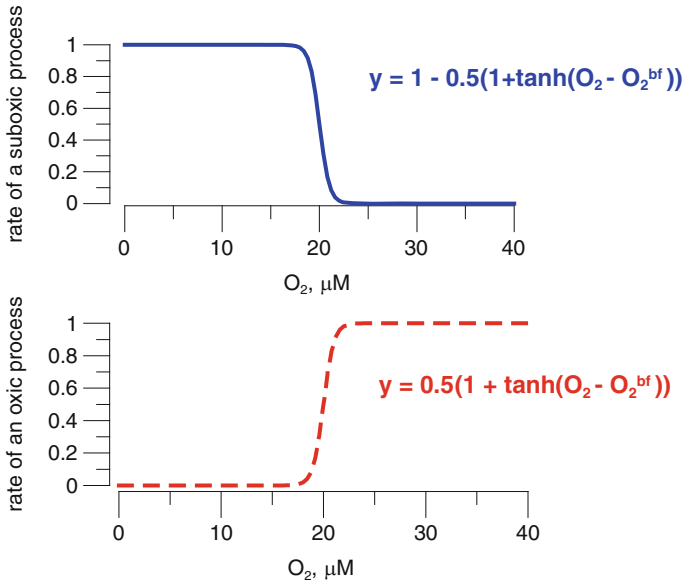

Fig. 4 Functions used as switches between oxic and suboxic processes (shown in Table 1.) assuming oxygen concentration $O_2^{bf} = 20$ μM as a threshold value

Changes in the OXY content were calculated with the Redfield ratio. Besides this, we parameterized an additional sink of oxygen for oxidation of reduced forms of sulphur and Mn. On the base of the estimates received in [14], we assumed for the oxygen deficient and suboxic conditions the consumption of oxygen for the mentioned purpose is similar to that for ammonia (that is a dominant part of DOM in OxyDep):

$$SMnOXY = f_S(\mathrm{OXY})K_{DOM}f_t^D(t)\mathrm{DOM}.$$

Changes in the NUT due to denitrification on particulate and dissolved organic were described as:

$$\begin{aligned} DenitrOM = {} & K_{POM}^S f_t^D(t) f_S(\mathrm{OXY}) f_N^D(\mathrm{NUT})\mathrm{POM} \\ & + K_{DOM}^S f_t^D(t) f_S(\mathrm{OXY}) f_N^D(\mathrm{NUT})\mathrm{DOM}. \end{aligned}$$

Loss of NUT for oxidation of the reduced forms of sulphur and metals was ignored.

Therefore, OxyDep parameterize the changes in the main biogeochemical processes connected with variations of oxygen concentrations between high normoxic to suboxic, with following oxygen depletion to 0.

Notations, values, units, and names of parameters used in the model are given in Table 2.

2.4 Sinking

The sinking parameterized as the last term of equation (1) was considered for BIO and POM with the same sinking velocity $w_{C.}$ (Table 2).

2.5 Boundary Conditions

In case of the upper boundary, the surface fluxes of the modelled chemical constituents were assumed to be zero, except for OXY. The O_2 surface flux is prescribed by:

$$Q_{O_2} = p_{vel}(Oxsat - OXY),$$

where p_{vel} is the wind coefficient, $Oxsat = a_0(a_1 + a_2t)$ is the concentration of oxygen saturation as a function of temperature t, according to [15].

Simulations were carried out based on a mean wind speed of 2 m s^{-1}.

Parameterization of the lower boundary conditions under changing redox conditions requires description of changes in intensity and even directions of fluxes of certain parameters.

For particulate organic matter (BIO, POM), we assumed the decrease of concentrations due to burial (modified on the base of an approach used in [16]):

$$Q_{C_i} = -B_u H_{vert} C_i,$$

where B_u is the burial rate. H_{vert} is the model's vertical resolution.

The changes of the bottom layer concentrations of DOM and NUT in oxic conditions, following the approach used in [17], we parameterized as:

$$Q_{C_i} = \tau_L^{-1}(C_{Li} - C_i).$$

The term on the right hand side describes a "relaxation" of C_i towards the constant C_{Li} in the sediment with the relaxation time scale τ_L. This term is used to ensure that the "observed" concentration in the sediment does not exceedingly diverge from simulated C_i which is strongly influenced by biogeochemical processes and by the horizontal advection.

When oxic conditions are present in the bottom water, the flux of oxygen nitrate into the sediments along with the absence of fluxes of H_2S, Mn(II), Fe(II) into the water should be observed.

In the case of suboxic conditions in the bottom water, there should be an increased flux of oxygen into the sediments. To reflect this we assumed for OXY:

$$Q_{C_i} = \tau_L^{-1}(C_{Li}^O - OXY) + f_s(OXY)\tau_L^{-1}(C_{L0}^O - OXY),$$

where C_{Li}^O and C_{L0}^O are concentrations of OXY in the sediments in oxic and suboxic conditions The same dependence was used for NUT, that should reflect the flux of nitrate into the sediments necessary to support denitrification there.

For DOM, we assumed the same dependence modified:

$$Q_{C_i} = \tau_L^{-1}(C_{Li}^D - DOM) + f_s(OXY)\tau_L^{-1}(C_{L0}^D - DOM),$$

where C_{Li}^D and C_{L0}^D are concentrations of DOM in the sediments in oxic and suboxic conditions, correspondingly, that allowed to parameterize a sudden increase of ammonia in case of depletion of oxygen at the water/sediment boundary. An additional term of oxygen sink *SMnOXY* allowed also to parameterize a flux from the sediment of reduced forms of sulphur, Mn, and Fe that occur in suboxic conditions [18].

At the open channel boundary that was positioned in 1.5 km from the Hunnbunn, we parameterized a uniform distributions of OXY (280 μM), NUT(0.5 μM), BIO (0.01 μM), DOM (0 μM), and POM (0 μM).

3 Results and Discussion

The results of modelling of the Fjord Hunnbunn structure along a transect from the channel mouth to the head of the Fjord (see Fig. 1 green line) in summer (a snapshot) is shown in Fig. 5.

According to the observation [6], the spring consolidation of the pycnocline and its subsequent dissolution from August is the most notable feature of the Hunnbunn hydrography. A goal of the hydrophysical block of the model was to reproduce a structure including a pycnocline that will be stable for a significant period of time necessary for a formation of anoxic layer.

Our model was able to reproduce the formation of pycnocline, but it was not stable and dissolved shortly after its formation. Numerical experiments with different vertical stretching of the model's layers (with decreased distance between the layers below the surface and increased above the bottom and visa versa) always demonstrated the dissolution of the pycnocline because of intense mixing along the slopes.

The calculated summer hydrophysical structure (Fig. 5) was characterized by a gradual decrease of temperature from about 15.3 °C at the surface to 15.0 °C over the bottom, while salinity increases from 14.0 PSU at the surface to 15.0 PSU at the bottom.

With this hydrophysical structure, the model allowed simulation of the main features of the vertical biogeochemical structure of a water body with the bottom anoxia. Using the BIO model compartment allowed parameterizing of processes of

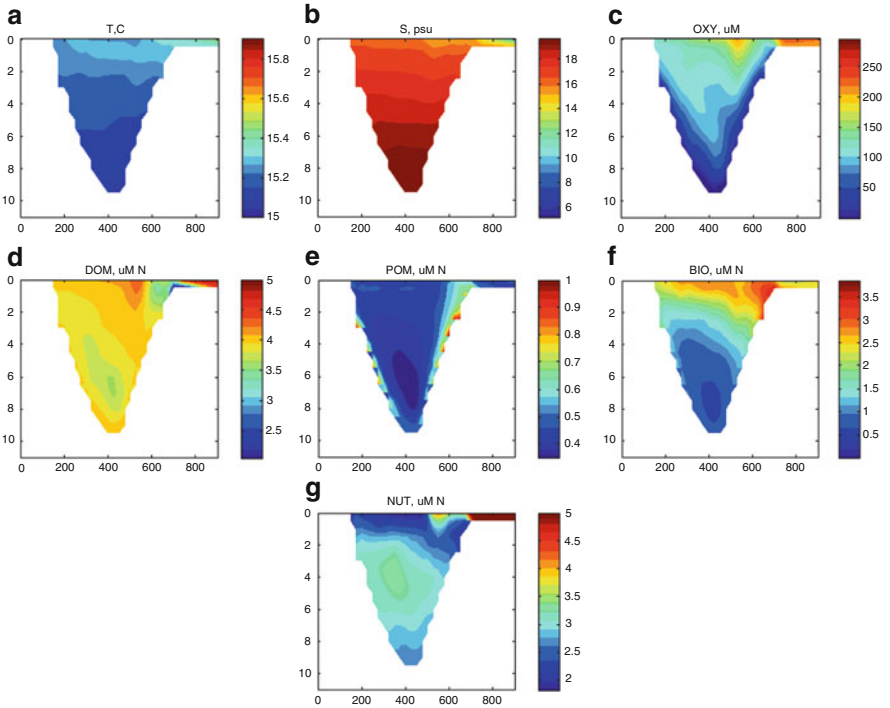

Fig. 5 The results of modelling of the Fjord Hunnbunn vertical structure at a transect from the channel mouth to the opposite coast in summer period for temperature, salinity, OXY, DOM, POM, BIO, and NUT

OM synthesis that resulted in the formation of high concentrations of DOM and POM. BIO had a maximum in the upper 0–2 m layer with concentrations 3.5 μM N (about 50 μg Chl-a L^{-1}) and decreased to 0 below 6 m depth. Concentrations of DOM varied from 5 μM in the euphotic later to approximately 3 μM at the 4–8 m depth, and increased to about 4–4.5 μM above the bottom. Maximum concentrations of POM were found directly at the bottom. The bottom layer near the channel mouth was enriched with BIO and organic matter compounds compared with the opposite flow slope.

Oxygen regime was determined by three factors: (1) production and consumption due to the synthesis and decay of OM, (2) exchange with the atmosphere, and (3) exchange at the bottom. OXY was characterized by maximum concentrations (200–280 μM) in the surface 0–2 m layer, where photosynthesis took place. Gas exchange secured high concentrations of oxygen in the surface layer. Below this layer oxygen was consumed by mineralization of OM (first of all in the dissolved form, DOM). The sinking of POM and BIO led to an enrichment of the bottom layer with OM. Here dissolved oxygen was quickly depleted for the mineralization of the water column POM and DOM, bottom POM and securing the flux from the sediments of DOM and reduced forms of sulphur and metals. This facilitated the

reproduction of anoxic conditions directly in the bottom and suboxic conditions in the 1–2 m layer above the bottom. The NUT (nitrate and nitrite) concentrations increased from about 2 μM N in the upper layer to 3.5–4 μM N at 4–6 m depth following by a decrease of concentrations above the bottom due to denitrification.

The model failed to simulate the formation of a thick 5 m anoxic zone in the modern Fjord Hunnbunn, but allowed reasonable reproduction of the characteristic features of a vertical biogeochemical structure with the bottom anoxia. The oxygen concentrations corresponding to suboxic conditions (less than 30 μM) were observed in the deep part of the modelled basin in a 2-m layer above the bottom. We hypothesise that a similar structure was in the Fjord Hunnbunn earlier when the oxygen regime was better [6].

The main reason for the difference between the simulated results and observed picture is that the hydrophysical block of the model failed to simulate the formation of a permanent developed pycnocline (halocline) that prevents the vertical exchange between the upper and low layers. We hypothesise that using a model with vertical sigma-coordinates (i.e. GETM) makes it very difficult to simulate a hydrophysical structure of shallow regions with pronounced pycnocline/halocline feature such as Fjord Hunnbunn and similar Fjords, lagoons and inlets. A necessity for the same amount of layers in all the grid points of the sigma-coordinates models results in significant changes of the physical vertical resolution (from about 1 m to 0.2 m in this model). At the slopes of the water body the enhanced exchange along the sigma-surfaces leads to an increased vertical transport of heat and salt that doesn't exist in nature.

4 Conclusions

We hypothesise that an application of a simplified biogeochemical model, OxyDep coupled with a 3D model (such as GETM, ROMS, HAMSOM) can be a useful tool for analysing and forecasting of oxygen and nutrient regime changes. In particular, it is possible to use the parameterized seasonal organic matter variability for studying of propagation of pollutants and carbonate system dynamics.

Special attention must be paid when using terrain following vertical coordinates to avoid spurious vertical mixing. The setup for the vertical coordinates in this particular model application needs to be tuned further to achieve more realistic vertical mixing. A z-coordinate model would probably conserve the vertical stratification like the one observed in Hunnbunn better.

Acknowledgements This research was supported by the Norwegian Institute for Water Research project 29083. The research leading to these results has received funding from the European Union's Seventh Framework Programme HYPOX under grant agreement n° 226213. We appreciate the help of colleagues for performing of the chemical analyses: S.V. Pakhomova, O.I. Podymov, and A.V.Kostyleva. We thank A.K. Sweetman for discussions and editing of the manuscript.

References

1. Diaz RJ, Rosenberg R (2008) Spreading dead zones and consequences for marine ecosystems. Science 321(5891):926–929
2. Yakushev EV (2011) RedOx layer model. In: Yakushev EV (ed.), Chemical Structure of Pelagic Redox Interfaces: Observation and Modeling, Hdb Env Chem (this volume)
3. Savchuk OP (2010) Large-scale dynamics of hypoxia in the Baltic Sea. In: Yakushev EV (ed.), Chemical Structure of Pelagic Redox Interfaces: Observation and Modeling, Hdb Env Chem DOI 10.1007/698_2010_53
4. Murray JW, Codispoti LA, Friederich GE (1995) The suboxic zone in the Black Sea. In: Huang CP, O'Melia R, Morgan JJ (eds) Aquatic chemistry: interfacial and interspecies processes. Adv Chem Ser 244. American Chemical Society, Washington DC, pp 157–176
5. Staalstrøm A, Bjerkeng B, Yakushev E, Christie H (2009) Water exchange and water quality in Hunnbunn – evaluation of dredging in the Thalbergsund with regard to improved water quality. NIVA report no. 5874–2009, p 53
6. Ström TE, Klaveness D (2003) Hunnebotn: a seawater basin transformed by natural and antohropogenic processes. Estuar Coast Shelf Sci 56(5–6):1177–1185
7. Grashoff K, Kremling K, Ehrhard M (1999) Methods of seawater analysis, 3rd completely revised and extended edition. Wiley–VCH, Weinheim
8. Pakhomova SV, Yakushev EV (2011) Manganese and iron at the redox interfaces in the Black Sea, the Baltic Sea, and the Oslo Fjord. In: Yakushev EV (ed.), Chemical Structure of Pelagic Redox Interfaces: Observation and Modeling, Hdb Env Chem DOI 10.1007/698_2011_98
9. Pavlidou A, Kontoyiannis H, Anagnostou Ch, Siokou–Frangou I, Pagou K, Krasakopoulou E, Assimakopoulou G, Zervoudaki S, Zeri K, Chatzianestis J, Psyllidou-Giouranovits R (2010) Biogeochemical Characteristics in the Elefsis Bay (Aegean Sea, Eastern Mediterranean) in relation to anoxia and climate changes. In: Yakushev EV (ed.), Chemical Structure of Pelagic Redox Interfaces: Observation and Modeling, Hdb Env Chem DOI 10.1007/698_2010_55
10. Berge JA, Amundsen R, Bjerkeng B, Bjerknes E, Espeland SH et al (2010) Overvåking av forurensningssituasjonen i Indre OsloFjord 2009. NIVA report no. 5985–2010, p 145
11. Stips A, Bolding K, Pohlman T, Burchard H (2004) Simulating the temporal and spatial dynamics of the North Sea using the new model GETM (General Estuarine Transport Model). Ocean Dyn 54:266–283
12. Shchepetkin AF, McWilliams JC (2005) The region ocean model system (ROMS): a split-explicit, free-surface, topography-following-coordinate oceanic model. Ocean Modell 9:347–404
13. Yakushev EV (2002) On parameterization of biogeochemical processes in modelling objects at different time scales. Electronic Journal Studies in Russia (Issledovano v Rossii) 141:1587–1594. http://zhurnal.ape.relarn.ru/articles/2002/141.pdf (in Russian)
14. Yakushev EV, Pollehne F, Jost G, Umlauf L, Kuznetsov I, Schneider B (2007) Analysis of the water column oxic/anoxic interface in the Black and Baltic seas with a Redox-Layer Model. Mar Chem 107:388–410
15. Neumann T, Fennel W, Kremp C (2002) Experimental simulations with an ecosystem model of the Baltic Sea: a nutrient load reduction experiment. Global Biogeochem Cycles 16(3)
16. Savchuk OP, Wulff F (2009) Long-term modelling of large-scale nutrient cycles in the entire Baltic Sea. Hydrobiologia 629:209–224
17. Yakushev EV, Kuznetsov IS, Podymov OI, Burchard H, Neumann T, Pollehne F (2011) Modeling of influence of oxygenated inflows on biogeochemical structure of the Gotland Sea, central Baltic Sea: changes in distribution of manganese. Comput Geosci 37:398–409
18. Skei J, Melsom S (1982) Seasonal and vertical variations in the chemical composition of suspended matter in an oxygen deficient Fjord. Estuar Coast Shelf Sci 14:61–78
19. Schrum C, Janssen F, Hubner U (2000) Recent climate modelling for North Sea and Baltic Sea. Part A: model description and validation. – Berichte des Zentrums für Meeres- und Klimaforschung, Universität Hamburg, p 37

Numerical Modelling of Biogeochemical Regime Response to Decadal Atmospheric Variability During 1960–2000 in the Black Sea

Yunchang He, Emil Stanev, Evgeniy Yakushev, and Joanna Staneva

Abstract Based on an analysis of observations and one-dimensional coupled hydrophysical biogeochemical model, long-term variability of the physical and biogeochemical structure of oxic and suboxic layers in the Black Sea is studied here. The correlation between large-scale atmospheric forcing [2 m air temperature, surface level pressure, surface wind and North Atlantic oscillation (NAO) index] and local responses is the main point. The comparison of model performance with respect to spatial and temporal distribution of biogeochemical variables against observed vertical distribution patterns is quite good. It is demonstrated that during 1960–2000, the long-term variability of winter-mean-simulated SST in the Black Sea is reasonably well correlated with the variability of 2 m air temperature. Furthermore, it is demonstrated that the thermal state of the upper ocean impacts largely the variability of concentration of biogeochemical variables, such as oxygen and nitrate. The teleconnection between NAO and Black Sea biogeochemistry manifests differently for the periods 1960–2000. The corresponding regime shifts are also associated in a vital way with the large-scale forcing.

Keywords Atmospheric forcing, Biogeochemical model, Black Sea, Decadal variability, Oxygen

Contents

Y. He (✉), E. Stanev, and J. Staneva
Helmholtz-Zentrum Geesthacht, Geesthacht 21502, Germany
e-mail: yunchang.he@hzg.de

E. Yakushev
Norwegian Institute for Water Research, Gaustadalleen 21, NO-0349 Oslo, Norway

E.V. Yakushev (ed.), *Chemical Structure of Pelagic Redox Interfaces: Observation and Modeling*, Hdb Env Chem (2013) 22: 253–272, DOI 10.1007/698_2011_103,

Abbreviations

AT	Air temperature
CIL	Cold intermediate layer
DPT	Dew point temperature
GOTM	General Ocean Turbulent Model
NAO	North Atlantic oscillations
OM	Organic matter
ROLM	Redox-Layer Model
SST	Sea surface temperature

1 Introduction

Permanent anoxic conditions are observed in lakes, fjords and ocean basins such as Black Sea, Baltic Sea and Cariaco Trench, which are characterized by extremely stable stratification. In the Black Sea, the biogeochemical system adjusted to the physical stratification in an unique way, building thus the largest anoxic environment in the world. Major changes of biogeochemical variables are observed across levels of constant density, while gradients along density are extremely small [1–3]. A typical vertical profiles observed in the centre of the Black Sea are shown in Fig. 1. Oxygen is almost at atmospheric saturation in the upper layer (0–40 m) and drops sharply below the detection limit of 3 μM at about the depth of 60 m. The first appearance of the hydrogen sulphide occurs at about 80 m and then increased continuously to more than 40 μM of about 150 m. The nitrate maximum appears at about 60 m, and the ammonia starts to increase at about 75 m several metres above the sulphidic boundary. The same profiles are shown versus density in the figure on the right (Fig. 1). It is noteworthy that biogeochemical structure of the water column is characterized by no-overlap of dissolved oxygen and hydrogen sulphide layers. The corresponding layer is known as the suboxic layer (the zone without oxygen and hydrogen sulphide, [4]). Yakushev et al. [5] numerically proved with the model that the manganese cycle in the Black Sea could explain this layering.

The present-day vertical structure is very stable and has been established as a consequence of the re-connection between the Black Sea and the Mediterranean. Some analyses of long-term variations of chemical [6] and ecological [7, 8] systems in the Black Sea identify regime shifts, which could be due to either anthropogenic or climatic forcing.

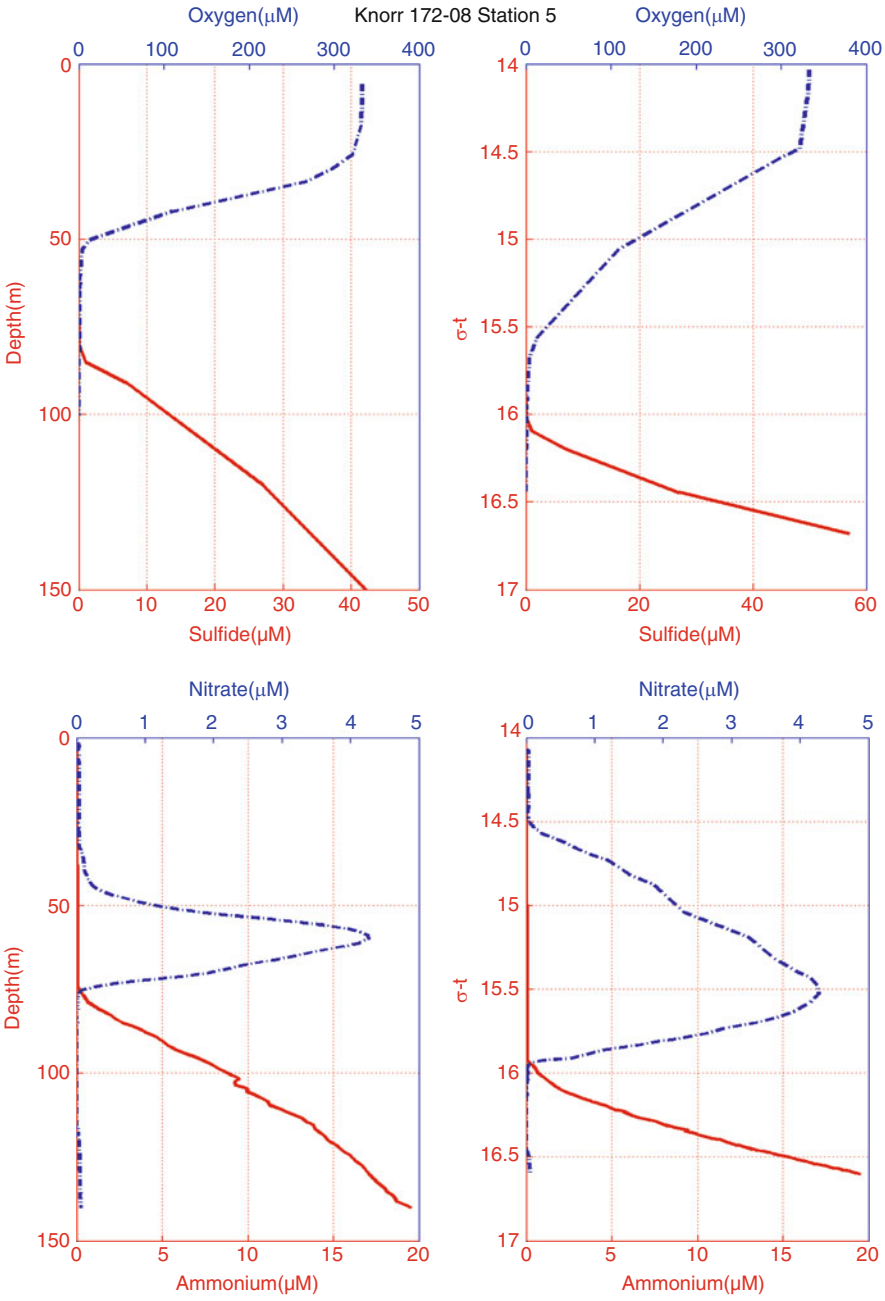

Fig. 1 Vertical profiles of basic chemical end ecological variables in the Black Sea (*Leg* 8, *Stn* 5); *top*: oxygen/sulphide data in situ; *bottom*: nitrate/nitrite/ammonia pump cast data, during R/V Knorr Cruise 2003: The Black Sea; for more details, see: http://www.ocean.washington.edu/cruises/Knorr2003/data/Vol_Oxygen_Sulfide/08-5.html

The motivation for this study is to test the capability of a complex biogeochemical model to reproduce interannual variability triggered by the atmosphere. In this chapter, we use a 1D model, a first step that is necessary to understand the possible reaction of natural water systems to atmospheric forcing. Testing performance of 1D biogeochemical model and validation against observations will also be illustrated here. Major interest is on the upper layer variability. The chapter is structured as follows. We first describe the numerical model and sensitivity experiments carried out, which is followed by a discussion of results and short conclusions.

2 Model and Materials

2.1 Description of the Model

The biogeochemical model used in this study is Redox-Layer Model (ROLM, [5]). This model includes production and decay of organic matter (OM), and reduction and oxidation of nitrogen, sulphur, manganese and iron. The following compartments are included (Fig. 2): dissolved oxygen (O_2), hydrogen sulphide (H_2S), total

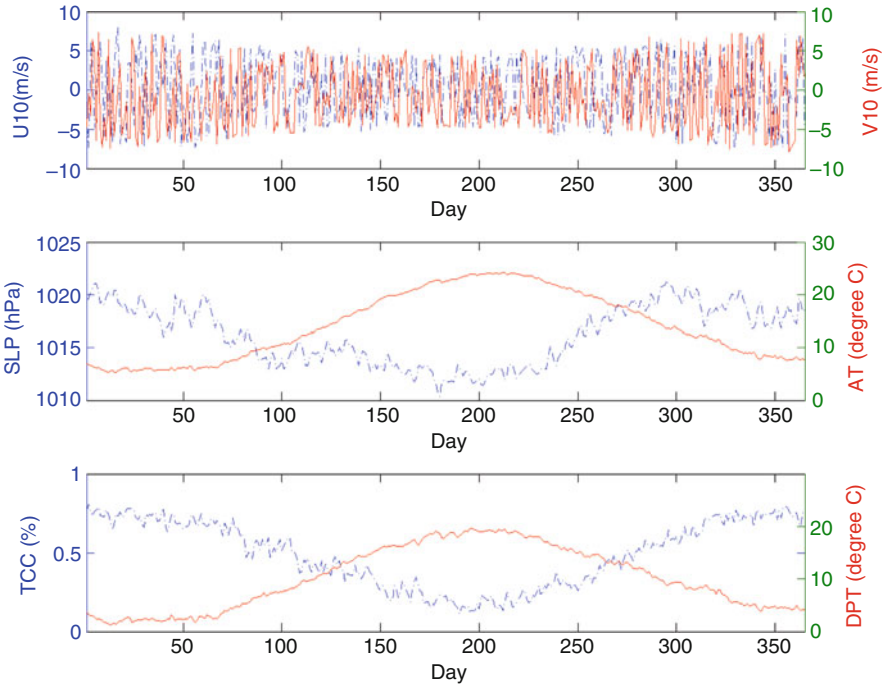

Fig. 2 Forty-five-year mean value for meteorological forcing data of wind speed, sea level pressure, air temperature, dew point temperature and total cloud cover

elemental sulphur (S_0), thiosulphate (S_2O_3), sulphate (SO_4), ammonia (NH_4), nitrite (NO_2), nitrate (NO_3), particulate organic nitrogen (PON), dissolved organic nitrogen (DON), phosphate (PO_4), particulate organic phosphorus (POP), dissolved organic phosphorus (DOP), bivalent manganese (Mn_2), trivalent manganese (Mn_3), quadrivalent manganese (Mn_4), bivalent iron (Fe_2), trivalent iron (Fe_3), phytoplankton (Phy), zooplankton (Zoo), aerobic heterotrophic bacteria (Bhe), aerobic autotrophic bacteria (Bae), anaerobic heterotrophic bacteria (Bha) and anaerobic autotrophic bacteria (Baa). ROLM was chosen for the multi-decadal calculations because this model describes losses of oxygen for both mineralization of organic matter and oxidation of the reduced forms of sulphur, nitrogen, manganese and iron. ROLM considers also the transformation of nitrogen from reduced to oxidized forms (i.e. between NO_3, NO_2 and NH_4). Unlike the other existing models for the Black Sea [9, 10], organic mater production due to photosynthesis and chemosynthesis is parameterized, and thus feedbacks between the upward fluxes of nutrients and organic mater production are accounted for. A detailed description of the model is presented by Yakushev [5].

The model is coupled online with the General Ocean Turbulent Model (GOTM, [11]). This is a one-dimensional water column model for the most important hydrodynamic and thermodynamic processes related to vertical mixing. The basic set of equations (1–7) for temperature T, salinity S, mean horizontal velocity components u and v, pressure P, turbulent kinetic energy (TKE) k and the TKE dissipation rate ε are:

$$\frac{\partial T}{\partial t} = \frac{\partial}{\partial z}\left((\upsilon'_t + \upsilon')\frac{\partial T}{\partial z} \right) - \gamma^T (T - T_o), \tag{1}$$

$$\frac{\partial S}{\partial t} = \frac{\partial}{\partial z}\left((\upsilon'_t + \upsilon')\frac{\partial S}{\partial z} \right) - \gamma^S (S - S_o), \tag{2}$$

$$\frac{\partial u}{\partial t} = \frac{\partial}{\partial z}\left((\upsilon_t + \upsilon)\frac{\partial u}{\partial z} \right) + fv, \tag{3}$$

$$\frac{\partial v}{\partial t} = \frac{\partial}{\partial z}\left((\upsilon_t + \upsilon)\frac{\partial v}{\partial z} \right) - fu, \tag{4}$$

$$\frac{\partial P}{\partial z} = -g\rho, \tag{5}$$

$$\frac{\partial k}{\partial t} = \upsilon_k \frac{\partial^2 k}{\partial z^2} + P + B - \varepsilon, \tag{6}$$

$$\frac{\partial \varepsilon}{\partial t} = \upsilon_\varepsilon \frac{\partial^2 \varepsilon}{\partial z^2} + \frac{\varepsilon}{k}(c_{\varepsilon 1} P + c_{\varepsilon 3} B - c_{\varepsilon 2}\varepsilon), \tag{7}$$

where υ'_t and υ' are molecular and turbulent diffusivity of temperature and salinity, υ and υ_t are molecular and turbulent viscosity (momentum), f is the Coriolis parameter, and υ_ε and υ_k are the turbulent diffusivities of energy dissipation and TKE, respectively. Relaxation with the time scale $1/\gamma^{(T,\ S)}$ towards prescribed profiles (T, S) is enabled in deep layers to compensate for the missing fluxes in one-dimensional model.

The shear stress production P and the buoyancy production B are:

$$P = \upsilon_t \left(\left(\frac{\partial u}{\partial z} \right)^2 + \left(\frac{\partial v}{\partial z} \right)^2 \right), \tag{8}$$

$$B = -\upsilon'_t N^2, \tag{9}$$

where

$N^2 = \dfrac{-g}{\rho_0} \dfrac{\partial \rho}{\partial z}$ is the Brunt–Väisälä frequency.

The turbulent viscosity and diffusivity can be calculated using the relation of Kolmogorov and Prandtl:

$$\upsilon_t = c_\mu \frac{k^2}{\varepsilon}, \quad \upsilon'_t = c'_\mu \frac{k^2}{\varepsilon}. \tag{10}$$

The turbulent diffusivities for k and ε are:

$$\upsilon_k = \frac{c_\mu}{\sigma_k} \frac{k^2}{\varepsilon}, \quad \upsilon_\varepsilon = \frac{c_\mu}{\sigma_\varepsilon} \frac{k^2}{\varepsilon}. \tag{11}$$

All parameters in the above formula are listed in Table 1 [11, 12]. The surface fluxes is calculated by means of bulk formulae which was developed by Kondo [13]. Meteological forcing and dew point temperature are specified, while the solar radiation is not prescribed.

The physical model is coupled to and solves one-dimensional vertical diffusion equations for 24 non-conservative substances of the type:

$$\frac{\partial C_i}{\partial t} = \frac{\partial}{\partial z} \left((\upsilon'_t + \upsilon) \frac{\partial C_i}{\partial z} \right) - \frac{\partial}{\partial z} \left((W_C + W_M) \times C_i \right) + R_{C_i}, \tag{12}$$

Table 1 Parameters of the K-ε model [26]

Model constant	Value	Definition
$c_{\varepsilon 1}$	1.44	Empirical coefficient of dissipation equation
$C_{\varepsilon 2}$	1.92	Empirical coefficient of dissipation equation
$c_{\varepsilon 3}$ ($B < 0$)	−0.4	Empirical coefficient of dissipation equation for stable stratification
$c_{\varepsilon 3}$ ($B > 0$)	1	Empirical coefficient of dissipation equation for unstable stratification
σ_ε	1.3	Schmidt number for TKE diffusivity
σ_k	1	Schmidt number for TKE diffusivity

where C_i is the concentration of a model variable, W_C the sinking velocity of particulate matter; W_{Me} accounts for the contribution of settling of Mn hydroxides, and R_{C_i} describes biogeochemical production or consumption. These terms given by Yakushev [5] were used in the present study parameter values. Meanwhile, some parameters about phytoplankton on specific growth, respiration, mortality and excretion rate changed a little according to other literatures to make the model results more closer to the real situation.

2.2 Analysis of Forcing and Initial Data

2.2.1 Forcing Data

Forcing data for the physical model consists of radiation (including clouds), 10 m wind speed, 2 m air temperature and dew point temperature, as well as sea level pressure. They are produced by the European Centre for Medium-Range Weather Forecasts (ECMWF) and were kindly made available for the period 1958–2002 in the frame of Southern European Seas: Assessing and Modelling Ecosystem changes (SESAME) project by the INGV, Italy. The temporal sampling rate is 6 h. The data have spatial resolution of 0.25°. From these data, we extract forcing corresponding to an open sea location (32.625°E, 43.177°N). Atmospheric variability is characterized by a pronounced seasonal cycle, which is exemplified in Fig. 2 by the mean year for the 45-year model integration period. In the study, all the atmospheric forcing data are calculated in winter-mean (December–February).

The Black Sea regime shifts appear to be sporadic events forced by the strong transient decadal perturbations, and therefore differ from the multi-decadal scale cyclical events observed in pelagic ocean ecosystems under low-frequency climatic forcing [14]. The North Atlantic oscillation (NAO) index is known to be the most prominent mode of low-frequency variability controlling atmospheric circulation and climate over the North Atlantic and Eurasia [15]. The positive winter NAO index is associated with stronger north-south pressure gradient, more cold and dry air conditions in the Mediterranean and Black Sea region, and more moisture and heat transported in Scandinavian area. Conversely, the negative NAO index supports warmer air temperatures in the southern Europe. The NAO index for the period 1960–2000, defined as the normalized sea level pressure difference measured in meteorological stations located at Gibraltar and Iceland [16], was obtained from the Climate Prediction Centre of National Weather Service in NOAA (http://www.cpc.noaa.gov/products/precip/CWlink/pna/nao_index.html). Monthly values were averaged for winter season (December–February).

2.2.2 Initial Conditions

Initial conditions correspond to the annual mean temperature and salinity profiles for the interior part of the basin. Because the model is one-dimensional (no horizontal fluxes are computed or prescribed), we relax temperature and salinity below the depth of CIL to climatology. At every time step, temperature and salinity profiles used for relaxation are interpolated to the actual GOTM model grid. This procedure ensures that the simulations remain consistent with the dominating stratification in deep layers. At the same time, upper layer characteristics are free to adjust to surface forcing.

At the sea surface, all chemical and ecological constituents were set to zero except for O_2, NO_3 and PO_4 that were parameterized as follows [5]. At the lower boundary, which is at the depth of 200 m, constant values were specified: NH_4 = 20 μM, H_2S = 60 μM, MnII = 8 μM, FeII = 0.4 μM, PO_4 = 4.5 μM, which corresponds to existing observations.

2.3 Numerical Experiments

We define two scenarios, which we run for 45 years each with data described above. The difference between them is that in the first one called Scenario (I) we use the full atmospheric signal, which contains interannual (I) variability. In second scenario, we substitute the atmospheric forcing by the mean year, which is perpetually repeated for 45 times; therefore, the name of this scenario is perpetual (P).

In view of the simple conditions of the 1D physical biochemical model, the meteorological forcing was the only driving source. Four sensitivity experiments in 1-year run on air temperature, dew point temperature, wind and sea level pressure were designed to test the main affecting factors. On the basis of the scenario P, we designed six sensitivity experiments on AT, DPT, wind and SLP independently. The first sensitivity experiment run by increasing 2° on AT value, and the other meteorological forcing kept unchanged. The second sensitivity experiment run by decreasing 2° on AT value, and the others parameters kept unchanged. The similar experiments run with increasing and decreasing 2° on DPT, increasing and decreasing 1 m s^{-1} on wind, and increasing and decreasing 7 Pa on SLP independently. All the sensitivity experiments run 2 years, as well as the reference run without any change in meteorological forcing.

For oxygen distribution at CIL (between 50 and 75 m) in sensitivity experiments (Fig. 3), air temperature with reduction of 2° caused oxygen concentration go up to nearly 9 μM, from 30 μM at reference to 40 μM. On the contrary, air temperature increasing 2° made oxygen concentration go down around 10 μM all the year. The dew point temperature increased 2°, the oxygen concentration decreased to the maximum of 3 μM in summer when compared to that of reference, and vice versa. The wind either increased or decreased 1 m s^{-1}, and oxygen concentration at CIL

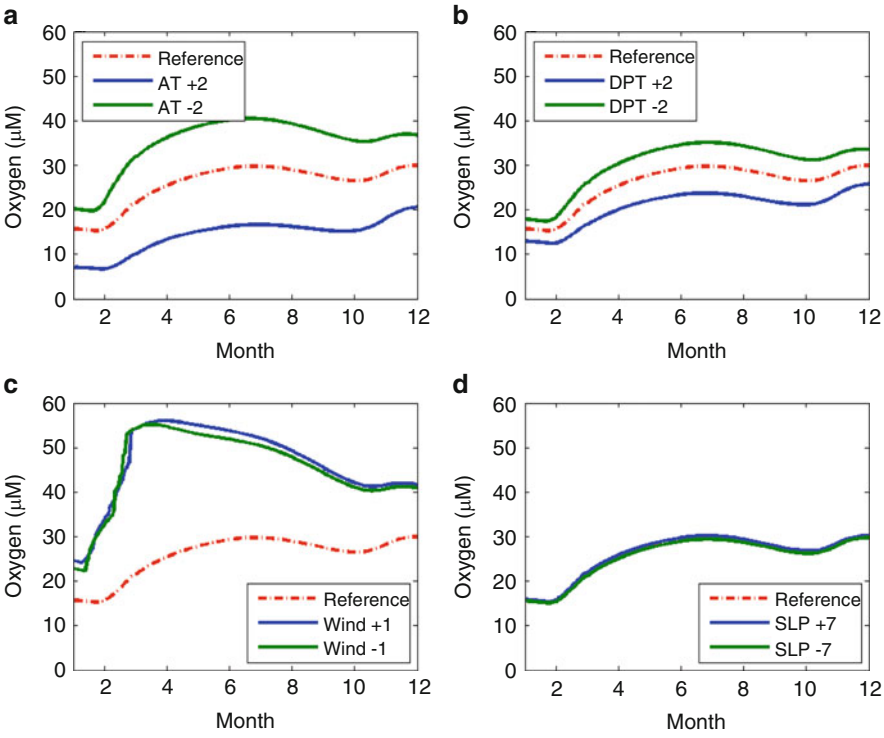

Fig. 3 Oxygen variations at CIL (50–75 m) in the different sensitivity experiments [(**a**) air temperature; (**b**) dew point temperature; (**c**) wind; (**d**) sea level pressure]. The oxygen concentration from perpetual scenario was the reference (*red dash line*)

goes up, especially in spring bloom. The change in sea level pressure had negligible effect on oxygen concentration at CIL. From the analysis and comparison, the effect on oxygen at CIL among all meteorological forcing in the sensitivity experiments, the changes in wind and air temperature, should be the more important factors, and then the dew point temperature was less important affecting factors on variability of oxygen at suboxic zone. For nitrate concentration experiments at the same layer (Fig. 4), the variability of air temperature and dew point temperature brought obvious change, and the decrease of 2° in air temperature caused nitrate concentration going up 1 μM. On the contrary, the increase of 2° in air temperature caused nitrate concentration going down 2 μM. The change in dew point temperature had a similar effect on nitrate, while the influence was less to half. Whether wind increased 1 m s^{-1} or decreased 1 m s^{-1}, the concentration of nitrate went up less than 1 μM. The variability of 7 Pa on sea level pressure caused very weak influence on nitrate concentration.

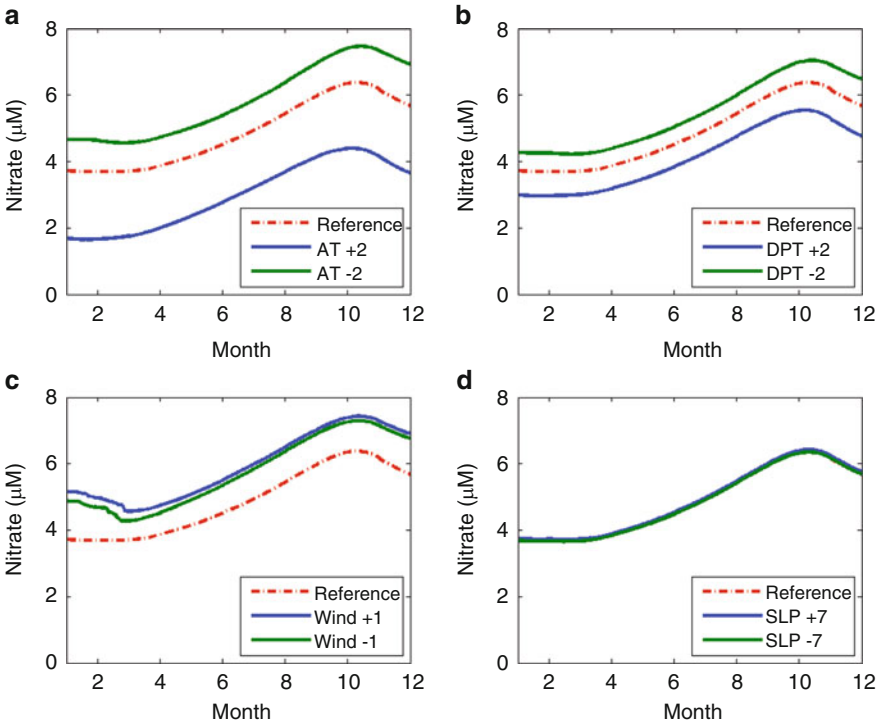

Fig. 4 Nitrate variations at CIL (50–75 m) in the different sensitivity experiments [(**a**) air temperature; (**b**) dew point temperature; (**c**) wind; (**d**) sea level pressure]. The nitrate concentration from perpetual scenario was the reference (*red dash line*)

2.4 Model Validations

The performance of the model is illustrated below by validating the simulations against observations from the Knorr Black Sea Cruise in the centre of the Black Sea Western Gyre in 2003. Because the processes in the Black Sea align to isopycnals, we present simulated profiles against depth and density separately. Figure 5 reveals the typical vertical distribution of temperature, salinity, oxygen and hydrogen sulphide. Overall, the comparison is quite good; however, some differences are to be mentioned: the cold intermediate layer (CIL) in the model is a little more diffuse than in the observations, and the oxygenated water penetrates slightly deeper in the upper layer. As a success of the simulation, one could mention the approximate agreement of the isopycnic depth of the suboxic layer (a layer characterized by the absence of dissolved oxygen and hydrogen sulphide; Murray et al. [4]) in the observations and simulations.

Here, we will describe the model performance at the depths above and around the depth interval where suboxic layer is usually observed (Fig. 6). In the numerical simulations, position of suboxic zone is at the density layer of 15.2–15.7 kg m^{-3}.

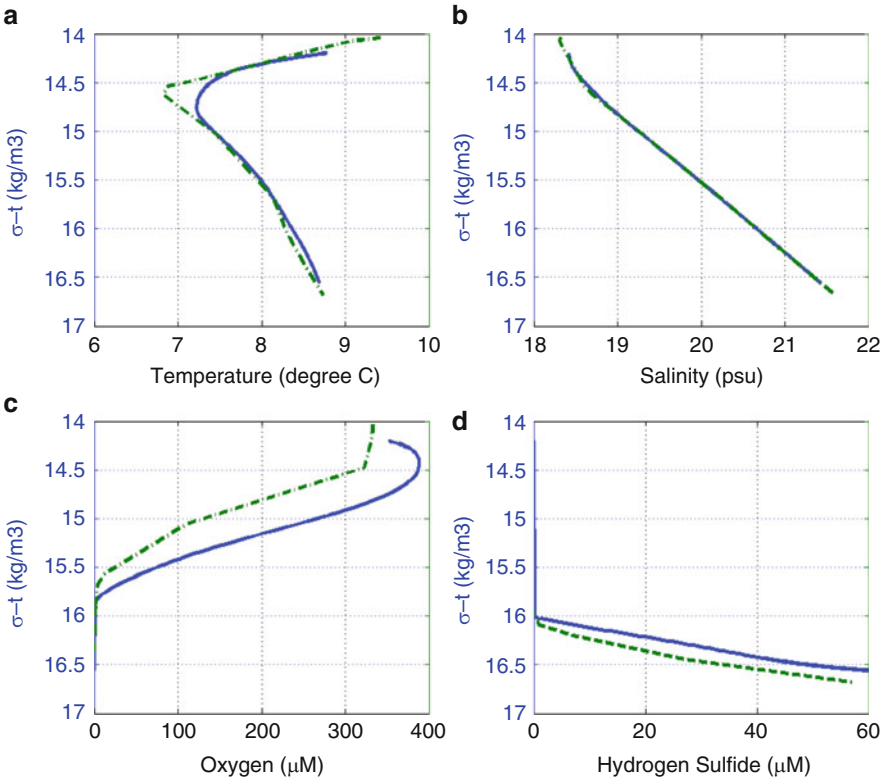

Fig. 5 Comparisons of vertical distribution of temperature, salinity, oxygen and hydrogen sulphide between simulation and observation versus depth and density. Observations used for intercomparisons are taken from Knorr Cruise in 2003

Large variations were observed in the distributions of oxygen in surface layers mostly due to temperature change. Maximum of oxygen of about 380 μM occurred at sea surface, which was similar to the observed data [8]. The profile reached zero concentration (less than 0.5 μM) at σ_θ 15.2 kg m^{-3}, which was little thinner than in the observed data (15.3–16.0 kg m^{-3}) [17]. Vertical distribution of nitrogen compounds (NH_4, NO_2, NO_3) showed that onset of NH_4 appears at about σ_θ 15.4 kg m^{-3}, and the maximum of NO_2 appeared at the depth where the concentrations of NH_4 and NO_3 were equal. The onset of Mn_2 increased greatly where the onset of H_2S occurred. The vertical distribution of H_2S was similar in summer and winter. The maximum of NO_3 appeared approximately at the depth where the O_2 dropped below 10 μM.

The depth of redox layer was 65 and 90 m, correspondingly. In the model, the oxidation of Mn_2 resulted in the formation of alternative electron acceptors, which had a sinking rate to accelerate the downward transport. O_2 dropped to 0 at the same depth where Mn_2 onset appeared that was same as in the observations [5].

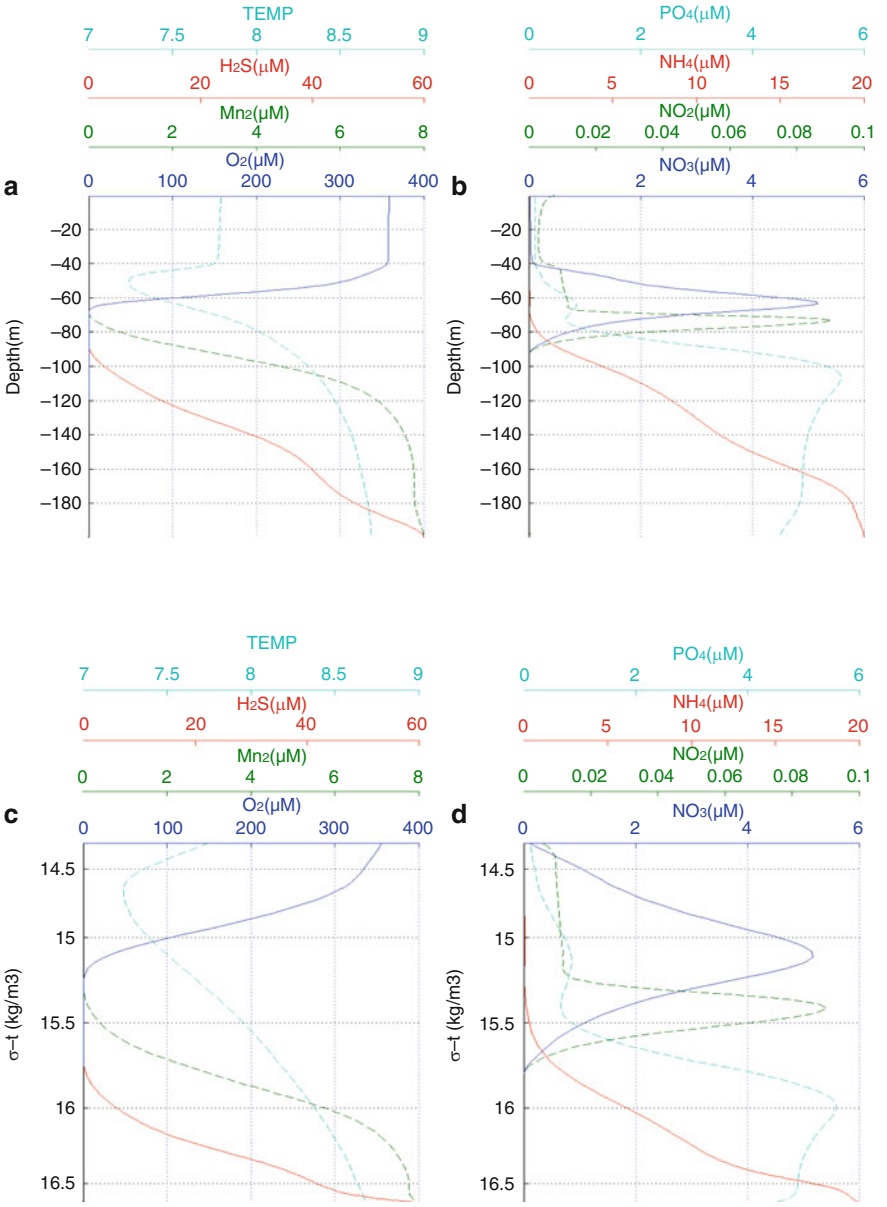

Fig. 6 Winter-mean (December–February) vertical distribution of the main chemical variables versus depth (**a**, **b**) and versus density (**c**, **d**) in 1960

Furthermore, Yakushev and Debolskaya [18] suggested that the reduction of Mn_4 by H_2S was very intensive, and the reaction can be balanced by the flux from below. Hence, we may conclude that the main biogeochemical features of

the redox layer in the central Black Sea known from observations are well reproduced by the 1D model.

3 Interannual Variability of Simulated Biogeochemistry Responses

Decadal and interannual variability in atmospheric state, in particular in the European region, is well pronounced when analysing data for winter months. Interannual variability in the physical system has been analysed by Stanev et al. [3, 19] and Tsimplis et al. [20]. One important result from the above studies is that the deep layers of the Black Sea do not show pronounced sensitivity to interannual variations in forcing. This is due to the strong stratification decoupling surface and deep layers. However, as it has been demonstrated by Staneva et al. [21], responses in the upper layers and down to the depth of CIL are very clear. Recently, the response of a number of biogeochemical parameters to long-term atmospheric variability has been addressed by Oguz [22].

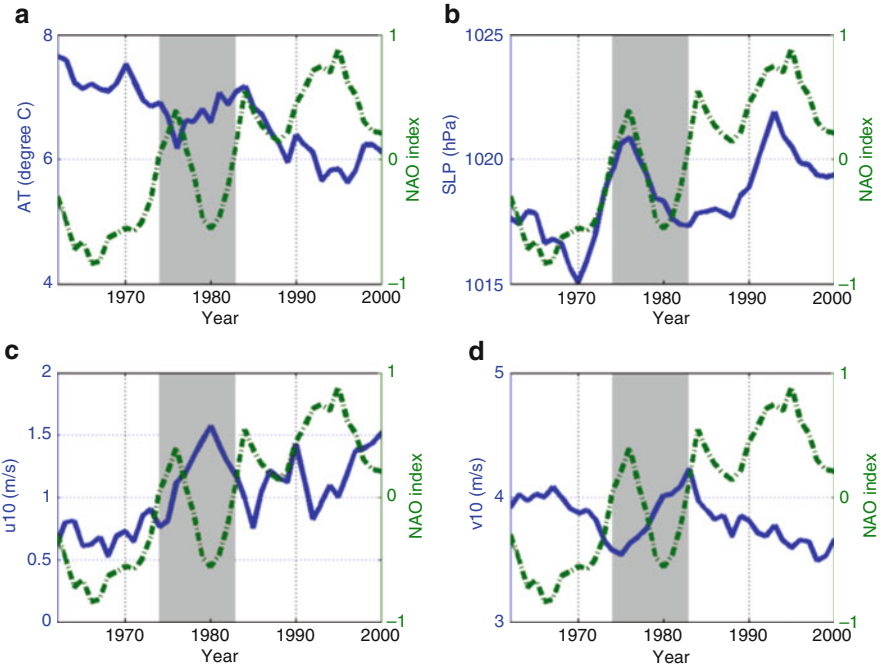

Fig. 7 Interannual variability of air temperature (**a**), SLP (**b**) and wind components u10 (**c**) and v10 (**d**) in winter (December–February) compared with the winter NAO index. Data were 5-year moving averaged

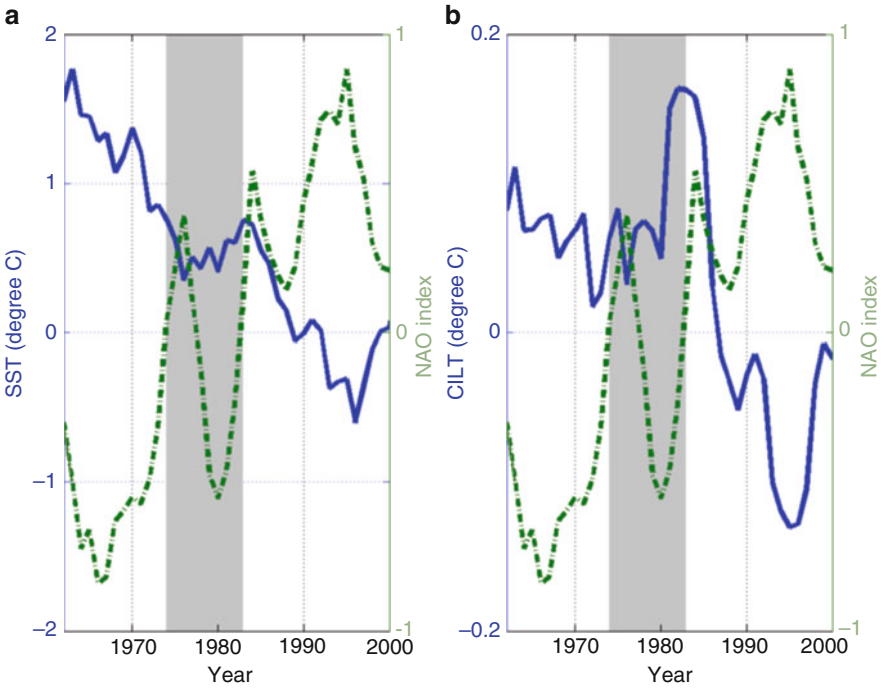

Fig. 8 Interannual variability of simulated annual SST (**a**) and CIL temperature (**b**) anomalies in winter (December–February) compared with the winter NAO index. Data were 5-year moving averaged

There is a consensus that during periods of positive winter NAO index, cold and dry air intrusions into the Black Sea region dominate. Conversely, during times of negative NAO index, warmer air temperatures dominate the Black Sea region. Figures 7 and 8 showed the comparison between winter NAO index and air temperature, sea level pressure, wind, SST anomaly and CIL temperature anomaly in winter during 1962–2000. All the data were 5-year moving averaged. Clearly, there were three peaks of the winter NAO index in 1976, 1984 and 1995, separately. From 1960s to 1973, the negative winter NAO index dominates; the air temperature had a decreasing trend, also with SST, CIL temperature and dew point temperature. The following 9 years between 1974 and 1982, the winter NAO index changed from positive to negative, also in turn, frequently. At the same time, the air temperature increased a little about 1°, and the same trends appeared for SST, CIL temperature and dew point temperature. At the third period in 1983–1995, positive winter NAO index took the main role, and the air temperature, SST, CIL temperature and dew point temperature also decreased. After 1995, all the situations varied again. From the wind components in winter time, the southwest wind prevailed the four decades from 1960s to 1990s in the observation station. It was similar to the observation statistics wind data [23], and an occurrence of the SW wind regime (61%) is approximately two times as much as of the NE regime (28%) during the

period 1950–2004 in the Black Sea. The interannual variability in the Black Sea diagnosed from GOTM does not reveal a very clear correlation between analysed variables and NAO index, in particular when shorter periods are concerned. As explained by Oguz [22], NAO is not the only one relevant for the region climatic index; therefore, perfect correlation is not to be expected.

Summarizing the above results, we remind that the trend variabilities of air temperature, dew point temperature, SST and CIL temperature show some correlation with winter NAO index. This could indicate that shifts in the response pattern of physical variables of the Black Sea are possible.

Long-term variations in the structure of thermohaline had been discussed by many scientists. According to Belokopitov [24], extreme cold winters occurred in 1964, 1972, 1976, 1985 and 1993.

A two-layer structure can be distinguished in the vertical distribution of oxygen in the Black Sea (Fig. 1). A 90–110% saturated with oxygen upper layer is at or above atmospheric solubility due to gas exchange and biological production. It shows significant seasonal variations, and the concentrations there vary from 300–370 μM in February–April to 200–250 μM in July–August depending on the seasonality of temperature-influenced air–water exchange and OM production and decomposition [8]. In the lower layer, the oxygen concentrations decrease. A layer of decreasing oxygen concentration (oxycline) coincides with the main pycnocline (halocline). Oxygen decreases quasi-linearly with depth from 250–300 μM above the main pycnocline to 10–20 μM at the density level of σ_θ 15.50–15.60 kg m^{-3}. The vertical gradient of oxygen in this layer is 7–10 μM m^{-1}. Below this depth, the vertical gradient of oxygen decreases significantly to 0.5–1.5 μM m^{-1}. Around the densities of σ_θ, 15.90–16.00 kg m^{-3} dissolved oxygen decreases to below detection [8].

A supply of oxygen from the upper layer to the lower one depends on an intensity of the vertical mixing. In case of the presence of a strong thermohaline structure, oxygen is consumed faster than it can be replaced by vertical and lateral fluxes at a depth of CIL, about 70 m. But after a cold winter, the vertical mixing intensifies and the oxygen concentrations increase. Such an increase in mixing should also affect supply of nutrients (i.e. nitrate) to the surface layer and therefore its potential biological productivity. This means that the yearly variability of oxygen, phytoplankton and nitrate concentrations at both surface and CIL may have also certain correlations with winter NAO index.

According to the model simulations (Fig. 9), the NAO index in winter influences the anomalies of oxygen, phytoplankton and nitrate concentrations at both surface and CIL. The oxygen concentration at the surface (Fig. 9a) had same trend of increasing with NAO in 1962–2000 that is opposite to temperature (Fig. 7a). Before 1990, the oxygen anomaly kept negative and became positive in the most time of 1990s, when it might be caused by high solubility of oxygen due to the colder SST. From the middle 1970s to middle 1980s, oxygen maintained relatively stable, while phytoplankton and nitrate appeared maximum. Furthermore, the correlation of general trend between winter NAO and phytoplankton and nitrate in surface layers was clearly negative. Noteworthy is that the correlation between above

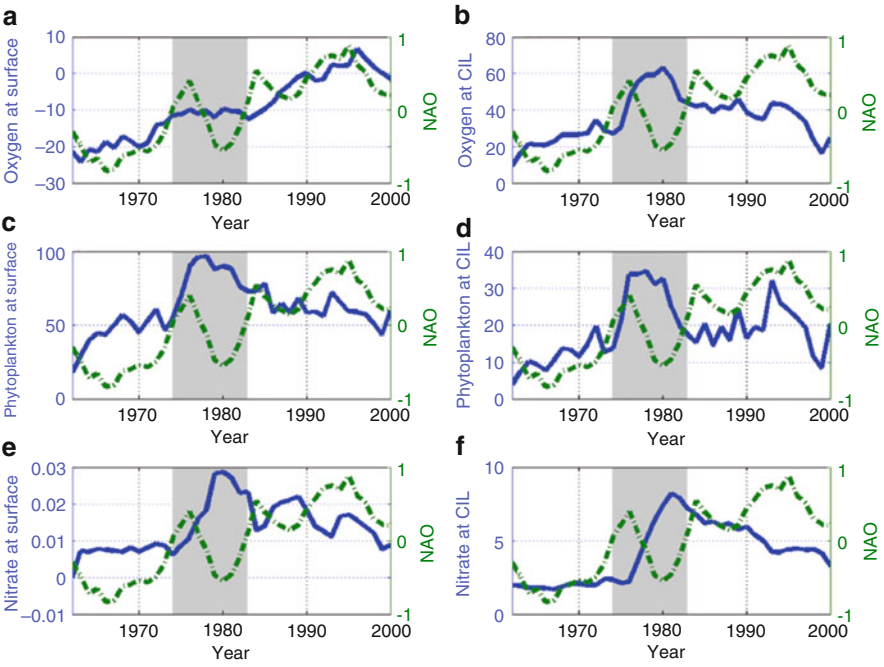

Fig. 9 Interannual variability in anomalies of oxygen, phytoplankton and nitrate concentrations in winter time simulated at sea surface (0–5 m) (*left*) and CIL (60–90 m) (*right*) versus winter NAO index (December–February). (**a**) Oxygen at surface versus winter NAO index; (**b**) oxygen at CIL versus winter NAO index; (**c**) phytoplankton at surface versus winter NAO index; (**d**) phytoplankton at CIL versus winter NAO index; (**e**) nitrate at surface versus winter NAO index; (**f**) nitrate at CIL versus winter NAO index

phytoplankton and nitrate in the surface layer is much stronger than oxygen, which may reflect that at surface phytoplankton concentration depends on nitrate, while the surface layer oxygen can be affected by other factors, i.e. temperature-forced changes in the air–water exchange (Figs. 5a and 7a).

Meanwhile, an interannual variability of oxygen at CIL correlate better with an interannual variability of phytoplankton and nitrate both in the CIL and at the surface (Fig. 9b–f). An increase in oxygen concentrations at CIL depends on the intensity of mixing as well as an increase in nitrate and phytoplankton. It was notable that nitrate was preserved stable in 1960s and in the first half of 1970s at surface and at CIL. Both surface and CIL phytoplankton and nitrate concentrations and oxygen at CIL increased very rapidly in the late half of 1970s, when the winter NAO shifted very intensively. Consistent with the above analysis, one comes to the conclusion that the winter NAO can be regarded as a potential long-term forcing explaining the decadal variability of biogeochemical process.

4 Discussion and Conclusions

We demonstrated in this chapter that the coupled numerical model simulations reveal a pronounced interannual variability of state variables in the Black Sea, allowing to conclude that changes in NAO during the past 40 years could be considered as important driver for changes in the Black Sea biogeochemistry. Both at surface layer and at CIL layer, the concentrations of oxygen, nitrate and phytoplankton directly or indirectly respond to the long-term winter NAO index. The basic points of our findings may be briefly summarized as follows:

(1) Winter NAO index had a overall increasing trend, except for the abrupt transitions during a decade from 1973 to 1982, when SST and CIL temperature followed generated echoes, that is, the trends changed correspondingly. The general decreasing trend of SST is opposite to the winter NAO index.
(2) Winter NAO index abrupt shift frequently may bring great changes on meteorological, physical and biogeochemical variables in the Black Sea. The variabilities in air temperature and wind caused by the winter NAO index influence SST and ventilation flux, and then affect oxygen, nitrate and phytoplankton. The ventilation flux from surface to CIL which led by wind variability changed the distributions of biogeochemical variables. After analysis on the results of the sensitivity experiments, the roles of meteorological forcing on affect oxygen, phytoplankton and nitrate from important to less important were air temperature, wind component U, then V, dew point temperature, and last sea level pressure.
(3) A performed model analysis can reveal a mechanism of reaction of the Black Sea biogeochemical regime on the decadal atmospheric variability. More intense ventilation should lead to an increase in both oxygen content in the CIL and supply of nutrient to the surface layer, which will potentially increase the biological productivity Therefore, the periods of increased concentrations of nitrate and phytoplankton should be correlated with the oxygen increase in the CIL, while the oxygen dynamics in the upper layer can be in a larger degree controlled by an interannual variability of the temperature.

The general response pattern of hydrophysical and biogeochemical variables in the Black Sea to NAO may be described as being mostly shaped by air temperature. However, taking into consideration the fact that most processes in the Black Sea are controlled by wind [25], one could expect that in 3D modelling framework wind will also have a pronounced impact. The fact that the results presented here do not fully support variations in temporal distribution of O_2 and H_2S derived from observations [6] could be due to the following problems: (1) in the present model, interannual changes in river runoff and eutrophication due to it has not been considered; (2) horizontal transport processes are also expected to play an important role. Therefore, the next step to do when simulating the long-term variability is to apply a 3D modelling framework.

Acknowledgements We would like to thank Dr. O. Podymov, Dr. J. Su and R. Kandilarov for their useful help. Atmospheric model data were produced by the European Centre for Medium-Range Weather Forecasts (ECMWF) and were kindly made available for the period 1958–2002 in the frame of SESAME project by the INGV, Italy. The study was funded by HYPOX project.

References

1. Spencer DW, Brewer PG (1971) Vertical advection diffusion and redox potentials as controls on the distribution of manganese and other trace metals dissolved in waters of the Black Sea. J Geophys Res 76:5877–5892
2. Shaffer G (1986) Phosphate pumps and shuttles in the Black Sea. Nature 321:515–517
3. Stanev EV, Staneva JV, Bullister JL, Murray JW (2004) Ventilation of the Black Sea Pycnocline. Parameterization of convection, numerical simulations and validations against observed chlorofluorocarbon data. Deep Sea Res 51(12):2137–2169
4. Murray JW, Codispoti LA, Friederich GE (1995) Oxidation-reduction environments: the suboxic zone in the Black Sea. Aquatic chemistry: interfacial and interspecies processes. Am Chem Soc Adv Chem Ser 244:157–176
5. Yakushev EV, Pollehne F, Jost G, Kuznetsov I, Schneider B, Urnlauf L (2007) Analysis of the water column oxic/anoxic interface in the Black and Baltic seas with a numerical model. Mar Chem 107:388–410
6. Konovalov SK, Murray JW (2002) Variations in the chemistry of the Black Sea on a time scale of decades (1960-1995). J Mar Syst 31:217–243
7. Oguz T (2005) Black sea ecosystem response to climatic teleconnections. Oceanography 18(2):122–133
8. Yakushev EV, Chasovnikov VK, Murray JW, Pakhomova SV, Podymov OI (2008) Vertical hydrochemical structure of the Black Sea. The Black Sea environment, The handbook of environmental chemistry, vol 5. Springer, Berlin, pp 277–307
9. Oguz T, Ducklow H, Malanotte-Rizzoli P, Murray JW (1998) Simulations of the Black Sea pelagic ecosystem by one-dimensional, vertically resolved, physical-biochemical models. Fish Oceanogr 7(3/4):300–304
10. Konovalov SK, Murray JW, Luther GW, Tebo BM (2006) Processes controlling the redox budget for oxic/anoxic water column of the Black Sea. Deep Sea Res II 53:1817–1841
11. Burchard H, Bolding K, Villareal MR (1999) GOTM, a general ocean turbulence model, theory, applications and test cases. European Commission Report EUR 18745 EN 103
12. Burchard H (2002) Applied turbulence modelling in marine waters. Lecture notes in earth sciences, vol 100. Springer, Berlin, p 229
13. Kondo J (1975) Air-sea bulk transfer coefficients in diabatic conditions. Bound Lay Meteor 9:91–112
14. Oguz T, Gilbert D (2007) Abrupt transitions of the top-down controlled Black Sea pelagic ecosystem during 1960-2000: evidence for regime-shifts under strong fishery and nutrient enrichment modulated by climate-induced variations. Deep Sea Res I. doi:10.1016/j.dsr.2006.09.010
15. Marshall FE, Cannizzo JK, Corbet RHD (1997) IAU Central Bureau for Astronomical Telegrams. Circular No. 6727. website: http://www.cfa.harvard.edu/iauc/06700/06727.html#Item1
16. Jones PD, Jonsson T, Wheeler D (1997) Extension to the North Atlantic oscillation using early instrumental pressure observations from Gibraltar and south-west Iceland. Int J Climatol 17:1433–1450

17. Murray JW, Stewart K, Kassakian S, Krynytzky M, Dijulio D (2005) Oxic, suboxic and anoxic conditions in the Black Sea. In: A. Gilbert, V. Yanko-Hombach and N. Panin (eds) Climate Change and Coastline Migration as Factors in Human Adaptation to the Circum-Pontic Region: From Past to Forecast. Kluwer Pub.
18. Yakushev EV, Debolskaya EI (2000) Particulate manganese as a main factor of oxidation of hydrogen sufide in redox zone of the Black Sea. IOC Workshop Report, vol 159. Kluwer Academic, Dordrecht, pp 592–597
19. Stanev EV, Peneva EL (2002) Regional sea level response to global climatic change: Black Sea examples. Glob Planet Change 32:33–47
20. Tsimplis MN, Josey SA, Rixen M, Stanev EV (2004) On the forcing of sea level in the Black Sea. J Geophys Res 109:C08015. doi:10.1029/2003JC002185
21. Staneva JV, Stanev EV (2002) Water mass formation in the Black Sea during 1991–1995. J Mar Syst 32:199–218
22. Tsimplis M, Zervakis V, Josey S, Peneva ES,Truglia MV, Stanev E, Lonello P, Malanotte-Rizzoli P, ArtaleV, Theocharis A, Tragou E, Oguz T (2006) Changes in the Oceanography of the Mediterranean Sea and their link to Climate Variability. In: Mediterranean Climate Variability, Lionello, Rizzoli and Boscolo (eds) Elsevier, Chapter 4, 217–272
23. Kazmin AS, Zatsepin AG, Kontoyiannis H (2010) Comparative analysis of the long-term variability of winter surface temperature in the Black and Aegean Seas during 1982–2004 associated with the large-scale atmospheric forcing. Int J Climatol 30:1349–1359
24. Belokopitov V (1998) Long-term variability of cold intermediate layer renewal conditions in the Black Sea. NATO TU-Black Sea Project Ecosystem Modelling as a Management Tool for the Black Sea, Symposium on Scientific Results. NATO ASI Series 2/47(2):47–52
25. Stanev EV, Bowman MJ, Peneva EL, Staneva JV (2003) Control of Black Sea intermediate water mass formation by dynamics and topography: comparisons of numerical simulations, survey and satellite data. J Mar Res 61:59–99
26. Rodi W (1987) Examples of calculation methods for flow and mixing in stratified fluids. J Geophys Res (C5), 92:5305–5328

Conclusions

E.V. Yakushev

Abstract This book is aimed at a systematic description of the knowledge accumulated on studying of chemical structure of pelagic redox interfaces, oxygen depletion and connected processes. It presents the principal particular features of the water column redox structure, including the distributions of certain parameters and microbiological features. The book also presents studies devoted to the inter-annual variability of some oxygen-depleted systems and modelling. The monograph is written by a team of scientists joined by a common understanding of the complicated phenomena and processes that are connected with the redox-interfaces structure formation and oxygen depletion development. The book is based on numerous observational data, collected by the authors of the chapters during sea and shore expeditions, on the archive data, as well as on a wide scientific literature.

Keywords Anthropogenic factor, Baltic Sea, Black Sea, Climate change, Oxygen depletion, Redox zone

This conclusion completes one more generalization concerning the investigations of water column redox interfaces and oxygen depletion events in the sea water. This scientific topic attracts an increasing interest of the marine science community in the recent years because of the global character of these events and their possible connection with Global Change. The research shows how complicated and diverse natural processes and phenomena are, their interaction in the redox layers and temporal changes of the redox-conditions. Redox interfaces are discussed in the context of studying of processes typical of the changeable redox conditions appearing during oxygen depletion. The oxygen depletion events are connected

E.V. Yakushev (✉)
Norwegian Institute for Water Research, Oslo, Norway

Shirshov Institute of Oceanology RAS, Gelendzhik, Russia
e-mail: eya@niva.no

E.V. Yakushev (ed.), *Chemical Structure of Pelagic Redox Interfaces: Observation and Modeling*, Hdb Env Chem (2013) 22: 273–284, DOI 10.1007/698_2012_181,

with anthropogenic and climatic forcing, and already oxygen-depleted systems are more sensitive to the potential future changes. Thus, this book presents a description of the knowledge accumulated today (2012) that is necessary for understanding of the changes in the marine oxygen-depleted systems in the future.

This new monograph significantly complements many issues assessed (that are listed in the Introduction) and also reflects the opinions of the scientists who prepared this book. Modern science, methods and priorities are developing fast. This requires an adequate scientific response, which is reflected in publications. This new book about the nature of the oxygen depletion events presents the scientific views of the researchers referring to different generations and scientific backgrounds and therefore from different perspective. However, they are centered on the general concept of oxygen depletion development, formation of the redox layers properties and basic principles. They refer to the interrelation between the natural environment and society, which is a "system approach" or view of the modern Ocean.

The book starts with an analysis of the vertical biogeochemical structure of the water column redox interface of the Black Sea. A characteristic feature of the Black Sea redox layer is that certain redox reactions occur in a very narrow layers (2–5 m) of a constant water density. That leads to the correspondence of vertical chemical distributions to specific density levels. Analysis of the vertical distributions of the ratios between C, S, Si, N, P revealed the layers with significant systematic differences from the theoretical Redfield's and Richard's values. These anomalies can testify to a presence of such processes as denitrification/anammox and the processes of the "phosphate dipole" formation.

The ranges of depth and density for reactions that control the decrease of nitrogen (denitrification/annamox) and the formation of the shallow minimum and deep maximum of phosphate in the redox layer are shown based on the analyses of stoichiometric ratios between the main nutrients. Assuming that silicate concentration does not change under the conditions of the redox layer, the rates of the processes of nitrogen decrease (denitrification/anommox) were calculated. According to these calculations, the range of the probable denitrification/anommox rates is (0.012–0.046) $\mu M\ day^{-1}$, which is in agreement with existing results of these processes measurements. Based on the same approach, the rates of formation of the shallow phosphate minima (0.008–0.032) $\mu M\ day^{-1}$ and the deep phosphate maxima (0.006–0.024) $\mu M\ day^{-1}$ were calculated. The obtained estimates of the rates of transformations of the main nutrients at the redox interface have a large significance for studying of the phosphorus and nitrogen dynamics at the seasonal and interannual scales in connection with different scenarios of climate variability and anthropogenic forcing.

Organisms living below the euphotic zone in marine environments are dependent on the organic matter supplied to this environment. Here, the quantity and quality of organic carbon is in most cases the limiting factor for heterotrophic growth. In some cases oxygen also becomes limiting for metabolic processes in deeper layers, mostly as an effect of reduced water circulation. The supply of both oxygen and organic carbon to layers below the euphotic zone of most marine systems is essential to maintain aerobic organisms, as nearly all eukaryotic living

organisms depend on oxygen as the terminal electron acceptor when generating energy by respiration of organic material.

Combining the assessment of fluxes of electron acceptors and donors that fuel chemolithoautotrophy with observations on the microbial taxonomic structure within marine redox gradients was made. Although modern molecular techniques help to identify the acting organisms and verify chemolithoautotrophy on the process level, there are still gaps that need to be solved. Within the energetic frame of contributing reactions, there is still the option of the presence of hitherto undescribed physiological pathways. In this environment, characterized by strong gradients, new approaches need verification by incubation independent methods to eliminate artifacts. At the moment, there is no satisfying explanation for the extent of the carbon dioxide fixation rates, especially in the anoxic part of the redox zones. An improvement of techniques of in situ rate measurements and the integration of in situ molecular approaches like metatranscriptomics or proteomics regarding carbon dioxide fixing key enzymes is needed.

Fluorescent in situ hybridization (FISH) was used to analyze the abundance and phylogenetic composition of physiological active anaerobic microbial communities (sulphate-reducing bacteria and methanogenic archaea) that lived in the aerobic waters and in the oxic/anoxic transitional zone (redox layer) of the Black Sea. Biogenic sulphate reduction and methane formation were detected at these interfaces by radioisotope techniques.

In the oxic subsurface water layer, the active cells of sulphate-reducing and methanogenic microorganisms were much more abundant in the samples collected in summer than in winter samples from the deep-sea zone. The presence of physiologically active anaerobic microorganisms in oxic and chemocline waters of the Black Sea correlates with the hydrochemical data on the presence of sulphide and methane at corresponding depths.

Thus, the results of both FISH and radioisotope measurement of the rates of sulphate reduction and methanogenesis indicate active sulphate reduction in the aerobic waters of the Black Sea. The aerobic surface waters and the redox layer differed in both the total microbial numbers and the phylogenetic composition of the physiologically active anaerobic microbial community. High abundance of SRB of the genera *Desulfotomaculum* and *Desulfovibrio,* which exhibit relatively high aerotolerance, was discovered in the oxidized surface horizons. In the chemocline zone, the cells of *Desulfomicrobium* and, to a lesser degree, *Desulfovibrio* were found. However, *Desulfomicrobium* and *Desulfomicrobium* prevailed in anaerobic enrichment cultures obtained from the water samples of the aerobic and chemocline zone, respectively.

These results demonstrate a significant biogeochemical and ecological role of sulphate-reducing bacteria and methanogenic archaea in the aerobic zone, chemocline and upper anaerobic horizons of the Black Sea.

The joint analysis of manganese and iron species distributions (dissolved Mn, dissolved bound Mn, dissolved Fe(II) and Fe(III), particulate Fe and Mn) data obtained in the north-eastern Black Sea, the Gotland and Landsort Deeps of the Baltic Sea and the Oslo Fjord enabled common features to be revealed that demonstrate the similarity of the redox-layer formation mechanism in these geographical regions.

The research shows that Mn bound in stable complexes with hypothetical organic matter or pyrophosphate is observed in the redox zones at significant concentrations (up to 2 μM), and is likely present as Mn(III), an intermediate product of the oxidation of Mn(II) and reduction of Mn(IV). This bound Mn plays an important role in the cycle of Mn, and in the cycles of other elements in the redox zone both as oxidizer and as complexing agent. The bound Mn existed in two forms – colloidal (0.02–0.40 μm) and truly dissolved (<0.02 μm) perhaps resulting from complexing with different types of ligands.

Redox interfaces are characterized by a formation of a so-called "phosphate dipole" with a minimum above the sulphidic boundary and a maximum just below, with a steep increase in concentrations between the two. The hypothesis that the P and Mn cycles are interconnected by the formation of complexes between Mn(III) and P-containing ligands can explain the presence of the shallow phosphate minimum above the sulphide-interface. The presence of the deep phosphate minimum (below the H_2S boundary) is probably due to the formation of P-containing iron particles. Further studies of the relation between the Mn(III), pyrophosphates and polyphosphates are necessary to better understand the ecology of seas with anoxic conditions, because the flux of phosphates to the anoxic zone affects the processes of OM production.

The flushing events, river input and sporadically increased mixing and anoxygenic photosynthesis play an important role in the formation of redox zones. Response time for changes in the microbial processes involved in reduction and/or reoxidation of Mn and Fe lags behind that for oxygen injection into water. Concentrations of redox-sensitive species of Mn and Fe should thus be useful for tracing of prior redox conditions changes.

Modelling results confirm that the manganese cycle (formation of sinking down Mn(IV) and presence of dissolved Mn(III)) is the main reason of absence of oxygen and hydrogen sulphide direct contact. Because of the low concentrations, the role of the iron cycle is insignificant in the formation of the main features of the boundary layer structure between the hydrosulphide and oxic waters. The model experiments enabled the role of a number of factors to be assessed. We suggest that in nature all the factors analyzed (amount of Mn, intensity of mixing, sinking rate) are not constant and can vary from region to region and from time to time. Their exact combination results in the shape of the distributions of the observed parameters.

Further studies of the manganese and iron cycling under the changeable redox conditions are necessary to understand the consequences of oxygen depletion development, i.e. effects for the transformation of nutrient and hazardous substances. It is necessary for understanding of the reaction of the oxygen-depleted systems to Global Change.

Depth profiles of sulphur species, including sulphide oxidation intermediates (zero-valent sulphur and thiosulphate), nutrients, metals (Mn, Fe), oxygen, temperature, salinity and turbidity were measured in the Gotland Deep, central in the eastern Gotland Basin (the Baltic Sea). It was found that the highest concentrations of more oxidized sulphide oxidation intermediate, thiosulphate, were located below the highest concentrations of zero-valent sulphur. This paradox was explained by

bacterial nitrate reduction coupled with thiosulphate oxidation. The same process utilizing zero-valent sulphur is less effective due to particulate form of the latter.

Oxic water intrusions were traced in both the redox transition zone (RTZ) and deep water column by decrease in concentrations of reduced sulphur and nitrogen species (sulphide, zero-valent sulphur, thiosulphate) as well as in increase of nitrate concentration. Two turbidity maxima were found in the redox transition zone. Turbidity maximum, which coincides with past oxic water intrusion, was found in the deep sulphide-rich water layer. The depth distributions of metals and nutrients in most of the profiles indicate instability of the redoxcline and oxic water intrusions at and below the redoxcline.

Detailed study of the RTZ and water column profiles of Gotland Deep revealed that RTZ in this system can be relatively stable and dominated by oxic water intrusions below the oxic–anoxic water boundary. Oxygen intrusion in the deep water was also documented. Though no oxygen was detected below the RTZ, decrease in ammonia, sulphide and thiosulphate concentrations and increase in temperature, salinity and turbidity at 180–220 m depth are the result of recent oxic water intrusion. Even in the profiles with relatively stable RTZ, no phosphate minimum above the sulphide onset and no maximum at sulphide detection depths were found.

Concentrations of sulphide oxidation intermediates were relatively low. At the RTZ the highest concentrations of zero-valent sulphur and thiosulphate were 1.10 μmol L^{-1} and 1.51 μmol L^{-1}, respectively. In the deep water below RTZ the highest concentrations of zero-valent sulphur and thiosulphate were found to be 1.27 μmol L^{-1} and 3.34 μmol L^{-1}, respectively. Similar concentrations for thiosulphate and zero-valent sulphur were reported in the RTZ of the other regions. Oxygen is the main electron acceptor for sulphide oxidation at RTZ. Below RTZ, Fe(III) and Mn(IV) are responsible for sulphide oxidation and production of sulphide oxidation intermediates in the deep water column. In profiles with relatively stable redoxcline, the maximum of thiosulphate concentrations was found at the level, which is 3–9 m deeper than that for the maximum of zero-valent sulphur concentrations. Onset of thiosulphate concentration coincides with depth of nitrate depletion. We propose that thiosulphate oxidation coupled to nitrate reduction is the reason for the thiosulphate depletion in the chemocline. Zero-valent sulphur is not removed by this mechanism due to its low solubility in non-sulphidic waters that makes zero-valent sulphur less bio-available.

Based on the measurements at more than 1,700 stations during the last three decades in the north-eastern Black Sea, analysis of seasonal and interannual variability of chemical characteristics of Cold Intermediate Layer (CIL) and redox layer is given. Studied species include main nutrients, dissolved oxygen, hydrogen sulphide and carbon system elements.

The reported investigations showed that the biogeochemical system of the redox layer and the CIL of the Black Sea are subject to interannual changes. Surface layers ventilation with dissolved oxygen (DO) down to the depth of the CIL occurs in winter. The intensity of ventilation is predetermined by climate forcing which is possibly regulated by the large-scale climate formations like the North Atlantic

Oscillation (NAO) that affects the temperature of air and surface water, and they in turn set up the upper boundary conditions for the downward transport of DO.

No clear trend of pH decrease in the Black Sea CIL testifying a progressive acidification was revealed. The CIL pH variability was significantly correlated with the CIL oxygen changes, which were logically consistent with the interannual variability of the winter vertical mixing intensity.

This ventilation sets the upper boundary conditions for the downward transport of DO. The Black Sea hydrogen sulphide boundary oscillates in the density field with an amplitude of $\sigma_\theta \sim 0.05–0.15$ kg m^{-3} depending on the climate variability, which is well related to the NAO index. The position of the sulphide boundary indicates on the volume of the oxic layer in the Black Sea and plays a major role in the functioning of the ecosystem. Therefore, the variations of chemical parameters distribution in the density field of the Black Sea redox layer are a good indicator of global climate change.

Historical data on physico-chemical and biological characteristics during the last 30 years were used to examine the seasonal nutrient and plankton dynamics in a semi-enclosed area of the Mediterranean Sea, Elefsis Bay, in phase with the development of intermittently hypoxic and anoxic conditions. Sediment records covering most of the Holocene showed that the area was affected by hypoxia and/or anoxia in the past. However, the occurrence of hypoxia in the Elefsis Bay need not necessarily be attributed to the anthropogenic activities but could be naturally driven by oceanographic-climate forcing.

The Elefsis Bay ecosystem seems to be very complicated and variable. Its variability over the last 30 years can be attributed to the differences in anoxia intensity and the amount of the accumulated organic material. The first observations in temporal variations of environmental parameters in the bay primarily reflect the impact of decreasing pollution during the last decade rather than climate variability. On the contrary, the observed variation in the intense of the hypoxia/anoxia developed in the bay appears to be related to local climate variability. However, this variation together with the decrease of the pollution in the bay during the last years, seems to have an effect on the N:P ratio that controls the planktonic production.

The physiography of Elefsis Bay leads to strong seasonal density stratification of the water mass and influence the oxygen distribution in the basin resulting in hypoxia and anoxia, existing for about 5 months annually. This situation retains nutrients and organic matter within the basin and leads to high nutrient accumulation. Relatively low nitrite concentrations (0.03–0.12 μM) characterize the anoxic, ammonium-rich waters of the Bay. The nitrite concentrations were rather elevated in the suboxic zone (0.03–2.40 μM). However, mineralization processes (i.e. ammonification) are favoured and supported by the high concentrations of organic matter. On the other hand, the data imply that "new" organic matter enriched in nitrogen is released into the bottom waters upon oxygen removal. It may be that the dying zoobenthic communities during anoxic periods contribute significantly to the observed distribution of organic matter. The mesozooplankton community of Elefsis Bay is characterized by low diversity, high dominance of opportunistic species and very strong temporal variability, reflecting the pollution of the bay.

The occurrence of hypoxia in Elefsis Bay on a "geological" timescale seems to be related to climate fluctuations. Warmer periods contributed to stratification of the water column and to relative higher productivity. These factors were the primary forcing for hypoxia in the Elefsis Bay.

The interannual variability of the biochemical parameters showed significant increasing trend of the N:P ratio and decreasing trend for chlorophyll, which indicates a change of the ecosystem after 2000. This possibly reflects the decrease of the pollution in the bay mainly due to the operation of the Sewage Treatment Plant in Psitallia in the end of 1994.

The Elefsis Bay ecosystem seems to be very complicated, variable and "fragile", due to its morphology (enclosed), bathymetry (shallow with two small basins) and intense anthropogenic activity (domestic, industrial and naval pollution). Its variability can be attributed to the differences in anoxia intensity and the amount of the accumulated organic material. The weak water mass renewal in combination with the organic load and the high biological production results in the entrapment and recycling of large amount of organic matter in the bay.

The first observations in temporal variations in nutrients in the bay primarily reflect the impact of decreasing pollution during the last decade rather than climate variability. On the contrary, the variation in the intense of the hypoxia/anoxia developed in the bay appears to be related to local climate variability.

The large-scale hypoxia is an inherent property of the Baltic Sea caused by geographically and climatically determined insufficiency of oxygen supply to the deep water layers. Occurrence of hypoxia was documented by direct oxygen measurements from the beginning of the twentieth century and inferred backwards over centuries and millennia from lamination and metallic indices in the dated sediment cores. Therefore, in contrast to local coastal areas, where the recent hypoxia is often related to man-made eutrophication, the anthropogenic contribution into extension and intensity of hypoxia in the deep offshore waters is still under debate. Apparently, the convincing quantitative estimates of such contribution should be obtained with the aid of mathematical models that are now capable to realistically simulate the long-term variations of large-scale hypoxia and its biogeochemical consequences.

The extension of hypoxia varies both seasonally and from year to year. During 1961–2005, the hypoxic zone covered by waters with oxygen concentration less than 2 mL L^{-1} extended on average over a huge area of about 50,000 km^2.

The interannual variations reaching dozens of thousand square kilometres generate large-scale effects in basin-wide nutrient pools. In the expansion phase, dissolved inorganic nitrogen (DIN) pool is reduced by denitrification and dissolved inorganic phosphorus (DIP) pool increases due to phosphate release from anoxic sediments, while in the shrinkage phase the changes are opposite. These changes reached hundreds thousand tonnes of N and P The resulting excess of phosphate pool over the "Redfield" demand by phytoplankton is favorable for the dinitrogen fixation by cyanobacteria in amounts sufficient to compensate for denitrification and to counteract possible reductions of the nitrogen land loads.

The expansion of hypoxia results in decreased N:P ratio that is favourable for the blooms of dinitrogen fixing cyanobacteria, another common feature of the Baltic Sea ecosystem. Nitrogen fixed by cyanobacteria becomes available for further biotic cycling, thus to a large degree compensating for the nitrogen removal by denitrification.

A historical imbalance between external input of phosphorus vs. its insufficient removal by advection and sediment burial resulted in an "extra" (200–300) $\times$ 10^3 tonnes of phosphorus, accumulated in the Baltic Proper since the 1960s, that in two ways counteract the environmental management measures aimed at reducing eutrophication. Firstly, a longer time is needed to deplete the larger phosphorus pool even by the drastic reductions of the phosphorus land loads. Secondly, this excessive phosphorus stock supports the cyanobacterial nitrogen fixation that counteracts the nitrogen land load reductions. Therefore, it is the phosphorus load reduction that should be the priority managerial target in the Baltic Proper. The possibility to speed up the reduction of excessive phosphorus pool by such engineering methods as the forced ventilation of intermediate water layers or the artificial co-precipitation of phosphate should be studied in a greater quantitative detail.

In contrast to modelling in the typical oceanic and marine waters oxic conditions, the modelling of the oxic/anoxic transformation can not only give numerical estimates, but can also reveal the mechanisms of the main processes occurring there, because there is still not much known about it. From this point of view the main goal of oxic/anoxic modelling is to compare knowledge of events, processes and systems with the observed situation. A model seems to be the single tool that will permit one to check the hypothesis of what processes are responsible for the origin and maintenance of the observed phenomena.

The goal of the elaboration of the RedOx Layer Model (ROLM) was to create an instrument for a complex analysis of the structures of the pelagic redox-interfaces in the seas with anoxic conditions. The processes of formation and decay of organic matter (OM), reduction and oxidation of species of nitrogen, sulphur, manganese and iron, and transformation of phosphorus forms were parameterized. ROLM can be used as a construction block of the vertical one-dimensional models (i.e. the General Ocean Turbulent Model, GOTM) or three-dimensional models.

The earlier performed applications of ROLM for analyzing the water column redox layer structure enabled common features to be revealed that demonstrate the similarity of the redox-layer formation mechanism in the different geographical regions. Modelling results demonstrate that formation of sinking Mn(IV) and presence of dissolved Mn(III) is the main reason of a presence of suboxic zone with absence of both oxygen and hydrogen sulphide. The particulate manganese may be a primary oxidant of hydrogen sulphide into elementary sulphur. The intense vertical transfer of detritus particles with the heavy particles of Mn(IV) oxide is a cause of the existence of the suboxic zone with no detectable oxygen concentrations. This makes possible the presence processes of anoxic oxidation of reduced compounds, such as methane, reduced iron and ammonium. The formation of Mn(IV) might considerably affect the distribution of the suspended matter and the formation the layer of turbidity. The theoretical requirement of the occurrence

of seasonal variations of the particulate manganese concentrations was also confirmed by means of the model that treated this phenomenon according to the competition for dissolved oxygen between the organic matter supplied from the upper layers and the reduced compounds supplied from the hydrosulphide zone. The competition results in the fact that the processes of organic matter mineralization become more intense in the summer; hence, less oxygen is available for the oxidation of the reduced forms of manganese, iron and sulphur. At the same time, more oxygen is available for the formation of particulate manganese and iron. Because of the small concentrations, the role of the iron cycle is insignificant in the processes of the redox interfaces in the water column compared with those in the sediments. Application of ROLM allowed to explain the formation of so-called "phosphate dipole". The shallow minimum of phosphate above the sulphidic boundary can be formed due to formation of complexes between Mn(III) and P-containing ligands.

The chapters included in this volume present examples of the ROLM application for analysis of the distributions of forms of manganese, iron and sulphur in the redox layer and for simulating of the Black Sea biogeochemical regime interannual changes.

A biogeochemical model OxyDep coupled with three-dimensional hydrodynamic model GETM (General Estuarine Transport Model) was used to simulate the hydrophysical and biogeochemical regimes of the meromictic Fjord Hunnbunn over the summer period. The main goal was to parameterize the oxygen depletion processes resulting in formation of suboxic and anoxic conditions in the water column. OxyDep considered five state variables: dissolved oxygen, inorganic nutrient, dissolved organic matter, particulate organic matter and biota. This model parameterized the main processes responsible for the changing of the water column oxygen conditions, i.e. OM synthesis; OM decay due to oxic mineralization and denitrification; consumption of oxygen from sulphur and metals oxidation and the processes at the boundaries (air–water exchange and the sediment-water exchange). Results of numerical experiments have reproduced the main features of the observed structure and have allowed to reveal the main components responsible for the formation of biogeochemical structure of the meromictic water objects.

With the hydrodynamical model block used it was impossible to reproduce the presence of a permanent pycnocline. Therefore a special attention must be paid when using terrain following vertical coordinates to avoid spurious vertical mixing. The setup for the vertical coordinates in this particular model application needs to be tuned further to achieve more realistic vertical mixing. A z-coordinate model would probably conserve the vertical stratification like the one observed in Hunnbunn better.

The results showed that an application of a simplified biogeochemical model, OxyDep coupled with a three-dimensional model (such as GETM, ROMS, HAMSOM) can be a useful tool for analyzing and forecasting of oxygen and nutrient regime changes. In particular, it is possible to use the parameterized seasonal organic matter variability for studying of propagation of pollutants and carbonate system dynamics.

A long-term variability of the physical and biogeochemical structure of oxic and suboxic layers in the Black Sea was studied on the basis of an analysis of observations and one-dimensional coupled hydrophysical (GOTM) biogeochemical (ROLM) model.

The comparison of model performance with respect to spatial and temporal distribution of biogeochemical variables against observed vertical distribution patterns is quite good. It is demonstrated that during 1960–2000, the long-term variability of winter-mean simulated SST in the Black Sea is reasonably well correlated with the variability of 2 m air temperature. Furthermore, it demonstrated that the thermal state of the upper ocean impacts largely the variability of concentration of biogeochemical variables, such as oxygen and nitrate. The teleconnection between NAO and Black Sea biogeochemistry manifests differently for the periods 1960–2000. The corresponding regime shifts are also associated in a vital way with the large-scale forcing.

The coupled numerical model simulations reveal a pronounced interannual variability of state variables in the Black Sea allowing to conclude that changes in NAO during the past 40 years could be considered as important driver for changes in the Black Sea biogeochemistry. Both at surface layer and CIL, the concentrations of oxygen, nitrate and phytoplankton directly or indirectly respond to the long-term winter NAO index.

The basic points of our findings may be briefly summarised as follows:

- Winter NAO index had an overall increasing trend, except for the abrupt transitions during a decade from 1973 to 1982, when SST and CIL temperature followed generated echoes, that is, the trends changed correspondingly. The general decreasing trend of SST is opposite to the winter NAO index.
- Winter NAO index abrupt shift frequently may bring great changes on meteorological, physical and biogeochemical variables in the Black Sea. The changes of air temperature and wind caused by the winter NAO index influences SST and ventilation flux then affect oxygen, nitrate and phytoplankton. The ventilation flux from surface to CIL led by wind variability changed the distributions of biogeochemical variables.
- A performed model analysis can reveal a mechanism of reaction of the Black Sea biogeochemical regime on the decadal atmospheric variability. More intense ventilation should lead to an increase of both oxygen content in the CIL and supply of nutrient to the surface layer. This will potentially increase the biological productivity. Therefore, the periods of increased concentrations of nitrate and phytoplankton should be correlated with the oxygen increase in the CIL, while the oxygen dynamics in the upper layer are in a larger degree controlled by an interannual variability of the temperature.

The general response-pattern of hydrophysical and biogeochemical variables in the Black Sea to NAO may be described as being mostly shaped by air temperature. However, taking in consideration the fact that in most processes in the Black Sea are controlled by wind one could expect that in 3-D modelling framework wind will also have a pronounced impact. The fact that the results presented do not fully

support variations in temporal distribution of DO and hydrogen sulphide derived from observations could be due to (1) absence in the model of interannual changes in river runoff and eutrophication, (2) absence of horizontal transport that is expected to also play an important role. Therefore the next step to do when simulating the long-term variability is to apply a 3-D modelling framework.

The presented in the book chapters reflect a snapshot of the present state of the investigations devoted to the studies of the water column redox interfaces and the oxygen-depleted systems.

The findings of this book show that oxygen depletion are affected by both anthropogenic and natural factors. The regulation of anthropogenic activity (i.e. treatment plant construction in the Elefsis Bay or a significant decrease of the nutrient discharge to the Baltic Sea) play an important role in the improvements of coastal systems. But climatic factors seem to play a more dominant role. In the Black Sea, nutrient controls in the Danube avoid hypoxia on the Northeastern Shelf, but the Sea hydrogen sulphide boundary position is NAO controlled. The Baltic Sea hypoxic water volume increases due to warming climate and due to an enrichment of the sediments with phosphorus caused by anthropogenic eutrophication that happened mainly in 1970s–1980s.

The oxygen condition of natural waters is an important element of water quality, and oxygen depletion need to be studied in the context of local or regional anthropogenic influence and Global Change.

Index

E.V. Yakushev (ed.), *Chemical Structure of Pelagic Redox Interfaces: Observation and Modeling*, Hdb Env Chem (2013) 22: 285–288, DOI 10.1007/698_2012,